DECLARATION

This work has not previously been accepted in substance for any degree and is not concurrently submitted in candidature for any degree.

Signed ..... (candidate) Date ...18/01/10.....

STATEMENT 1

This thesis is being submitted in partial fulfillment of the requirements for the degree of PhD

Signed ..... (candidate) Date ...18/01/10....

STATEMENT 2

This thesis is the result of my own independent work/investigation, except where otherwise stated. Other sources are acknowledged by explicit references.

Signed ..... (candidate) Date ...18/01/10....

STATEMENT 3

I hereby give consent for my thesis, if accepted, to be available for photocopying and for inter-library loan, and for the title and summary to be made available to outside organisations.

Signed ..... (candidate) Date ...18/01/10..

Cardiff University

SYNTHESIS AND CHARACTERISATION OF LANTHANIDE COMPLEXES FOR APPLICATION AS RESPONSIVE PROBES

By Michael Bryan Andrews

A thesis submitted for the Degree of Doctor of Philosophy

School of Chemistry

October 2009

ProQuest LLC
789 East Eisenhower Parkway
P.O. Box 1346
Ann Arbor, MI 48106-1346

CARDIFF UNIVERSITY

ABSTRACT

SCHOOL OF CHEMISTRY

Doctor of Philosophy

SYNTHESIS AND CHARACTERISATION OF LANTHANIDE COMPLEXES FOR APPLICATION AS RESPONSIVE PROBES

by Michael Bryan Andrews

A range of new lanthanide complexes have been synthesised. The ligands and ligand precursors were characterised by NMR (^{1}H, ^{13}C), electrospray mass spectrometry, UV-Vis and IR spectroscopy. Several ligands or ligand precursors have been crystallised and analysed by X-ray crystal diffraction. The complexes were characterised by electrospray mass spectrometry, UV-Vis, IR spectroscopy and luminescence spectroscopy.

In Chapter 2 a quinoxaline chromophore was incorporated in a macrocyclic ligand and it was shown that quinoxaline was capable of sensitising Ln(III) luminescence in the visible and NIR region. The Eu(III) emission intensity and lifetime were shown to be responsive to pH.

In Chapter 3 two N-(2-nitrophenyl)acetamide-derived chromophores were incorporated into macrocyclic ligands and shown to be capable of sensitising Ln(III) emission. A combined structural, spectroscopy and computation study was undertaken to investigate the spectral differences between the ligands.

In Chapter 4 a synthetic strategy towards the synthesis of metal-ion responsive lanthanide complexes is detailed. The Eu(III) complexes were titrated against various metals and it was shown that the metal-based luminescence was sensitive to the concentration of Hg(II) and Cu(II).

Hydroxyquinoline, aminoanthracene, amidopyrene, amidoquinoline and amidoanthraquinone chromophores were incorporated into macrocyclic ligands in Chapter 5 in order investigate the feasibility of adapting the synthetic strategy presented in Chapter 4 to synthesise responsive probes containing long-wavelength absorbing chromophores. Binding studies demonstrated the potential for these complexes to respond to the presence of Group 12 metals with changes in the overall emission intensity, relative intensity of hyperfine transitions and luminescence lifetimes.

In Chapter 6 the synthetic strategy presented Chapter 4 was utilised to synthesis a ligand capable of forming bimetallic complexes with Ln(III) ions. Combined luminescence and relaxivity studies indicated that the binding of Hg(II) resulted in a change in Ln(III) coordination environment, whereas the binding of Cu(II) caused quenching of emission without increasing q.

Acknowledgements

I would like to thank Dr. Simon Pope for his constant guidance, support and encouragement throughout the duration of this work. I am also sincerely grateful to Dr. Michael Coogan and Dr. Angelo Amoroso for their advice and assistance.

I am very grateful to Dr. Rebecca Laye and Dr. Benson Kariuki, for data collection and structure solution on the X-ray crystal structures, and Dr. Benjamin Ward for DFT investigations.

Many to thanks go to Dr. Andy Hallett, Lucy Mullice, Jenn Jones, Flora Thorp-Greenwood and everyone else with whom it has been my pleasure to share a lab.

My deepest thanks go to my parents and my family for a lifetime of support.

Three years of funding were provided by the EPSRC.

Contents

List of Tables

List of Figures

Abbreviations

Spectroscopy and Procedures

TLC	thin-layer chromatography
IR	infra red
UV-Vis	ultra violet
NMR	nuclear magnetic resonance
NMRD	nuclear magnetic resonance dispersion
MRI	magnetic resonance imaging
ES MS	electrospray mass spectrometry
HR MS	high resolution mass spectrometry
δ	chemical shift
ppm	parts per million
s	singlet
t	triplet
q	quartet
m	multiplet
br	broad

Photophysics

ISC	intersystem crossing
BET	back energy transfer
PeT	photoinduced electron transfer
CT	chart transfer
ILCT	intra-ligand charge transfer
MLCT	metal-ligand charge transfer
MMLCT	metal-metal-ligand charge transfer
HOMO	highest occupied molecular orbital
LUMO	lowest unoccupied molecular orbital

Solvents, Compounds and Chemicals

Et_2O	diethyl ether
EtOH	ethanol
MeCN	acetonitrile
MeOH	methanol
edda	ethylenediamine-N,N'-diacetic acid
edta	ethylenediaminetetraacetic acid
dtpa	diethylenetriaminepentaacetic acid
nota	1,4,7-triazacyclononane-N,N',N''-triacetic acid
dota	1,4,7,10-tetraazacyclododecane-N,N',N'',N'''-tetraacetic acid
Ln	lanthanide
Cyclen	1,4,7,10-tetraazacyclododecane
DO3A	1,4,7,10-tetraazacyclododecane 1,4,7-triacetic acid
DO3AM	1,4,7,10-tetraazacyclododecane 1,4,7-triamide
boc	butoxycarbonyl
TFA	trifluoroacetic acid
OTf/triflate	trifluoromethanesulfonate
Me	methyl
Et	ethyl
Ac	acetyl

Chapter One
Introduction to Lanthanide Chemistry, Spectroscopy and Paramagnetism

1.1 – Introduction

The chemistry of the lanthanides has found use in a wide variety of fields including homogeneous catalysts,[1, 2] permanent magnets,[3] lasers[4] and therapeutic medicine.[5, 6] However, over the last three decades their potential applications in diagnostic medicine have attracted an increasing amount of interest due to their interesting photophysical[7] and magnetic properties.[8] The work described in this thesis describes the synthesis and responsive luminescence and some selected relaxivity properties of new lanthanide complexes as potential biological probes.

1.2 – f-orbitals and Coordination Chemistry of Lanthanides

Symbol	Element	Electronic Configuration	Electronic Configuration Ln(III)
La	Lanthanum	[Xe]$5d^1 6s^2$	[Xe]
Ce	Cerium	[Xe]$4f^1 5d^1 6s^2$	[Xe]$4f^1$
Pr	Praseodymium	[Xe]$4f^3 6s^2$	[Xe]$4f^2$
Nd	Neodymium	[Xe]$4f^4 6s^2$	[Xe]$4f^3$
Pm	Promethium	[Xe]$4f^5 6s^2$	[Xe]$4f^4$
Sm	Samarium	[Xe]$4f^6 6s^2$	[Xe]$4f^5$
Eu	Europium	[Xe]$4f^7 6s^2$	[Xe]$4f^6$
Gd	Gadolinium	[Xe]$4f^7 5d^1 6s^2$	[Xe]$4f^7$
Tb	Terbium	[Xe]$4f^9 6s^2$	[Xe]$4f^8$
Dy	Dysprosium	[Xe]$4f^{10} 6s^2$	[Xe]$4f^9$
Ho	Holmium	[Xe]$4f^{11} 6s^2$	[Xe]$4f^{10}$
Er	Erbium	[Xe]$4f^{12} 6s^2$	[Xe]$4f^{11}$
Tm	Thulium	[Xe]$4f^{13} 6s^2$	[Xe]$4f^{12}$
Yb	Ytterbium	[Xe]$4f^{14} 6s^2$	[Xe]$4f^{13}$
Lu	Lutetium	[Xe]$4f^{14} 5d^1 6s^2$	[Xe]$4f^{14}$

Table 1.1 – Electronic configuration of the lanthanides in their atomic and dominant oxidation state

The lanthanides are elements in which the valence electrons are situated in the 4*f* orbital. The *f* electrons are poor at shielding other valence orbitals from nuclear charge, thus the increasing nuclear charge across the series results in a contraction and stabilisation of the 4*f* orbitals. As a result of this the 4f orbitals are typically filled preferentially over the 5*d* orbital, the exception to this is the transition from europium to gadolinium in which the stability of the half-filled 4*f* orbital is maintained by adding the additional electron to the 5*d* orbital (Table 1.1). On oxidation of the lanthanides, the electrons are first removed from the 6s orbital then from either the 5d or 4f orbital. The chemistry of the lanthanides

is dominated by the +3 oxidation state, since this configuration results in empty 5*d* and 6*s* orbitals combined with a further contraction and stabilisation of the 4*f* orbitals.[9]

The contraction of 4*f* orbitals means they are shielded by the 5*s* and 5*p* orbitals, and are therefore core-like and do not interact strongly with ligands. As a result of this the coordination chemistry of the trivalent lanthanide ions is considerably different to that of the transition metals.[9] Since the valence orbitals are not shape directing the coordination number and geometries of lanthanide complexes in solution are not known with any precision but coordination number and geometry appears to be based on interligand repulsion and crowding in the coordination sphere. X-ray crystallography of hydrated lanthanide ions in the solid state, for example in $Nd(BrO_3)_3$[10] and ErX_3 (X = Cl/I),[11] indicate that the earlier lanthanides tend to form nine-coordinate tricapped trigonal prismatic complexes whereas the later lanthanides tend form eight-coordinate square antiprismatic complexes. However, coordination numbers as high as 12 have been observed for complexes of larger lanthanide salts with bidentate ligands with small bite angles.[12] The general decrease in coordination numbers across the series is due to the lanthanide contraction, which arises from the increase in nuclear charge coupled with the poor shielding effect of the *f*-orbitals.

As hard Lewis acids lanthanide ions form more stable complexes with ligands incorporating hard donors such as oxygen and nitrogen, however even in these cases the complexes of lanthanides with monodentate ligands are extremely labile. The lifetime of exchange of water ligands is of the order of 10^{-9} s, essentially determined by the rate of diffusion of molecules into and out of the lanthanide coordination sphere.[13] In order to form kinetically stable complexes the *chelate* and *macrocyclic* effects must be exploited by utilising multidentate ligands. When a multidentate ligand coordinates with a metal ion in solution, for instance a lanthanide ion in water, the dissociation of two or more water molecules results in an increase in entropy of the system. This increases the stability of the complex formed compared to that of an analogous complex with monodentate ligands. The more donor atoms in the ligand the greater the

number of water molecules liberated, as the Equation 1 demonstrates the larger the increase in entropy the higher the stability of the resultant complex.[14]

$$\Delta G = \Delta H - T\Delta S$$

Equation 1

This is known as the chelate effect. In terms of kinetics, the stability of a chelate results from the need for all donor atoms to simultaneously dissociate from the metal, in order for decomplexation to occur. Due to the inherent stability of five- and six-membered rings metal ions form the most stable complexes with ligands in which there are two or three atoms between the donors.

Ligand	Number of donor atoms	LogK
edda[15]	4	7 – 9
edta[15, 16]	6	15 – 20
nota[16]	6	13 – 15
dtpa[16]	8	20 – 22
dota[16]	8	23 - 25

Table 1.2 – The stability of the lanthanide complexes with multidentate and macrocyclic ligands.

Although edta and nota have the same number of donor atoms the stability constant of edta complexes is generally much higher for two reasons (Table 1.2).[16] Firstly, edta has a higher portion of hard, oxygen-based donor atoms, and secondly nota is a cyclic molecule with a small internal cavity which is too restricted to adequately coordinate to lanthanide ions. However, larger cyclic ligands show a stability enhancement compared to acyclic ligands with similar donors, as observed for dtpa and dota. This is known as the macrocyclic effect and was first reported for the copper complex with 1,4,8,11-

tetraazacyclotetradecane, which is five orders of magnitude more stable than the analogous acyclic ligand.[17]

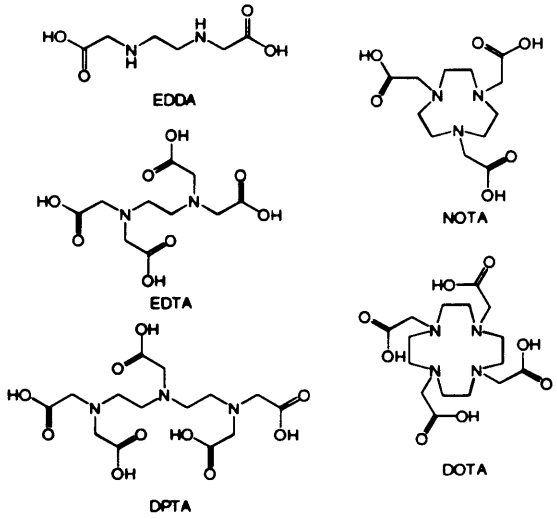

Figure 1.1 – The structures of the ligands presented in Table 1.2.

This enhancement of stability is due to the increased configurational entropy of the acyclic ligand in solution compared to its cyclic analogue.[18] In terms of kinetics, the macrocyclic effect may be attributed to the donors of a cyclic ligand being prearranged to bind to a metal and for dissociation to occur the ring must stretch, inducing an unfavourable strain across the ring, in order for several donor-metal bonds to be broken at once.

Through a combination of the chelate effect and the macrocyclic effect sufficient stability can be induced in gadolinium complexes to allow them to be used as magnetic resonance imaging (MRI) contrast agents (as discussed in more detail in Section 1.6). The gadolinium complexes with dtpa and dota can be administered to patients in gram quantities and go by the commercial names Magnevist® and Dotarem®, respectively.[9]

The work contained herein will use 1,4,7-tris(*tert*-butoxycarbonyl)-1,4,7,10-tetraazacyclododecane as a starting material, in which the secondary amine allows the addition of further functionality, as the precursor. This is formed

directly from cyclen according to the literature procedure reported by Sammes and coworkers.[19]

1.3 – Electronic Spectroscopy

Many of the lanthanide ions are slightly coloured, and this absorption is due to forbidden $f \rightarrow f$ transitions between different energy levels within the 4*f* orbitals. These energy levels arise due to spin-orbit coupling – the coupling of the angular momentum of the spin of an electron with the angular momentum of its orbital momentum. These energy levels are described using Russell-Saunders coupling, which represents energy levels as a term symbol-

$$^{(2S+1)}L_J$$

-where S equals the total spin angular momentum, *L* equals the total orbital angular momentum and *J* is the total angular momentum.[9]

In the case of transition metals the selection rules forbidding $d \rightarrow d$ transition are relaxed due to vibronic coupling, which arises from the vibrations of ligands temporarily lowering the symmetry of the d orbitals. However, in the case of the lanthanides the crystal field effect is weak due to the shielding of the 4f orbitals by the 5*s* and 5*p* orbitals, resulting in the much weaker absorbance, and subsequent phosphorescence on relaxation of the excited states, of lanthanide complexes compared to that of d-block metal complexes. The weak crystal field effect in lanthanide complexes also results in well-defined transitions which vary little in energy between different compounds. However, by close observation of the electronic spectra of lanthanide ions changes in the symmetry of the coordination sphere can be observed due to the presence of hypersensitive transitions. A comparison of the absorption spectrum of neodymium salts in solution[20] with those of hydrated neodymium bromate, sulphate and iodide salts indicate that Nd(III) aqua ion is nine coordinated, since the hypersensitive bands show a greater similarity with those of $Nd(BrO_3)_3.H_2O$.[10]

1.4 – Sensitised emission of lanthanide ions

In 1941 it was reported by Weissman that the irradiation of the organic chromophore in an europium salicylaldehyde complex resulted in strong, characteristic Eu(III) emission.[21] Over the next two decades it was established that this sensitisation of lanthanide ions in complexes, containing organic chromophores, typically occurs *via* the promotion of an electron into the excited singlet state of the ligand, followed by intersystem crossing (ISC) into the excited triplet state. Energy transfer from the triplet state of the ligand, to one or more excited states of the Ln(III) ion then occurs, followed by lanthanide luminescence (Figure 1.2).[22]

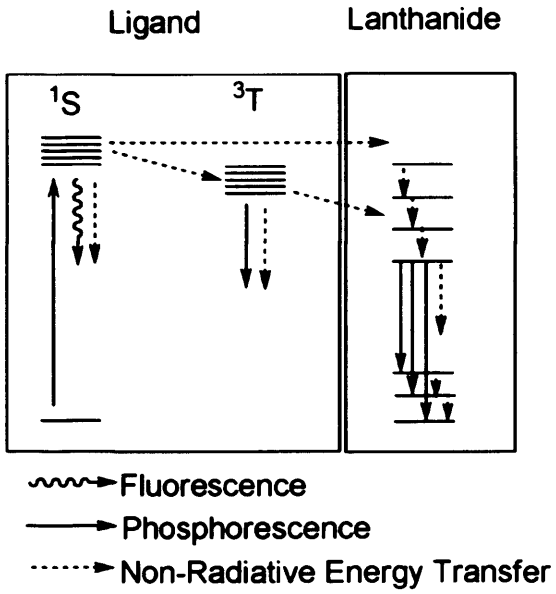

Figure 1.2 – Diagram of energy transfer process in a lanthanide complex.

Sensitisation is achieved by non-radiative energy transfer from the donor (organic chromophore) to the acceptor (lanthanide ion):

$$D^* + A \rightarrow D + A^*$$

In order for this to occur the donor and the acceptor must be in close proximity and there must be an overlap in the emission spectrum of the donor and the absorption spectrum of the acceptor. Non-radiative energy transfer may occur by two mechanisms- the Coulombic (also known as Förster's) or the exchange (known in this case as Dexter's) mechanisms.[23] In Förster's mechanism the donor-acceptor interaction is primarily dipole-dipole in nature, with contributions from dipole-quadrupole interactions. The rate of energy transfer is given by the equation below. The Förster distance, R_0, is characteristic of the spectral properties of the donor/acceptor pair and typically has a value of 20 – 60 Å. Since the rate of energy transfer is proportional to $1/r^{-6}$ (Equation 2) the transfer efficiency is highly distance dependant[24] but can be significant at distances of around 10 nm.[23]

$$k_T(r) = \frac{1}{\tau_D}\left(\frac{R_0}{r}\right)^6$$

$k_T(r)$ = rate of energy transfer

τ_D = decay time of donor excited state

R_0 = distance at which energy transfer is 50 % efficient (known as the Förster distance)

r = donor to acceptor distance

Equation 2

The rate of energy transfer by Dexter's mechanism, $k_E(r)$, is given below (Equation 3), where r is the separation between the donor and the acceptor, L is a constant related to the orbital radii of the donor and the acceptor, and J is the extent of spectral overlap.[23] The exponential drop in the exchange rate with increasing separation reflects the fact that the orbitals must be in very close proximity (~ 2 Å[24]) to each other in order for Dexter exchange to take place. This requires the donor to be in direct contact with the acceptor.

$$k_E(r) = \exp\left(\frac{-2r}{L}\right)J$$

Equation 3

In 1968 Kleinerman observed that in some Tb(III) complexes sensitisation occurs despite the fact that the lowest emissive state of Tb(III) ($^5D_4$) was higher in energy than the ligand triplet state.[25] It was also noted that the λ_{max} of the Tb(III) excitation spectrum showed a hypsochromic shift compared to that of the excitation spectrum for the ligand luminescence in the Gd(III) and the excitation spectrum of Eu(III), in which the lowest lanthanide excited state ($^5D_0$) was low enough to receive energy from the ligand triplet state. This was attributed to energy transfer from the upper ligand singlet states directly to the emissive lanthanide states by an electron transfer process, which caused structural or energetic changes in the complexes which prevented quenching of the Ln(III) emissive level by the ligand triplet state. Direct singlet to lanthanide transfer was supported by the observation that many complexes, in which the lowest lanthanide excited energy level is between the ligand triplet and singlet states, show a much greater degree of ligand emission quenching than the gadolinium complexes, in which the lowest Gd(III) excited state ($^6P_{7/2}$) is higher in energy than the ligand singlet state. This showed that the quenching cannot be attributed to the heavy atom effect and suggests that energy is being transferred directly from the singlet state to the lanthanide ion, the emission of which is then quenched due to BET to the ligand triplet state.[25] Since then several systems have been developed which efficiently sensitise lanthanide emission *via* direct energy transfer from a singlet state.[26-28] It has also been shown that complexes of d-block metals such as Cr, Fe, Co, Ru, Rh, Re, Os, Ir and Pt can act as sensitising chromophores for lanthanide emission,[29] either by ligand field or CT excited states.

As discussed previously both the Förster energy transfer mechanism and Dexter exchange mechanism require an overlap in the emission spectrum of the donor and the excitation spectrum of the acceptor. However NIR emission from Yb(III), which has no energy levels below approximately 10300 cm^{-1},[22] can be

sensitised by short wavelength chromophores despite the lack of spectral overlap. In 1985 Horrocks and coworkers reported that the tryptophan (Trp) fluorescence of a parvalbumin protein was significantly decreased on binding to Eu(III) and Yb(III), an effect which was not observed for other members of the lanthanide series.[30] This was later attributed to an electron transfer mechanism in which the excited state tryptophan reduces the lanthanide ion.[31] In the case of europium, the Trp+ Eu(II) state is lower in energy than the lowest emissive state of Eu(III) ($^5D_0$) and a second redox process returns the system to the ground state without emission.. However, ytterbium(II) is more readily oxidised than europium(II) , therefore the Trp+ Yb(II) state is higher in energy than the lowest emissive state of Yb(III) ($^2F_{5/2}$). Trp+ then oxidises the Yb(II), which may form Yb(III) in its excited state. This is then followed by NIR emission from ytterbium, returning the system to the ground state and accounting for the sensitisation despite the lack of spectral overlap.[31]

As is the case for the absorption spectra of Ln(III), the emission spectra are largely unaffected by the coordination environment due to the shielding of the f orbitals by the 5*s* and 5*p* orbitals. However, there are also hyperfine transitions in the emission spectra of several lanthanides, most notably that of Eu(III). The Eu(III) emission spectrum is dominated by the $^5D_0 \rightarrow {}^7F_J$ transitions ($J = 0 - 4$). The $^5D_0 \rightarrow {}^7F_1$ transition is of purely magnetic dipole character so its intensity and energy is largely independent of ligand field. The $^5D_0 \rightarrow {}^7F_{0,2,4}$ transitions are electric dipole transition and thus sensitive to the ligand field. In particular the intensity of $^5D_0 \rightarrow {}^7F_2$ varies greatly depending on the symmetry of the ligand field.[32] If Eu(III) has an inversion centre it can be totally absent whereas in a highly polar environment it can be an order of magnitude more intense than the $^5D_0 \rightarrow {}^7F_1$ transition.[9]

The most significant mechanism by which lanthanide luminescence is quenched is by non-radiative energy transfer to nearby vibrational modes. In particular, for lanthanide complexes in water, interactions with the O-H oscillations of both inner and outer sphere solvent molecules have a dramatic quenching effect on the intensity and lifetime of the lanthanide emission.[33] Although C-H and N-H oscillators also quench lanthanide luminescence[34] the effect is not as severe as

that of O-H vibrations, therefore the luminescence efficiency of a lanthanide ions can be maximised by using multidentate ligands which shield them from interactions with surrounding solvent molecules.

The quenching effect of inner sphere water molecules on the lifetime of lanthanide luminescence has been quantified, providing a means to calculate the degree of solvation of lanthanide ions in complexes. The initial work was carried out by Horrocks.[35] Crystals of known Eu(III) and Tb(III) compounds were prepared in which the metal ion was coordinated to either H_2O or D_2O. These samples were then subjected to direct laser excitation and the lifetime of the lanthanide luminescence was measured. It was found that the difference between the decay rate constant in deuterated and non-deuterated samples has a linear correlation with the number of inner sphere solvent molecules, allowing the number of inner sphere solvent molecules, q, to be expressed as Equation 4.

$$q = A\left(\frac{1}{\tau_{H_2O}} - \frac{1}{\tau_{D_2O}}\right)$$

Equation 4

A is an experimentally determined factor relating to the efficiency of quenching of the particular lanthanide ion by interactions with the O-H oscillations of surrounding solvent molecules. It was also shown that this applied not only to crystalline samples but also to lanthanide chelates in solution and proteins in which a lanthanide ion occupied a metal binding site.[35] Further modifications of this equation added a correction factor to take into account the quenching effect of outer-sphere solvent molecules on Eu(III), Tb(III) and Yb(III) and the effect of N-H oscillations on Eu(III).[36] It has been observed that Nd(III) is particularly sensitive to the quenching effect of C-H oscillations, and a modified form of the equation has been developed to take this into account. In this case the results tend to be accurate for systems in which the ligand contains a high number of C-H bonds close to the metal binding site, for example EDTA and DPTA, but may

give anomalous results for ligand systems in which the number of these bonds is limited, such as the Lehn cryptand.[37]

1.5 – The use of lanthanide complexes as luminescent probes

The use of luminescent probes in cellular imaging and fluoroimmuno assays has typically relied on the use of organic chromophores, some of the most widely used are fluoresceins, rhodamines and derivatives thereof. These have the advantages of high extinction coefficients (~80,000 $M^{-1}cm^{-1}$), absorption and emission bands at long wavelengths and fluorescence spectra which are largely insensitive to solvent polarity.[24] More recently BODIPY® dyes containing boron-based fluorophores have been introduced, which are insensitive to pH, have quantum yields near to unity and more well-defined peaks in their fluorescence emission spectra.[38] However, these fluorophores have several drawbacks. Their small Stokes shifts can result in self-quenching by Förster energy transfer as well as cause technical problems such as the autofluorescence of biological tissue and their short lifetimes (on the order of nanoseconds) make them vulnerable to interference by light scattering.

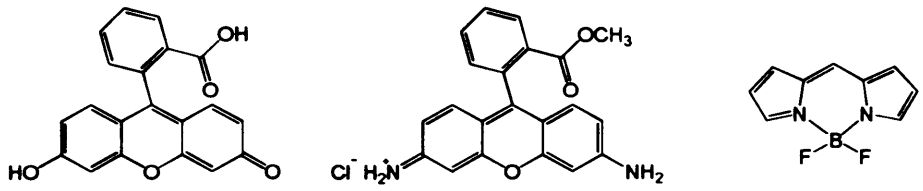

Figure 1.3 – Three commonly used organic dyes.

Although the conditions required to induce lanthanide luminescence are demanding, once they have been met a number of useful properties arise. Population of the excited states requires the careful selection of sensitising chromophore, with a donor energy level approximately 1000 – 2000 cm^{-1} higher than the lowest emissive state of the lanthanide to prevent BET[39] and the large lanthanide ions and the lability of their bonding require large, multidentate

ligands to produce stable complexes and shield the ion from the quenching effect of surrounding solvent molecules. The fluorescence quantum yield of sensitised lanthanide complexes vary greatly, depending on the efficiency of ISC in the organic chromophore, the energy gap between the chromophore donor level and the lanthanide excited state, the energy gap between the lanthanide emissive and ground states and the extent of non-radiative quenching. High quantum yields (> 0.5 Φ) have been reported for Eu(III) and Tb(III) complexes, particularly with aromatic ketones as sensitising chromophores.[40, 41] In contrast to this, quantum yields of around 0.03 achieved for the NIR emission of Nd(III) have only been achieved in organic solvents.[42]

Since the 1970s the long lifetimes of the lanthanide excited states, particularly Eu(III), has prompted the development of time-resolved fluoroimmunoassays based on fluorescence resonance energy transfer (FRET).[43] In homogeneous assays an Eu(III) complex is used as an energy donor and is linked to a specific antibody while a suitable acceptor, such as a fluorescent protein, is linked to a second antibody. When both antibodies bind to an antigen, energy is transferred from the Eu(III) complex to the acceptor, causing protein fluorescence. As the Eu(III) excited state is long-lived, the lifetime of the protein fluorescence of the bound antibodies is much longer than that of unbound antibodies, allowing the two to be distinguished by time-gating.[44, 45]

The use of fluorescence microscopy is a valuable tool in life sciences. The high specificity of fluorescent stains makes it possible to study tissue and cell structure with a level of detail and resolution that is unavailable to traditional optical microscopy. The sample is typically irradiated from above, through a filter which selects the excitation wavelength of the fluorophore being used, this light then passes through a dichromatic mirror and the objective then onto the sample, this process of illumination from above is known as epi-illumination. The epi-fluorescence induced in the sample passes back through the objective, is reflected by the dichromatic mirror and passes through an emission filter to remove reflected light or unwanted fluorescence before reaching the detector.[24] Extremely high resolution and depth selection can be obtained by using confocal microscopy. In this technique the objective focuses the incident light onto a

point on the focal plane within the sample, however since the light passes through a cone-like shape of the sample out-of-plane fluorescence is also produced. Before reaching the detector, the epifluorescence is focused through a lens and a pin-hole aperture which is positioned at the focal point of the light beam, removing most out-of-plane fluorescence. By recording multiple points a two-dimensional cross section or a three-dimensional model of the sample may be produced.[24]

Fluorophores with small Stokes shifts may have a significant overlap between the absorption and the emission spectra. Using an emission filter with a cut-off point at short wavelength would allow light reflected from the sample to reach the detector, causing interference and a loss of contrast. Alternatively, a filter with a higher wavelength cut-off would only allow light from the long wavelength tail of the emission spectrum to reach the detector, reducing image intensity. These difficulties could be overcome using luminescent lanthanide complexes since the indirect sensitisation process required to populate Ln(III) emissive states results in large Stokes shifts, ranging from ~ 200 nm, in the case of visible sensitisation of Eu(III), to > 1000 nm, in the case of ultraviolet sensitisation of near-infrared emissive ions Nd(III), Er(III) and Yb(III).

A variation of emission profile in response to environmental factors is an important property in probes designed to measure the intracellular concentration of ions. When the presence of an external ion causes a simple increase or decrease in the intensity of emission, the concentration of that probe must be known in order to infer the concentration of the analyte. However, in cellular staining the local concentration of a probe may not be known, therefore the target ion must induce a ratiometric response in the probe.[24] This would allow the concentration of the ion to be calculated based on the ratio of the emission intensities at two wavelengths, which would be independent of the probe concentration. The hypersensitive bands of the lanthanide ions provide a means of producing a ratiometric response. For instance, if a target ion can induce a change in the coordination environment of Eu(III), the concentration of that ion could be calculated by comparing the intensity of the $J = 1$ ($\lambda \sim 590$ nm) peak to that of the $J = 2$ peak ($\lambda \sim 615$ nm). Another form of output that is independent

of probe concentration is the luminescence lifetime. Ln(III) complexes in which the degree of hydration is altered by the presence of a particular ion can be used as 'hydration switch' style probes, by monitoring the lifetime of the lanthanide luminescence using fluorescence lifetime imaging microscopy (FLIM).[24]

Epifluorescence and confocal microscopy experiments have demonstrated the potential for lanthanide complexes to act as cellular stains and biological probes. A study carried out by Parker and coworkers followed the uptake of several emissive Eu(III) and Tb(III) complexes based around a core cyclen structure.[46] The rate of uptake was studied in the presence of inhibitors and stimulators of different modes of endocytosis and co-localisation experiments with fluorescent probes with known uptake modes were carried out to observe the early localisation of lanthanide complexes within cells. The results indicated that the lanthanide complexes entered the cells *via* macropinocytosis. This is a form of endocytosis which is not receptor mediated, solute macromolecules are taken up in large vesicles, independently of charge or structure, and once inside the cell the contents of macropinosomes readily escape, allowing uptake by other organelles.[46]

Co-localisation studies indicate that the distribution of lanthanide complexes within cells is determined primarily by the nature of the sensitising chromophore and its mode of linkage to the macrocyclic ligand core rather than by complex charge, lipophilicity and the number and identity of other donor atoms.[47-49] Gadolinium complexes bearing an N-coordinated azathiaxanthone chromophore have been shown to reversibly bind to serum albumin and the corresponding europium complexes show a selective staining of the protein-rich nucleoli and ribosomes of cells and could be used to signal the intracellular concentration of citrate (Figure 1.4, A).[50, 51] The azathiaxanthone chromophore was later incorporated into a complex bearing a reversibly bound sulphonamide pendant arm to form a probe for intracellular pH (Figure 1.4, B).[49]

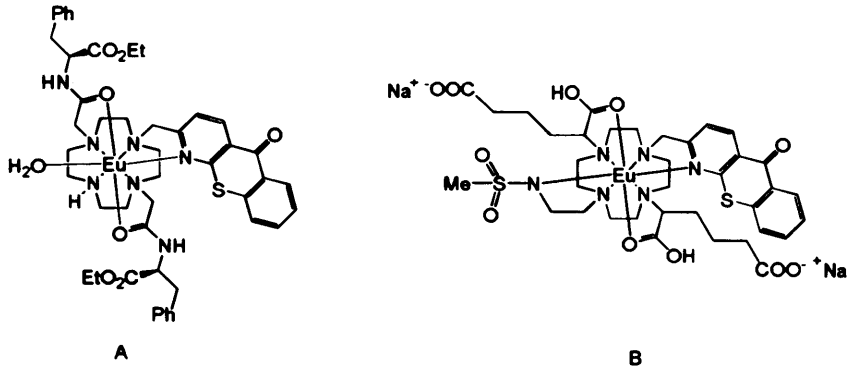

Figure 1.4 – Two complexes bearing azathiaxanthone chromophores.

A different localisation profile has been observed for several lanthanide complexes, typically those bearing ester-substituted azaxanthone-based chromophores.[48] These tend to transfer between endosomes/lysosomes and mitochondria, likely due to association with a particular carrier protein. The complexes that show slower egress from the mitochondria have a higher toxicity and induce apoptotic cell death.[52]

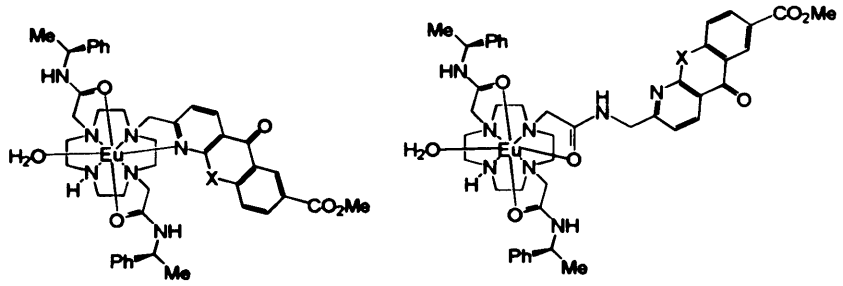

Figure 1.5 – Eu(III) complexes shown to localise in cell mitochondria.

The majority of complexes which have undergone fluorescence microscopy studies show a third type of distribution. They tend to localise in the late endosomes and lysosomes of cells. These complexes show fast uptake and egress by cells and have low toxicity.[52] In addition to the cyclen-based complexes developed by Parker and coworkers bimetallic helicates developed by Bünzli *et al.* show a similar distribution.[53-55]

In addition to the pH and citrate probes mentioned above, lanthanide complexes have been developed as ratiometric probes for the intracellular concentration of

various biorelevant anions, such as hydrogencarbonate.[47] Although the charge of a complex does not effect the distribution of a luminescent probe within cells it can alter the responsive properties, with cationic probes showing greater affinity for anions than neutral or negatively charged species. A Eu(III) complex developed by Nagano and coworkers has been shown capable of signalling changes in intracellular Zn(II).[56] However, the presence of Zn(II) increased the Eu(III) luminescence intensity but did not result in a ratiometric change in the emission profile.[56]

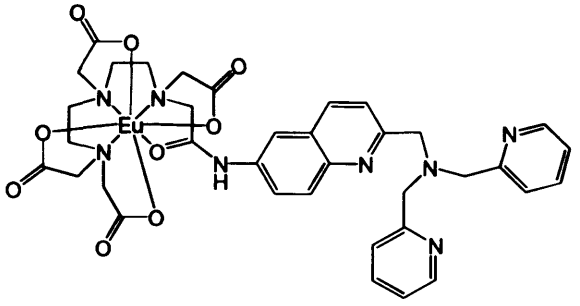

Figure 1.6 – Zn(II) sensor suitable for *in cellulo* use.

Biological chromophores, particularly haemoglobin, absorb strongly in the visible region, while the vibrational modes of water absorb strongly in the Mid IR. This leaves a 'window of transparency' in the NIR, between approximately 650 nm and 1300 nm.[57] Therefore, if the use of lanthanide probes is to be expanded to *in vivo* applications suitable Nd(III) and Yb(III) complexes must be developed. These would need to efficiently shield the ions from the surrounding solution, since the small energy gap between the excited and ground states make them vulnerable to quenching *via* non-radiative energy transfer to the vibrational modes of surrounding solvent molecules. Ideally, these probes could be administered in a quenched state and would be activated on contact with a specific molecule or ion, this would enable probe emission to be distinguished from that of background fluorophores. These developments, along with a comprehensive understanding of the light absorbing properties of tissues and technological increases in the sensitivity of detectors may enable luminescent lanthanide probes to play an important future role in diagnostic medicine. Recent advances in the field of NIR tomography have shown that quantum dots

can be used to map the lymph nodes in large animals[58] and indocyanine green can be used to image breast cancer in human patients.[59]

1.6 – Paramagnetism

The paramagnetism of the Ln(III) ions arises from the unpaired 4*f* electrons, which are found in all members of the series except La(III) and Lu(III). Their paramagnetism is generally determined by the ground state electron configuration, since in most cases the magnitude of spin-orbit coupling makes the excited states thermally inaccessible.[13] The high paramagnetism of the lanthanides has been used in the synthesis of magnetic contrast agents,[8] the development of strong magnets[3] and refrigeration, in which the removal of gadolinium and dysprosium salts from a magnetic field causes adiabatic demagnetisation, which results in cooling.

1.7 – Gd(III) complexes as MRI contrast agents

As the 4f orbitals are shielded from crystal field effects by the 5s and 5p orbitals the magnetic properties of lanthanide complexes are similar to those of Ln(III) aqua ions. This has lead to the application of Gd(III) complexes as contrast agents for magnetic resonance imaging (MRI).

In pulsed NMR an applied magnetic field along the z axis brings the net macroscopic magnetisation of proton spins into alignment, parallel to the field. This is then perturbed by radiofrequency pulses and the magnetisation relaxes back to alignment. Recovery of magnetisation along the z axis occurs with an exponential time component, T_1, and is known as longitudinal relaxation whereas the recovery of magnetisation perpendicular, T_2, is known as transverse relaxation. T_1 is typically on the order of a second whereas T_2 is on the order of milliseconds. The magnetisation recovery times are often expressed as the relaxation rates, $1/T_1$ and $1/T_2$, and the method of pulsing can be calibrated to emphasise differences in either rate. The image intensity of MRI can be

increased by increasing $1/T_1$ or decreasing $1/T_2$ and gadolinium contrast agents increase both longitudinal and transverse relaxation rates by the same amount, but since the percentage difference is greatest for $1/T_1$ these agents are used in conjunction with T_1-weighted scans.[8, 60]

It has been estimated that 40 – 50 % of MRI scans use contrast agent.[61] There is a range of gadolinium-based contrast agents currently approved for use in the EU and the USA, most of which are derivatives of DPTA or DOTA.[8] As discussed previously, these compounds have stability constants of logK > 20,[9] allowing them to be used at concentrations of approximately 0.1 mmol kg^{-1}.[13] Currently there is a great deal of interest in improving the relaxivity of gadolinium contrast agents in order to develop site-specific probes.[62]

The development of Gd(III)-based contrast agents requires slightly different structural restrictions than that of Ln(III)-based luminescent biological probes. The ability of a complex to increase the relaxation rates of surrounding solvent molecules, known as its *relaxivity*, is due to dipole-dipole interactions of the unpaired 4f electrons of the Gd(III) ion with the proton nuclei of surrounding water molecules. These interactions are characterised as either inner-sphere, in which the interactions are between water molecules that are bound directly to the metal (which are in exchange with the bulk solvent), or outer sphere interactions directly between the contrast agent and the surrounding solvent molecules. While the toxicity of Gd(III) complexes must be minimised by forming kinetically inert complexes with multidentate ligands, the metal should not be fully coordinated in order to allow inner-sphere interactions.

1.8 – Experimental

General physical measurements

All photophysical data were obtained on a JobinYvon-Horiba Fluorolog spectrometer fitted with a JY TBX picosecond photodetection module and a Hamamatsu R5509-73 detector (cooled to –80 °C using a C9940 housing). Luminescence lifetimes were obtained using either a flash lamp or a pulsed laser

source from a Continuum Minilite Nd:YAG configured for 355 nm output. Lifetimes were obtained using the JY-Horiba FluoroHub single photon counting module. IR spectra were recorded on a Varian 7000 FT-IR. LR Mass spectra were obtained using a Bruker MicroTOF LC. UV-vis data were recorded as solutions on a Jasco 570 spectrophotometer. Proton NMRD profiles were obtained using a Stelar Spinmaster FFC 200 fast field cycling NMR relaxometer.

1.9 - References

1. G. A. Molander, *Chem. Rev.*, 1992, **92**, 29-68.
2. M. Shibasaki and N. Yoshikawa, *Chem. Rev.*, 2002, **102**, 2187-2209.
3. D. Gatteschi and C. Benelli, *Chem. Rev.*, 2002, **102**, 2369-2387.
4. A. A. Kaminskii, *Phys. Stat. Sol.*, 2003, **200**, 215-296.
5. K. Wang, R. Li, C. Y and B. Zhu, *Coord. Chem. Rev.*, 1999, **190-192**, 297-308.
6. S. P. Fricker, *Chem. Soc. Rev.*, 2006, **35**, 524-533.
7. A. Beeby, S. W. Botchway, I. M. Clarkson, S. Faulkner, A. W. Parker, D. Parker and J. A. G. Williams, *J. Photochem. Photobiol. B*, 2000, **57**, 83-89.
8. P. Caravan, J. J. Ellison, T. J. McMurry and R. B. Lauffer, *Chem. Rev.*, 1999, **99**, 2293-2352.
9. S. Cotton, *Lanthanide and Actinide Chemistry*, John Wiley and Sons Ltd, Chichester, 2006.
10. L. Helmholz, *J. Am. Chem. Soc.*, 1939, **61**, 1544-1550.
11. G. W. Brady, *J. Chem. Phys.*, 1960, **33**, 1079-1082.
12. A. Clearfield, R. Gopal and R. W. Olsen, *Inorg. Chem.*, 1977, **16**, 911-915.
13. N. Kaltsoyannis and P. Scott, *The f Elements*, Oxford University Press, Oxford, 1999.
14. A. W. Adamson, *J. Am. Chem. Soc.*, 1954, **76**, 1578-1579.
15. C. A. Chang and M. E. Rowland, *Inorg. Chem.*, 1983, **22**, 3866-3869.
16. A. D. Sherry, W. P. Cacheris and S. K. Nickle, *Inorg. Chem.*, 1987, **26**, 958-960.
17. D. K. Cabbiness and D. W. Margerum, *J. Am. Chem. Soc.*, 1969, **91**, 6540-6541.
18. P. Paoletti, A. Sabatini and M. Micheloni, *J. Chem. Soc.Dalton Trans.*, 1983, 1189-1191.
19. A. Dadabhoy, S. Faulkner and P. G. Sammes, *J. Chem. Soc. Perkin Trans. 2*, 2002, 348-357.
20. D. G. Karraker, *Inorg. Chem.*, 1968, **7**, 473-479.
21. S. I. Weissman, *J. Chem. Phys.*, 1942, **10**, 214-217.
22. G. A. Crosby, R. M. Alire and R. E. Whan, *J. Chem. Phys.*, 1961, **34**, 743-&.
23. M. Klessinger and J. Michl, *Excited States and Photochemistry of Organic Molecules*, VCH Publishers, Inc., New York, 1995.
24. J. R. Lakowicz, *Principles of Fluorescence Spectroscopy*, Third Edition edn., Springer Science, New York, 2006.
25. M. Kleinerman, *J. Chem. Phys.*, 1969, **51**, 2370-2381.
26. V. Vicinelli, P. Ceroni, M. Maestri, V. Balzani, M. Gorka and F. Vogtle, *J. Am. Chem. Soc.*, 2002, **124**, 6461-6468.
27. G. A. Hebbink, S. I. Klink, L. Grave, P. Alink and F. van Veggel, *Chem. Phys. Chem.*, 2002, **3**, 1014-1018.
28. C. Yang, L. M. Fu, Y. Wang, J. P. Zhang, W. T. Wong, X. C. Ai, Y. F. Qiao, B. S. Zou and L. L. Gui, *Angew. Chem. Int. Ed. Engl.*, 2004, **43**, 5010-5013.
29. M. D. Ward, *Coord. Chem. Rev.*, 2007, **251**, 1663-1677.
30. P. J. Breen, E. K. Hild and W. D. Horrocks, *Biochem.*, 1985, **24**, 4991-4997.
31. W. D. Horrocks, J. P. Bolender, W. D. Smith and R. M. Supkowski, *J. Am. Chem. Soc.*, 1997, **119**, 5972-5973.

32. A. F. Kirby, D. Foster and F. S. Richardson, *Chem. Phys. Lett.*, 1983, **95**, 507-512.
33. J. L. Kropp and M. W. Windsow, *The J. Chem. Phys.*, 1965, **42**, 1599-1607.
34. Y. X. Zheng, M. Motevalli, R. H. C. Tan, I. Abrahams, W. P. Gillin and P. B. Wyatt, *Polyhedron*, 2008, **27**, 1503-1510.
35. W. D. Horrocks and D. R. Sudnick, *J. Am. Chem. Soc.*, 1979, **101**, 334-340.
36. A. Beeby, I. M. Clarkson, R. S. Dickins, S. Faulkner, D. Parker, L. Royle, A. S. de Sousa, J. A. G. Williams and M. Woods, *J. Chem. Soc. Perkin Trans. 2*, 1999, 493-503.
37. S. Faulkner, A. Beeby, M. C. Carrie, A. Dadabhoy, A. M. Kenwright and P. G. Sammes, *Inorg. Chem. Comm.*, 2001, **4**, 187-190.
38. T. Yogo, Y. Urano, Y. Ishitsuka, F. Maniwa and T. Nagano, *J. Am. Chem. Soc.*, 2005, **127**, 12162-12163.
39. M. Latva, H. Takalo, V. M. Mukkala, C. Matachescu, J. C. RodriguezUbis and J. Kankare, *J. Lum.*, 1997, **75**, 149-169.
40. A. Beeby, L. M. Bushby, D. Maffeo and J. A. G. Williams, *J. Chem. Soc.-Perkin Trans. 2*, 2000, 1281-1283.
41. J. C. Rodriguez-Ubis, M. T. Alonso, O. Juanes, R. Sedano and E. Brunet, *J. Lum.*, 1998, **79**, 121-125.
42. Y. Hasegawa, T. Ohkubo, K. Sogabe, Y. Kawamura, Y. Wada, N. Nakashima and S. Yanagida, *Angew.Chem. Int. Ed.*, 2000, **39**, 357-+.
43. E. Soini and I. Hemmila, *Clin. Chem.*, 1979, **25**, 353-361.
44. G. Mathis, *Clin. Chem.*, 1995, **41**, 1391-1397.
45. M. Gabourdes, V. Bourgine, G. Mathis, H. Bazin and W. Alpha-Bazin, *Anal. Biochem.*, 2004, **333**, 105-113.
46. E. J. New and D. Parker, *Org. Biomol. Chem.*, 2009, **7**, 851-855.
47. Y. Bretonniere, M. J. Cann, D. Parker and R. Slater, *Org. Biomol. Chem.*, 2004, **2**, 1624-1632.
48. B. S. Murray, E. J. New, R. Pal and D. Parker, *Org. Biomol. Chem.*, 2008, **6**, 2085-2094.
49. R. Pal and D. Parker, *Org. & Biomol. Chem.*, 2008, **6**, 1020-1033.
50. J. H. Yu, D. Parker, R. Pal, R. A. Poole and M. J. Cann, *J. Am. Chem. Soc.*, 2006, **128**, 2294-2299.
51. D. Parker and J. H. Yu, *Chem. Comm.*, 2005, 3141-3143.
52. C. P. Montgomery, B. S. Murray, E. J. New, R. Pal and D. Parker, *Acc. Chem. Res.*, 2009, **42**, 925-937.
53. E. Deiters, B. Song, A. S. Chauvin, C. D. B. Vandevyver, F. Gumy and J. C. G. Bunzli, *Chem. Eur. J.*, 2009, **15**, 885-900.
54. A. S. Chauvin, S. Comby, B. Song, C. D. B. Vandevyver and J. C. G. Bunzli, *Chem. Eur. J.*, 2008, **14**, 1726-1739.
55. N. Dalla-Favera, J. Hamacek, M. Borkovec, D. Jeannerat, F. Gumy, J. C. G. Bunzli, G. Ercolani and C. Piguet, *Chem. Eur. J.*, 2008, **14**, 2994-3005.
56. K. Hanaoka, K. Kikuchi, H. Kojima, Y. Urano and T. Nagano, *J. Am. Chem. Soc.*, 2004, **126**, 12470-12476.
57. R. Weissleder, *Nature Biotechnol.*, 2001, **19**, 316-317.
58. S. Kim, Y. T. Lim, E. G. Soltesz, A. M. De Grand, J. Lee, A. Nakayama, J. A. Parker, T. Mihaljevic, R. G. Laurence, D. M. Dor, L. H. Cohn, M. G. Bawendi and J. V. Frangioni, *Nature Biotechnol.*, 2004, **22**, 93-97.
59. V. Ntziachristos, A. G. Yodh, M. Schnall and B. Chance, *Proc. Nat. Acad. Sci. USA*, 2000, **97**, 2767-2772.

60. R. B. Lauffer, *Chem. Rev.*, 1987, **87**, 901-927.
61. K. N. Raymond and V. C. Pierre, *Bioconj. Chem.*, 2005, **16**, 3-8.
62. S. Aime, C. Cabella, S. Colombatto, S. G. Crich, E. Gianolio and F. Maggioni, *J. Magn. Res. Imag.*, 2002, **16**, 394-406.

Chapter Two

Quinoxaline as a sensitizer for lanthanide luminescence

2.1 - Introduction

Quinoxaline is a bicyclic heterocycle, isoelectronic with naphthalene, which features nitrogen atoms at the 1- and 4- positions (Figure 2.1). The quinoxaline unit has been incorporated into systems with a wide variety of applications. In biomedicinal chemistry it is present in antitumor and antiviral drugs which induce autophagy in cancer cells[1] and has been used as a fluorescent tag to probe polypeptide structure and stability in which the presence of quinoxaline resulted in a marked increase in the intensity of the fluorescence at 363 nm.[2] The electron donating properties of the nitrogen atoms have been exploited in ligands to study redox processes in rhenium(I) complexes[3] and are responsible for conformational switching in a series of cavitands and velcrands.[4] It has been incorporated into polymers for use as high-stability thermoplastics[5] and electron-transport materials in electroluminescent devices (OLEDs).[6] The aim of this chapter is to develop a new ligand system incorporating a quinoxaline unit as a chromophore to sensitise visible and NIR emission.

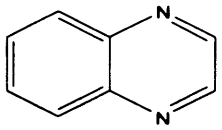

Figure 2.1 – Quinoxaline.

The individual quinoxaline unit has absorption maxima at 234 and 314 nm with a tail extending to around 350 nm. However, the utility of quinoxaline extends beyond its absorption characteristics, the incorporation of nitrogen atoms into the aromatic system may allow direct coordination -and therefore more efficient energy transfer- to the lanthanide. Heterocyclic chromophores such as this include terpyridine,[7] azathiaxanthone,[8] hydralazine-derived systems,[9] pyrazoyl-1-azaxanthone[10] and, most significantly, a series of quinolines (Figure 2.2, A-E respectively), [11] closely related to quinoxaline. In work by Nagano and co-workers these were found to coordinate to europium and allowed sensitisation with wavelengths of over 300 nm.

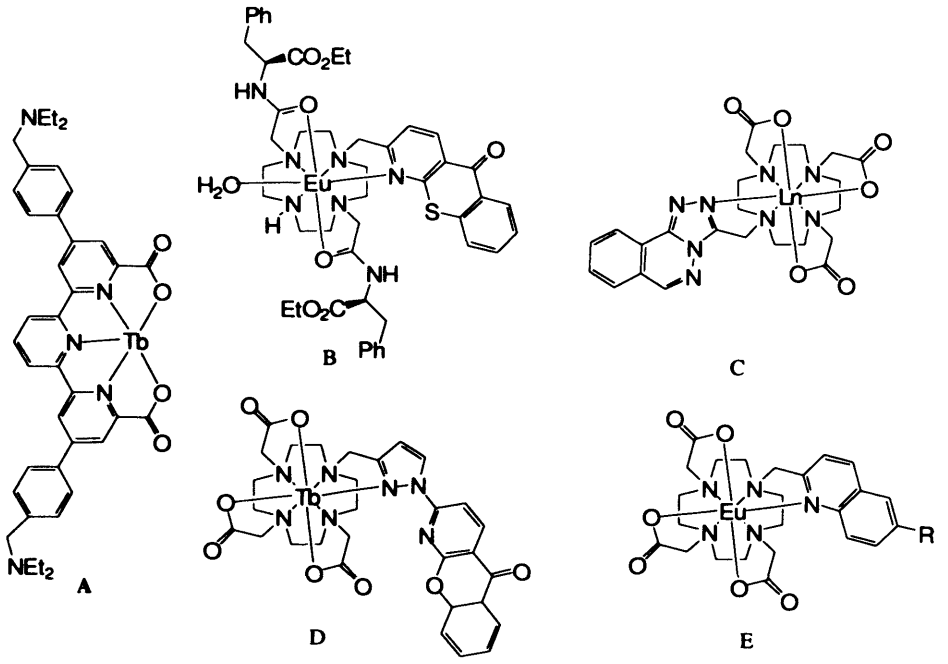

Figure 2.2 – Various examples of nitrogen-containing heterocycles as lanthanide sensitisers.

The direct binding of nitrogen to the lanthanide ion has other benefits when designing luminescent probes. As hard Lewis acids lanthanides are not ideally suited to coordination by nitrogen donors, particularly aryl nitrogen atoms. This means that in the presence of an external stimulus they may dissociate from the lanthanide ion and change the coordination sphere and degree of solvation. Although a study by Parker[12] found that the intramolecular ligation of pyridine to Gd(III) and Eu(III) is independent of pH in the range of 2.5 – 12.5 a 'hydration switch' style pH probe was later developed which was based on reversible binding by a phenylsulfonamide (Figure 2.3, A).[13] The use of coordinating, nitrogen-containing chromophores in the hydration switch response mode has also been utilised in probes for other analytes, such as the Pope Zn(II) sensor (Figure 2.3 B).[14]

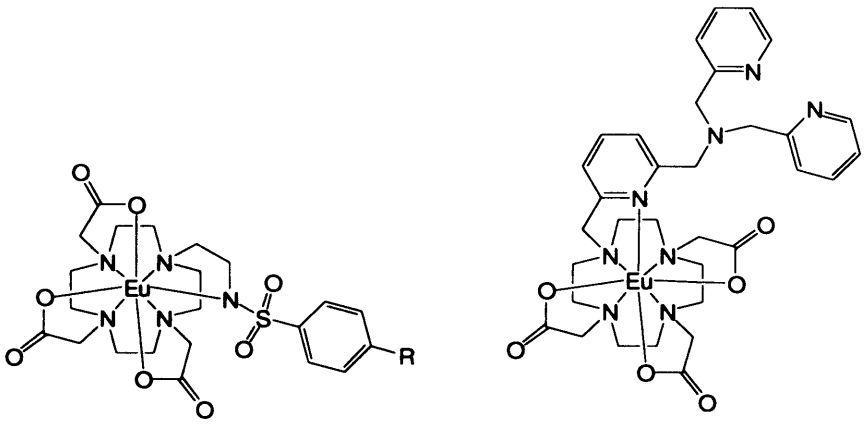

Figure 2.3 – 'Hydration switch' sensors.

When incorporated into a sensitising chromophore the ability of nitrogen to act as an electron donor can form the basis of an alternative mode of response. Systems in which quinolyl amides are bound to the lanthanide *via* an amide group in the *meta* or *para* position to the aryl nitrogen can act as pH sensors by the protonation-dependant alteration of the chromophore energy level (Figure 2.4, A).[15, 16] Other systems which rely on nitrogen protonation to alter the energy level of the chromophore, and thus the degree of energy transfer to the lanthanide, include phenthridinyl amides (Figure 2.4 B)[17] and phenanthroline(Figure 2.4 C).[18]

It was later found that the phenanthroline-based system developed by Gunnlaugsson and co-workers could also respond to the presence of Cu(II) by the formation of tetranuclear complexes in solution, in which the two *phen* nitrogen atoms in three europium complexes coordinate with a single copper cation.[19] In this case the singlet excited state of the *phen* group is quenched by electron transfer to Cu(II), preventing energy transfer to, and subsequent luminescence from, the lanthanide ion. The alteration of energy levels was also utilised in a Zn(II) responsive system developed by Nagano (Figure 2.4, D), in which coordination of zinc reduces the energy level of the quinoline triplet state, increasing the efficiency of energy transfer to europium and hence the intensity of the europium emission.[20]

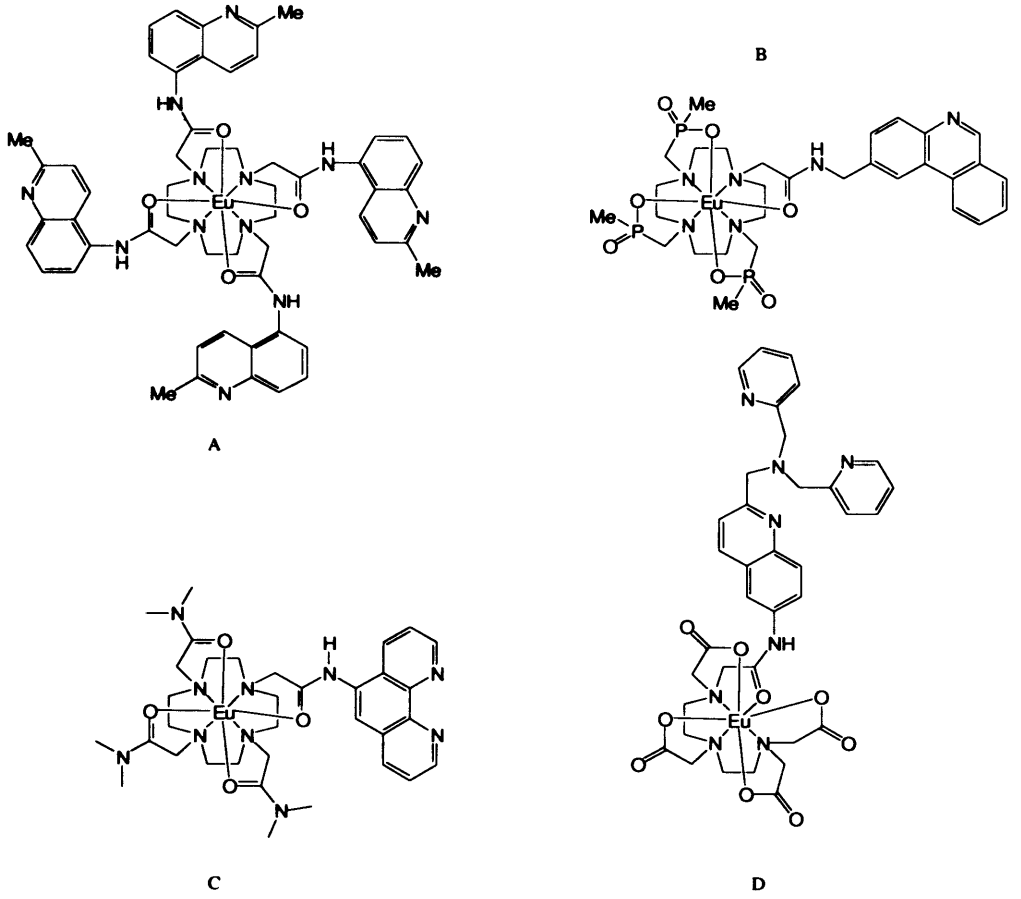

Figure 2.4 – Several 'energy level' switches.

In a system based around a tetraza-macrocycle that incorporates quinoxaline it is likely that the lanthanide could coordinate to the quinoxaline *via* one of the aryl nitrogen atoms, as seen in the system developed by Nagano,[11] but since the two nitrogen atoms are *para*- to each other coordination to both would be prohibited.

The aim of this work was to incorporate quinoxaline into a cyclic ligand suitable for forming complexes with Ln(III) ions and to examine the potential for the these ligands to respond to species in its environment

2.2 - Results and Discussion

2.2.1 – Viability of quinoxaline as a sensitising chromophore

It has been shown by Faulkner and co-workers that the viability of a potential chromophore to sensitise lanthanide emission may be explored by solution state self-assembly.[21] An aromatic carboxylic acid is added to a solution of a lanthanide complex with the heptadentate ligand and a ternary species is formed in which excitation of the chromophore can result in energy transfer to, and subsequent emission from, the lanthanide ion. A solution of Nd-DO3A, a complex with no organic chromophore and a hydration state of 2,[22] was irradiated with laser light at 355 nm, at which wavelength neodymium has no absorption band. As expected no NIR emission was observed. 2-quinoxalinecarboxylic acid was then synthesised according to a modified literature procedure[23] and added to the solution of the coordinatively unsaturated metal complex (Figure 2.5) and laser excitation now resulted in characteristic neodymium NIR emission at 1058 nm, arising from the $^4F_{3/2} \rightarrow {}^4I_{11/2}$ transition. This indicated that ligand systems involving quinoxaline may sensitise lanthanide emission. In the self-assembly studies the binding mode of the quinoxaline is through the carboxylate group, which is conjugated with the delocalised π-system, whereas a single ligand system would rely on binding *via* one of the aryl nitrogen atoms. Both binding modes would involve electronic interaction between the chromophore and the lanthanide ion, enabling energy transfer to occur by the Dexter exchange mechanism. However, previous work by Faulkner and co-workers[24] has indicated that sensitisation of lanthanide luminescence can occur without direct binding of the chromophore, therefore Förster energy transfer cannot be ruled out.

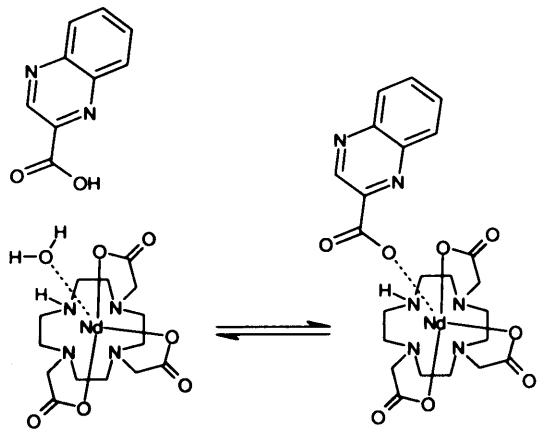

Figure 2.5 - Formation of self-assembly complex.

2.2.2 - Synthesis and characterisation of ligand and complexes

The initial synthetic methodology to incorporate quinoxaline into a system capable of chelating lanthanide ions involved coupling commercially available 2,3-bis(bromomethyl)-quinoxaline with two 1,4,7-functionalised tetraaza macrocycles. This would be similar to a zinc complex reported by Bencini *et al*[25] in which quinoxaline acted as a spacer between two 1,4,7-triazacyclononane rings. A 2:1 molar ratio of the starting materials was dissolved in acetonitrile in the presence of two equivalents of base (sodium hydrogen carbonate) and a catalytic amount of potassium iodide and the mixture was heated to reflux for two days, after which time TLC indicated that the quinoxaline starting material had been consumed. The crude reaction mix was separated by column chromatography and a large amount (~ 1 equivalent) of the macrocyclic starting material was recovered along with a small amount of a compound containing both the macrocycle and the chromophore. ^{1}H NMR indicated that the quinoxaline was symmetrical but that the ratio of macrocycle to quinoxaline was 1:1, suggesting that a quaternary nitrogen species had been formed (figure 2.6). This was confirmed by mass spectrometry. It is likely that the short distance between the bromomethyl groups and the steric bulk of the boc-protected macrocycle prevented the formation of the desired product.

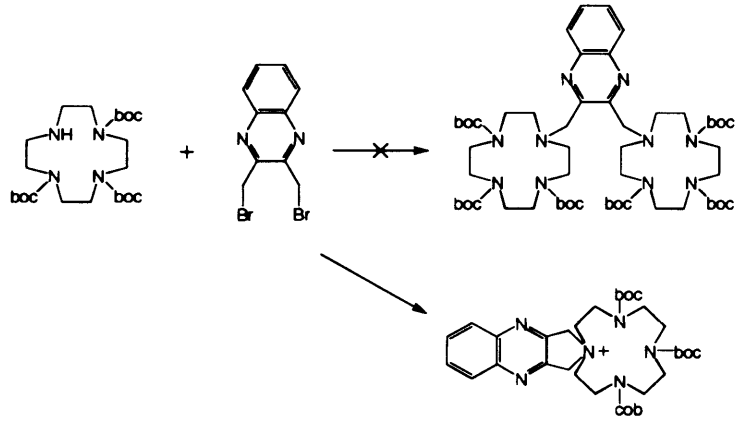

Figure 2.6 – Attemped synthesis of quinoxaline-bridged bis-macrocycle.

In light of this, 2-bromomethylquinoxaline was prepared according to a modified literature precedent,[26] reacting 2-methylquinoxaline with *N*-bromosuccinimide in CCl_4, but using benzoyl peroxide as the radical initiator. After several hours at reflux the reaction resulted in a statistical mixture of unreacted quinoxaline starting material and the desired product, as

well as the bisbromo- and trisbromo-substituted methylquinoxaline (Figure 2.7).

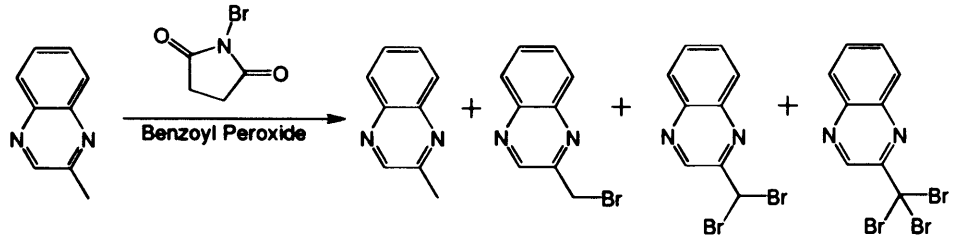

Figure 2.7 – Reaction of 2-methylquinoxaline with *N*-bromosuccinimide.

Column chromatography afforded the pure 2-bromomethylquinoxaline which was then coupled with 1,4,7-tris(*tert*-butoxycarbonylmethyl)-1,4,7,10-tetraazacyclododecane. The *tert*-butoxy-esters could then be cleaved to form 1,4,7-tris(carboxymethyl)-10-(methylquinoxaline)-1,4,7,10-tetraazacyclododecane, which would be a suitable chelating unit for lanthanide ions. However, after the ester deprotection step (CF_3CO_2H, CH_2Cl_2) ^1H NMR and mass spectrometry indicated that the aromatic moiety had been cleaved from the macrocycle. Although there are alternative routes to the DO3A unit which do not require an acidic deprotection step, for example *via* 1,4,7-tris(ethoxycarbonylmethyl)-1,4,7,10-tetraazacyclododecane, a diethylamido functionalised macrocycle (**1**) was considered to be the more favourable alternative. An amide-functionalised macrocycle would result in a lanthanide/chelate unit with a total charge of 3+ (Figure 2.8), which would cause electrostatic repulsion of cations and prevent quenching by external metal ions. The presence of the ethyl groups would result in an amphiphilic complex with the potential to dissolve in water as well as penetrate cell membranes in future applied studies.

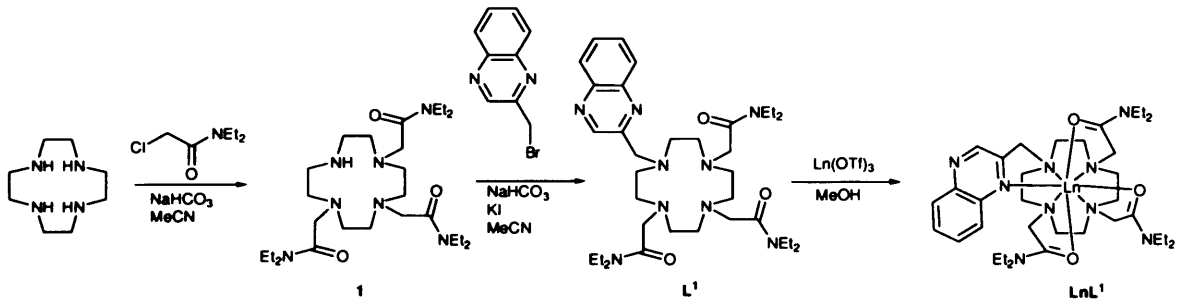

Figure 2.8 - Synthetic approach to LnL1

Mass spectrometry indicated that the ligand had been synthesised as a sodium complex with a chloride counter-ion, *m/z* = 654. The IR spectrum showed the amide carbonyl stretching frequency at 1703 cm^{-1}. Single crystals of the ligand suitable for x-ray diffraction were

grown from a concentrated toluene solution at -20 °C. Parameters associated with data collection are presented in table 2.2 bond length and angles are presented in table 2.3. Structural studies confirmed the proposed binding mode with the ligand coordinating to a sodium ion *via* the four macrocyclic nitrogen atoms, the three amide oxygen atoms and the proximate quinoxaline nitrogen (Figure 2.9). The charge is balanced by the I_3^- counterion. Previous work by Pope *et al*[14] indicates that coordination mode of sodium ions in functionalised tetraazamacrocyclic ligands is comparable to the coordination mode adopted by lanthanide ions. IR spectra of the complexes showed a low energy shift of the carbonyl stretching frequency of *ca.* 100 cm^{-1} indicative of the weakening of these bonds on coordination of the oxygen to the lanthanide ion. Mass spectra of each the complexes showed monocationic species corresponding to the loss of a single counter-ion (Table 2.1). Expected isotopic patterns for the lanthanide complexes were calculated and comparison with the observed data showed an extremely close correlation.

Complex	Ion Peak Observed (*m/z*)	Corresponding Species
NdL1	1095	$\{M\text{-}OTf\}^+$
EuL1	1104	$\{M\text{-}OTf\}^+$
GdL1	1109	$\{M\text{-}OTf\}^+$
TbL1	1110	$\{M\text{-}OTf\}^+$
YbL1	1013	$\{M\}^+$
	991	$\{M\text{-}NO_3\text{+}MeCN\}^+$
	951	$\{M\text{-}NO_3\}^+$

Table 2.1 – MS data for LnL1.

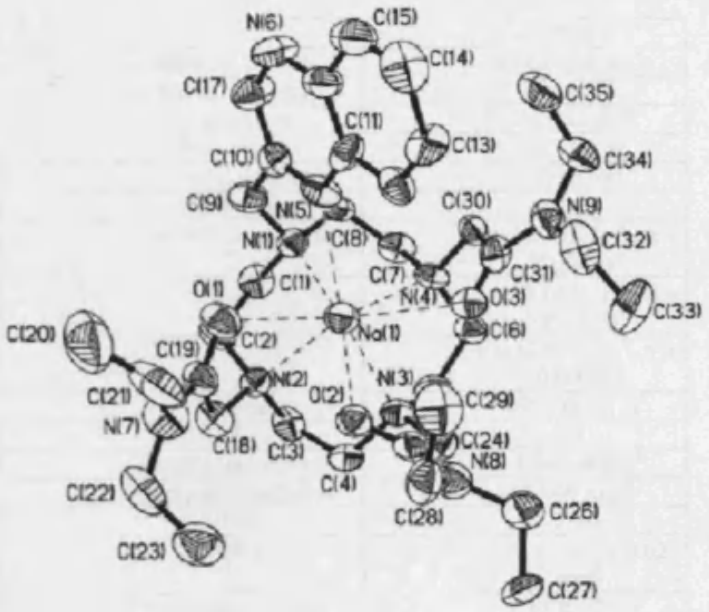

Figure 2.9 - Structural representation of NaL1 (counter ion and solvent of crystallisation omitted for clarity).

	NaL1
Empirical formula	$C_{42}H_{67}I_3N_9NaO_3$
Formula weight	1149.74
Temperature	150(2)K
Wavelength	0.71073Å
Crystal system	Triclinic
Space group	P-1
Unit cell dimensions	a = 12.562(3) Å, α = 99.34(3)°
	b = 18.648(4) Å, β = 103.65(3)°
	c = 22.955(5) Å, γ = 103.09(3)°
Volume	4955.6(17) $Å^3$
Z	4
Density (calculated)	1.541 Mg/m^3
Absorption coefficient	1.946 mm^{-1}
F(000)	2304
Crystal size	0.35 × 0.03 × 0.02 mm^3
Theta range for data collection	1.15 to 27.08°
Reflections collected	20579
Independent reflections	20579 [R(int) = 0.0000]
Completeness to theta = 27.08°	94.4 %
Absorption correction	Multi-scan
Max. and min. transmission	0.9621 and 0.5492
Refinement method	Full-matrix least squares on F
Goodness-of-fit on F	0.950
Final R indices [I > 2sigma(I)]	R1 = 0.0839, wR2 = 0.2065
R indices (all data)	R1 = 0.2597, wR2 = 0.3138

Table 2.2 - Crystal data collection and refinement details for the crystal structure of NaL1

The structure was refined on F_O^2 using all data.

Bond lengths (Å)			
Na(1)-O(1)	2.551(12)	Na(2)-O(4)	2.543(11)
Na(1)-O(2)	2.421(11)	Na(2)-O(5)	2.406(11)
Na(1)-N(1)	2.564(13)	Na(2)-O(6)	2.542(11)
Na(1)-N(2)	2.585(13)	Na(2)-N(10)	2.599(13)
Na(1)-N(3)	2.583(13)	Na(2)-N(11)	2.595(12)
Na(1)-O(3)	2.617(11)	Na(2)-N(12)	2.635(11)
Na(1)-N(4)	2.663(13)	Na(2)-N(13)	2.552(12)
Na(1)-N(5)	2.659(13)	Na(2)-N(14)	2.692(12)
Na(1)-C(25)	3.084(17)	Na(2)-C(66)	3.071(15)
I(1)-I(2)	2.901(2)	I(4)-I(5)	2.923(2)
I(1)-I(3)	2.929(2)	I(4)-I(6)	2.935(2)
Bond angles (°)			
O(2)-Na(1)-O(1)	81.3(4)	O(5)-Na(2)-O(6)	81.1(3)
O(2)-Na(1)-N(1)	157.3(4)	O(5)-Na(2)-O(4)	79.0(3)
O(1)-Na(1)-N(1)	85.4(4)	O(6)-Na(2)-O(4)	133.6(4)
O(2)-Na(1)-N(3)	65.5(4)	O(5)-Na(2)-N(13)	84.5(3)
O(1)-Na(1)-N(3)	125.2(4)	O(6)-Na(2)-N(13)	64.5(3)
N(1)-Na(1)-N(3)	108.9(4)	O(4)-Na(2)-N(13)	151.9(4)
O(2)-Na(1)-N(2)	85.3(4)	O(5)-Na(2)-N(11)	123.7(4)
O(1)-Na(1)-N(2)	64.3(4)	O(6)-Na(2)-N(11)	154.5(4)
N(1)-Na(1)-N(2)	72.4(4)	O(4)-Na(2)-N(11)	63.9(4)
N(3)-Na(1)-N(2)	70.4(4)	N(13)-Na(2)-N(11)	108.9(4)
O(2)-Na(1)-O(3)	79.4(4)	O(5)-Na(2)-N(10)	156.2(4)
O(1)-Na(1)-O(3)	136.9(4)	O(6)-Na(2)-N(10)	84.8(4)
N(1)-Na(1)-O(3)	122.3(4)	O(4)-Na(2)-N(10)	124.2(4)
N(3)-Na(1)-O(3)	79.8(4)	N(13)-Na(2)-N(10)	72.0(3)
N(2)-Na(1)-O(3)	150.0(4)	N(11)-Na(2)-N(10)	69.9(4)
O(2)-Na(1)-N(5)	127.6(4)	O(5)-Na(2)-N(12)	65.2(3)
O(1)-Na(1)-N(5)	75.6(4)	O(6)-Na(2)-N(12)	124.9(3)
N(1)-Na(1)-N(5)	65.5(4)	O(4)-Na(2)-N(12)	82.7(4)
N(3)-Na(1)-N(5)	158.9(4)	N(13)-Na(2)-N(12)	69.8(4)
N(2)-Na(1)-N(5)	123.1(4)	N(11)-Na(2)-N(12)	69.3(3)
O(3)-Na(1)-N(5)	86.4(4)	N(10)-Na(2)-N(12)	108.9(4)
O(2)-Na(1)-N(4)	123.5(4)	O(5)-Na(2)-N(14)	127.0(4)
O(1)-Na(1)-N(4)	154.6(4)	O(6)-Na(2)-N(14)	74.2(3)
N(1)-Na(1)-N(4)	69.5(4)	O(4)-Na(2)-N(14)	85.3(4)
N(3)-Na(1)-N(4)	69.0(4)	N(13)-Na(2)-N(14)	122.6(4)
N(2)-Na(1)-N(4)	109.0(4)	N(11)-Na(2)-N(14)	91.8(4)
O(3)-Na(1)-N(4)	61.1(3)	N(10)-Na(2)-N(14)	66.1(4)
N(5)-Na(1)-N(4)	90.4(4)	N(12)-Na(2)-N(14)	160.7(4)
I(2)-I(1)-I(3)	177.93(5)	I(5)-I4)-I(6)	178.82(5)

Table 2.3 - Selected bond lengths and angles for NaL1.

2.2.3 - Photophysical Studies

The UV/Vis absorption spectrum of the ligand showed a π-π^* transition at 294 nm and a π-π^* or n-π^* transition at 357 nm. Following irradiation of the low energy band absorption band, a broad, structureless fluorescence was observed with a maximum at 415 nm, due to the aerated nature of the solution this was probably due to a singlet excited state. The

absorption spectra of the lanthanide complexes showed a single transition which is red-shifted with respect to the free ligand, potentially indicating the coordination between the quinoxaline and the lanthanide ion. In order to study the ligand-based excited-state energy levels in a lanthanide complex the luminescence spectrum of **GdL1** in an optical glass was measured at 77 K, since the lowest gadolinium excited state energy level ($^6P_{7/2}$) is approximately 32000 cm^{-1} it cannot accept any energy from long-wavelength chromophores.[27] Therefore the structured emission band which was observed in the phosphorescence spectrum was assigned to the ligand $^3\pi\pi^*$ state (Figure 2.10). The band had a peak separation of approximately 1400 cm^{-1}, consistent with aromatic C-C vibrational modes. From the 0-0 transition it was calculated that the energy of the triplet level was *ca.* 22000 cm^{-1}. The europium $^5D_1$ and $^5D_0$ levels lie at 19020 and 17250 cm^{-1} respectively,[27] thus the energy gap between the emitting level of the chromophore and the absorption band of the lanthanide ion is suitably small to allow energy transfer but large enough to prevent back-transfer.

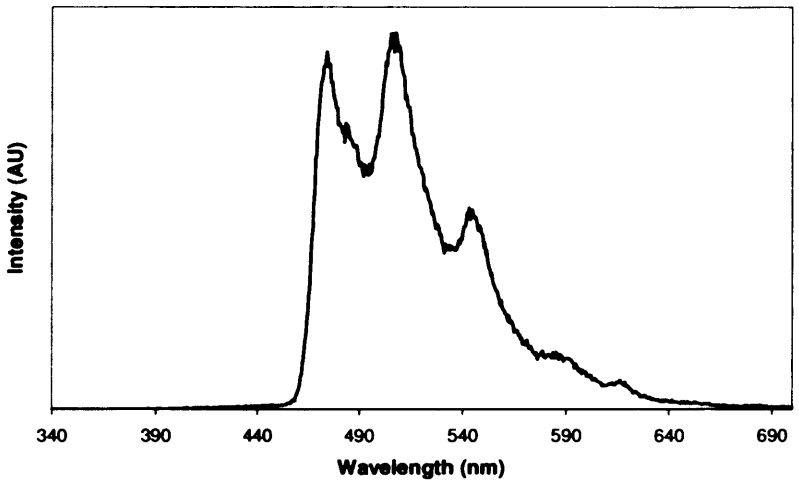

Figure 2.10 - Structured emission from ligand $^3\pi\pi^*$ state.

Each of the complexes gave emission spectra characteristic of the coordinated lanthanide ion and the excitation spectrum of the J = 2 peak of Eu^{III} (615 nm) coincided well with the absorption spectra of the complexes (Figure 2.11), with the two maxima at *ca.* 310-330 nm, confirming that irradiation of the quinoxaline chromophore can sensitise lanthanide emission.

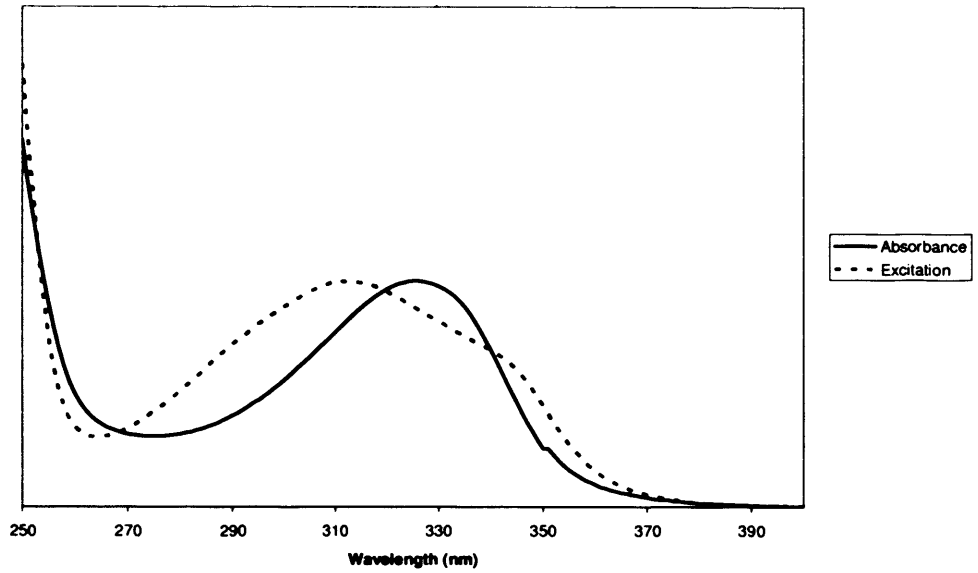

Figure 2.11 – **EuL1** excitation spectrum superimposed upon the absorbance spectrum.

Following indirect excitation (320 nm) of **EuL1** two sets of peaks were observed. A relatively weak set of peaks were observed on the high-wavelength tail of the ligand emission at 525, 535 and 555 nm. These were assigned to the $^5D_1 \rightarrow {}^7F_0$, $^7F_1$ and $^7F_2$ transitions,[28] further $^5D_1 \rightarrow {}^7F_J$ transitions were not observable since they coincide with the much stronger $^5D_0 \rightarrow {}^7F_J$ transitions. Emission from the $^5D_0$ state was well-resolved, allowing the $J = 0$ (579 nm), $J = 1$ (592 nm), $J = 2$ (616 nm), $J = 3$ (651 nm) and $J = 4$ (688 and 699 nm) transitions to be distinguished without the need to time-gate the emission (Figure 2.12). The **TbL1** spectrum showed two bands at 546 nm and 587 nm arising from transitions from the $^5D_4$ state to the $^7F_5$ and $^7F_4$ ground states, respectively (Figure 2.13). The $J = 6$ transition is known to give rise to a band at approximately 490 nm, however in this case the intensity of the ligand luminescence prevented this peak from being observed. The relative intensity of the ligand fluorescence compared to the lanthanide emission implies that energy transfer to Tb^{III} is probably much less efficient than the energy transfer to Eu^{III}. Since the lowest energy resonance level of terbium lies at 20430 cm^{-1} it is likely that radiative decay of this state is competitive against back transfer to the quinoxaline triplet state.[27]

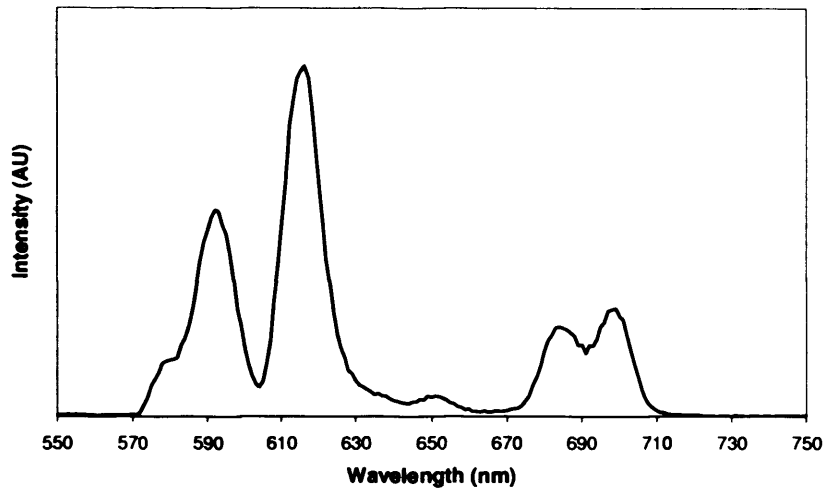

Figure 2.12 - Emission spectrum of **EuL1**.

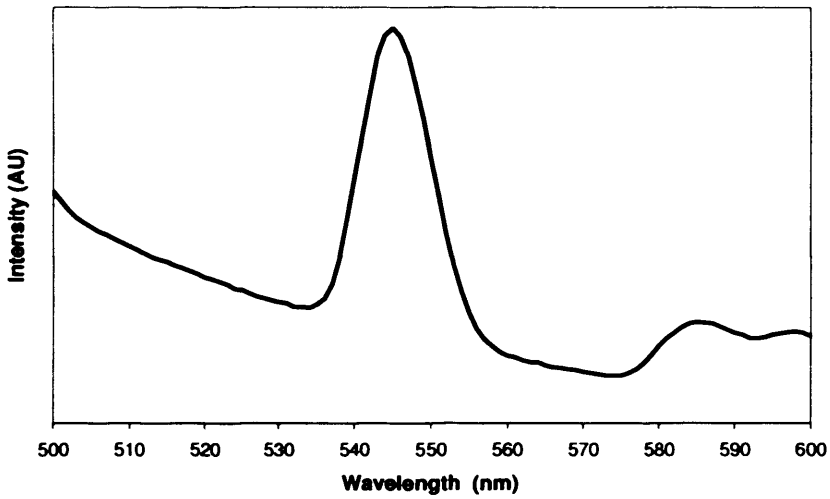

Figure 2.13 - Emission spectrum of **TbL1**.

Following laser excitation at 355 nm the two near-IR emitting species, **NdL1** and **YbL1**, gave characteristic steady-state spectra. The Nd^{III} spectrum was dominated by the $^4F_{3/2} \rightarrow {}^4I_{11/2}$ transition, with a peak at 1058 nm, shorter wavelength bands arising from the $^4F_{3/2} \rightarrow {}^4I_{9/2}$ transition were not observed due to filtering. The steady-state emission spectrum of the Yb^{III} complex showed the $^2F_{5/2} \rightarrow {}^2F_{7/2}$ transition with a peak 972 nm and a broad, lower energy shoulder indicative of ligand field induced splitting of the $^2F_{7/2}$ manifold (Figure 2.14).

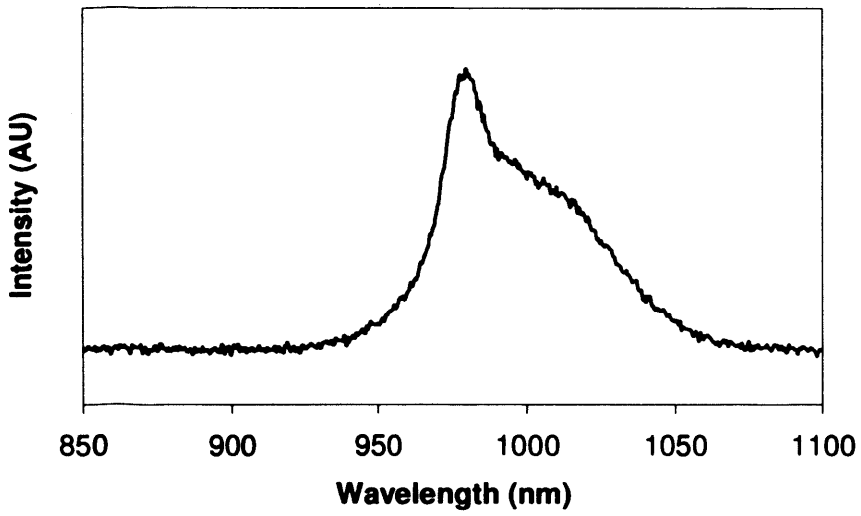

Figure 2.14 - Emission spectrum of **YbL1**.

λ_{ex} = 355 nm.

Luminescence lifetimes were obtained for each of the lanthanide complexes in deuterated and non-deuterated solvents, and are summarised in Table 2.4. The europium complex was excited with a wavelength of 355 nm (indirect excitation) and 395 nm (direct excitation) and in both cases the resulting luminescence lifetime of the peak at 615 nm fit a single exponential decay, indicating the presence of only one emissive species. The lifetime of the europium complex was 1250 μs in D_2O and 551 μs in H_2O. These lifetime measurements were applied to the modified versions of Horrocks equation (Equation 5 and Equation 6)[29, 30] which take into account the quenching effect of outer sphere solvent molecules and quenching by C-H and N-H oscillations, in order to determine the degree of inner sphere solvation; q, values of A and B are metal-specific and shown in Table 2.4 For the europium complex this resulted in q = 0.9, which corresponds to an eight coordinate ligand with one inner sphere solvent molecule.

$$q = A(\tau_H^{-1} - \tau_D^{-1} - B)$$

Equation 5 – Modified Horrocks equation for Eu(III), Tb(III) and Yb(III)

$$q = 290(\tau_H^{-1} - \tau_D^{-1}) - 0.4$$

Equation 6 – Modified Horrocks equation for Nd(III)

Metal	A	B
Eu(III)	1.25 ms	0.25 ms^{-1}
Tb(III)	5.0 ms	0.06 ms^{-1}
Yb(III)	1.0 μs	0.2 μs^{-1}

Table 2.4 – Values of A and B for Lanthanide ions.

This degree of solvation correlates with the hypothesis that the lanthanide ion is binding directly to the quinoxaline unit as well as the four macrocyclic nitrogen atoms and three amide oxygen atoms. These lifetimes are slightly shorter than those reported by Nagano for the related quinoline-DO3A europium complex,[11] although the *q* values indicate a similar binding mode between the two species. This is possibly due to the quenching effect of the greater number of proximate C-H oscillators in the diethyl amide pendant arms. The europium emissions observed between 525 and 555 nm had a much shorter lifetime, in the region of 5.6 μs (in H_2O), this is consistent with transitions from the $^5D_1$ state since the radiative emission is in competition with non-radiative decay to the $^5D_0$ state. The neodymium complex was irradiated at 355 nm and the lifetime of the $^4F_{3/2} \rightarrow {}^4I_{11/2}$ (1058 nm) and $^4I_{13/2}$ (1340 nm) transitions were measured, these were also analysed as a single exponential decay. The proposed binding mode is further supported by the low *q* value of the neodymium, however as neodymium is more vulnerable to quenching by proximate C-H oscillators this result must be treated with caution.[30]

The lifetime of the ytterbium species was more complicated. In methanol the lifetime of the $^2F_{5/2} \rightarrow {}^2F_{7/2}$ transition was 0.904 μs and could be modelled as a single exponential decay. However, in deuterated methanol the lifetime was best fitted as a double exponential decay. The dominant component (87 %) had a lifetime of 1.37 μs whereas the lesser component (13 %) had a lifetime of 2.59 μs. It is possible that the two components represented the reversible binding of the quinoxaline unit which is resolved on the time-scale of the measurements. This conclusion is supported by the UV-Vis absorption spectrum of the ytterbium complex, which showed a lesser degree of red-shifting compared to the other lanthanide complexes. It's likely that this process also occurred in non-deuterated methanol, but the two species had a very similar lifetime.

Complex	τ_H / μs	τ_D / μs	*q*
NdL1[a]	0.186	0.399	0.4
EuL1[b]	551	1250	0.9
TbL1[b]	772	2050	0.4
YbL1[a]	0.904	1.370	0.7

Table 2.5 - Lifetimes and *q* values of lanthanide complexes.

[a] Measurements obtained in MeOH/CD_3OD, λ_{ex} = 355 nm

[b] Measurements in H_2O/D_2O, λ_{ex} = 355, 396 nm

2.2.4 - Quinoxaline-based complexes as pH chemosensors

Once sensitisation of lanthanide emission *via* excitation of quinoxaline had been confirmed the viability of **L1** as a pH sensor was investigated. As an aromatic heterocycle, quinoxaline has the potential to be protonated in acidic media, which may affect the emissive properties of the complex in several ways. It may influence the excited state energy level of the chromophore, which would alter the extent of energy transfer to the lanthanide and hence the intensity of lanthanide luminescence. Since one of the quinoxaline nitrogen atoms is directly coordinated to the lanthanide ion its protonation would affect the coordination sphere which could result in a change in the degree of solvation, observable *via* lifetime of the decay. The europium complex is of particular interest, since the peak at 615 is due to an electric-dipole its intensity is strongly affected by the degree of symmetry in the coordination sphere, the $J = 4$ transition is also known to have electric-dipole components while intensity of the $J = 1$ peak is primarily magnetic-dipole in nature and largely unaffected by changes of the coordination sphere. This allows a change in the coordination sphere to be observed as a ratiometric response. Thus, the pH sensitivity of **EuL1** was assessed in H_2O using an excitation wavelength of 320 nm, at which the absorption of the complex is the same is neutral, basic and acidic environments. The titration was carried out in a constant ionic background and the concentration of the complex was kept the same throughout.

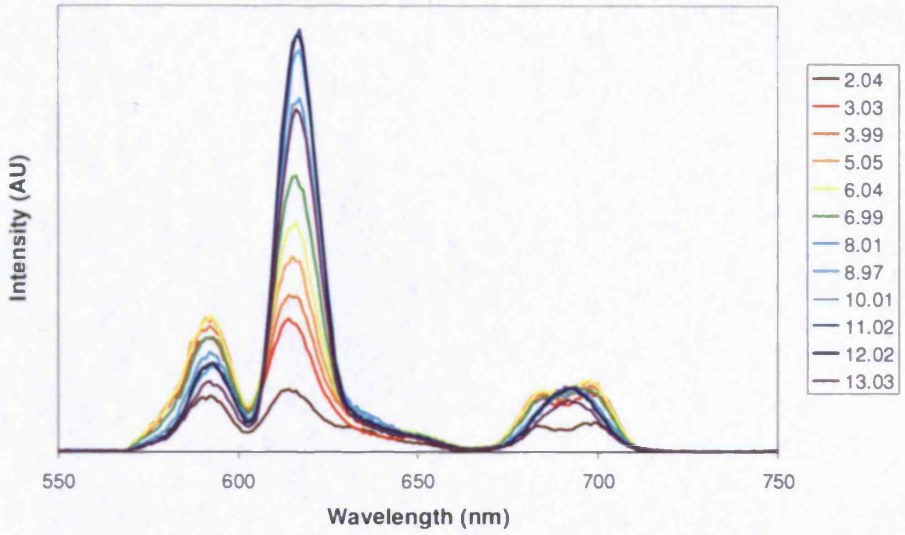

Figure 2.15 - Change in EuL1 emission as a factor of pH.
(λ_{ex} = 320 nm, H_2O, I = 0.1 M NaCl, 298 K)

It was found that as the environment changed from pH 12 to pH 2 the overall intensity of the europium emission spectrum decreased dramatically, the bulk of this change occurring in the biorelevant region between 9 and 6. Furthermore, these changes altered the overall structure of the emission (Figure 2.15). In basic conditions the $J = 4$ transition appears as a single peak at 692 nm but as the pH decreases this is resolved into two separate peaks at 684 and 699 nm. As pH decreases the intensity of the $J = 1$ transition increases to a broad maximum from pH 7 to pH 3, before decreasing slightly, while the intensity of the $J = 2$ transition reaches its maximum at approximately 9.5 before sharply decreasing (Figure 2.16). Overall the total change in the $J = 2$ to $J = 1$ ratio was a decrease from approximately 4.9 down to 1.1 (Figure 2.17). In light of this change the decay profile of the europium emission was analysed at pH/pD 2, these measurements could be modelled as single exponential decays, which indicated that decomplexation had not occurred. It was found that the while the lifetime in deuterated solvents remained the same the lifetime in protonated solvent had decreased by about 40 % compared to neutral conditions. This brought the degree of solvation to $q = 2.2$. These changes are consistent with the hypothesis that in the acidic conditions the quinoxaline unit is protonated and becomes uncoordinated from the europium ion. The value of q obtained from a solution at pH/pD 12 was approximately 0. Since the solutions were not degassed it is likely that at high pH the binding of CO_3^{2-} to Eu(III) prevented the coordination of solvent molecules. As the pH of

the solution decreased CO_3^{2-} was converted to CO_2, resulting in the increase of q. From figure 2.17 the pK_a of the system can be estimated as approximately 7.7, this is higher than reported values for quinoxaline derivatives most likely due to the coordination of the nitrogen to the lanthanide inhibiting protonation.

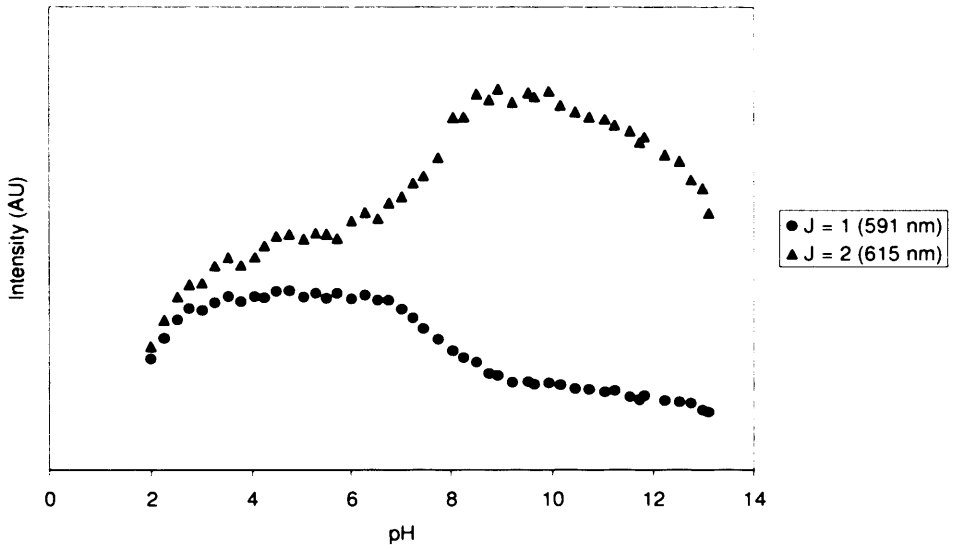

Figure 2.16 - Change in intensity of europium emission as a factor of pH.

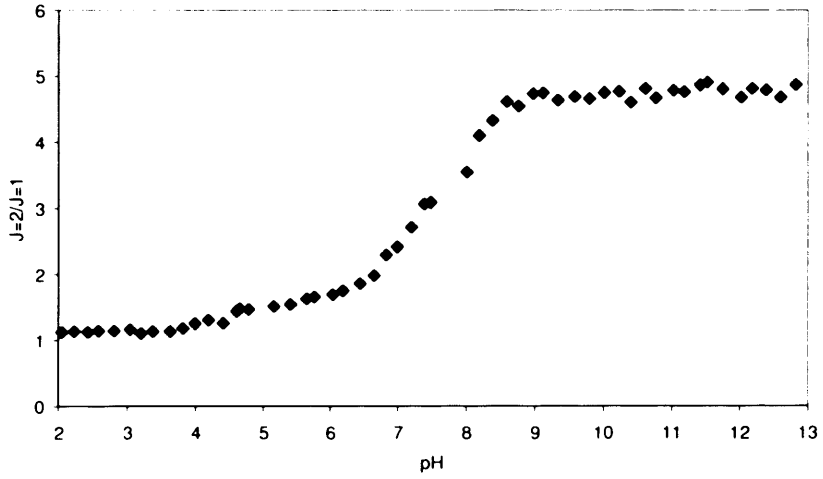

Figure 2.17 - Change in J =1/J=2 intensity as a factor of pH.

2.2.5 - Resistance of complexes to quenching by external metal ions

An affective chemosensor must be selective in its response to the chosen target. In order to test the selectivity of **EuL1** as a pH probe the luminescence of buffered solutions of the complex were measured in the presence of various concentrations of metal ions. Zn(II) is a common target for organic quinoline based sensors and Cu(II) is a well known quencher of organic and europium luminescence. However, even in the presence of ten equivalents of metal the Eu(III) emission was not effected at all by zinc and the copper only had a slight quenching effect. This may be due to the overall 3+ charge on the lanthanide/macrocycle array, which was hypothesised to prevent interactions with surrounding cations.

2.3 - Conclusions

A ligand system has been synthesised incorporating a chromophore, quinoxaline, which has been shown to be capable of sensitising lanthanide emission in the visible and NIR region following excitation between 300 – 400 nm. A combined structural and spectroscopic approach has shown that the new quinoxaline-functionalised macrocycle is octadentate, with the central lanthanide ion coordinating to four macrocyclic nitrogen atoms, three amide oxygen atoms and one quinoxaline nitrogen atom. It was found that in acidic environments the quinoxaline becomes protonated and dissociates from the lanthanide, increasing the degree of solvation. This alters the intensity and form of the europium emission and decreases its lifetime. The complex was resistant to quenching by external metal ions, possibly because the neutral ligand results in the lanthanide/ligand unit carrying a 3+ charge, thus discouraging the binding of external cations.

2.4 - Experimental

1,4,7-Tris[(*N*-diethyl)carbamoylmethyl]-1,4,7,10-tetraazacyclododecane[31] A mixture of 1 equiv. cyclen (0.25 g, 1.45 mmol), 3 equiv. $NaHCO_3$ (0.37 g, 4.35 mmol) and a catalytic amount of KI were stirred in acetonitrile (50 ml) under nitrogen and cooled to 0 °C. A solution of 3 equiv. *N*-diethyl-2-chloroacetamide (0.65 g, 4.35 mmol) in acetonitrile (20 ml) was added dropwise over 30 min. The mixture was allowed to warm to room temperature and stirred for a further 72 h. The solvents were removed in vacuo and the crude reaction mix was purified by recrystallisation with diethyl ether followed by recrystallisation from hot toluene to give the pure product as a brown oil. Yield: 0.429 g, 52%. ^{1}H NMR (400 MHz, $CDCl_3$, 300 K): δ_H = 9.96 (1H, br s, NH), 3.52 (2H, s, $COCH_2$), 3.45 (4H, s, $COCH_2$), 3.27 (8H, q, $^3J_{HH}$ = 7.2 Hz, CH_2CH_3), 3.18 (4H, q, $^3J_{HH}$ = 7.1 Hz, CH_2CH_3), 3.04 (4H, s, ring CH_2), 3.02 (4H, s, ring CH_2), 2.81 (8H, s, ring CH_2), 1.10 (6H, t, $^3J_{HH}$ = 7.1 Hz, CH_2CH_3) and 1.02 (12H, t, $^3J_{HH}$ = 7.1 Hz, CH_2CH_3). ES+ MS (MeCN): found *m/z* 512. $\{M+H\}^+$ requires *m/z* 512.

{1,4,7-Tris[(*N*-diethyl)carbamoylmethyl]-1,4,7,10-tetraazacyclododecane-10-(2-methylquinoxaline)}•NaCl(2) One equivalent of 2-bromomethyl quinoxaline (0.035 g, 0.157 mmol) was added to a stirred solution of 1 equiv. of the cyclen triamide (0.08 g, 0.157 mmol) in dry acetonitrile (20 ml) and heated to 60 °C under nitrogen. After 1 h 1.1 equiv. $NaHCO_3$ (0.0145 g, 0.168 mmol) and a catalytic amount of KI were added and the reaction was stirred for a further 18 h. The reaction mixture was filtered, the solvent was removed in vacuo and the crude reaction mixture was purified by recrystallisation from hot toluene to give the pure product as a yellow-brown solid, isolated as the sodium chloride salt. Yield: 0.047 g, 42%. ^{1}H NMR (400 MHz, $CDCl_3$, 300 K): δ_H = 8.85 (1H, s, aromatic), 8.00 (2H, m, aromatic), 7.63 (1H, m, aromatic), 7.56 (1H, m, aromatic), 3.42 (8H, br m, CH_2CO and $-CH_2-$quin), 3.20 (8H, m, CH_2CH_3), 2.97 (8H, br s), 2.73 (4H, m, CH_2CH_3), 2.1–2.7 (8H, br m), 1.11 (12H, m, CH_2CH_3) and 0.83 (6H, t, $^3J_{HH}$ = 6.4 Hz, CH_2CH_3) ppm. ^{13}C{1H} NMR (101 MHz, $CDCl_3$, 300K): δ_C 13.1, 14.5, 14.8, 40.9, 41.5, 41.6, 55.3, 56.1, 129.5, 129.8, 129.9, 130.0, 146.5, 169.3, 170.5 ppm. IR ν_{max}(ATR, solid): 1703, 1588, 1503, 1458, 1372, 1290, 1267, 1202, 1107, 1015, 881, 838, 791, 748 cm^{-1}. ES+ MS: found *m/z* 654. $\{M+H-NaCl\}^+$ requires *m/z* 654.

General method for lanthanide complexation

The lanthanide complexes were prepared by stirring the ligand (0.020 g, 1 eq., 0.3 mmol) with 1 eq. of $Ln(OTf)_3$ or $Yb(NO_3)_3$ in MeOH (approx. 15 ml) for approximately 24 h at 50 °C. The reaction was followed by TLC ($MeOH:CH_2Cl_2$ 1:9) and judged to be complete when free ligand was no longer observed on the TLC plate. The resulting mixture was concentrated and the desired product precipitated from solution upon addition of diethyl ether. The complexes were obtained as light brown solids in high yield.

{NdL1}(OTf)$_3$

0.032 (89 %) ES+ MS (MeCN): found *m/z* 1095. $\{M\text{-}OTf\}^+C_{37}H_{59}F_6N_9NdO_9S_2$ requires *m/z* 1095. IR ν_{max}(ATR, solid): 1598, 1482, 1445, 1256, 1160, 1078, 1027, 954, 918, 793, 636 cm^{-1}. UV–Vis $\lambda_{max}(\varepsilon/mol^{-1}dm^3cm^{-1})$: 241 (12377), 323 (4725) nm.

{EuL1}(OTf)$_3$

0.032 g (89 %), ES+ MS (MeCN): found *m/z* 1104. $\{M\text{-}OTf\}^+C_{37}H_{59}EuF_6N_9O_9S_2$ requires *m/z* 1104. IR ν_{max}(ATR, solid): 1600, 1458, 1250, 1155, 1079, 1028, 954, 918, 636 cm^{-1}. UV–Vis $\lambda_{max}(\varepsilon/mol^{-1}dm^3cm^{-1})$: 238 (14942), 324 (3718) nm.

{GdL1}(OTf)$_3$

0.034 (94 %), ES+ MS (MeCN): found *m/z* 1109. $\{M\text{-}OTf\}^+C_{37}H_{59}GdF_6N_9O_9S_2$ requires *m/z* 1109. IR ν_{max}(ATR, solid): 1884, 1604, cm^{-1}. UV–Vis. λ_{max} (ε / mol^{-1} dm^3 cm^{-1}) 242 (14102) 324 (5257).

{TbL1}(OTf)$_3$

0.033 (92 %), ES+ MS (MeCN): found *m/z* 1110. $\{M\text{-}OTf\}^+C_{37}H_{59}TbF_6N_9O_9S_2$ requires *m/z* 1110. IR ν_{max}(ATR, solid): 2399.7, 1884.4 and 1603.7. cm^{-1}. UV–Vis $\lambda_{max}(\varepsilon/mol^{-1}dm^3cm^{-1})$: 242 (10491) 324 (3808).

{YbL1}$(NO_3)_3$

0.022 (79 %), (ES+ MS (MeCN): found *m/z* 1013, 991 and 951. $\{M\}^+$ $C_{35}H_{59}N_{12}O_{12}Yb$ requires m/z 1013, $\{M\text{-}NO_3\text{+}MeCN\}$+$C_{37}H_{62}$-$N_{12}O_9Yb$ requires m/z 992, $\{M\text{-}NO_3\}$+$C_{35}H_{59}N_{11}O_9Yb$ requires m/z 951. IR ν_{max}(ATR, solid): 1605, 1404, 1295, 1260, 1075, 1023, 952, 793, 636 cm^{-1}. UV–Vis $\lambda_{max}(\varepsilon/mol^{-1}dm^3cm^{-1})$: 219 (18785), 319 (2503) nm.

2.5 - References

1. M. Montana, T. Terme and P. Vanelle, *Tet. Lett.*, 2005, **46**, 8373-8376.
2. H. E. Rongqiao and C.-L. Tsou, *Biochem. J.*, 1992, **287**, 1001-1005.
3. S. E. Page, A. Flood and K. C. Gordon, *J. Chem. Soc., Dalton Trans.*, 2002, 1180-1187.
4. M. Frei, F. Marotti and F. Diederich, *Chem. Commun.*, 2004, 1362-1363.
5. P. M. Hergenrother, *Polym. Eng. Sci.*, 1976, **16**, 303-305.
6. D. O'Brien, M. S. Weaver, D. G. Lidzey and D. D. C. Bradley, *Appl. Phys. Lett.*, 1996, **69**, 881-883.
7. A. P. de Silva, H. Q. N. Gunaratne and T. E. Rice, *Angew. Chem. Int. Ed. Engl.*, 1996, **35**, 2116-2119.
8. D. Parker and J. Yu, *Chem. Commun.*, 2005, 3141-3143
9. B. P. Burton-Pye, S. L. Heath and S. Faulkner, *J. Chem. Soc. Dalton Trans.*, 2005, 146-149.
10. C. P. Montgomery, D. Parker and L. Lamarque, *Chem. Commun.*, 2007, 3841-3843.
11. K. Hanaoka, K. Kikuchi, S. Kobayashi and T. Nagano, *J. Am. Chem. Soc.*, 2007, **129**, 13502-13509.
12. S. Aime, A. S. Batsanov, M. Botta, J. A. K. Howard, M. P. Lowe and D. Parker, *New J. Chem.*, 1999, 669-670.
13. M. P. Lowe and D. Parker, *Chem. Commun.*, 2000, 707-708.
14. S. J. A. Pope and R. H. Laye, *J. Chem. Soc. Dalton Trans.*, 2006, 3108-3113.
15. T. Gunnlaugsson and D. Parker, *Chem. Commun.*, 1998, 511-512.
16. T. Gunnlaugsson, D. A. Mac Donaill and D. Parker, *J. Am. Chem. Soc.*, 2001, **123**, 12866-12876.
17. D. Parker, J. A. G. Williams, *Chem. Commun.*, 1998, 245-246.
18. T. Gunnlaugsson, J. P. Leonard, K. Senechal and A. J. Harte, *J. Am. Chem. Soc.*, 2003, **125**, 12062-12063.
19. T. Gunnlaugsson, J. P. Leonard, K. Senechal and A. J. Harte, *Chem. Commun.*, 2004, 782-783.
20. K. Hanaoka, K. Kikuchi, H. Kojima, Y. Urano and T. Nagano, *J. Am. Chem. Soc.*, 2004, **126**, 12470-12476.
21. S. Faulkner, B. P. Burton-Pye, T. Khan, L. R. Martin, S. D. Wray and P. J. Skabara, *Chem. Commun.*, 2002, 1668-1669.

22. A. Riesen, T. A. Kaden, W. Ritter and H. R. Maecke, *J. Chem. Soc., Chem. Comm.*, 1989, 460-461.

23. J. Jampilek, M. Dolezal, J. Kunes, V. Buchta, L. Silva and K. Kralova, *Med. Chem,*. 2005, 591-593.

24. S. Faulkner, M.-C. Carrie, S. J. A. Pope, J. Squire, A. Beeby and P. G. Sammes, *J. Chem. Soc., Dalton Trans.*, 2004, 1405-1409.

25. M. Arca, A. Bencini, E. Berni, C. Caltairone, F. A. Devillanova, F. Isaia, A. Garau, C. Giorgi, V. Lippolis, A. Perra, L. Tei and B. Valtancoli, *Inorg. Chem.*, 2003, **42**, 6929-6939.

26. L. S. Hegedus, M. M. Greenberg, J. J. Wendling and J. P. Bullock, *J. Org. Chem.*, 2003, **68**, 4179-4188.

27. G. A. Crosby, R. E. Whan and R. N. Alire, *J. Chem. Phys.*, 1961, 743.

28. E. V. Sayre and S. Freed, *J. Chem. Phys.*, 1956, 1211-1212.

29. A. Beeby, B. P. Burton-Pye, S. Faulkner, G. R. Motson, J. C. Jeffery, J. A. McCleverty and M. D. Ward, *J. Chem. Soc. Dalton Trans.*, 2002, 48-54.

30. S. Faulkner, A. Beeby, M. C. Carrie, A. Dadabhoy, A. M. Kenwright and P.G. Sammes, *Inorg. Chem. Commun.*, 2001, **4**, 187-190.

31 During the course of this work this compound was isolated using different conditions, although spectroscopic data correlates: K. Nwe, J. P. Richard and J. R. Morrow, *J. Chem. Soc. Dalton Trans.*, 2007, 5171-5178.

32 J. H. Markgraf, R. A. Blatchly, B. M. Peake and A. S. Huffadine, *J. Chem. Eng. Data*, 1982, **27**, 474-475.

Chapter Three

N-(2-nitrophenyl)acetamide-derived chromophores as sensitizers for lanthanide luminescence

3.1 - Introduction

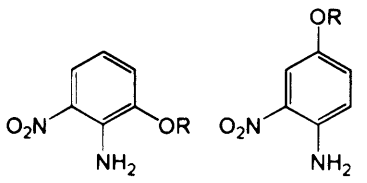

Figure 3.1 – Substituted benzamines.

The aim of this chapter was to determine the viability of derivatives of two isomeric, substituted benzamines (Figure 3.1) to act as chromophores and efficiently transfer energy to lanthanide ions. They are closely related to nitroaniline and aminophenol which are used as precursors to many azo-dyes including paranitraniline red (Para Red), Disperse orange 1, Alizarine yellow R and Amido black 10B. In these dyes the nitro-, methoxy- and other functional groups contribute to the aromaticity, red-shifting the absorption. This is demonstrated by substituting one aryl group of a simple azo dye, azo-benzene (Figure 3.2), with various functional groups (Table 3.1).

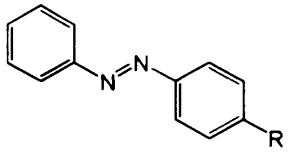

Figure 3.2 – Azo-benzene.

R	λ_{max}
-H	320 nm[1]
-Me	327 nm[2]
$-NO_2$	335 nm[3]
-OH	342 nm[4]
-OMe	346 nm[2]
$-NMe_2$	420 nm[5]

Table 3.1 - The effect of various functional groups on the absorption profile of azo-benzene

Functional groups can also act as electron donors or electron acceptors and establish a degree

of charge transfer character. This is seen in Para Red and the closely related 'Sudan' family of dyes. Sudan I (Figure 3.3, A) is made up of naphthol (incorporating an electron donating hydroxy group) and an aryl-ring, bound *via* an azo group, and has been used as yellow/orange dye (λ_{max} 450 nm)[6] whereas Para Red (Figure 3.3, B), in which the *para* position of the aryl ring is substituted with a strong electron acceptor nitro- group, has an intense red absorbance (λ_{max} ~ 480 nm). However, if the aryl ring is substituted with another electron donor, a methoxy group (Figure 3.3, C), the charge transfer character is disrupted and the absorption is blue shifted (λ_{max} ~ 420 nm).[7]

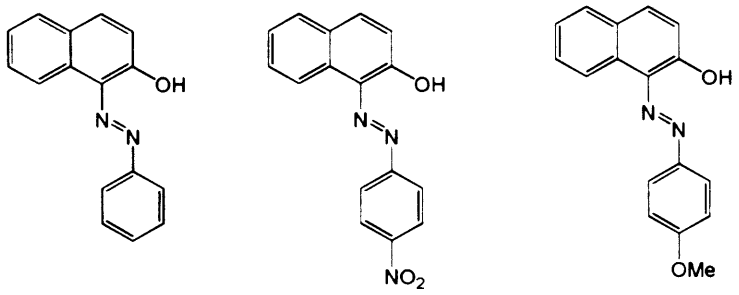

Figure 3.3 – Structure of Sudan I (A) and Para Red (B) and an isomer of Sudan Red G (C).

The addition of functional groups to increase the extent of aromaticity and add a degree of ILCT character has been utilised in the field of lanthanide photochemistry. The effect of varying the *para*-substituent of an acetophenone chromophore (Figure 3.4) has been studied by Beeby *et al.*[8] It was found that more strongly electron-donating substituents caused a greater red-shift to the ligand absorption and allowed lower energy sensitisation of europium. In the case of the ligand with the strongest electron donor, a dimethylamino group, the chromophore showed a significant red-shift on coordination to the metal, indicating that the more polarised π system had a stronger interaction with the europium ion. This was reflected in the europium spectra of the complexes. The stronger electron donors resulted in a more polarised, negatively charged carbonyl group, which enhanced the relative intensity of the hypersensitive $J = 2$ band of the europium emission.

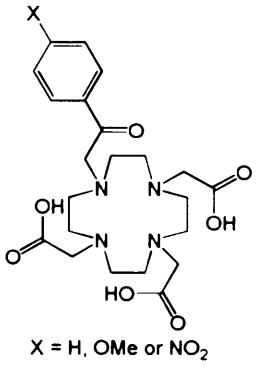

Figure 3.4 – Ligand with substituted acetophenone chromophore.

Complexes of nitrophenoxides (Figure 3.5) have been known to show lanthanide luminescence in the solid state.[9] Ytterbium and erbium complexes of a tetrafluoronitrophenoxide were shown to absorb light in the UV and visible regions, with λ_{max} at around 406 nm. The luminescence excitation spectra of the complexes in the solid state showed broad peaks at ~400 nm and ~520 nm. The higher energy peak was characterised as lanthanide sensitisation following absorption into the ligand $^1\pi\pi^*$ state, whereas the lower energy peak was assigned to direct excitation into the ligand $^3\pi\pi^*$ followed by energy transfer to the metal ion. In both cases the luminescence lifetimes were unusually long, due to the absence of vibrational quenching by C-H bonds.

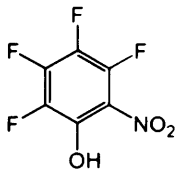

Figure 3.5 – Tetrafluoronitrophenoxide used to sensitise Yb^{III} and Er^{III} emission.

Kiefer and Sherry and co-workers reported a responsive MRI contrast agent based around the pH-dependant dissociation of a nitrophenolic pendant arm of DO3A and DO3AM macrocycles (Figure 3.6).[10] On attempting to determine the degree of hydration by comparing the lifetime of the europium emission in deuterated and non-deuterated solvents it was discovered that europium based emissions were negligible, despite the separation of the triplet state of the nitrophenol group and the europium excited states being well suited for efficient energy transfer. This was due to quenching of the excited state of the relatively readily reduced Eu^{III} by ligand-metal charge transfer upon oxidation of the nitrophenol group. Tb^{III} emission was observed, however with short lifetimes indicating a significant amount of back energy transfer (BET).

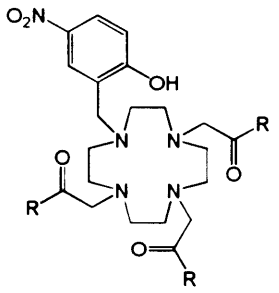

Figure 3.6 – Ligand incorporating a nitrophenol pendant arm.

In a study into the energy transfer processes in complexes of europium and terbium with substituted diketonates and salicylates[11] it was found that excitation of europium dinitrisalicylate (Figure 3.7) in the UV and visible region resulted in strong, lanthanide-based emission. The luminescence excitation spectrum of the complex showed a band with λ_{max} at 360 nm, which was assigned to a $\pi\pi^*$ transition as well as a strong band at 450 nm which was assigned as an ILCT band, induced by the π-acceptor properties of the multiple nitro- groups.

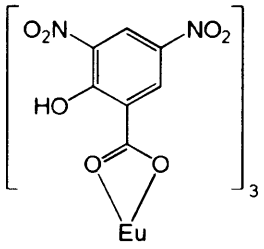

Figure 3.7 – Europium dinitrosalicylate.

As mentioned earlier, lanthanide sensitisation *via* ILCT states has been observed in several ligand systems.[12-15] In a study by Kim *et al.* on lanthanide complexes with 4-naphthalen-1-yl-benzoic acid derivatives (Figure 3.8) the absorption and emission properties of the ligands were found to be highly solvatochromic, with the maxima more red-shifted as solvent polarity increased. This is due to the stabilisation of the ILCT excited state in more polar solvents. In the europium complexes the metal based emission was highly solvent dependant with strong phosphorescence observed in acetonitrile but no emission seen in toluene. No ligand based phosphorescence was observed in the gadolinium complex and the europium emission was completely independent of oxygen concentration. This indicated that europium sensitisation takes place exclusively *via* an ILCT state. In a study by Bünzli *et al.* substitution of the electron-donating and accepting groups allowed a modulation of the efficiency of Eu(III) sensitisation by modulating the energy of the ILCT. It was also shown that NIR emission Ln(III) ions Nd(III) and Yb(III) could be sensitised *via* an ILCT state.[16]

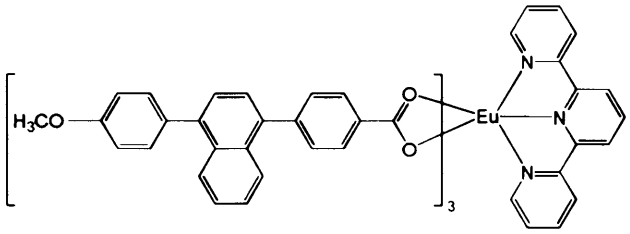

Figure 3.8 – Eu(III) complex with 4-naphthalen-1-yl-benzoic acid derivative.

In contrast to this is a study into europium complexes of functionalised β-diketonates (Figure 3.9), which displayed both ILCT fluorescence and sensitised europium emission.[17] The ILCT fluorescence in the free ligand was compared to that in the europium and gadolinium complexes and it was found that coordination of either metal resulted in no change in the lifetime but a decrease in the quantum yield. This indicated that sensitisation of europium was not occurring *via* an ILCT state, instead it was found that a ligand triplet state was responsible for the metal emission. On coordination with either gadolinium or europium the ISC rate was enhanced due to the heavy atom effect and the population of the triplet state became more competitive against the ILCT state, reducing the quantum yield. This indicates that in some cases the presence of an ILCT band may partially quench lanthanide luminescence.

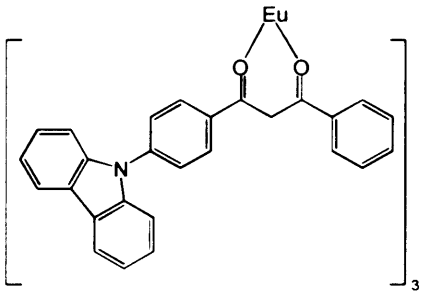

Figure 3.9 – Eu(III) complex with functionalised β-diketonates.

In light of these issues the aim of this chapter was to examine the viability of incorporating the simple nitrobenzamides into an azamacrocyclic framework, capable of forming water stable complexes with lanthanide ions and sensitising lanthanide luminescence following UV-visible excitation. Particular attention shall be paid to the effect of varying the position of substitution around the aryl ring.

3.2 – Results and Discussion

3.2.1 - Synthesis and characterisation of ligand precursors, ligands and lanthanide complexes

Before the chromophores could be appended to a suitable macrocycle they were converted to chloroacetamides. This is a convenient conversion in that it is synthetically facile and can extend the delocalised π system to a suitable donor group, allowing the chromophore to bind directly to the lanthanide ion. 2-nitro-6-hydroxyaniline (**1**) reacts readily with chloracetyl chloride to form 2-chloro-N-(6-hydroxyl-2-nitrophenyl)acetamide (**2**), which upon drying formed crystals suitable for X-ray diffraction studies (Table 2, Figure 3.11). This was then mixed with 1,4,7-tris(*tert*-butoxycarbonylmethyl)-1,4,7,10-tetraazacyclododecane (**3**) in the presence of an organic base and the reaction was monitored by thin-layer chromatography. After 6h the reaction appeared to be complete and the ^{1}H NMR of the crude reaction mixture confirmed the absence of the aromatic starting material. However, ES$^+$ MS of the mixture indicated that the desired product had not been formed; instead only macrocyclic starting material and a new product at *m/z* 194 were observed. The molecular weight of the new product corresponded to the cyclised acetamide (**5**, Figure 3.10). Although the *ortho-* isomer was prearranged to react intramolecularly, no such process could occur in the *para-* isomer. However, attempts to append 2-chloro-N-(6-hydroxyl-2-nitrophenyl)acetamide **2** to the macrocycle **3** failed. TLC indicated the formation of more than five new chromophoric species. It is likely that due to deprotonation of the phenol group intermolecular polymerisation between chloroacetamide molecules had occurred.

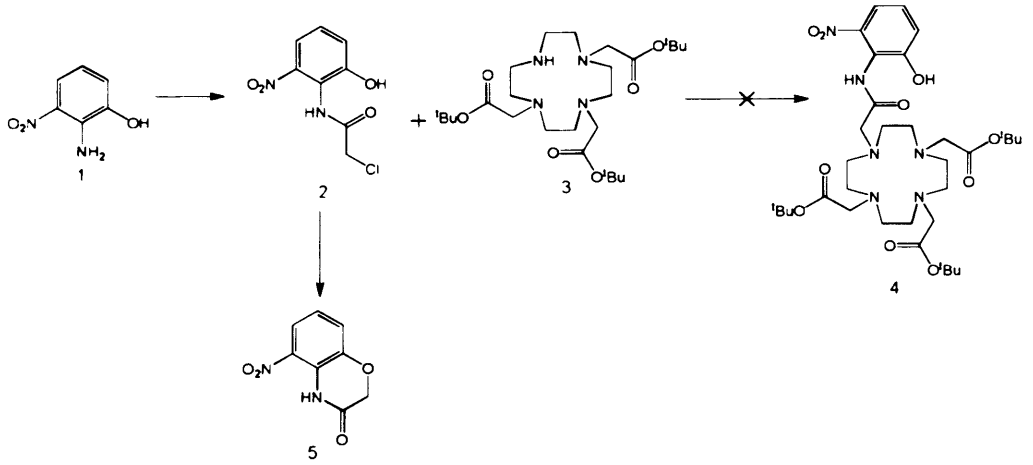

Figure 3.10 – Attempted route to new ligand precursor and the resulting intramolecular cyclisation.

	2	**6**
Empirical formula	$C_9H_9ClN_2O_4$	$C_8H_7ClN_2O_4$
Formula weight	244.63	230.61
Temperature	100(2)K	100(2)K
Wavelength	0.71073Å	0.71073Å
Crystal system	Monoclinic	Monoclinic
Space group	P2(1)/c	P2(1)/n
Unit cell dimensions	a = 4.6925(3) Å, α = 90.00°	a = 6.2783(6) Å, α = 90.00°
	b = 14.8214(8) Å, β = 97.287(4)°	b = 14.9977(13) Å, β = 100.430(4)°
	c = 14.9223(10) Å, γ = 90.00°	c = 9.8799(9) Å, γ = 90.00°
Volume	1029.45(11) $Å^3$	914.92(14) $Å^3$
Z	4	4
Density (calculated)	1.578	1.674
Absorption coefficient	4.289	4.289
F(000)	504	472
Crystal size	0.27 × 0.22 × 0.15 mm^3	0.20 × 0.09 × 0.09 mm^3
Theta range for data collection	2.75 to 27.47°	2.50 to 27.65°
Reflections collected	3627	2128
Independent reflections	3083	1962
Goodness-of-fit on F	1.059	1.070
Final R indices [I > 2sigma(I)]	R1 = 0.0377, wR2 = 0.1050	R1 = 0.0285, wR2 = 0.0782
R indices (all data)	R1 = 0.0446, wR2 = 0.1093	R1 = 0.0311, wR2 = 0.0803

Table 3.2 – Crystal data collection and refinement details for the crystal structure of **2** and **6**.

In light of this the chromophore starting materials were methylated using MeI in acetone with potassium carbonate as a base. This was carried out and the products were characterised according to literature precedent.[18, 19] This had to take place prior to the conversion to the chloroacetamide as the conditions required for methylation also resulted in cyclisation. 2-Nitro-6-methoxyphenylcarbamoyl methyl chloride (**6**) and 2-nitro-3-methoxyphenylcarbamoyl methyl chloride (**7**) were synthesised with the same ease as the *ortho*-hydroxy analogue and were characterised by ^1H NMR, carried out in $CDCl_3$. In each case unique methoxy, methylene and aromatic peaks were observed but the most dramatic difference between the two isomers was in the position of the amide proton resonance which appears at 9.2 ppm in the *ortho* isomer, whereas in the *para* isomer it is shifted downfield to 11.5 ppm, indicating a more desheilded environment. Allowing a solution of **6** in ethyl acetate to dry in air resulted in crystals of suitable quality to carry out X-ray diffraction structural studies, the results of this are compared to those of the *hydroxy* analogue (Table 3.2, Figure 3.11).

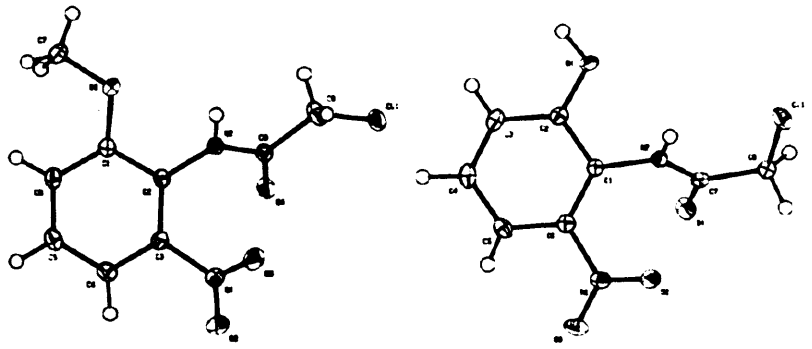

Figure 3.11 – X-ray crystal structures of **2** and **6**.

The chromophores were then appended to a suitable macrocycle by reacting 1.5 equivalents of the chloroacetamide with 1,4,7-tris(tert-butoxycarbonylmethyl)-1,4,7,10-tetraazacyclododecane in the presence of a base (sodium hydrogen carbonate) and a catalytic amount of KI (Figure 3.12).

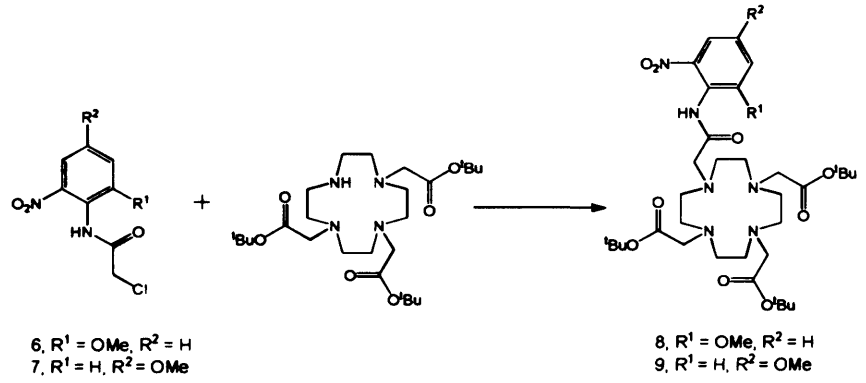

Figure 3.12 – Formation of **8** and **9**, new ligand precursors.

The excesses of chloroacetamide were then separated by column chromatography to give the desired products as pure brown oils. ^{1}H NMR confirmed the absence of methylene chloride protons and there were slight shifts in the methoxy, aromatic and amide peaks compared to the starting materials. Again the amide resonance of the *para* analogue was shifted further downfield than that of the *ortho* analogue, 11.1 ppm compared to 9.21 ppm. ES$^+$MS of both compounds showed a peak for the protonated parent ion, $\{M+H\}^+$, at *m/z* 723. Single crystals of the *ortho*-methoxy ligand precursor were grown from a concentrated hexane/toluene solution at -20 °C and crystals of the *para*-methoxy ligand precursor were grown by slow vapour diffusion of diethyl ether into a concentrated chloroform solution. Although the goodness-of-fit for the *ortho*- isomer (1.413) was poorer than that of the *para*- isomer (1.027) (table 3.3) both allowed a structural comparison (table 3.3).

	K8	**K9**
Empirical formula	$C_{35}H_{58}IKN_6O_{10}$ $(H_2O)0.75(C_4H_8O_2)$	$C_{35}H_{58}IKN_6O_{10}$ $0.75(H_2O)$
Formula weight	971.96	902.39
Temperature	150(2)K	150(2)K
Wavelength	0.71073Å	0.71073Å
Crystal system	Triclinic	Monoclinic
Space group	P-1	C2/c
Unit cell dimensions	a = 16.9830(7) Å, α = 101.560°	a = 21.3350(4) Å, α = 90.00°
	b = 17.0630(8) Å, β = 105.440(7)°	b = 23.2170(5) Å, β = 97.0750(10)°
	c = 21.3680(9) Å, γ = 111.950°	c = 17.8310(4) Å, γ = 90.00°
Volume	5215.1(4) $Å^3$	8765.1(3) $Å^3$
Z	4	8
Density (calculated)	1.238	1.368
Absorption coefficient	4.439	4.439
F(000)	3756	3756
Crystal size	0.3 x 0.22 x 0.06 mm^3	0.22 x 0.16 x 0.06 mm^3
Theta range for data collection	1.05 to 21.97°	2.8 to 27.54°
Reflections collected	12477	8918
Independent reflections	8564	5365
Goodness-of-fit on F	1.413	1.027
Final R indices [I > 2sigma(I)]	R1 = 0.1265, wR2 = 0.1768	R1 = 0.0755, wR2 = 0.1852
R indices (all data)	R1 = 0.3493, wR2 = 0.3853	R1 = 0.1363, wR2 = 0.2174

[a] The structure was refined on F_o^2 using all data

Table 3.3 - Crystal data collection and refinement details for the crystal structures of **K8** and **K9**.

Both compounds crystallised as potassium complexes with the metal ion coordinating to the four macrocyclic nitrogen donors, the three ester carbonyl oxygen atoms and the amide carbonyl oxygen atom, the charge was balance by an iodide counterion (Figures 3.13 and 3.14). Previous work has shown that the coordination mode adopted by alkali metal ions with the ester precursors to functionalised-DO3A ligands is comparable with the coordination mode adopted by lanthanide ions in the final deprotected ligands.[20] This supports the proposed binding mode of **L1** and **L2**, with the lanthanide ion binding directly to the amide group.

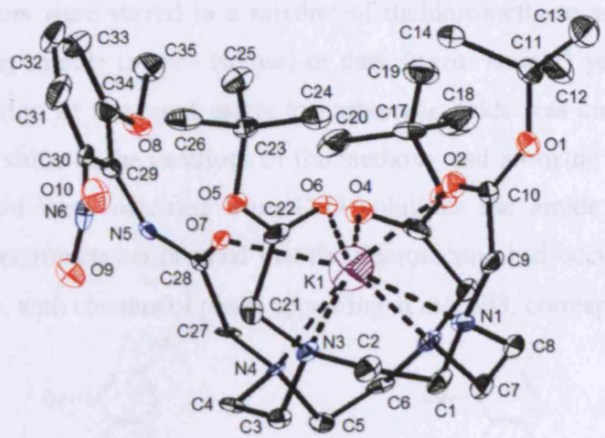

Figure 3.13 – X-ray crystal structure of **K8** (counterion omitted for clarity).

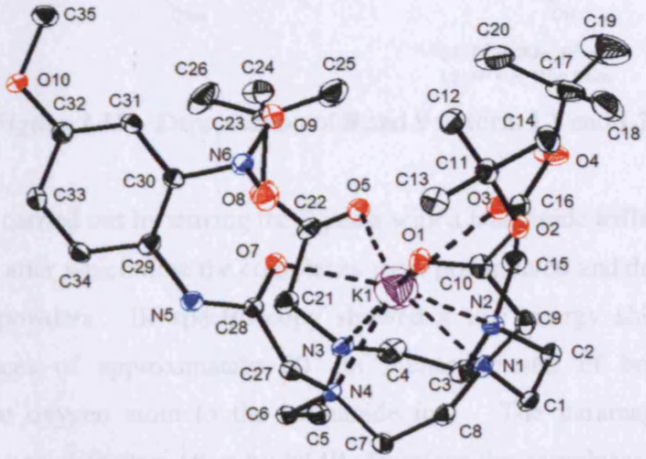

Figure 3.14 – X-ray crystal structure of **K9** (counterion omitted for clarity).

The ligand precursors were stirred in a mixture of dichloromethane and trifluoroacetic acid (1:1, 24 h), resulting in pale (*ortho-* isomer) or dark (*para-* isomer) yellow powders (Figure 3.15). The conversion of tert-butyl esters to carboxylic acids was confirmed by ^{1}H NMR, which also showed shifts in the positions of the methoxy and aromatic resonances. However as the NMR spectra were obtained from D_2O solutions the amide resonances were not observed. Mass spectrometry confirmed that the deprotection had occurred without cleavage of the chromophore, with clusters of peaks appearing at *m/z* 593, corresponding to $\{M+K\}^+$.

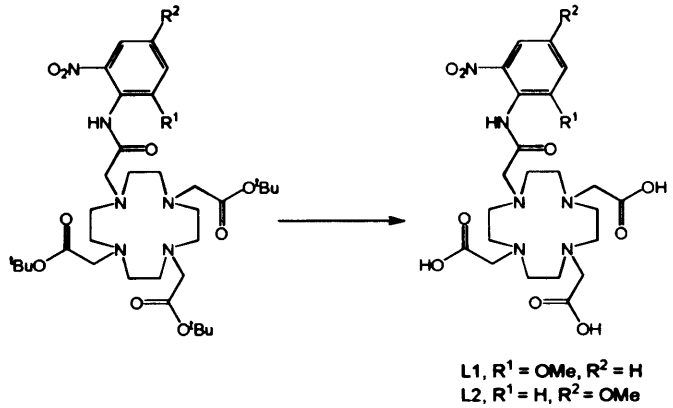

Figure 3.15 – Deprotection of **8** and **9** to form **L1** and **L2**.

Complexation was carried out by stirring the ligands with a lanthanide triflate salt in methanol, at 50 °C overnight, after which time the complexes were precipitated and dried to result in pale cream or yellow powders. IR spectroscopy showed a low energy shift of the carbonyl stretching frequences of approximately 80 cm^{-1}, characteristic of bond weakening on coordination of the oxygen atom to the lanthanide ion. The paramagnetic character of lanthanide ions limited characterisation by NMR, therefore the complexes were characterised primarily by HRMS. Each spectrum showed an *m/z* corresponding to the calculated mass of the desired complex, typically accurate to three decimal places, and the observed isotopic patterns corresponded extremely well with those predicted (see Figure 3.16 for examples).

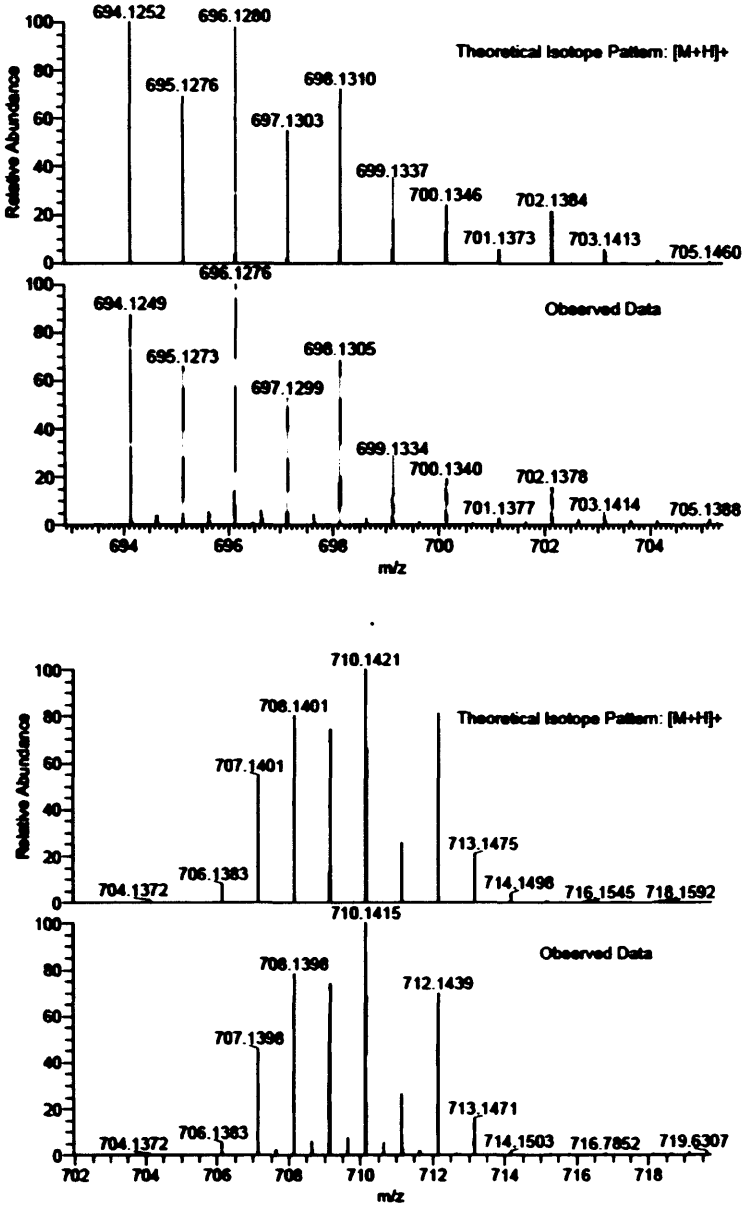

Figure 3.16 – Comparison of theoretical and observed isotope pattern for NdL2 (top) and GdL2 (bottom).

3.2.2 - Photophysical Studies

The UV-Vis absorption spectrum of each of the chloroacetamide precursors showed a $\pi\pi^*$ transition below 250 nm as well as a weaker, broader transition at low energy which was red shifted for the *para* isomer (λ_{max} = 373 nm) compared to the *ortho* isomer (λ_{max} = 323 nm). In order to assign this peak the spectra were measured in several different solvents. Charge transfer transitions are known to be highly solvatochromic with increasing polarity of the solvent resulting in a red-shift of the absorption.[15] This was not observed in the case of the

chloroacetamides, in both cases the λ_{max} was at the same wavelength in diethyl ether, chloroform and acetonitrile but was blue-shifted in DMSO. This indicates that although there may be a charge transfer component the transition is primarily of $\pi\pi^*$ or $n\pi^*$ character. Very slight changes were observed in the absorption spectra when the chromophores were bound to the macrocycle and when the pendant arms of the macrocycle were deprotected. Upon complexation of the ligands with lanthanide ions only the *para*-methoxy showed significant changes in its absorption profile. Typically the electron withdrawing effect of complexation with a lanthanide ion causes a red shift in the absorption spectrum of the chromophore, with heavier lanthanides having a greater effect due to increased Lewis acidity.[12] However in this case the low energy absorption band was blue-shifted from λ_{max} = 365 nm to approximately λ_{max} = 340 nm (Figure 3.17 for example) and the effect was independent of the mass of the lanthanide ion, indicating that on coordination an alternative process, unrelated to the electron withdrawing effect of the lanthanide, was responsible for the shift.

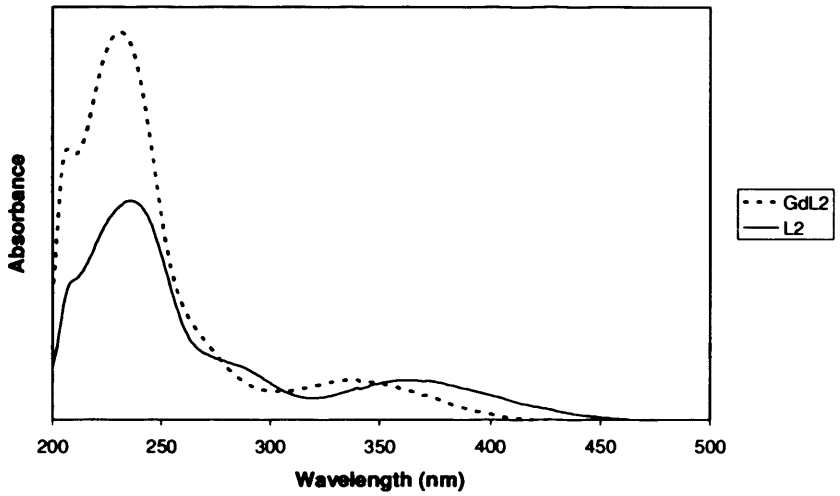

Figure 3.17 – Blue shift to absorption profile of L2 on complexation with Gd(III).

Following excitation at 290 nm of the gadolinium complexes at room temperature, it showed only broad, short-lived ligand fluorescence. However, following excitation of the gadolinium complexes in an optical glass (ethanol, 77K) broad structureless phosphorescence was observed, with the onset of the peak at *ca.* 425 nm and the maxima at 440 nm. This allowed an estimation of the triplet state of the chromophore of approximately 23400 cm^{-1}. This was to be expected as the lowest excited state of Gd(III), the $^6P_{7/2}$ level, is at *ca.* 32000 cm^{-1} and therefore it cannot receive energy from chromophores which absorb at long wavelength.[21] The energy gap between the triplet state of the ligand and the excited states of visible and NIR emissive lanthanides is suitable for efficient sensitisation.[21]

Following excitation of the Tb, Eu, Nd and Yb complexes of **L1** and **L2** between 300 and 350 nm the steady state spectra showed transitions characteristic of the lanthanide ion, this is significantly red-shifted compared to an unsubstituted benzamide, which can sensitise terbium emission but only following excitation at higher energy (266 nm).[22] The Tb(III) emission arising from the $^5D_4 \rightarrow {}^7F_5$ and $^5D_4 \rightarrow {}^7F_4$ transitions were visible only in the fluorescence spectrum of **TbL1** as slight shoulders on the low energy edge of the ligand emission (Figure 3.18). In **TbL2** the ligand emission was red shifted and too intense to distinguish the terbium emission although decay measurements at 487 nm and 545 nm showed a lifetime in the millisecond range, indicating that lanthanide sensitisation had been achieved. Eu(III) emission from the $^5D_0 \rightarrow {}^7F_J$ transitions were visible over the tail of the ligand emission and were intense enough to allow the resolution of the $J = 0 - 4$ peaks (Figure 3.19).[23]

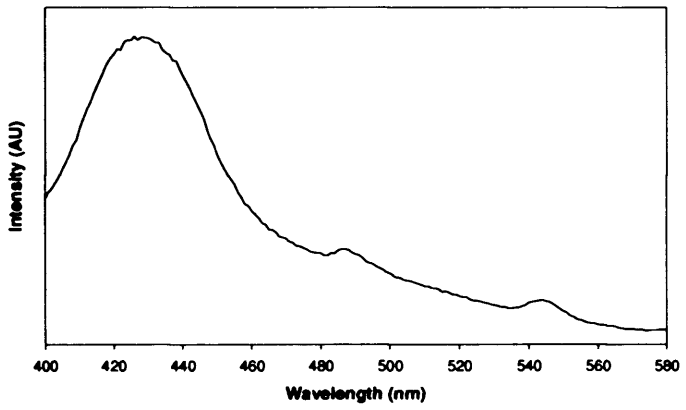

Figure 3.18 – Superimposed ligand and terbium emission for **TbL1**.

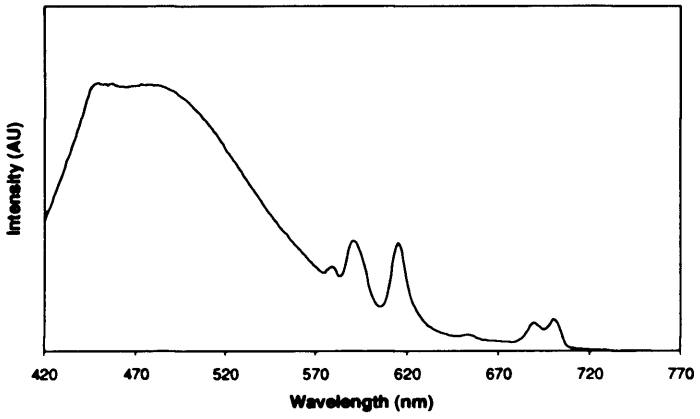

Figure 3.19 – Superimposed ligand and europium emission for **EuL2**.

Following excitation at 320-370 nm the Nd(III) showed NIR emission due to the $^4F_{3/2} \rightarrow {}^4I_{9/2}$ (weak peaks at approx. 875 and 895 nm), $^4F_{3/2} \rightarrow {}^4I_{11/2}$ (strong peak at approx. 1058 nm) and

$^4F_{3/2} \rightarrow {}^4I_{13/2}$ (weak peak at approx. 1350 nm) transitions (Figure 3.20).[24] The steady state emission spectra of **YbL1** and **YbL2** showed a peak at 975 nm, due to the $^2F_{5/2} \rightarrow {}^4F_{7/2}$ transition, with a broadened shoulder due to vibronic interactions (Figure 3.21).[25]

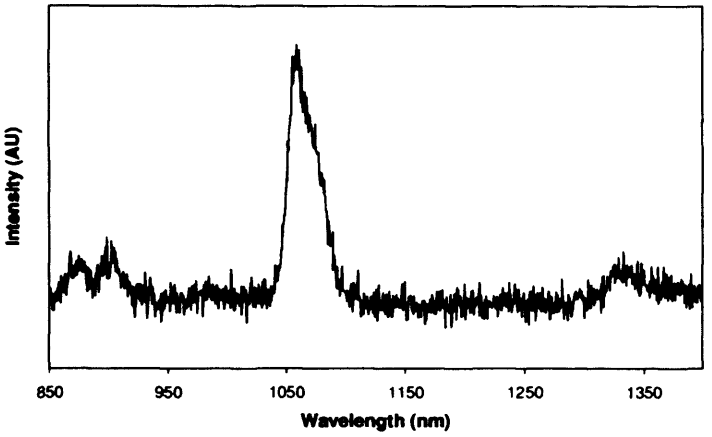

Figure 3.20 – Neodymium emission of **NdL1**.

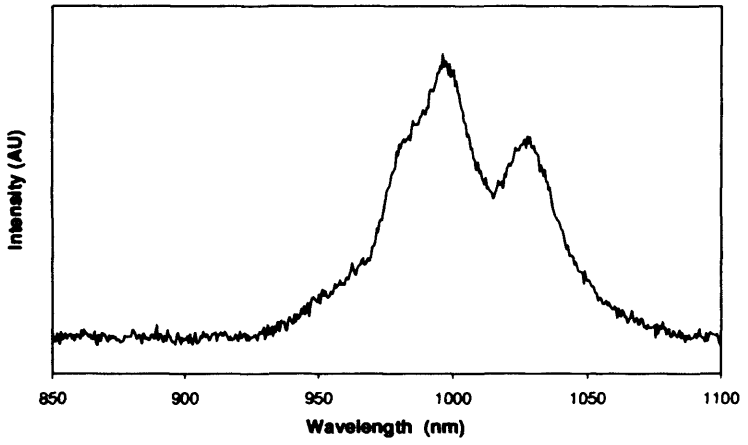

Figure 3.21 – Ytterbium emission of **YbL1**.

For each of the emissive complexes the luminescence lifetimes were obtained in H_2O and D_2O and analysed as single exponential decay profiles, indicative of a single emissive species. The difference in lifetimes in deuterated and non-deuterated solvents was used to calculate the degree of inner sphere hydration, q, of Eu, Tb and Yb, by application of Horrocks equation, [$q = A(\tau_H^{-1} - \tau_D^{-1} - B)$] where A = 1.2 ms (Eu), 5 ms (Tb) and 1 μs (Yb) and B = 0.5 ms^{-1} (Eu), 0.06 ms^{-1} (Tb) and 0.2 μs^{-1}(Yb).[26] The q value of Nd was calculated using the modified version of the equation [$q = 130(\tau_H^{-1} - \tau_D^{-1}) - 0.4$] to take into account quenching by C-H oscillations.[27] In each case the value of q was approximately 1 (Table 3.4), corresponding to a

single inner sphere solvent molecule. From this it can be deduced that the ligands adopt the proposed octadentate binding mode, coordinating *via* the four amines, the three carboxylate groups and the amide carbonyl oxygen, as observed in the X-ray crystal structures of the protected ligand precursors. Interestingly the value of q for the Nd complex was lower than would be expected for DO3A-based ligand and were similar to cases where quenching by proximate C-H bonds is minimised, such as in complexes with the Lehn cryptand.[27] However, the lifetimes and q values for the Yb complexes did not show the same discrepancy and were very similar to those reported in the literature for complexes with a similar binding mode.[26, 28] Although the q values of the europium and terbium complexes approximately correlated with the proposed coordination mode the lifetimes were shorter than is usually observed in many related aminocarboxylate species, comparable to the terbium lifetimes reported by Sherry and co-workers in which the ligand bore a nitrophenolic pendant arm, this was thought to be a result of BET to the ligand.[21] Due to the high energy of the terbium excited state (20500 cm^{-1}) it is more susceptible to quenching by BET to a low lying ligand $^3\pi\pi^*$ state. However, since ligand triplet states are quenched by triplet oxygen carrying out the measurements in anaerobic conditions should prolong the lifetime of the terbium emission and degassed experiments showed no such enhancement. Tsaryuk and co-workers have observed that energy transfer to the $n\pi^*$ transition of a nitro-group can have a quenching effect, decreasing the relative luminescence efficiency of europium and terbium.[29, 30] The extent of this effect is determined by the energy of the $n\pi^*$ transition relative to that of the energy of the lanthanide excited state, with smaller energy gaps allowing more effective quenching. Although the effect of quenching by nitro-groups on luminescence lifetime was not studied, energy transfer from the lanthanide excited state to the nitro group is likely to shorten the lifetime of lanthanide luminescence. As observed, this effect would be stronger in cases where the energy difference between the ligand transition and the lanthanide excited state are smaller, such as in terbium complexes compared to europium complexes and in complexes of **L2** compared to those of **L1**.

Lanthanide	Ligand	Lifetime in D_2O (μs)	Lifetime in H_2O (μs)	*q*
Nd	1	0.327	0.095	0.6
	2	0.270	0.085	0.6
Eu	1	1507	530	1.2
	2	922	429	1.2
Tb	1	1120	920	0.9
	2	450	410	1.1
Yb	1	7.629	0.776	1.0
	2	8.611	0.802	0.9

Table 3.4 – Lifetime data for emissive lanthanide complexes.

3.2.3. - Density Functional Theory Calculations

In order to rationalise the spectroscopic differences observed between the two isomers a density functional theory (DFT) study was undertaken by Dr. Ben Ward to probe the energetic consequences of substitution at different positions around the aryl ring. As mentioned earlier the synthesis of the chloroacetamides yielded the pure products which crystalised on drying and the crystals of the *ortho*-methoxy isomer **6** were suitable for X-ray diffraction anaylsis. Structural studies revealed that the amide group was twisted away from the plane of the ring, minimising the steric clash with the nitro group. In order to test the validity of DFT computational methods to these systems the structure of **6** was calculated and compared to those obtained by the X-ray diffraction study (Table 3.5). The only major difference was that the torsion angle of the amide was predicted to be smaller than was observed in the crystal structure, otherwise the bond lengths and angles were in good agreement, lending credibility to the application of computational methods to these systems.

Selected bond lengths	**Measured**	**Calculated**
N(1)-C(6)	1.4711(17) Å	1.469 Å
N(1)-O(2)	1.2215(15) Å	1.223 Å
N(1)-O(3)	1.2344(15) Å	1.223 Å
O(1)-C(2)	1.3491(15) Å	1.360 Å
N(2)-C(1)	1.4177(15) Å	1.397 Å
Cl(1)-C(8)	1.7787(13) Å	1.799 Å
O(4)-C(7)	1.2323(16) Å	1.217 Å
N(2)-C(7)	1.3340(16) Å	1.366 Å
Selected bond angles		
O(2)-N(1)-O(3)	122.99(11)°	125.24°
C(1)-N(2)-C(7)	122.85(11)°	124.33°
C(7)-C(8)-Cl(1)	114.84(9)°	116.74°
Selected torsion angles		
O(4)-C(7)-C(8)-Cl(1)	170.9(1)°	166.75°
C(6)-C(1)-N(2)-C(7)	60.49(17)°	44.26°
O(2)-N(1)-C(6)-C(1)	19.98(17)°	33.51°

Table 3.5 – Comparison between properties of 6 measured from X-ray crystal diffraction studies and those predicted from DFT calculations.

As a comparison between systems in which the aryl group is substituted in different positions the two isomers of methoxy-2-nitro-N-methylbenzamide (**10** and **11**, Figure 3.22) were modelled using DFT (B3PW91) methods. As observed in the chloroacetamide the amide group of the *ortho-* isomer twists out of the plane of the aryl ring, with an energy barrier for rendering bringing the amide group into planarity with the aryl ring of 11 kcal mol^{-1}, this allows the nitro- group to reside closer to co-planarity whereas the *para-* isomer, 4-methoxy-6-nitro-N-methylbenzamide, is a much more planar system. The energy barrier of rotation of the amide is group is 10 kcal mol^{-1}, consistent with a fully π-delocalised system. The energy barrier for rotation of an amide group linking two aromatic rings has been calculated as 4.65 kcal mol^{-1} and the configuration of minimum energy of 0°, with the amide group coplanar with the aryl ring.[31] The higher barrier of the current system is possibly due steric hindrance caused by the nitro- group, which also causes the slight shift away from coplanarity. Although these systems lack the steric bulk of the ligands or the ligand precursors these findings correlate with the observed crystal structures of the ^{t}butyl-protected macrocycles. Presumably the difference is due to the degree of steric hindrance caused by the position of the methoxy group and although the amide is conjugated with the π system in both cases the degree of torsion is likely to dictate the extent of delocalisation, thereby affecting the HOMO-LUMO energy gap (Figure 3.23).

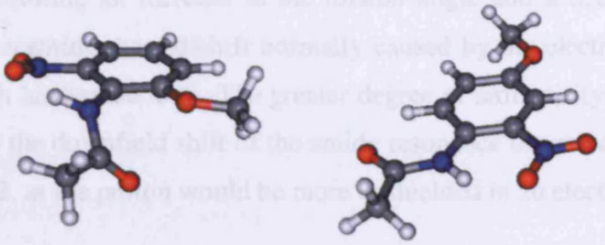

Figure 3.22 – Modelled systems, 6-methoxy-2-nitro-N-methylbenzamide **10** (left) and 4-methoxy-2-nitro-N-methylbenzamide **11** (right).

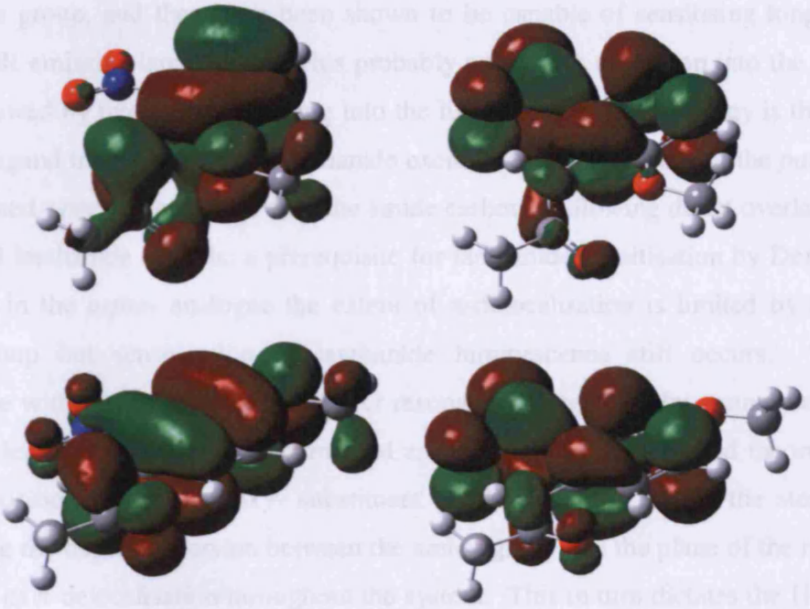

Figure 3.23 – HOMOs (left) and LUMOs (right) of model systems **10** (top) and **11** (bottom).

UV-Vis absorption studies have shown that at all stages of the synthesis of **L1** and **L2** the absorption of the *para*- isomer of the precursors are red-shifted compared to the *ortho*- isomer precursors, indicating a greater degree of aromaticity and a smaller HOMO-LUMO gap. The energy difference between the orbitals of the model systems was calculated to be 3.73 eV (332 nm) for the *ortho*- isomer and 3.46 eV (358 nm) for the *para*- isomer. This is in good agreement with the transitions observed in the UV-Vis spectra of the ligands and the ligand precursors, however on coordination of the **L2** with lanthanide ions there was a high energy

shift to the absorption. This is potentially due to coordination of the amide carbonyl causing steric hindrance, requiring an increase in the torsion angle and a decrease in the extent of aromaticity, hence negating the red-shift normally caused by the electron-withdrawing effect of coordination with lanthanide ions. The greater degree of aromaticity extended to the amide group also explains the downfield shift of the amide resonance observed in the ^{1}H NMR of all the precursors to **L2**, as the proton would be more deshielded in an electron deficient amide.

3.3 – Conclusions

In conclusion two new chromophores have been utilised in which nitro- and methoxy-substituents of an aryl ring cause a red shift of the absorption bands compared to a basic benzamide group, and they have been shown to be capable of sensitising long-lived visible and near-IR emissive lanthanides. This probably occurs *via* excitation into the ligand singlet state, followed by intersystem crossing into the ligand triplet state. Energy is then transferred from the ligand triplet state to the lanthanide excited state. In the case of the *para*- isomer the π-delocalised system is extended onto the amide carbonyl, allowing direct overlap between the ligand and lanthanide orbitals; a prerequisite for lanthanide sensitisation by Dexter exchange. However, in the *ortho*- analogue the extent of π-delocalisation is limited by torsion of the amide group but sensitisation of lanthanide luminescence still occurs. Therefore, in accordance with literature reports[28] Förster resonance energy transfer cannot be ruled out. It has been demonstrated through a combined spectroscopic, structural and theoretical analysis that the position of the methoxy- substituent on the aryl ring causes the steric hindrance, influencing the degree of torsion between the amide group and the plane of the ring and hence the extent of π-delocalisation throughout the system. This in turn dictates the HOMO-LUMO energy gap, which is observed in the red shifting of the less hindered *para*-methoxy isomer as well as the extent of shielding extended to the amide proton.

3.4 - Experimental

General Procedure for the formation of the chloro-acetamides

A large excess (approximately 3 eq.) of chloroacetyl chloride was added to a stirring solution of the substituted aniline (1.0 g) in MeCN (200 mL) and the mixture was stirred for 1 h. The solvent was removed *in vacuo* and ethyl acetate was added, the organic phase washed with water, dried over $MgSO_4$, before the organic washing were removed *in vacuo* to give the title compounds in high yield (typically 95 %). The chloroacetamides were used without further purification.

2-chloro-N-(6-methoxy-2-nitrophenyl)acetamide was isolated as pale yellow crystals (yield 1.41 g, 97%). ^{1}H NMR (400 MHz, $CDCl_3$): δ_H = 3.90 (3H, s, OCH_3), 4.13 (2H, s, CH_2Cl), 7.12 (1H, dd J_{HH} = 1.1 and 8.3, aromatic), 7.28 (1H, t J_{HH} = 8.3 aromatic), 7.48 (1H, dd J_{HH} = 1.1 and 8.3 aromatic) and 9.2 (1H, s br, amide) ppm. UV-VIS λ_{max} (ε / mol^{-1} dm^3 cm^{-1}): 323 (2173) nm. IR ν_{max} ($CHCl_3$): 1698 (C=O), 1512 (NO_2) cm^{-1}. ES$^+$ MS: m/z 245 $\{M + H\}^+$.

2-chloro-N-(4-methoxy-2-nitrophenyl)acetamide was isolated as dark yellow crystals (yield, 93%). ^{1}H NMR (400 MHz, $CDCl_3$): δ_H = 3.81 (3H, s, OCH_3), 4.16 (2H, s, CH_2Cl), 7.18 (1H, dd J_{HH} = 3.0 and 9.3, aromatic), 7.64 (1H, d J_{HH} = 3.0, aromatic), 8.58 (1H, d J_{HH} = 9.3, aromatic) and 11.5 (1H, s br, amide) ppm. UV-VIS λ_{max} (ε / mol^{-1} dm^3 cm^{-1}): 373 (2091) nm. IR ν_{max} ($CHCl_3$): 1694 (C=O), 1514 (NO_2) cm^{-1}. ES$^+$ MS: m/z 244 $\{M+H\}^+$.

General Procedure for the formation of protected ligand precursors

The 2-nitromethoxyphenylcarbamoyl methyl chloride (1.5 eq.) was added to a mixture of the bromide salt of the cyclen triester (0.4 g, 1 eq.), triethylamine (3 eq.) and KI in MeCN and the mixture was heated to reflux for 48 h. The solution was filtered and reduced *in vacuo* and the crude reaction mixture was purified by column chromatography over alumina gel, eluting with DCM → 9:1 DCM:MeOH.

1-(2-nitro,6-methoxyphenylcarbamoyl methyl)-4,7,10-tris(*tert*-butoxycarbonyl)-1,4,7,10-

tetraazacyclododecane was isolated as a brown oil (0.39 g, 75 %). NMR (400 MHz, $CDCl_3$): δ = 1.33 (27H, s, $COOC(CH_3)_3$), 1.90 – 3.74 (24H, br-m, CH_2 ring, NCH_2COO and NCH_2CON), 3.84 (3H, s, OCH_3), 7.06 (1H, dd J_{HH} = 1.1 and 8.3, Ar), 7.18 (1H, d J_{HH} = 8.3, Ar), 7.36 (1H, dd J_{HH} = 1.1 and 8.3, Ar) and 9.21 (1H, s, NH). λ_{max} (ε / mol^{-1} dm^3 cm^{-1}); 220 (10799) and 328 (709). $\upsilon_{max}(CHCl_3)$; 1727 (C=O), 1682 (NC=O), 1522 (NO_2) and 1217 (O-CH_3) ES^+ MS: *m/z* 723 $\{M+H\}^+$.

1-(2-nitro,4-methoxyphenylcarbamoyl methyl)-4,7,10-tris(*tert*-butoxycarbonyl)-1,4,7,10-tetraazacyclododecane was isolated as a brown oil. (0.35 g, 67 %) NMR (400 MHz, $CDCl_3$): δ = 1.35 (27H, s, $COOC(CH_3)_3$), 1.88 – 3.68 (24H, br-m, CH_2 ring, NCH_2COO and NCH_2CON), 3.76 (3H, s, OCH_3), 7.01 (1H, dd J_{HH} = 2.9 and 8.9, aromatic), 7.36 (1H, d J_{HH} = 2.9, aromatic) 7.81 (1H, d J_{HH} = 8.9, aromatic) and 10.10 (1H, s, NH). λ_{max} (ε / mol^{-1} dm^3 cm^{-1}); 239 (87185) and 362 (14267). $\upsilon_{max}(CHCl_3)$; 1732 (C=O), 1518 (NO_2) and 1218 (O-CH_3) ES^+ MS: *m/z* 723 $\{M+H\}^+$.

General Procedure for the deprotection of ligands

The protected ligand precursor (0.2 g) was added to a 1:1 mixture of trifluoroacetic acid:DCM (10 mL) and the mixture was stirred at room temperature overnight. The solvent was removed *in vacuo* and the residue was re-dissolved three times in MeOH to eliminate excess acid. The residue was then dissolved in the minimum volume of MeOH and added dropwise to a stirred diethyl ether at 0 °C. The precipitate was filtered and dried to give the deprotected ligand.

1-(6-methoxy-2-nitrophenyl-N-carbamoylmethyl)-4,7,10-tris(carboxymethyl)-1,4,7,10-tetraazacyclododecane (L1) was isolated as a pale yellow powder. (0.138 g, 86 %); ^1H NMR (400 MHz, D_2O): δ_H = 2.95 – 4.05 (27H, br-m, CH_2 ring, NCH_2COO, NCH_2CON and OCH_3), 7.32 -7.50 (overlapping 3H, Ar). $^{13}C\{^1H\}$ (100 MHz, D_2O) δ_C 49.3 (br), 55.1 (br), 57.0 (-OCH_3) 57.8, 115.2, 117.0, 117.8 (q, CF_3CO_2H), 128.6, 145.6, 152.1, 154.5, 163.2 (q, CF_3CO_2H), 174.5 (br, CO). ES^+ MS: *m/z* 593 $\{M + K\}^+$. Found C, 41.21; H, 5.11; N, 10.22; Expected for $C_{24}H_{34}N_6O_{10}.(CF_3CO_2H)_2$: C, 41.44; H, 4.64; N, 10.74.

1-(4-methoxy-2-nitrophenyl-N-carbamoylmethyl)-4,7,10-tris(carboxymethyl)-1,4,7,10-tetraazacyclododecane (L2) was isolated as a yellow powder (0.102 g. 67 %); ^1H NMR (400 MHz, D_2O): δ_H 2.7-4.1 (27 H, br, m) 3.81 (3H, s, OMe), 7.30-7.49 (2H, overlapping

multiplet, Ar), 7.51 (1H, d, $^1J_{HH}$ = 8.0 Hz, Ar). $^{13}C\{^1H\}$ (100 MHz, D_2O) δ_C 49.4 (br), 53.4 (br), 57.0, 57.8, 62.0, 115.2, 117.8 (q, CF_3CO_2H), 128.5, 145.6, 154.5, 163.2 (q, CF_3CO_2H), 165.2, 174.7, 175.0 (CO). ES^+ MS: *m/z* 593 $\{M + K\}^+$ and 617 $\{M + Cu\}^+$. Found C, 41.15; H, 5.40; N, 10.28; Expected for $C_{24}H_{34}N_6O_{10}.(CF_3CO_2H)_2$: C, 41.44; H, 4.64; N, 10.74.

General Procedure for the formation of lanthanide complexes

A mixture of the ligand (0.020 g) and $Ln(OTf)_3$ was stirred in MeOH (10 mL) at 50 °C for 24h. The solution was reduced *in vacuo* then added dropwise to stirring diethyl ether at 0 °C. The precipitate was filtered, washed with diethyl ether and dried to give the lanthanide complex.

NdL1 was isolated as a pale yellow powder (0.021 g, 95 %). λ_{max} (ε / $mol^{-1}\,dm^3\,cm^{-1}$); 209 (8551) and 327 (964). υ_{max}(nujol); 1600 and 1645 (C=O). ES^+ MS: *m/z* 696 $\{M + H\}^+$. HRMS (ESI^+) found *m/z* 694.1259 $\{M + H\}^+$; $C_{23}H_{32}N_6O_{10}{}^{142}Nd$ requires 694.1252.

EuL1 was isolated as a pale yellow powder (0.020 g, 91 %). λ_{max} (ε / $mol^{-1}\,dm^3\,cm^{-1}$); 210 (8870) and 325 (1014). υ_{max}(nujol); 1599 and 1648 (C=O). ES^+ MS: *m/z* 703 $\{M + H\}^+$. HRMS (ES^+) found *m/z* 703.1383 $\{M + H\}^+$;$C_{23}H_{32}N_6O_{10}{}^{151}Eu$ requires 703.1373.

GdL1 was isolated as a pale yellow powder (0.021 g, 95 %). λ_{max} (ε / $mol^{-1}\,dm^3\,cm^{-1}$); 210 (9381) and 324 (1143). υ_{max}(nujol); 1601 and 1635 (C=O). ES^+ MS: *m/z* 708$\{M + H\}^+$. HRMS (ES^+) found 707.1397 $\{M + H\}^+$;$C_{23}H_{32}N_6O_{10}{}^{154}Gd$ requires 707.1401.

TbL1 was isolated as a pale yellow powder (0.019 g, 86 %). λ_{max} (ε / $mol^{-1}\,dm^3\,cm^{-1}$); 210 (9746) and 325 (1130). υ_{max}(nujol); 1600 and 1635 (C=O). ES^+ MS: *m/z* 711 $\{M + H\}^+$. HRMS (ESI^+) found *m/z* 711.1424 $\{M + H\}^+$; $C_{23}H_{32}N_6O_{10}{}^{159}Tb$ requires 711.1228.

YbL1 was isolated as a pale yellow powder (0.020 g, 87 %). λ_{max} (ε / $mol^{-1}\,dm^3\,cm^{-1}$); 214 (15378) and 321 (1022). υ_{max}(nujol); 1598 and 1630 (C=O). ES^+ MS: *m/z* 724 $\{M + H\}^+$. HRMS (ES^+) found *m/z* 722.1520 $\{M + H\}^+$;$C_{23}H_{32}N_6O_{10}{}^{170}Yb$ requires 722.1522.

NdL2 was isolated as a yellow powder (0.021, 95%). λ_{max} (ε / $mol^{-1}\,dm^3\,cm^{-1}$); 232 (11321) and 340 (1000). υ_{max}(nujol); 1607 and 1635 (C=O). ES^+ MS: *m/z* 694 $\{M + H\}^+$. HRMS

(ES^+) found *m/z* 694.1249 $\{M + H\}^+$;$C_{23}H_{32}N_6O_{10}{}^{142}Nd$ requires 694.1252.

EuL2 was isolated as a yellow powder (0.021, 95 %). λ_{max} (ε / mol^{-1} dm^3 cm^{-1}); 233 (9212) and 338 (1139). υ_{max}(nujol); 1603 and 1638 (C=O). ES^+ MS: *m/z* 703 $\{M + H\}^+$. HRMS (ES^+) found 703.1375 $\{M + H\}^+$;$C_{23}H_{32}N_6O_{10}{}^{153}Eu$ requires 703.1373.

GdL2 was isolated as a yellow powder (0.020, 91 %). λ_{max} (ε / mol^{-1} dm^3 cm^{-1}); 231 (11393) and 338 (1182). υ_{max}(nujol); 1598 and 1640 (C=O). ES^+ MS: *m/z* 708 $\{M + H\}^+$. HRMS (ES^+) found *m/z* 706.1383 $\{M + H\}^+$;$C_{23}H_{32}N_6O_{10}{}^{154}Gd$ requires 706.1383.

TbL2 was isolated as a yellow powder (0.019, 86 %). λ_{max} (ε / mol^{-1} dm^3 cm^{-1}); 238 (5979) and 340 (778). υ_{max}(nujol); 1599 and 1644 (C=O). ES^+ MS: *m/z* 711$\{M + H\}^+$. HRMS (ESI^+) found *m/z* 733.1247 $\{M + Na\}^+$; $C_{23}H_{31}N_6O_{10}{}^{159}TbNa$ requires 733.1255.

YbL2 was isolated as a yellow powder (0.021, 91 %). λ_{max} (ε / mol^{-1} dm^3 cm^{-1}); 214 (13870) and 340 (1164). υ_{max}(nujol); 1635 and 1674 (C=O). ES^+ MS: *m/z* 724 $\{M + H\}^+$. HRMS (ES^+) found *m/z* 722.1521 $\{M + H\}^+$;$C_{23}H_{32}N_6O_{10}{}^{170}Yb$ requires 722.1522.

3.5 - References

1. H. Takahashi, K. Fujita and H. Ohno, *Chem. Lett.*, 2007, **36**, 116-117.
2. A. Fraleoni-Morgera, L. Giorgini and P. Zanirato, *Dyes Pigm.*, 2008, **76**, 394-399.
3. N. Biswas, B. Abraham and S. Umapathy, *J. Phys. Chem. A*, 2002, **106**, 9397-9406.
4. M. R. Han and M. Hara, *New J. Chem.*, 2006, **30**, 223-227.
5. T. Saito and T. Kobayashi, *Opt. mater.*, 2003, **21**, 301-305.
6. F. Xu, Q. P. Yuan and H. R. Dong, *J. Chromatogr. B*, 2006, **838**, 44-49.
7. C. Boga, J. Degani, E. Del Vecchio, R. Fochi, L. Forlani and P. E. Todesco, *Eur. J. Org. Chem.*, 2002, 3837-3843.
8. A. Beeby, L. M. Bushby, D. Maffeo and J. A. G. Williams, *Dalton Trans.*, 2002, 48-54.
9. Y. X. Zheng, M. Motevalli, R. H. C. Tan, I. Abrahams, W. P. Gillin and P. B. Wyatt, *Polyhedron*, 2008, **27**, 1503-1510.
10. M. Woods, G. E. Kiefer, S. Bott, A. Castillo-Muzquiz, C. Eshelbrenner, L. Michaudet, K. McMillan, S. D. K. Mudigunda, D. Grin, G. Tircso, S. R. Zhang, P. Zhao and A. D. Sherry, *J. Am. Chem. Soc.*, 2004, **126**, 9248-9256.
11. V. Tsaryuk, V. Zolin and J. Legendziewicz, *J. Lumin.*, 2003, **102**, 744-750.
12. N. M. Shavaleev, R. Scopelliti, F. Gumy and J. C. G. Bunzli, *Eur. J. Inorg. Chem.*, 2008, 1523-1529.
13. V. F. Zolin, L. N. Puntus, V. I. Tsaryuk, V. A. Kudryashova, J. Legendziewicz, P. Gawryszewska and R. Szostak, *J. Alloys Compd*, 2004, **380**, 279-284.
14. L. N. Puntus, A. S. Chauvin, S. Varbanov and J. C. G. Bunzli, *Eur. J. Inorg. Chem.*, 2007, 2315-2326.
15. Y. H. Kim, N. S. Baek and H. K. Kim, *Chem. Phys. Chem*, 2006, **7**, 213-221.
16. A. D'Aleo, A. Picot, A. Beeby, J. A. G. Williams, B. Le Guennic, C. Andraud and O. Maury, *Inorg. Chem.*, 2008, **47**, 10258-10268.
17. D. B. Nie, Z. Q. Chen, Z. Q. Bian, J. Q. Zhou, Z. W. Liu, F. F. Chen, Y. L. Zhao and C. H. Huang, *New J. Chem.*, 2007, **31**, 1639-1646.
18. M. L. Morningstar, T. Roth, D. W. Farnsworth, M. K. Smith, K. Watson, R. W. Buckheit, K. Das, W. Y. Zhang, E. Arnold, J. G. Julias, S. H. Hughes and C. J. Michejda, *J. Med. Chem.*, 2007, **50**, 4003-4015.
19. M. Makosza and M. Bialecki, *J. Org. Chem.*, 1998, **63**, 4878-4888.
20. S. J. A. Pope and R. H. Laye, *Dalton Trans.*, 2006, 3108-3113.
21. G. A. Crosby, R. M. Alire and R. E. Whan, *J. Chem. Phys.*, 1961, **34**, 743.
22. S. Faulkner and S. J. A. Pope, *J. Am. Chem. Soc.*, 2003, **125**, 10526-10527.

23. E. V. Sayre and S. Freed, *J. Chem. Phys.*, 1956, **24**, 1211-1212.

24. A. Beeby and S. Faulkner, *Chemical Physics Letters*, 1997, **266**, 116-122.

25. W. D. Horrocks, J. P. Bolender, W. D. Smith and R. M. Supkowski, *J. Am. Chem. Soc.*, 1997, **119**, 5972-5973.

26. A. Beeby, I. M. Clarkson, R. S. Dickins, S. Faulkner, D. Parker, L. Royle, A. S. de Sousa, J. A. G. Williams and M. Woods, *J. Chem. Soc. Perkin Trans. 2*, 1999, 493-503.

27. S. Faulkner, A. Beeby, M. C. Carrie, A. Dadabhoy, A. M. Kenwright and P. G. Sammes, *Inorg. Chem. Comm.*, 2001, **4**, 187-190.

28. S. Faulkner, M. C. Carrie, S. J. A. Pope, J. Squire, A. Beeby and P. G. Sammes, *Dalton Trans.*, 2004, 1405-1409.

29. V. Tsaryuk, K. Zhuravlev, V. Zolin, P. Gawryszewska, J. Legendziewicz, V. Kudryashova and I. Pekareva, *J. Photochem. Photobiol. A* 2006, **177**, 314-323.

30. V. I. Tsaryuk, K. P. Zhuravlev, V. F. Zolin, V. A. Kudryashova, J. Legendziewicz and R. Szostak, *J. Appl.Spectrosc.*, 2007, 51-59.

31. J. Nishikawa, T. Imase, M. Koike, K. Fukuda, M. Tokita, J. Watanabe and S. Kawauchi, *Journal of Mol. Struct.*, 2005, **741**, 221-228.

Chapter Four
The development of metal ion responsive luminescent lanthanide complexes

4.1 - Introduction

In order to form a kinetically inert, luminescent lanthanide complex two conditions must be met. Firstly, the ligand must contain a suitable sensitising chromophore, with a donor energy level approximately 2000 cm^{-1} above the excited state of the lanthanide. Secondly, the ligand must be multidentate, in order to fulfil the coordination requirements of large Ln(III) ions and shield the excited states from quenching by contact with surrounding solvent molecules. Although synthetically demanding, these requirements offer several paths by which a target ion or molecule may induce a response in lanthanide luminescence based probe. The presence of the analyte may alter or disrupt the energy transfer process from the chromophore to the metal or change in the coordination sphere of the lanthanide ion, which may involve a change in the degree of solvation. Stable, luminescent lanthanide complexes have been designed which respond to changes in a wide variety of analytes, including pH,[1-3] pO_2[4, 5] and pX (X= halide, hydroxide).[3] The aim of this chapter is to develop systems which respond to the presence of metal ions.

4.1.1 – Lanthanide probes to signal the concentration of s-block metals

Alkali and alkali earth metals are ubiquitous in biological organisms. Sodium and potassium are vital for maintaining fluid and electrolyte homeostasis and changes in their concentration are responsible for the changes in the action potential of neuron membranes. Defects in sodium and potassium ion channels can cause paralysis, epilepsy and deafness and many potent venoms and toxins act by blocking these ion channels.[6] Variations in the concentration of calcium across cell membranes are responsible for muscle contraction and the signalling of light by rod cells in the retina.[7] Proteins bearing phosphate groups are stabilised by chelation to magnesium and ATP, the primary source of energy in cells, exists in cells as a complex of Mg(II), making magnesium vital to all living organisms.[8] The concentration of these ions can vary dramatically between intracellular and extracellular environments, therefore fluorescent probes that can signal their concentration have received a great deal of interest.[9]

One of the earliest examples of a responsive probe based around the modulation of lanthanide luminescence was a complex incorporating a lanthanide binding site, a functionalised terpyridine as an organic chromophore and two monoazacrown ether rings.[10] In pure methanol solution the europium complex is only very weakly luminescent, as PeT from the nitrogen present in the azacrown quenches europium emission. On binding of Na(I) or K(I) the PeT is suppressed and the europium emission, sensitised by irradiation of the terpyridine, was greatly enhanced. Crown and azacrown ethers are well known to bind alkali and alkali earth metals and can be tailored to bind specifically to a particular ion by changing the size of the ring. This versatility has resulted in them being incorporated into several other responsive lanthanide probes.

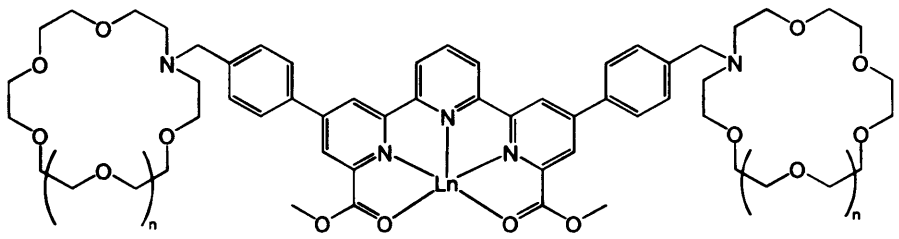

Figure 4.1 – da Silva's s-block metal responsive lanthanide complex.

An early example of a metal ion probe based on a functionalised tetraazamacrocycle was reported by Gunnlaugsson and co-workers.[11] In this case the ligand provided the metal lanthanide ion with an eight coordinate binding site. One of the pendant arms bore an anisidine-functionalised azacrown ether. Between pH 4 and pH 9 the terbium complex showed no emission following excitation of the organic chromophores but on addition of potassium ions the emission was switched 'on'. This was due to binding of potassium by the azacrown ether and the anisidine groups. Coordination of the potassium to the anisidine methoxy and aniline groups caused deconjugation of the nitrogen lone pair from the aromatic system, preventing PeT and allowing terbium sensitisation.

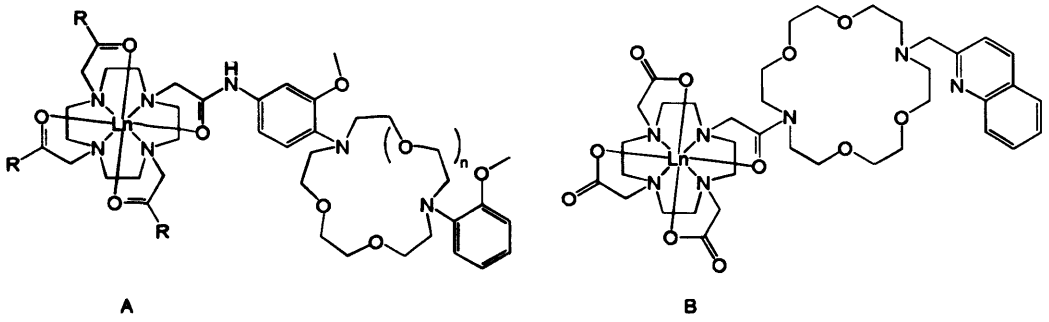

A B

Figure 4.2 – Gunnlaugsson's (A) and Wong's (B) sensors for s-block metals.

A dual pH and K(I) system was developed by Wong and co-workers in which a quinoline functionalised azocrown ether acted as the sensitiser/analyte receptor. Between pH 1 and pH 12 the terbium emission showed two maxima at ~ pH 2 and ~ pH 6, with a trough at ~ pH 4. The resulting four changes were assigned to sequential protonation of the aryl nitrogen, the tertiary amine, the amide nitrogen and the amide oxygen, as the conditions became more acidic. Upon addition of K(I) the terbium emission intensity was modulated with no change in lifetime, indicating the ion had been bound in the azacrown ether and was influencing energy transfer to the terbium. Interestingly the specific effect of K(I) depended on the pH, at pH 2.2 the emission was quenched whereas at pH 6.3 the emission intensity was enhanced.[12]

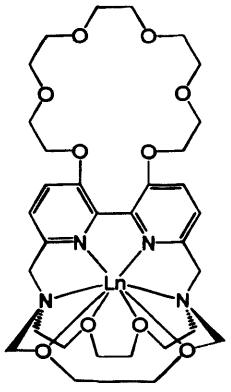

Figure 4.3 – A barium sensor based on a bipyridyl cryptate.

As mentioned above one of the potential benefits of luminescent lanthanide probes is the possibility of using NIR emissive metals, which could allow the imaging of biological tissue at greater depth. The first case of an *s*-block metal modulating the emission of a NIR emissive metal was reported by Pope and co-workers. In this case

a bipyridine-based chromophore is functionalised on one side with an octadentate binding site, suitable for binding lanthanide ions, and on the other side with a hexadentate crown ether unit, suitable for binding *s*-block metals. It was found that on addition of barium the absorption profile of the neodymium complex was significantly blue-shifted. This change was observed in the neodymium emission spectrum (λ_{ex} = 350 nm) as a decrease in intensity on addition of barium. The change was attributed to the binding of barium to the crown ether increasing the torsion angle between the two pyridine rings.[13]

4.1.2 - Lanthanide probes to signal the concentration of d-block metals

Sensors for Zinc(II)

Of the *d*-block elements, the metal that has attracted the most attention as the target for luminescent lanthanide probes has been zinc. Zinc is the second most abundant heavy metal in the human body, with a serum concentration of ~ 14 μM.[14] It is the most frequently utilised metal in protein and enzyme function.[15] The concentration of chelatable zinc varies throughout the body, but is particularly high in the synapses in the brain where it acts as an endogenous signalling substance.[16] High concentrations of free zinc have been shown to cause neuronal degeneration and have been implicated in the development of Alzheimer's disease.[17] In order to elucidate the various roles of zinc in the normal functioning of cells and its mishandling in disease there has been a great deal of interest in developing luminescent probes capable of signalling the intra- and intercellular concentration of free zinc.

The earliest reported zinc-responsive lanthanide complex utilised a tetraazamacrocycle functionalised with a receptor which also acted as the sensitising chromophore. The receptor site was similar to the 'London' type ligand, however the aniline had been replaced with a benzylic nitrogen, which promoted selectivity towards zinc over magnesium or calcium. The addition of zinc resulted in an enhancement of europium and terbium emission following excitation of the chromophore at 262 nm. This enhancement was not associated with a change in lifetime or the structure of the emission, indicating that the coordination environment had not been influenced. The increase in intensity was attributed to the zinc induced

suppression of PeT.[18]

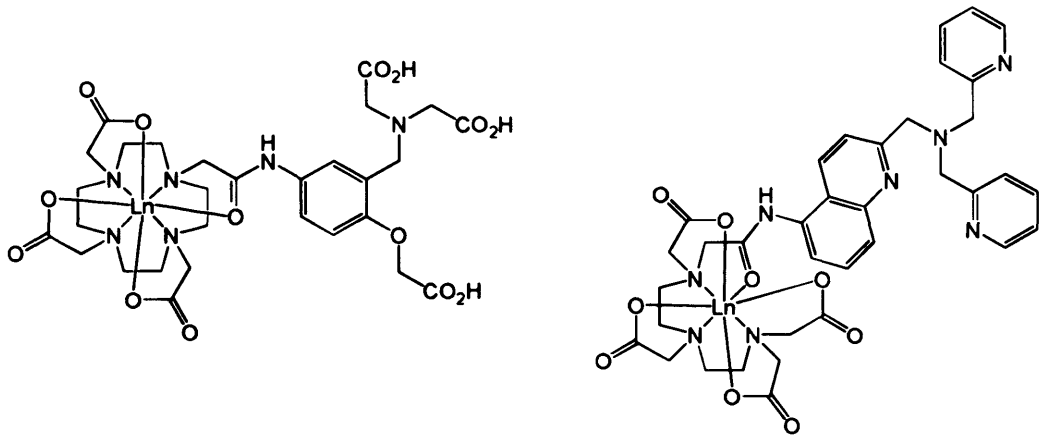

Figure 4.4 – Parker's (A) and Kikuchi and Nagano's (B) luminescent lanthanide sensors for Zn(II).

A system reported by Kikuchi, Nagano and co-workers demonstrated the potential of europium based complexes to monitor zinc concentration in a cellular environment. The complex was made up of an octadentate, lanthanide binding site and a zinc receptor which incorporated an amido quinolyl chromophore, allowing excitation wavelengths of up to 340 nm. The addition of zinc caused slight changes in the absorption spectrum of the europium complex but a significant enhancement in the ligand and metal-based emission spectrum. As the change in the number of inner sphere solvent molecules and the change in structure of the europium emission were negligible it was deduced that there was very little change in the coordination sphere of the europium. Instead the changes in the emission spectrum were attributed to a zinc induced lowering of the organic triplet state energy level, allowing more efficient sensitisation of europium.[19]

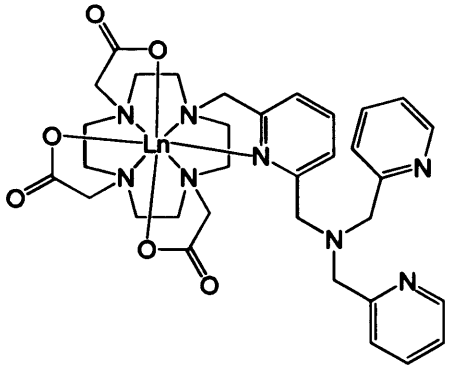

Figure 4.5 – A 'hydration switch' style luminescent lanthanide sensor for Zn(II).

One of the limitations of 'emission intensity'-based responsive probes is the inability to distinguish between changes in the concentration of the analyte and changes in the concentration of the probe. Ideally the presence of an analyte should induce a change in the coordination sphere of the lanthanide, this could induce a change in the lifetime of the metal-based luminescence and in the case of terbium and europium a change in the relative intensity of the hypersensitive emission bands. Both of these would allow probe concentration independent signalling of the presence of an analyte. The potential for zinc to influence changes in the coordination sphere europium was demonstrated by a system reported by Pope and co-workers. The receptor site was formed from three pyridine units linked by a tertiary amine. In the absence of zinc one of the pyridine units bound directly to the europium. In the presence of zinc this pyridine became unbound from the europium and participated in the coordination of zinc. This allowed an additional solvent molecule to bind to the metal centre, which was observed as a decrease in the luminescence lifetime and a change in the emission profile.[20] Zinc induced changes in the q value of a lanthanide has also been reported in work towards responsive MRI contrast agents by Nagano and co-workers[21] and Sherry and co-workers.[22] In these systems zinc induces a folding in the ligand, limiting access of the solvent molecules to the gadolinium and decreasing relaxivity.

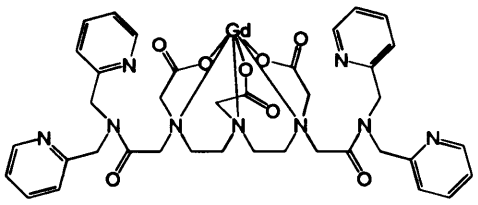

A

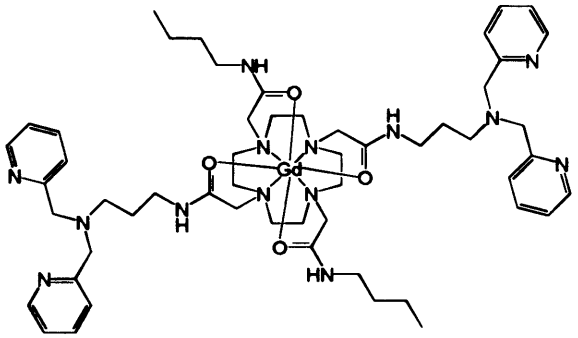

B

Figure 4.6 – Nagano (A) and Sherry's (B) Zn(II) responsive MRI contrast agents.

Sensors for Copper(II)

As a redox active metal copper is less prevalent in biological systems than zinc. However, there are still a great number of copper containing proteins and enzymes and a loss of control of copper homeostasis can result in oxidative stress, which is thought to be implicated in Alzheimer's, Parkinson's and Prion diseases.[23] Given its vital role in the healthy function of cells as well as the wide range of adverse effects associated with the mismanagement of copper, a luminescent probe capable of signalling its concentration at low level would be of great interest in the fields of biochemistry and pathology.

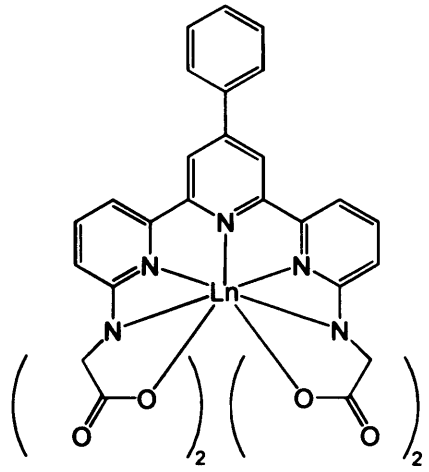

Figure 4.7 – Kessler's Cu(II) responsive lanthanide probe.

Among the first responsive luminescent lanthanide probes to be reported was a copper sensitive system developed by Kessler. The ligand was formed of a functionalised terpyridine chromophore and although it had no additional metal binding site it was found that the addition of Cu(II) strongly quenched both the intensity and the lifetime of the europium emission. The mechanism of the quenching was attributed to the overlap between the absorption bands of the Cu(II) and the emission bands of the europium. However, although other coloured ions such as Cr(III) had a slight quenching effect it was not as strong as would be expected from the extent of overlap between their absorption bands and the europium emission bands, indicating that an alternative quenching process is responsible for the effect of Cu(II).[24]

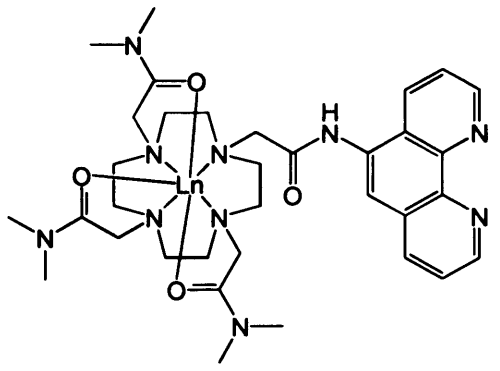

Figure 4.8 – Gunnlaugsson's Cu(II) responsive luminescent lanthanide probe.

A copper-responsive probe based around a tetraazamacrocyclic ligand was reported by Gunnlaugsson *et al.* The complex incorporated a *phen* chromophore and had

previously shown to be sensitive the pH, due to protonation of the aryl nitrogen atoms. In the presence of copper supramolecular ternary (CuL_2) and quaternary (CuL_3) complexes were formed, with two or three europium complexes coordinating to the copper ions *via* the *phen* groups. This induced a strong quenching effect on both the ligand and the Eu(III)-based emission which was attributed to electron-transfer quenching of the ligand singlet state, which prevented population of the lanthanide excited state.[25]

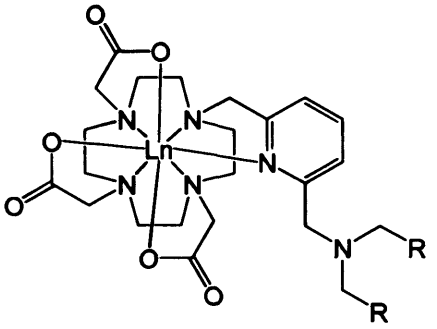

Figure 4.9 – The general design of Chang's copper responsive MRI contrast agents.

The potential of Cu(II) to alter the hydration state of lanthanide ions has been demonstrated by Chang *et al.* who have exploited the concept developed by Pope *et al* and designed a series of complexes in which binding of copper causes a pyridine unit to dissociate from gadolinium, increasing the relaxivity of the complex. By incorporating thioether donors a selectivity towards Cu(I) was established.[26]

The aim of this chapter was to examine the potential of three new lanthanide complexes to act as metal ion sensors. The effect of modifying a binding site by incorporating harder or softer donors was studied. The mode of response was intended to be a change in coordination sphere of metal accompanied with an increase in the number of inner sphere solvent molecules, rather than simply a change in intensity of emission.

4.2 – Results and Discussion

4.2.1 – Synthesis and characterisation of ligands and complexes

The synthetic target was based on that of the Pope zinc sensor.[20] However, rather than a chromophoric metal-ion receptor site being pre-formed and then appended to the macrocycle, a pyridine-functionalised macrocyclic was synthesised as a versatile synthon to various derivatives. The *tert*-butyl triester derivative of cyclen **1** was reacted with two equivalents of 2,6-bis-(chloromethyl)-pyridine **2**. The excess pyridine starting material was then separated by column chromatography to give the desired product, a chloromethyl-pyridine functionalised macrocycle **3**, as a pure, pale yellow oil at ~ 80 % yield. ^{1}H NMR indicated the presence of two unique *tert*-butyl groups, a methylene group at 4.58 ppm and three unique aromatic proton resonances. Electrospray mass spectrometry (ES+ MS) revealed a parent ion peak assigned to $\{M+H\}^+$ at *m/z* 654, indicating the presence of chloride and confirming that the reaction had occurred without hydrolysis.

Firstly this was reacted with an excess of diethyl iminodiacetate and the desired product **4** was purified by column chromatography. ^{1}H NMR showed very slight shifts in the *tert*-butyl ester, methylene and aromatic groups as well as the presence of two ethyl ester groups. From this protected precursor two different ligands were obtained. The *tert*-butoxy groups could be deprotected with trifluoroacetic acid in dichloromethane (1:1), leaving the two ethyl esters intact to give **L1**. ^{1}H NMR was used to confirm that this reaction had gone to completion and ES+ MS showed ion peaks corresponding to $\{M+Na\}^+$ and $\{M+K\}^+$ at *m/z* 661 and 677 respectively, confirming that the deprotection had occurred without cleavage of the ethyl esters. Alternatively the ethyl esters could be deprotected in a concentrated sodium hydroxide solution of aqueous ethanol. The completion of this reaction was confirmed using ^{1}H NMR, which indicated the absence of ethyl ester groups, before the *tert*-butoxy groups were deprotected in trifluoroacetic acid : dichloromethane to give **L2**. Again ^{1}H NMR confirmed this reaction had proceeded to completion and ES+ MS indicated that it had occurred without cleavage of the chromophoric metal binding site, with a peak at *m/z* 621 corresponding to $\{M+K\}^+$. Each ligand was reacted with $Eu(OTf)_3$ in methanol at 50 °C for 24 h to yield the complexes **EuL1** and

EuL2. HRMS was carried out on **EuL1**, which confirmed the isolation of the desired complex and showed the isotope pattern characteristic of europium. The mass spectrum of **EuL2** showed the desired species as an ammonium adduct, presumably due to the conditions used for ionisation.

((2-pyridylmethyl)(2-thiophenemethyl))-amine was synthesised according to literature precedent[27] before being coupled with **3** to give ligand precursor **5**. The reaction mix was filtered to remove inorganic salts and the solvent was removed *in vacuo*. The residue was dissolved in the minimum amount of hot toluene and left to precipitate at – 20 °C for three days, after which time the solvent was decanted to leave the pure product as a brown oil. ^{1}H NMR indicated the absence of methylene chloride and ES+ MS showed a parent ion peak at *m/z* 822 corresponding to $\{M+H\}^+$. Conversion of the *tert*-butyl esters to the carboxylic acids was carried out with trifluoroacetic acid to give **L3**, using ^{1}H NMR to confirm the reaction had gone to completion. ES+ MS showed a peak at *m/z* 676 corresponding to $\{M+Na\}^+$ and a peak at *m/z* 692 corresponding to $\{M+K\}^+$. EuL3 was formed as previously described for EuL1 and EuL2 and characterised by HRMS, which showed the desired species had been isolated and gave the predicted isotope pattern.

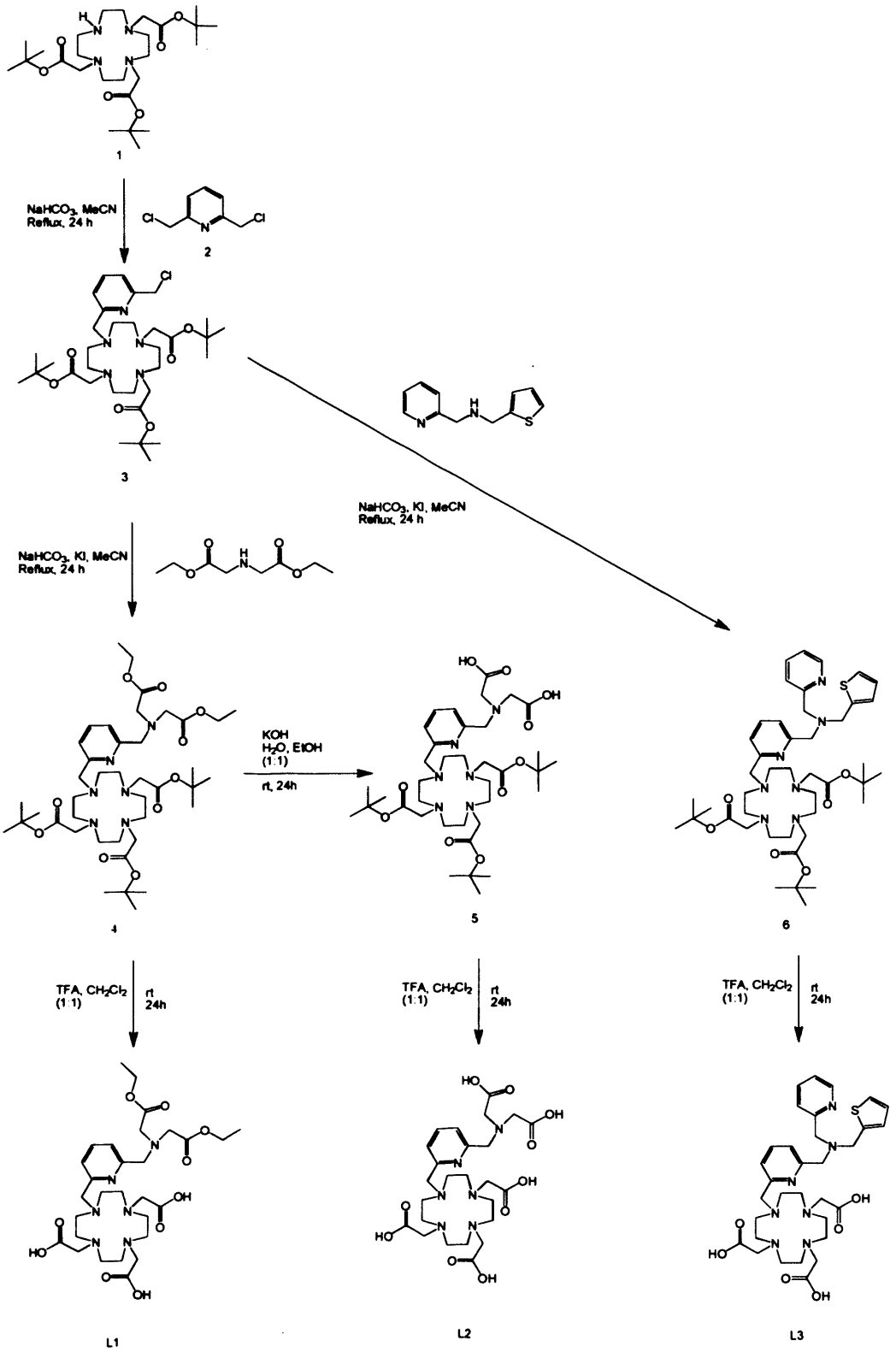

Figure 4.10 – Synthetic strategy towards L1, L2 and L3.

Slow diffusion of hexane into a concentrated chloroform solution of **5** yielded block-like yellow crystals suitable for structural analysis by X-ray crystallography (figure 4.11), which revealed the ligand precursor encapsulating a sodium ion with an iodide counterion. The sodium ion was bound by the four macrocyclic amines, the three ester carbonyl groups and the proximate pyridine nitrogen, neither the terminal pyridine nor the thiophene were bound to the central ion. This confirms the proposed formulation and supports the hypothesised binding mode of **L3** with a lanthanide ion, as the sodium complex of the precursor of the closely related dipicoline analogue was found to predict the coordination environment of the lanthanide ion in the final ligand.[20] The parameters associated with the crystal data are shown in table 1.

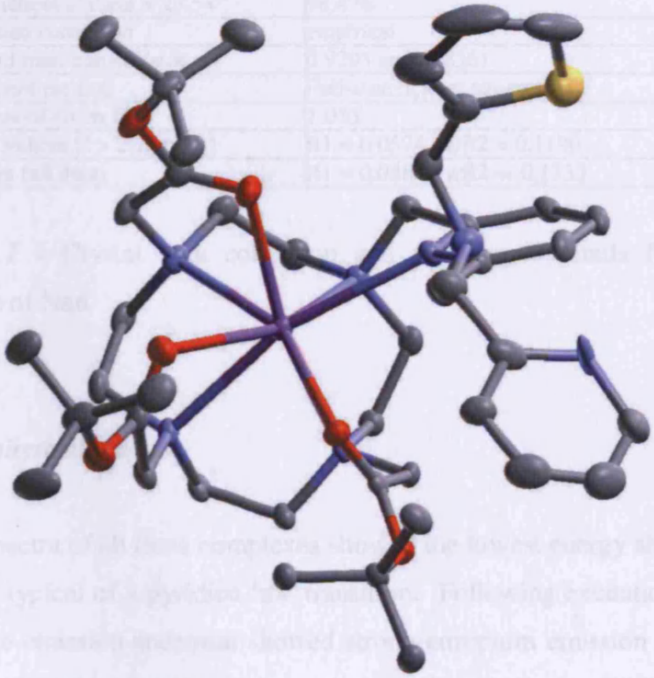

Figure 4.11 – Crystal structure of the *tert*-butyl ester precursor to **L3**, as a sodium complex (counter ion omitted for clarity).

Na6	
Empirical formula	$C_{44}H_{69}IN_7NaO_7S$
Formula weight	990.01
Temperature	150 K
Wavelength	0.71073
Crystal system	Triclinic
Space group	P-1
Unit cell dimensions	a = 12.3890(2)Å, α = 81.823(1)°
	b = 14.0610(2)Å, β = 85.133(1)°
	c = 16.1550(4)Å, γ = 64.010(1)°
Volume	2503.11(8) $Å^3$
Z	2
Density (calculated)	1.314 Mg/m^3
Absorption coefficient	0.742 mm^{-1}
F(000)	1036
Crystal size	0.25 x 0.20 x 0.10 mm
Theta range for data collection	2.92 to 27.54°
Reflections collected	11357
Independent reflections	8284
Completeness to theta = 27.54°	98.4 %
Absorption correction	empirical
Max. and min. transmission	0.9295 and 0.8361
Refinement method	Full-matrix least squares on F
Goodness-of-fit on F	1.033
Final R indices [I > 2sigma(I)]	R1 = 0.0574 , wR2 = 0.1190
R indices (all data)	R1 = 0.0887 , wR2 = 0.1333

Table 4.1 - Crystal data collection and refinement details for the crystal structure of **Na6**.

4.2.2 – Photophysical studies

The UV-Vis spectra of all three complexes showed the lowest energy absorption at *ca.* 260 - 265 nm, typical of a pyridine $^1\pi\pi^*$ transition. Following excitation of this band the steady state emission spectrum showed strong europium emission due to the $^5D_0 \rightarrow {}^7F_J$ transitions. The intensity of the emission allowed the J = 0,1,2,3 and 4 peaks to be resolved. Significant differences in the relative intensity of these peaks were observed between the three complexes which indicates that the terminal donors in the metal receptor site are binding to the lanthanide to some extent. In particular the $J = 2$ band is known to be hypersensitive, and is enhanced by increased donor polarity.[28] In the current series of complexes increasing the chemical hardness of the donor in the metal receptor site significantly increases the $J = 2/J = 1$ ratio (Figure 4.12), from ~ 0.8 for **L3** (thiophene donor) to ~ 2 for **L2** (carboxylate donors). This was confirmed

by time-resolved data obtained in H_2O and D_2O (Table 4.2). The lifetimes of the europium phosphorescence in all three complexes were very similar and on the millisecond scale, which correlates well with literature precedent. Application of the Parker modification of the Horrocks equation to the lifetimes in deuterated and non-deuterated solvents allows an estimation of the number of inner sphere solvent molecules; $q = 1.2(\tau_H^{-1} - \tau_D^{-1} - 0.25)$.[29] In this case q was approximately 0 for each complex, as reported for the original zinc receptor, indicating that the ligand is nine-coordinate, completely encapsulating the lanthanide ion.

Complex	τ_H (ms)	τ_D (ms)	q
EuL1	1.0	1.6	0
EuL2	0.9	1.5	0
EuL3	1.0	1.5	0
EuL3 + Hg(II)	0.4	1.5	2

Table 4.2 – Lifetimes and number of inner sphere solvent molecules (q) for **EuL1**, **EuL2** and **EuL3**.

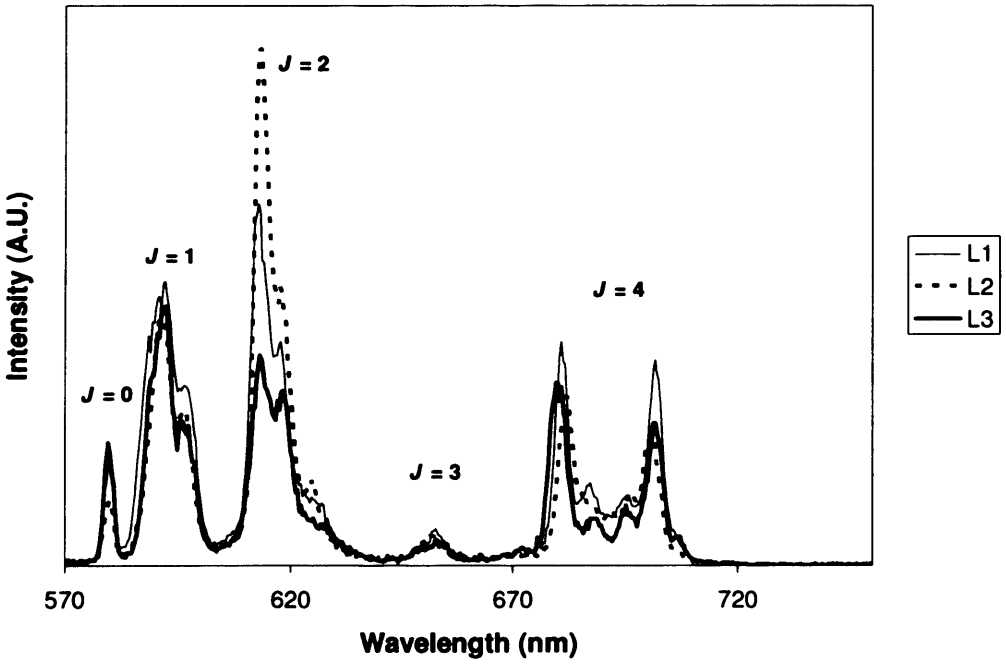

Figure 4.12 – Emission profile of **L1**, **L2** and **L3**, showing the relative increase in intensity of the $J = 2$ peak with the increase in donor hardness.
$\lambda_{ex} = 280$ nm, H_2O, 298 K

4.2.3 – Metal binding studies

S-block metals

The potential for **EuL2** to act as a sensor for harder metals was examined by titration with Li(I), K(I) and Ca(II), however neither the overall intensity or the structure of the europium emission were influenced. It is likely that in an aqueous environment the presence of only two hard donors in a chelating receptor site, as well as the proximity of a hard lanthanide ion, was not sufficient to induce binding of these alkali metal ions.

Group 12 metals

In order to study the effect of incorporating donors of different chemical hardness into the metal receptor site the complexes were first titrated against the group twelve metals. Unlike the closely related complex reported by Pope the complexes showed little response to zinc and the quenching effect of cadmium was only very slight even after the addition of ten equivalents of $Cd(ClO_4)_2$. However all the complexes showed a significant decrease in the intensity of the europium emission in the presence of mercury.

EuL3 showed the greatest selectivity. The slight drop in emission intensity after the addition of ten equivalents of Zn(II) and Cd(II) (< 10 %) could be attributed to dilution during the course of the titration. However, on addition of ten equivalents of Hg(II) the emission intensity of the $J = 2$ peak dropped by 80 %, this was accompanied by a change in ratio of the $J = 1/J = 2$ peaks (Figure 4.13), indicating a change in the coordination environment of the europium. Analysis of the lifetime of the europium complex in H_2O in the presence of mercury showed a bi-exponential decay, indicating the presence of two emissive species. One of these was very similar to the lifetime obtained for the free complex, the other was significantly shorter. It is likely that the shorter lifetime was due to a species in which mercury occupied the receptor site. The lifetime of **EuL3** in D_2O did not change on addition of mercury. It is probable that the mercury ions were still occupying the binding site, but the resultant species had a very similar lifetime to the free complex. Applying the

Horrocks equation to the lifetimes assigned to the mercury-bound species in water and D_2O resulted in a new q value approximately 2. This is consistent with the hypothesised binding mode of the receptor site, which reduces the ligand to heptadentate with respect to the europium ion, leaving it available to coordination by two solvent molecules as observed in the closely related zinc sensor.

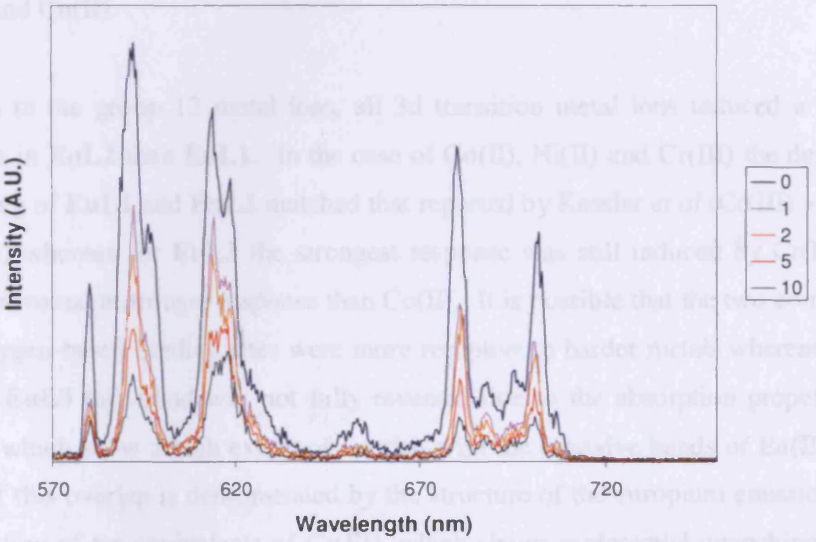

Figure 4.13 – Change in emission spectrum of **EuL3** on addition of Hg(II).
λ_{ex} = 280 nm, H_2O, 298 K, [**EuL3**] = 1.2 mmol.

This correlates well with literature precedent as mercury is well known thiophilic metal and replacing a single nitrogen-based donor with a sulphur-based donor has been known to completely shift the selectivity of a metal probe from zinc to mercury. A Zn(II) probe developed by Lippard and co-workers, Zinpyr 1, replied on a bis(2-pyridylmethyl)aminomethylaniline receptor site to selectively bind to zinc.[30] Replacing a single pyridine donor with a thioether (MS4) induced a selectivity for Hg(II) over Zn(II) and Ni(II).[31]

EuL1 and **EuL2** were less selective but showed the same trend. Despite bearing two harder donors **EuL2** was more efficiently quenched by each metal than **EuL1**. It is possible that the ethyl ester groups caused steric hindrance, preventing the binding of the metals.

Cu(II) and other 3d transition metal ions.

As a comparison with the MRI contrast agents developed by Chang[26] and the degree of quenching observed in the luminescent europium complexes reported by Kessler[24] and Gunnlaugsson[25] the complexes L1, L2 and L3 were titrated against Co(II), Ni(II), Cr(III) and Cu(II).

As seen in the group 12 metal ions, all 3d transition metal ions induced a greater response in **EuL2** than **EuL1**. In the case of Co(II), Ni(II) and Cr(III) the degree of quenching of **EuL1** and **EuL2** matched that reported by Kessler *et al* (Cr(III) > Co(II) > Ni(II)) whereas for **EuL3** the strongest response was still induced by Cr(III) but Ni(II) provoked a stronger response than Co(II). It is possible that the two complexes with oxygen-based binding sites were more receptive to harder metals whereas in the case of **EuL3** this trend was not fully reversed due to the absorption properties of Cr(III), which show a high extent of overlap with the emissive bands of Eu(II). The effect of this overlap is demonstrated by the structure of the europium emission after the addition of ten equivalents of Cr(III), which shows preferential quenching of the shorter-wavelength J = 0,1 and 2 peaks (Figure 4.14), most likely due to an internal filter effect.

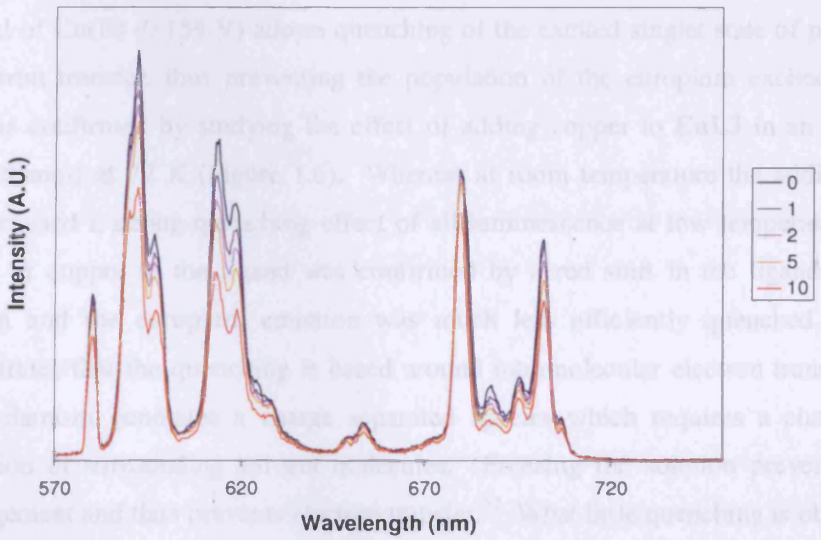

Figure 4.14 – Effect of Cr(III) on emission of **EuL3**.
λ_{ex} = 280 nm, H_2O, 298 K, [**EuL3**] = 1.2 mmol.

In all cases the addition of Cu(II) caused a much greater quenching effect than can be justified in term of its chemical softness or absorption properties, with intensity of the europium emission reduced by *ca.* 90 % after the addition of five equivalents.

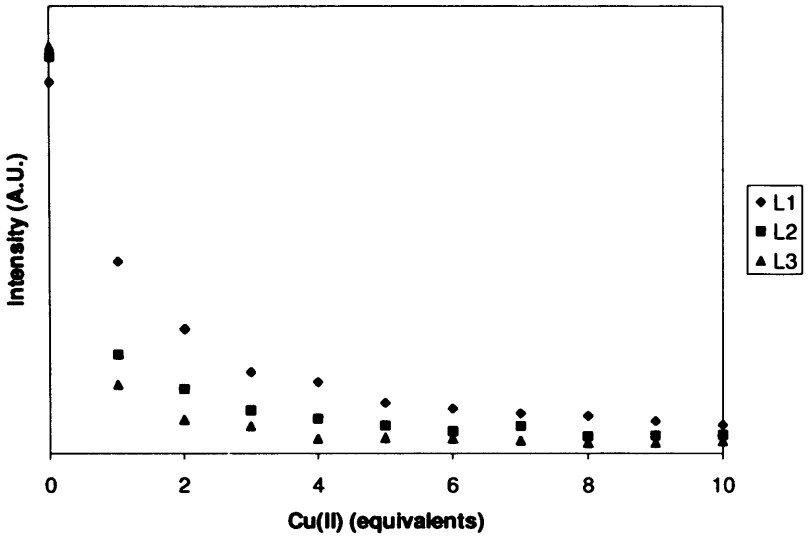

Figure 4.15 – Quenching effect of Cu(II) on emission intensity of the $J = 1$ peak of **EuL1**, **EuL2** and **EuL3**.

This is in accordance with the results reported by Gunnlaugsson.[25] The low reduction potential of Cu(II) (0.159 V) allows quenching of the excited singlet state of pyridine by electron transfer, thus preventing the population of the europium excited state. This was confirmed by studying the effect of adding copper to **EuL3** in an optical glass (ethanol) at 77 K (Figure 1.6). Whereas at room temperature the addition of copper caused a strong quenching effect of all luminescence at low temperature the binding of copper to the ligand was confirmed by a red shift in the ligand triplet emission and the europium emission was much less efficiently quenched. This demonstrates that the quenching is based around intramolecular electron transfer, as this mechanism generates a charge separated species which requires a change in orientation of surrounding solvent molecules. Freezing the solution prevents this rearrangement and thus prevents electron transfer.[32] What little quenching is observed may be attributed to Förster energy to the absorption bands of Cu(II), as observed with the other coloured metal ions, since this mechanism does not require solvent

reorganisation.

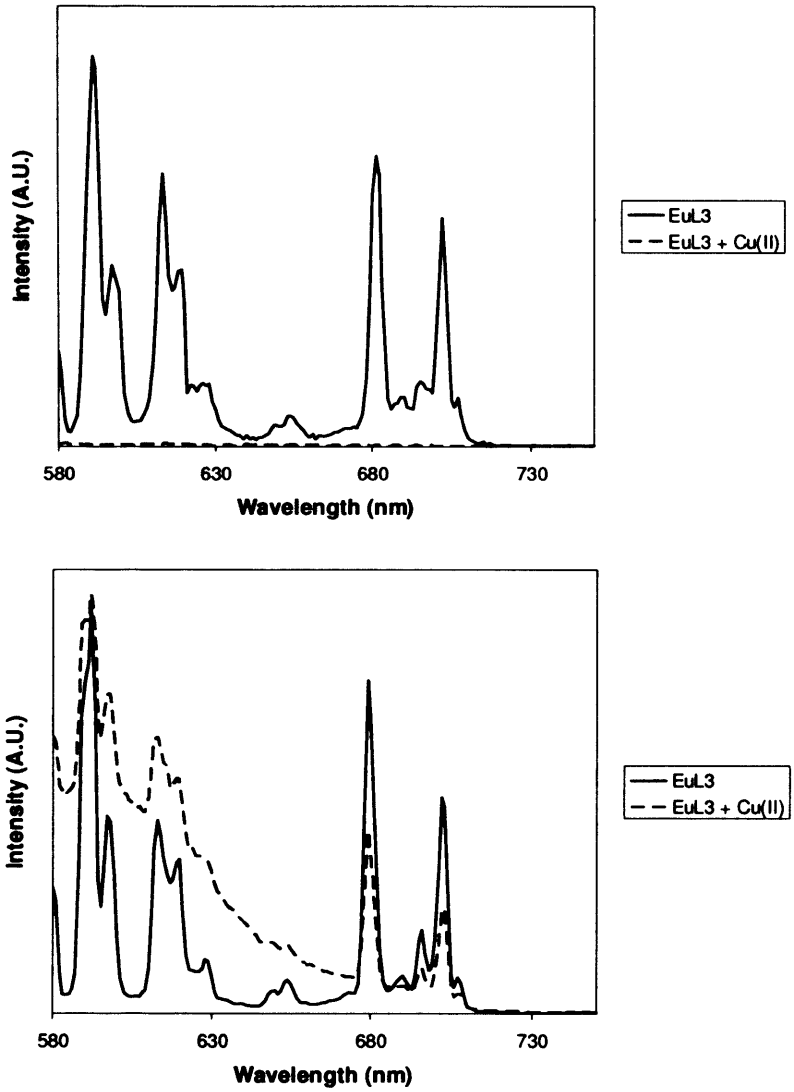

Figure 4.16 – Emission spectra of **EuL3** with and without Cu(II) at room temperature (top) and at 77 K (bottom).

4.3 – Conclusions

Three new ligands and the corresponding luminescent europium complexes bearing metal ion receptor sites have been synthesised. Following irradiation at 280 nm all complexes show intense, well-resolved europium emission and by comparison of the lifetime in deuterated and non-deuterated solvent and by utilisation of the Horrocks

equation it has been shown that the ligands are all nine-coordinate, completely encapsulating the europium ion. Direct coordination of the pyridine to the europium would allow sensitisation by a Dexter mechanism, however due to the proximity of the donor energy transfer by a Förster-type mechanism cannot be ruled out. It has been shown that incorporating a soft, thiophene donor into the receptor site induces a high degree of selectivity for mercury over other group 12 metals in **EuL3**. Based on steady state and luminescence lifetime data it can be deduced that the presence of mercury causes the pyridine to become unbound from the europium. This allows direct coordination of solvent molecules, which is observed as a decrease in the luminescent lifetime as well as a change in ratios of the intensity of the $J = 1/J = 2$ peaks. The general decrease in emission intensity may also be due to a decrease in the efficiency of energy transfer from the chromophore to the europium ion as a result of the groups no longer directly binding to each other.

While selectivity towards soft metals can be induced by incorporating a soft donor into the metal receptor site incorporating hard carboxylate donors, as in **EuL2**, does not induce selectivity towards hard, s-block metals. This is likely due to the small number of hard donors in the receptor site, the proximity of a hard lanthanide ion and coordination of the s-block metal by surrounding water molecules. However, in the case of the borderline d-block metals a slight preference for harder metals is observed.

In the case of **EuL3** the greater quenching effect of metals with a higher extent of overlap between the europium emissive bands and the guest-metal absorption bands indicates that quenching can take place via a Förster resonance energy transfer mechanism. The extremely efficient quenching of luminescence by copper indicates that an alternative process is taking place, most likely quenching of the pyridine singlet excited state by electron transfer to the copper.

4.4 – Experimental

1-(6-chloromethylpyridine-2-methyl)-4,7,10-tris(tert-butoxycarbonyl)-1,4,7,10-tetraazacyclododecane (1) 2,6-bis(chloromethyl)pyridine (0.102 g, 2 eq) and NaHCO3 (0.048 g, 2 eq) was added to a solution of 4,7,10-tris(carboxymethyl)-1,4,7,10-tetraazacyclododecane (0.172 g, 1 eq) in MeCN (10 mL) and the mixture was heated to reflux for 1d with stirring after which time it was allowed to cool, filtered over gravity and the solvent was removed in vacuo. The mixture was separated by column chromatography (silica gel, CH_2Cl_2 → 1:9 MeOH:CH_2Cl_2) to give the desired product as a pale yellow oil (0.16 g, 84%). ^{1}H NMR (400 MHz, $CDCl_3$): δ = 1.32 (18H, s, $C(CH_3)_3$), 1.43 (9H, s, $C(CH_3)_3$), 2.15 – 2.78 (16H, br-m, ring CH_2), 2.72 – 2.90 (6H, br-m, NCH_2COO), 2.97 (2H, br-s, NCH_2), 4.58 (2H, s, CH_2Cl), 7.16 (1H, d J_{HH} = 7.6 , Aro), 7.35 (1H, d J_{HH} = 7.7, Aro) and 7.69 ppm (1H, t J_{HH} = 7.7, Aro). ^{13}C{1H} (62.5 MHz, $CDCl_3$) δC 26.9, 27.0, 45.2, 49.5 (br), 52.5, 55.0, 55.7, 58.5, 66.9, 81.2, 81.4, 120.3, 122.3, 137.3, 156.1, 156.9, 171.1 and 172.0 ppm. λ_{max} (ε / mol^{-1} dm^3 cm^{-1}); 210 (7396) and 265 (3505) nm. ES+ MS: m/z 654 {M+H}+. IR υ_{max} ($CHCl_3$): 1101, 1228, 1370, 1426, 1474, 1522, 1727, 1794, 2253 and 2400 cm^{-1}.

***N*(diethylacetate)-6-aminomethylpyridine-2-methyl-4,7,10-tris(*tert*-butoxycarbonyl)-1,4,7,10-tetrazacyclododecane (3)** diethyl iminodiacetate (0.034 g, 1.8 x 10^{-4} mol, 1 eq.), $NaHCO_3$ (0.045 g, 5.4 x 10^{-4} mol 3 eq.) and KI (cat.) were added to a stirred solution of 1-(6-chloromethylpyridine-2-methyl)-4,7,10-tris(*tert*-butoxycarbonyl)-1,4,7,10-tetraazacyclododecane (1) (0.118 g, 1.8 x 10^{-4} mol, 1 eq.) in MeCN and the mixture was heated to reflux under N_2. After 16h the mixture was allowed to cool and filtered over gravity before being reduced *in vacuo*. The crude reaction mixture was purified by column chromatography over silica gel, eluting with Et_2O → CH_2Cl_2 to gain the title product as a pure yellow oil (0.096 g, 66 %); NMR (400 MHz, $CDCl_3$): δ_H = 1.18 (6H, t J_{HH} = 7.1, CH_2CH_3), 1.35 (18H, s, $C(CH_3)_3$), 1.43 (9H, s, $C(CH_3)_3$), 2.15 – 2.60 (6H, br-m, NCH_2COO), 2.65 – 3.10 (16H, br-m, ring CH_2), 2.99 (2H, br-s, ring-CH_2-pyr), 3.42 (4H, s, NCH_2), 3.90 (2H, s, pyr-CH_2-N), 4.08 (4H, t J_{HH} = 7.1, CH_2CH_3), 7.20 (1H, d J_{HH} = 10, Aro), 7.56 (1H, d J_{HH} = 10.6, Aro) and 7.61 ppm (1H, t J_{HH} = 12, Aro). ^{13}C{^{1}H} (62.5 MHz, $CDCl_3$) δ_C = 13.3,

1083, 1157, 1247, 1408, 1444, 1581, 1728, 2037, 2162 and 2361 cm^{-1}.

***N*(diaceticacid)-6-aminomethylpyridine-2-methyl-4,7,10-tris(*tert*-butoxycarbonyl)-1,4,7,10-tetrazacyclododecane (4)** A solution of NaOH (2M) was added to a solution of **3** (0.200 g, 2.4 mmol, 1 eq.) in EtOH and the mixture was stirred at room temperature overnight. The solution was then neutralised by addition of 2M HCl and the solvent was removed *in vacuo*. Ethyl acetate was added and the mixture was sonicated before being filtered over gravity to remove inorganic salts. The solvent was removed *in vacuo* to give the title product as a pure yellow solid. Cleavage of the ethyl groups was confirmed by ^1H NMR (400 MHz, $CDCl_3$): δ_H = 1.40 (27H, s, $C(CH_3)_3$), 2.10 – 2. 60 (6H, br-m, NCH_2COO), 2.60 – 3.05 (16H, br-m, ring CH_2), 2.95 (2H, br-s, ring-CH_2-pyr), 3.40 (2H, br-s, pyr-CH_2-N) 3.60 (4H, br-s, NCH_2), 7.34 (2H, m, Aro) and 7.61 ppm (1H, t J_{HH} = 7.6, Aro). The product was then deprotected according to the standard procedure to give ***N*(diacetic acid)-6-aminomethylpyridine-2-methyl-4,7,10-tris(carboxymethyl)-1,4,7,10-tetrazacyclododecane (3) (L2)** as a red powder (0.078 g, 54 %); NMR (400 MHz, D_2O): δ_H = 2.80 – 3.73 (22 H, br-m, ring H), 3.69 (2H, s, ring-CH_2-pyr), 3.82 (4H, s, CH_2COOH), 4.51 (2H, s, pyr-CH_2-pyr), 7.40 (1H, d J_{HH} = 7.8, pyr), 7.64 (1H, d J_{HH} = 7.8, pyr) and 7.83 ppm (1H, t J_{HH} = 8, pyr). ES+ MS: *m/z* 621 $\{M+K\}^+$. UV-VIS λ_{max} (ε/$mol^{-1}dm^3cm^{-1}$): 207 (5808) and 263 (3020) nm. IR ν_{max}($CHCl_3$): 1124, 1179, 1348, 1383, 1631, 1673, 2048 and 2164 cm^{-1}.

EuL2 was isolated as a pale yellow powder (0.02, 87 %); ES+ MS: *m/z* 782 $\{M+3NH_3\}^+$. λ_{max} (ε/$mol^{-1}dm^3cm^{-1}$): 216 (3577) and 268 (2478) nm. IR ν_{MAX}(ATR, solid): 1028, 1160, 1247, 1409, 1442, 1586, 1726, 1979, 2038, 2162, 2334, 2361, 2852 and 2919 cm^{-1}.

{(2-pyridylmethyl)(2-thiophenemethyl)}amino-6-methylpyridinyl-2-methyl-4,7,10-tris(*tert*-butoxycarbonyl)-1,4,7,10-tetrazacyclododecane (6) {(2-pyridylmethyl)(2-thiophenemethyl)}amine (**5**) (0.063 g, 2.1 x 10^{-4} mol, 1 eq.), $NaHCO_3$ (0.078 g, 6.3 x 10^{-4} mol, 3 eq.) and KI (cat.) were added to a stirred solution of **1** (0.202 g, 2.1 x 10^{-4} mol, 1 eq.) in MeCN (20 mL) and the mixture was heated to

reflux under N_2. After 16h the mixture was allowed to cool then filtered over gravity before the solvent was removed *in vacuo*. The residue was dissolved in the minimum amount of hot toluene (~ 5 mL) and left to cool at -5 °C for 3d, after which time the solvent was decanted to give the pure product as a brown oil (0.138 g, 53 %); NMR (400 MHz, $CDCl_3$): δ_H = 1.49 (9H, s, $C(CH_3)_3$), 1.50 (18H, s, $C(CH_3)_3$), 2.12 – 2.45 (6H, br-m, NCH_2), 2.58 – 3.10 (16H, br-m, ring-CH_2), 2.97 (2H, br-s, ring-CH_2-pyr), 3.69 (2H, s, CH_2-thio), 3.71 (4H, br-s, CH_2NCH_2), 6.78 (1H, m, thio-H), 6.81 (1H, m, thio-H), 7.08 (1H, m, pyr-H), 7.11 (3H, m, pyr-H, thio-H), 7.53 (1H, d J_{HH} = 7.9, pyr-H), 7.60 (2H, m, pyr-H) and 8.39 ppm (1H, d J_{HH} = 4.1, pyr-H). $^{13}C\{^1H\}$ (62.5 MHz, $CDCl_3$) δ_C = 27.97, 28.22, 50.32, 53.30, 56.08, 56.70, 59.83, 60.16, 82.05, 82.32, 122.10, 122.18, 122.33, 122.92, 124.81, 125.25, 126.54, 128.21, 129.02, 136.61, 137.58, 143.38, 148.80, 156.98, 159.61, 160.55, 172.13 and 172.90 ppm. ES+ MS: *m/z* 822 $\{M+H\}^+$. λ_{max} (ε/mol^{-1}dm^{3}cm^{-1}): 227 (8041) and 264 (4738) nm. IR ν_{max}($CHCl_3$): 1227, 1425, 1521, 1726, 2400, 2836 and 3016 cm^{-1}.

{(2-pyridylmethyl)(2-thiophenemethyl)}amino-6-methylpyridinyl-2-methyl-4,7,10-tris(carboxymethyl)-1,4,7,10-tetrazacyclododecane (6) (L3) was isolated as a brown powder (0.070 g, 64 %); NMR (400 MHz, D_2O): δ_H = 2.72 – 3.03 (6H, br-m, NCH_2COOH), 3.03 – 3.82 (16H, br-m, ring-CH_2), 3.27 (2H, br-s, ring N-CH_2-pyr), 4.10 (2H, s, NCH_2), 4.19 (2H, s, NCH_2), 4.34 (2H, s, NCH_2), 6.78 (1H, t J_{HH} = 4.8, thio-H), 6.88 (1H, m, thio-H), 7.19 (1H, m, thio-H), 7.42 (1H, d J_{HH} = 8.3, linker pyr-H), 7.73 (1H, m, pyr-H), 7.78 (1H, t, pyr-H), 7.94 (1H, d J_{HH} = 6.5, linker pyr-H), 8.27 (2H, m, pyr-H) and 8.54 ppm (1H, d J_{HH} = 5.2, pyr-H). ES+ MS: *m/z* 676 $\{M+Na\}^+$ and 692 $\{M+K\}^+$. λ_{max} (ε/mol^{-1}dm^{3}cm^{-1}): 228 (3972) and 260 (3855) nm. IR ν_{max}(ATR, solid): 1124, 1174, 1462, 1642, 1673, 2044, 2167, 2335 and 2362 cm^{-1}.

EuL3 was isolated as a brown powder (0.022 g, 89 %). ES+ MS: *m/z* 804 $\{M+H\}^+$. HRMS (ES^+) found *m/z* 804.2043 {M + H} calc requires 804.2047. λ_{max} (ε/mol^{-1}dm^{3}cm^{-1}): 217 (5793) and 265 (4805) nm. IR ν_{max}(ATR, solid): 1028, 1083, 1159, 1247, 1410, 1444, 1581, 1728, 2037, 2162 and 2361 cm^{-1}.

4.5 - References

1. T. Gunnlaugsson, J. P. Leonard, K. Senechal and A. J. Harte, *J. Am. Chem. Soc.*, 2003, **125**, 12062-12063.
2. T. Gunnlaugsson and D. Parker, *Chem. Comm.*, 1998, 511-512.
3. D. Parker, K. Senanayake and J. A. G. Williams, *Chem. Comm.*, 1997, 1777-1778.
4. D. Parker and J. A. G. Williams, *Chem. Comm.*, 1998, 245-246.
5. D. Parker, *Coord. Chem. Rev.*, 2000, **205**, 109-130.
6. A. Meir, S. Ginsburg, A. Butkevich, S. G. Kachalsy, I. Kaiserman, R. Ahdut, S. Demirgoren and R. Rahamimoff, *Physiol. Rev.*, 1999, **79**, 1019-1088.
7. M. P. Blaustein and W. J. Lederer, *Physiol. Rev.*, 1999, **79**, 763-854.
8. P. L. Jorgensen, K. O. Hakansson and S. J. D. Karlish, *Annu. Rev. Physiol.*, 2003, **65**, 817-849.
9. D. L. Nelson and M. M. Cox, *Principles of Biochemistry*, Fifth edn., W. H. Freeman and Company, New York, 2008.
10. A. P. deSilva, H. Q. N. Gunaratne, T. E. Rice and S. Stewart, *Chem. Comm.*, 1997, 1891-1892.
11. T. Gunnlaugsson and J. P. Leonard, *Dalton Trans.*, 2005, 3204-3212.
12. C. Li, G. L. Law and W. T. Wong, *Org. Lett.*, 2004, **6**, 4841-4844.
13. J. B. Coldwell, C. E. Felton, L. P. Harding, R. Moon, S. J. A. Pope and C. R. Rice, *Chem. Comm.*, 2006, 5048-5050.
14. M. M. Parker, F. L. Humoller and D. J. Mahler, *Clin. Chem.*, 1967, **13**, 40.
15. B. L. Vallee and K. H. Falchuk, *Physiol. Rev.*, 1993, **73**, 79-118.
16. T. Budde, A. Minta, J. A. White and A. R. Kay, *Neurosci.*, 1997, **79**, 347-358.
17. J. Kaiser, *Science*, 1994, **265**, 1365-1365.
18. O. Reany, T. Gunnlaugsson and D. Parker, *J. Chem. Soc.Perkin Trans. 2*, 2000, 1819-1831.
19. K. Hanaoka, K. Kikuchi, H. Kojima, Y. Urano and T. Nagano, *J. Am. Chem. Soc.*, 2004, **126**, 12470-12476.
20. S. J. A. Pope and R. H. Laye, *Dalton Trans.*, 2006, 3108-3113.
21. K. Hanaoka, K. Kikuchi, Y. Urano, M. Narazaki, T. Yokawa, S. Sakamoto, K. Yamaguchi and T. Nagano, *Chem. & Biol.*, 2002, **9**, 1027-1032.
22. R. Trokowski, J. M. Ren, F. K. Kalman and A. D. Sherry, *Angew. Chem.-Int.*

Ed. Engl., 2005, **44**, 6920-6923.

23. E. Gaggelli, H. Kozlowski, D. Valensin and G. Valensin, *Chem. Rev.*, 2006, **106**, 1995-2044.
24. M. A. Kessler, *Analytica Chimica Acta*, 1998, **364**, 125-129.
25. T. Gunnlaugsson, J. P. Leonard, K. Senechal and A. J. Harte, *Chem. Comm.*, 2004, 782-783.
26. E. L. Que, E. Gianolio, S. L. Baker, A. P. Wong, S. Aime and C. J. Chang, *J. Am. Chem. Soc.*, 2009, **131**, 8527-8536.
27. S. R. Banerjee, M. K. Levadala, N. Lazarova, L. H. Wei, J. F. Valliant, K. A. Stephenson, J. W. Babich, K. P. Maresca and J. Zubieta, *Inorg. Chem.*, 2002, **41**, 6417-6425.
28. A. Beeby, L. M. Bushby, D. Maffeo and J. A. G. Williams, *Dalton Trans.*, 2002, 48-54.
29. A. Beeby, I. M. Clarkson, R. S. Dickins, S. Faulkner, D. Parker, L. Royle, A. S. de Sousa, J. A. G. Williams and M. Woods, *J. Chem. Soc. Perkin Trans. 2*, 1999, 493-503.
30. C. J. Chang, J. Jaworski, E. M. Nolan, M. Sheng and S. J. Lippard, *Proc. Natl. Acad. Sci. USA*, 2004, **101**, 1129-1134.
31. E. M. Nolan and S. J. Lippard, *J. Mat. Chem.*, 2005, **15**, 2778-2783.
32. G. DeSantis, L. Fabbrizzi, M. Licchelli, C. Mangano, D. Sacchi and N. Sardone, *Inorg, Chim. Acta*, 1997, **257**, 69-76.

Chapter Five

The development of responsive luminescent lanthanide complexes incorporating long-wavelength chromophores

5.1 – Introduction

Since biological material strongly absorbs and scatters ultraviolet light the use of chromophores, which absorb longer wavelength light, is prefered in the design of responsive probes for medicinal application and fluoroimmuno-assay labelling agents. The range of wavelengths capable of sensitising lanthanide emission depends largely on the energy levels of the emissive states of the metal being used. Eu(III) and Tb(III) have been extensively studied due to their visible emission and long lifetimes (on the order of milliseconds). Eu(III) has two accessible excited states, $^5D_0$ and $^5D_1$, which are situated at 17250 and 19020 cm^{-1} respectively, whereas the emissive $^5D_4$ state of Tb(III) is at 20430 cm^{-1}.[1] In a report by Steemers[2] calixarenes incorporating near-ultraviolet chromophores (Figure 5.1, A – C) were synthesised and found to be capable of sensitising terbium and europium luminescence following excitation at approximately 350 and 380 nm, respectively. At the time these were estimated to be the upper limits of the wavelengths capable of sensitising emission from each metal ion, however this approximation was based on a minimum singlet-triplet separation of 5000 cm^{-1} and an optimum separation of the ligand triplet energy and the emissive state of the lanthanide of 3500 cm^{-1}. In a study by Latva[3] on the quantum yields of Eu(III) and Tb(III) complexes with 41 different ligands (for example, Figure 5.1, D) of varying triplet state energy levels it was found that terbium luminescence was most efficiently sensitised by ligands with a lowest triplet state energy level about 1850 cm^{-1} higher than the $^5D_4$ level. The precise relationship between the lowest triplet state energy level and the quantum yield of europium was more complicated, probably due to the close proximity of several Eu(III) excited states, but in general the most efficient sensitisation occurred when the triplet energy of the ligand was approximately 21600 cm^{-1}. In ligands with lower lying triplet states back-energy transfer from the lanthanide decreases the quantum yield of the emission. However, in these cases the large separation between ligand singlet and triplet states places the absorption maxima of the most efficient sensitizers at approximately 310 – 330 nm.

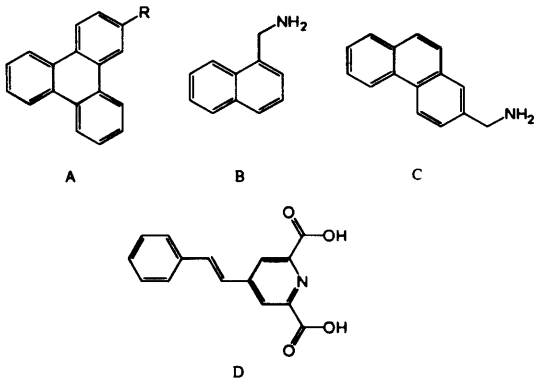

Figure 5.1 – Three chromophores used by Steemer (A – C) and a ligand used by Latva (D) for the sensitisation of Eu(III).

The longest wavelengths of efficient europium sensitisation have been achieved by minimising the gap between the singlet and the triplet energy levels and reducing the gap between the triplet state of the ligand and the excited state of europium to approximately 2000 cm^{-1}. In particular, ketone-containing chromophores display small singlet-triplet gaps as well as very efficient ISC. It has been shown that that Michler's ketone (Figure 5.2, A),[4] benzophenone (B),[5] acridone-based chromophores (C)[6] and hydroxyphenalone (D)[7] can sensitise Eu(III) emission following irradiation at wavelengths in excess of 400 nm. Longer wavelengths have been used to sensitise Eu(III) in mixed metal d-f arrays. The MLCT states of most d-block metal complexes are too low in energy to allow sensitisation of europium. However, bimetallic assemblies containing Ir(III)[8, 9] and Pt(II)-based[10] chromophores have been shown to sensitise Eu(III) emission by energy transfer *via* the ^{3}MLCT state, following excitation at wavelengths of up to 530 nm.

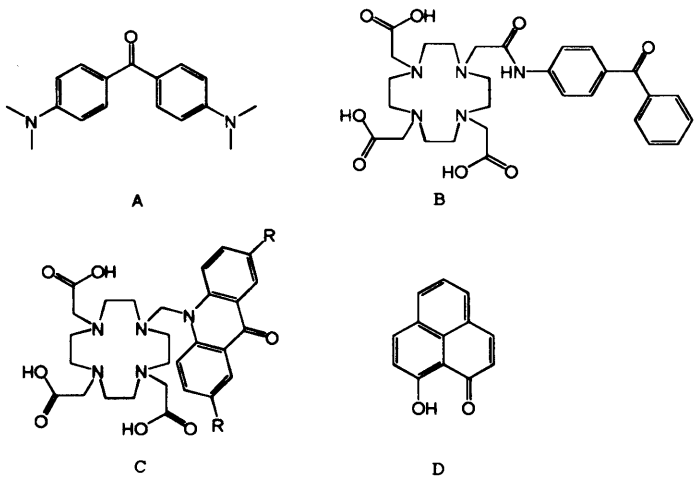

Figure 5.2 – Several ligands incorporating aromatic ketones as sensitising chromophores for Eu(III).

In terms of wavelength of sensitisation the near-infrared (NIR) emissive lanthanides are much more versatile than those that emit in the visible region. NIR luminescence is of considerable interest in the field of biological imaging due to the relative transparency of biological tissue in this region. Light with a wavelength of less than approximately 800 nm is efficiently absorbed by porphyrin chromophores present in haemoglobin and other proteins whereas the vibrational modes of water absorb further into the NIR region. Neodymium shows emission bands at ~ 880 nm (due to the $^4F_{3/2} \rightarrow {}^4I_{9/2}$ transition), 1055 nm ($^4F_{3/2} \rightarrow {}^4I_{11/2}$) and 1350 ($^4F_{3/2} \rightarrow {}^4I_{13/2}$) whereas Ytterbium shows a single broad emission band around 975 nm ($^2F_{5/2} \rightarrow {}^4F_{7/2}$),[11] making these metals ideal candidates for the luminescent component of biological imaging agents. Nd(III) has absorption bands throughout the visible and NIR region of the spectrum, Yb(III) has a single absorption band at 970 nm, but can be sensitised by much higher energy chromophores, with the large energy gap being bridged either by an internal redox process as proposed by Horrocks[12] or by vibronic interactions with surrounding solvent molecules. In each case the energy of the lowest emissive state determines the maximum wavelength of sensitisation available. The lowest emissive states of Nd(III) and Yb(III) lie at 11300 cm^{-1} and 6500 cm^{-1} respectively. As is the case with Eu(III) and Tb(III) an energy gap between the donating and accept states of approximately 2000 cm^{-1} is required to prevent BET, this places absorption of the lowest potential sensitizers of neodymium

and ytterbium in the red and NIR regions of the spectrum, respectively.

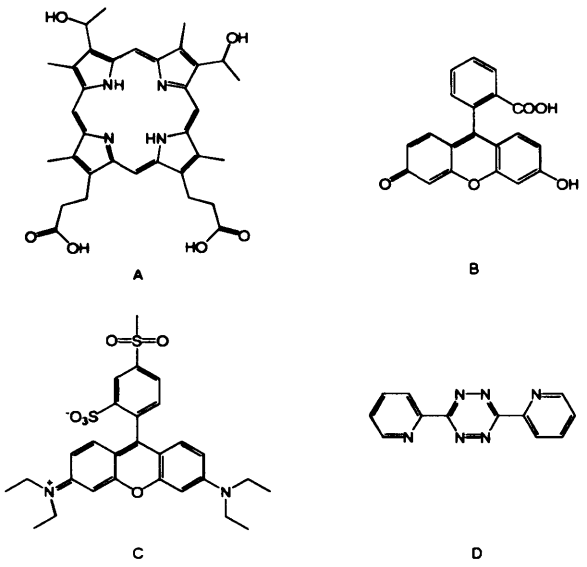

Figure 5.3 – Various organic chromophores used to sensitise NIR emission from lanthanide ions.

Long wavelength excitation of neodymium and ytterbium has been achieved by a variety of different forms of chromophore. Organic chromophores such as porphyrins (Figure 5.3, A),[13] fluorescein (B),[14-16] lissamine (C)[17] and bis-pyridyl-tetrazine (D)[18] have been shown to be capable of sensitising NIR emission from Nd(III) and Yb(III) following excitation at 500 – 600 nm. Bünzli *et al.* have reported emissive Nd(III), Yb(III) (Figure 5.4, A) and Er(III) complexes incorporating a boradiazaindacene dye[19] which absorb strongly in the visible region (λ_{max} ~ 515 nm) and emit NIR light. Multimetallic arrays incorporating chromophores based on a range of d-block metals including Fe(II) (C),[20] Pt(II) (B),[21-23] Ru(II)[20, 24, 25] and Re(I) (D)[23, 26] can sensitise NIR emission from lanthanide ions following excitation of the MLCT state.

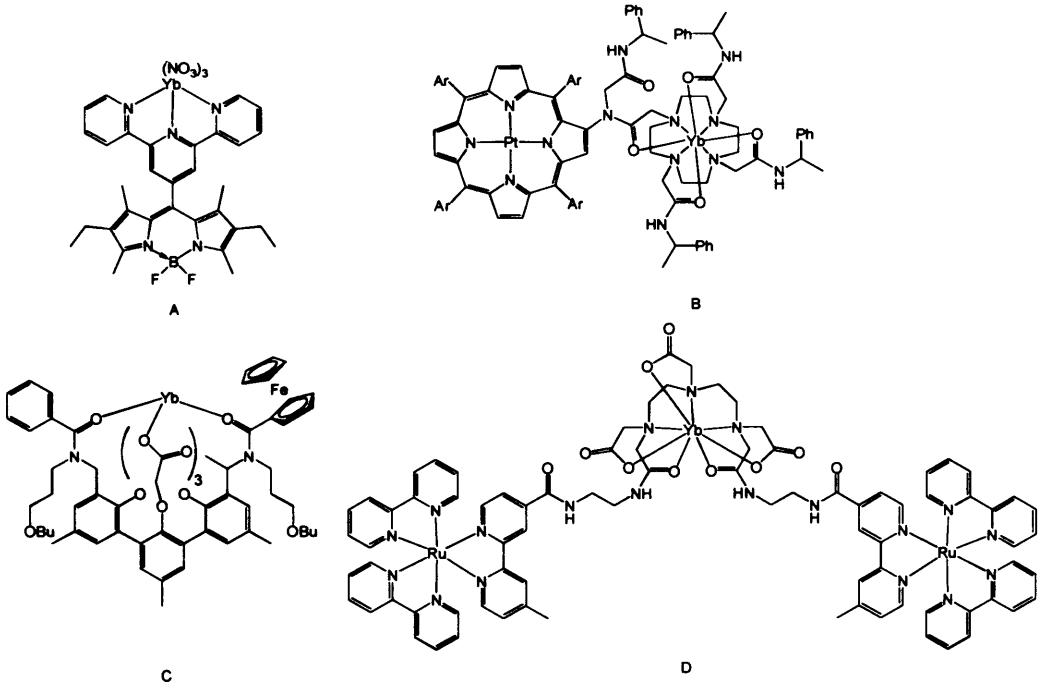

Figure 5.4 – Several complexes capable of emitting in the NIR following excitation by visible light.

The aim of this chapter was to incorporate relatively long-wavelength absorbing chromophores (λ_{max} > 300 nm) into complexes designed to respond to the presence of metal ions. Despite the amount of attention devoted to sensitising lanthanide luminescence using chromophores that absorb at long wavelengths relatively few of these chromophores have been incorporated into responsive probes.

An early s-block metal probe based on a lanthanide complexes was reported by de Silva *et al.* and incorporated a substituted terpyridine unit as a sensitising chromophore (Figure 5.5, A).[27] In the presence of Na(I) or K(I) photo-induced electron transfer (PET) from the nitrogen of an azacrown macrocycle to the chromophore was surpressed and excitation at 340 nm sensitised Eu(III) emission. A terpyridine-based chromophore was also used in a sensor developed by Kessler (Figure 5.5, B) in which the Eu(III) emission (λ_{exc} = 337 nm) was quenched upon addition of Cu(II).[28]

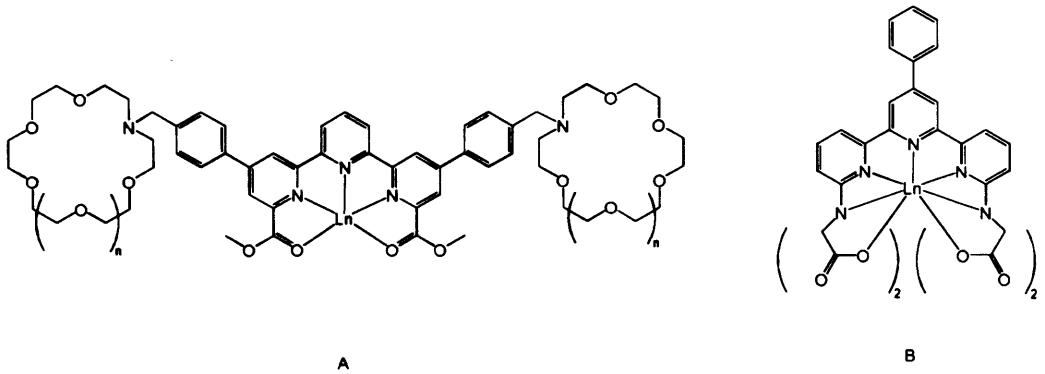

A B

Figure 5.5 – de Silva's Na(I)/K(I) sensor (A) and Kessler's Cu(II) sensor (B).

Quinoline has been incorporated into chemosensors for K(I) and Zn(II). The probe reported by Wong and co-workers (Figure 5.6, A) represents a dual responsive system,[29] with the intensity of Tb(III) emission (λ_{exc} = 313 nm) sensitive to changes in both pH and K(I) concentration. Protonation of the ligand or the binding of K(I) by the quinoline and the azacrown macrocycle altered the energy transfer process between the chromophore and the Tb(III), modulating emission intensity without changing the lifetime. In the sensor reported by Kikuchi and Nagano[30] (Figure 5.6, B) the Zn(II) receptor site included an amido-quinolyl group, allowing the sensitisation of Eu(III) emission by irradiation at wavelengths of up to 340 nm. The binding of Zn(II) lowered the triplet energy of the chromophore, allowing more efficient energy transfer to the Eu(III) and enhancing the emission intensity. The long wavelength of excitation allowed fluorescence microscopy measurements which showed the uptake of Zn(II) by living cells.

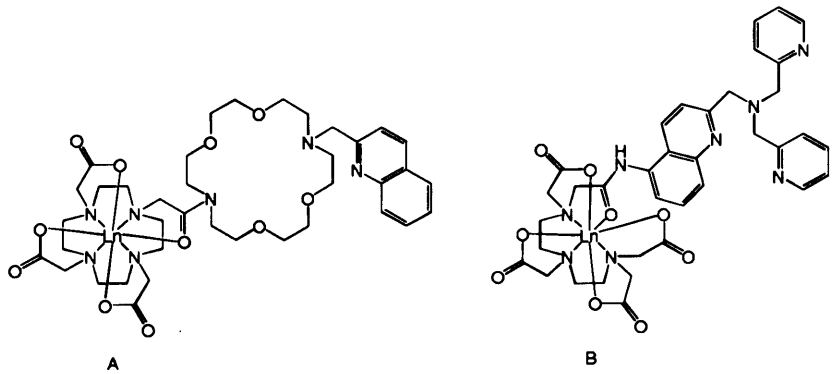

A B

Figure 5.6 – Wong's K(I) sensor (A) and Kikuchi and Nagano's Zn(II) sensor (B).

A sensor for Ba(II)[31] (Figure 5.7) is notable for the use of a NIR emissive metal as well as a substituted bipyridine chromophore allowing sensitisation at wavelengths in excess of 355 nm. Upon binding Ba(II) the bipyridine unit adopts a more twisted conformation, blue-shifting the absorption profile and decreasing the intensity of the Nd(III) emission when using an excitation wavelength of 335 nm.

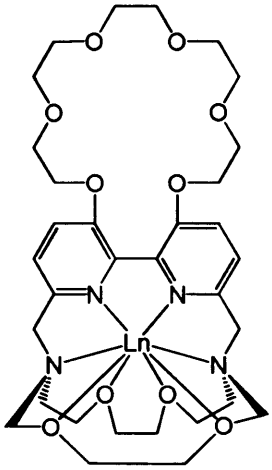

Figure 5.7 – Bipyridine-based Ba(II) sensor.

This chapter features ligands incorporating four organic chromophores: substituted quinolines (Figure 5.8, A), anthracene (B), pyrene (C) and anthraquinone (D). Typically quinoline-containing compounds typically show broad, structureless absorption (λ_{max} ~ 315) which a similar fluorescence (λ_{max} ~ 400). The triplet emission (recorded at 77 K) shows a large peak with vibronic structure, with an onset at approximately 450 nm.[32] This corresponds to a triplet energy level of about 21800 cm^{-1} which is ideal for the sensitisation of Eu(III) emission. As mentioned above quinoline has been incorporated into lanthanide complexes with metal-ion binding properties. It also forms the basis for many organic probes for metal-ion concentration, most commonly Zn(II),[33-35] which binds to the aryl nitrogen and prevents PeT, causing an enhancement in the fluorescence intensity.

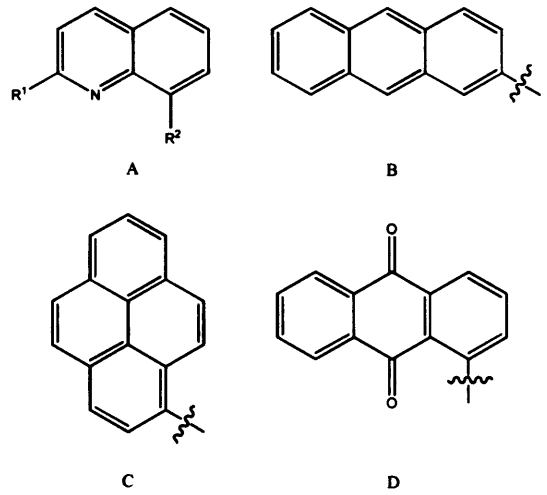

Figure 5.8 – Chromophores used in this chapter. Quinoline (A), anthracene (B), pyrene (C) and anthraquinone (D).

Anthracene typically shows a structured absorption between 300 and 420 nm with a mirroring fluorescence emission spectrum > 350 nm. The lowest triplet energy has been calculated as ~ 15000 cm^{-1},[36] making it theoretically possible to sensitise NIR emission from Nd(III), Yb(III) and Er(III) via transfer from the triplet state. Anthracene has been shown to sensitise lanthanide emission, however it seems this does not always occur through a typical $^*S \rightarrow {}^*T \rightarrow {}^*Ln$ process, instead energy transfer has been proposed to proceed *via* a direct $^*S \rightarrow {}^*Ln$[37] process or to be mediated by a charge separated state.[38] Anthracene has been incorporated into transition metal probes which can show either fluorescence enhancement or fluorescence quenching depending on the structure of the probe and the identity of the metal. In a probe reported by Fabrizzi *et al.* the binding of Cu(II) or Ni(II) resulted in electron transfer from the excited anthracene singlet state, quenching the luminescence.[39] Alternatively the presence of a metal ion can cause an enhancement of anthracene luminescence by inhibiting PeT.[40, 41]

The absorption profile of pyrene shows a series of transitions with the most intense peak around 350 nm. This structure is mirrored in the fluorescence spectrum at > 380 nm. The triplet level is generally situated around 16500 cm^{-1},[42] making it well suited to sensitise NIR emissive lanthanides.[43, 44] It has also been shown capable of sensitising Eu(III) emission, albeit with very low

quantum yield due to the significant level of BET.[45] Pyrene has been incorporated into a variety of metal sensors. In some systems the metal provokes a response in the pyrene fluorescence by the surpression of PeT,[46] as is the case in quinoline and anthracene probes however, in many pyrene-based metal probes an alternative mode of response is available. In systems in which the presence of a metal ion can either bring pyrene into close proximity with another aromatic system or prevent the aggregation of pyrene-containing molecules the concentration of the metal ion can be signalled in the fluorescence spectrum *via* the degree of excimer or exciplex emission, compared to typical monomeric pyrene emission.[47, 48]

Although anthraquinone has a relatively high triplet state (~20400 cm^{-1})[49] it has a small singlet-triplet gap (1400 cm^{-1})[50] as well as a high ISC quantum efficiency, making it a promising sensitising chromophore which has good absorbance at wavelengths in excess of 400 nm. Despite these useful properties the possibility of sensitising lanthanide emission has not been explored. Its fluorescence and donor properties have been utilised in metal,[51, 52] anion[53] and cation[54] sensors. The redox sensitivity of anthraquinone has also been exploited in the design of probes for pH and oxygen.[55]

This chapter is focussed on incorporating these long wavelength chromophores into macrocyclic ligands suitable for forming water-stable luminescent lanthanide complexes which respond to the local presence of metal ions. The chromophores were prepared as amines before incorporated into the target metal receptor site which also participated in the lanthanide coordination sphere. As demonstrated in Chapter 4, the binding of a target metal can not only influence energy transfer processes from the chromophore, but can also alter the local environment of the lanthanide. This results in a change in the hyperfine structure of the lanthanide emission, thus allowing changes in the concentration of the target metal to be distinguished changes in the concentration of the probe. The primary target was zinc due to its importance in protein function[56] and neuronal signalling[57] and its implication in the development of Alzheimer's disease.[58]

5.2 – Results and Discussion

5.2.1 – Synthesis and characterisation of ligand precursors, ligands and their corresponding lanthanide complexes

5.2.1.1 – Hydroxyquinoline-based ligands

The synthetic strategy (Figure 5.9) adopted to incorporate the chromophores into metal receptor sites was based on that of the Pope sensor for Zn(II).[59] Initial attempts focused on pre-forming a metal ion receptor site featuring 8-hydroxyquinoline before appending it to the *tert* butyl ester of cyclen **1** (Figure 5.9). 2-methyl-8-hydroxyquinoline **2** was readily converted to 8-hydroxyquinoline-2-carboxaldehyde **3** according to literature precedent before being coupled with glycine ethyl ester **4** by selective reductive amination to form the secondary amine **5**, using sodium triacetoxyborohydride to prevent the reduction of the aldehyde to the corresponding alcohol.[60]

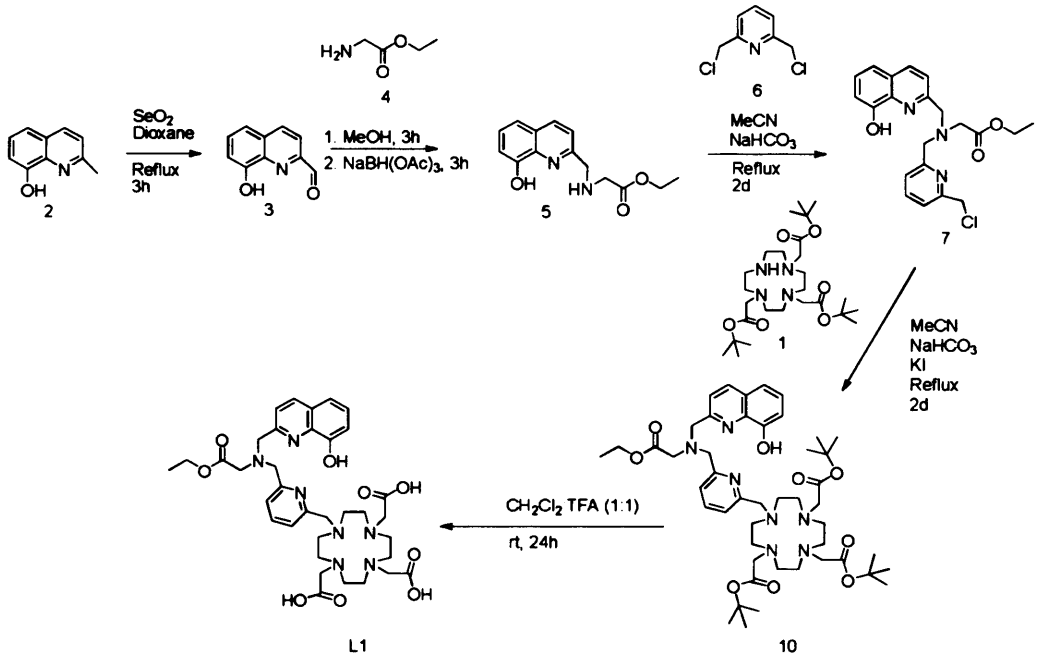

Figure 5.9 – Initial synthetic strategy towards new responsive ligand.

Product **5** was purified by acidic aqueous extraction and was characterised by

^{1}H and ^{13}C NMR and electrospray mass spectrometry (ES+ MS). However further functionalisation proved problematic. The reaction with 2,6-bis(chloromethyl)pyridine **6** resulted in a mix of mono- and di- substituted pyridine (**7** and **8**) as well as unreacted bis(chloromethyl)pyridine (Figure 5.10) starting material. This mixture could not be purified by column chromatography, recrystallisation, precipitation or acidic extraction. Therefore, an alternative route was attempted.

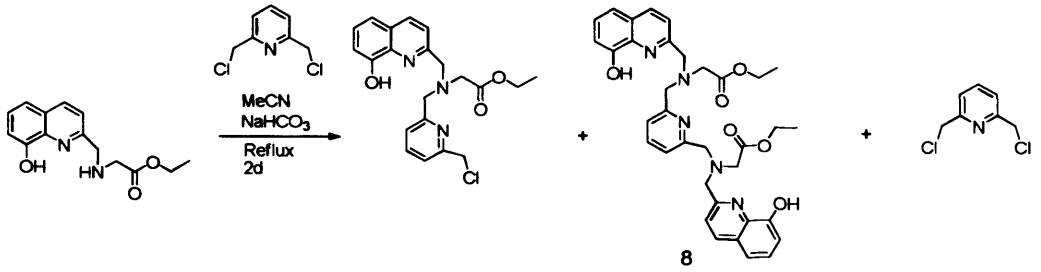

Figure 5.10 – Mixture of products resulting from reaction of **5** and **6**.

Since the secondary amine **5** could be easily synthesised at relatively high yield and a good degree of purity, the bis(chloromethyl)pyridine would instead be coupled with the macrocycle to form **9** before being reacted with the amine to form the metal receptor site (Figure 5.11).

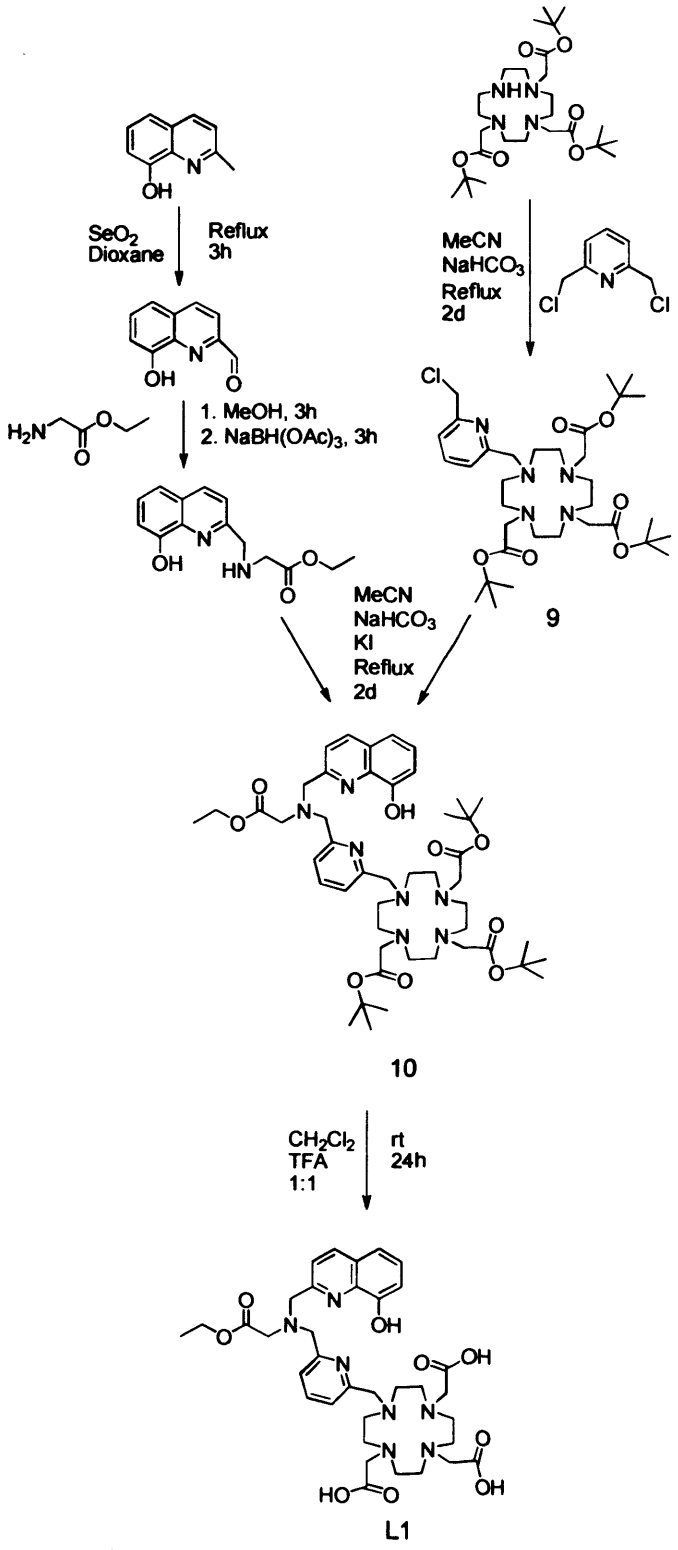

Figure 5.11 – Alternative synthetic approach to **L1**.

The chloromethyl-pyridine functionalised macrocycle was then coupled with the secondary amine bearing the hydroxyquinoline chromophore. The reaction was monitored by ^{1}H NMR and after two days the absence of the peak associated with methylene chloride group (4.58 ppm) indicated the reaction was complete. The crude product was dissolved in hot toluene and left to precipitate over three days to removed trace impurities. The protected ligand precursor **10** was characterised by ^{1}H and $^{13}C\{H\}$ NMR and ES MS which showed a parent ion peak at *m/z* 900 which corresponded with $\{M+Na\}^{+}$. The *tert* butyl esters were then deprotected by reaction with trifluoroacetic acid (TFA) in CH_2Cl_2 (1:1) to form **L1**. ^{1}H NMR showed an absence of peaks associated with *tert* butyl ester, indicating the reaction had gone to completion. ES^{+} MS showed a parent ion peak at *m/z* 836, the mass and isotope pattern corresponded to $\{M+2Cu\}^{+}$, presumably due to the free ligand scavenging copper from the mass spectrometry system. This confirmed that the reaction occurred without cleavage of the metal receptor site, or any of the aromatic groups within the receptor site.

5.2.1.2 – Anthracene-based ligands

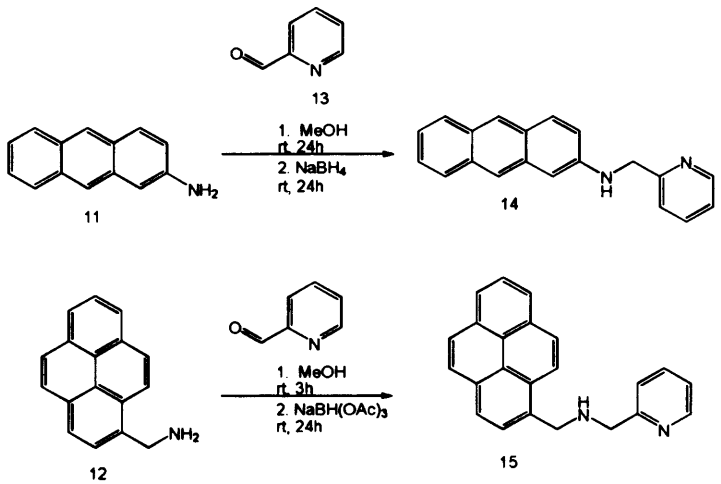

Figure 5.12 – Formation of chromophoric secondary amines by reductive amination.

Due to the ease and good yield of both the reductive amination and the synthesis

of the chloromethylpyridine-functionalised macrocycle this synthetic strategy was applied to several other chromophoric variants. Both 2-aminoanthracene (**11**) and 1-aminomethylpyrene (**12**) were coupled with pyridine-2-carboxaldehyde (**13**) to form **12** and **15** respectively. 2-methylquinoline (**15**) was brominated to form **16** by reaction with *N*-bromosuccinimide in CCl_4, using benzoyl peroxide as the radical initiator, according to a modified literature report.[61] This was then converted to 2-aminomethylquinoline (**18**) by the Gabriel synthesis, before being coupled with quinoline-2-carboxaldehyde (**19**) to form bis(quinolin-2-ylmethyl)amine (**20**).[60]

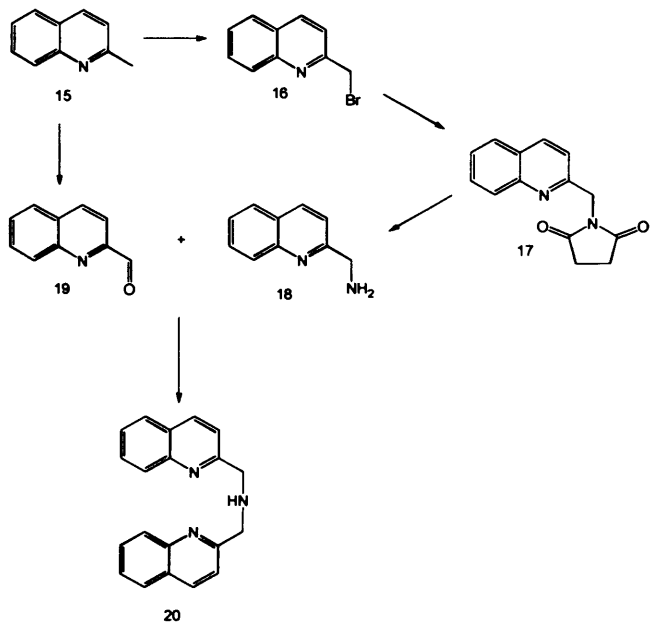

Figure 5.13 – Synthesis of bis(quinolin-2-ylmethyl)amine.

Each of the secondary amines were purified by mild acidic extraction to remove unreacted aldehyde starting material before being coupled with the chloromethylpyridine-functionalised cyclen triester and purified by column chromatography over silica gel (**21**, **22**, **23**). All secondary amines and *tert* butyl protected ligand precursors were characterised by ^1H and ^{13}C NMR and ES+MS, which, in the case of the amines showed the presence of a parent ion peak with an *m/z* corresponding to $\{M+H\}^+$ and in the case of the ligand precursors showed a parent ion peak corresponding to either $\{M+Na\}^+$ or $\{M+K\}^+$. Deprotection of the ester groups was attempted for each ligand

precursor as described above. ^{1}H NMR confirmed the absence of *tert* butyl groups, however in the case of **22** and **23** the ES MS indicated that the chromophores had been cleaved during the deprotection.

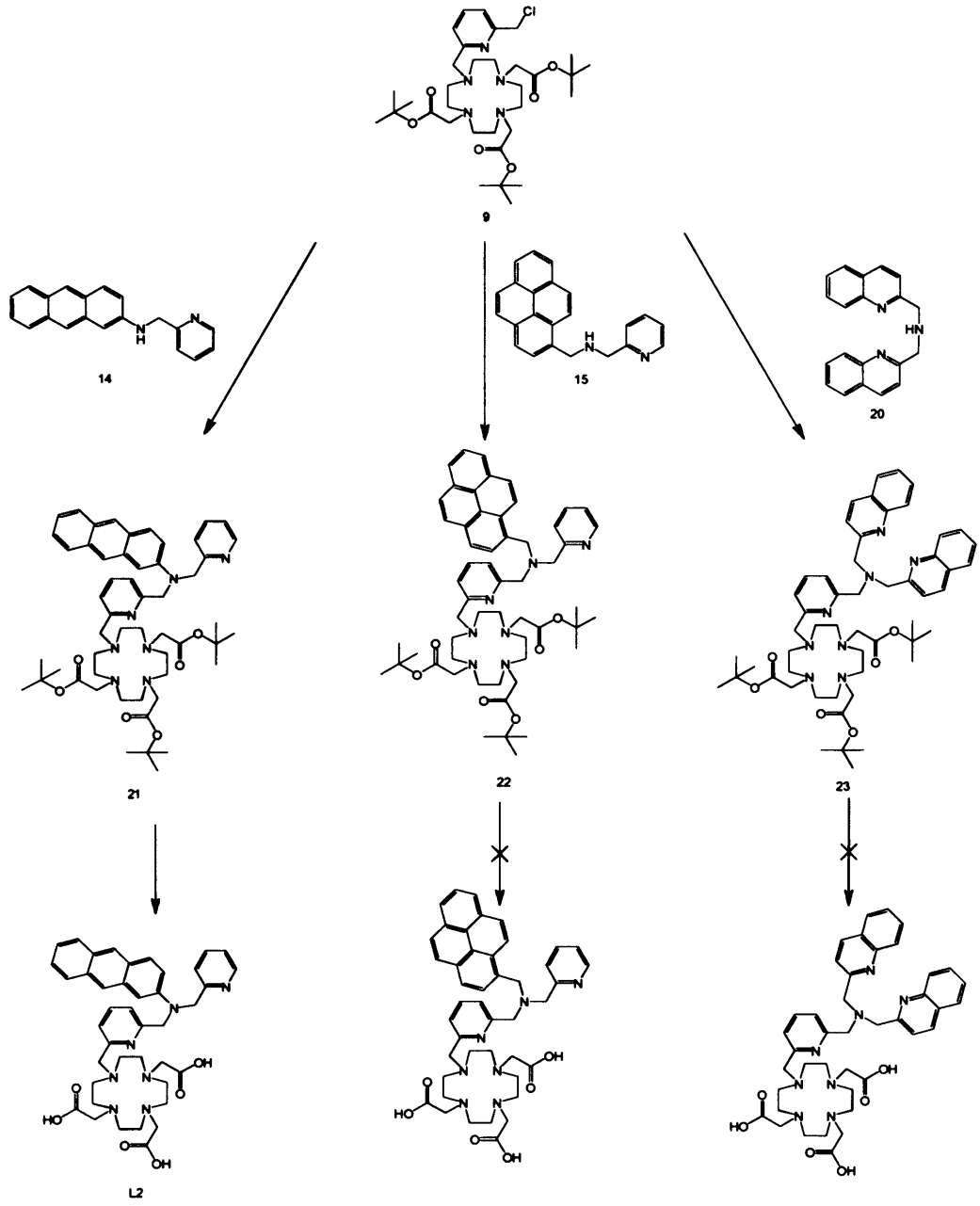

Figure 5.14 – Synthetic strategy towards three new ligands.

5.2.1.3 – Pyrene-, Quinoline- and Anthraquinone-based ligands

In light of this an alternative route was adopted to incorporate a range of other chromophores into the binding site. The three amino-chromophores, 2-aminopyrene (**24**), 8-aminoquinoline (**25**) and 1-aminoanthraquinone (**26**), were converted to chloroacetamides **27** - **29** by reaction with chloracetyl chloride (**30**) according to literature precedent[62-64] and were then reacted with 2-(aminomethyl)-pyridine (**31**) to form a series of secondary amines (**32** – **34**) which were purified by column chromatography and characterised by ES+MS which in each case showed a peak associated with $\{M+H\}^+$. These were then reacted with **9** to give the protected ligand precursors (**35** – **37**), which were then deprotected with TFA to form **L3**, **L4** and **L5** without cleavage of the chromophores.

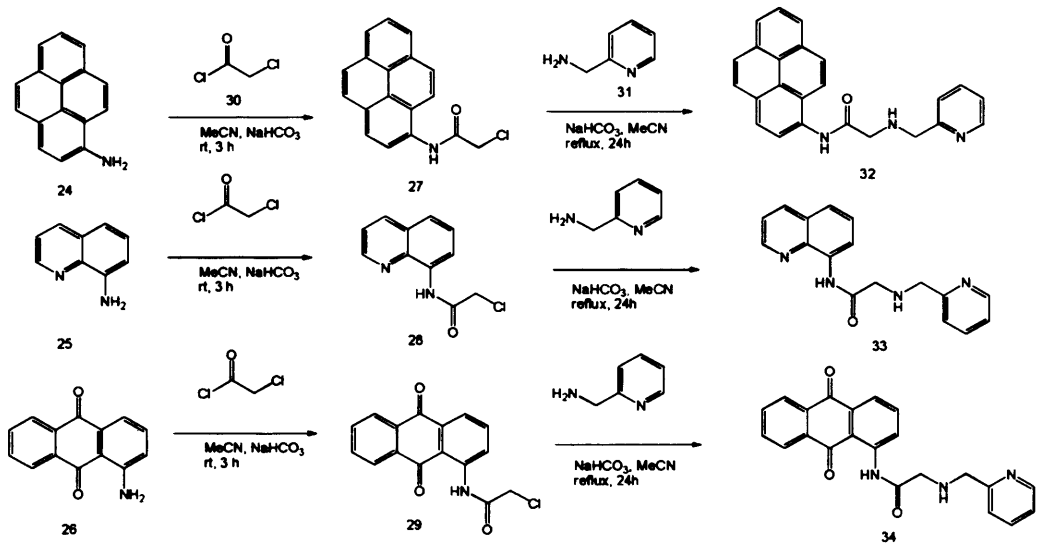

Figure 5.15 – Synthesis of several chromophoric secondary amines.

Lanthanide complexes were formed by mixing the ligand with a lanthanide triflate salt in methanol at 50 °C for 24 hour. In each case they were characterised by HR MS, which in each case showed the correct mass and correlated well to the predicted isotope pattern.

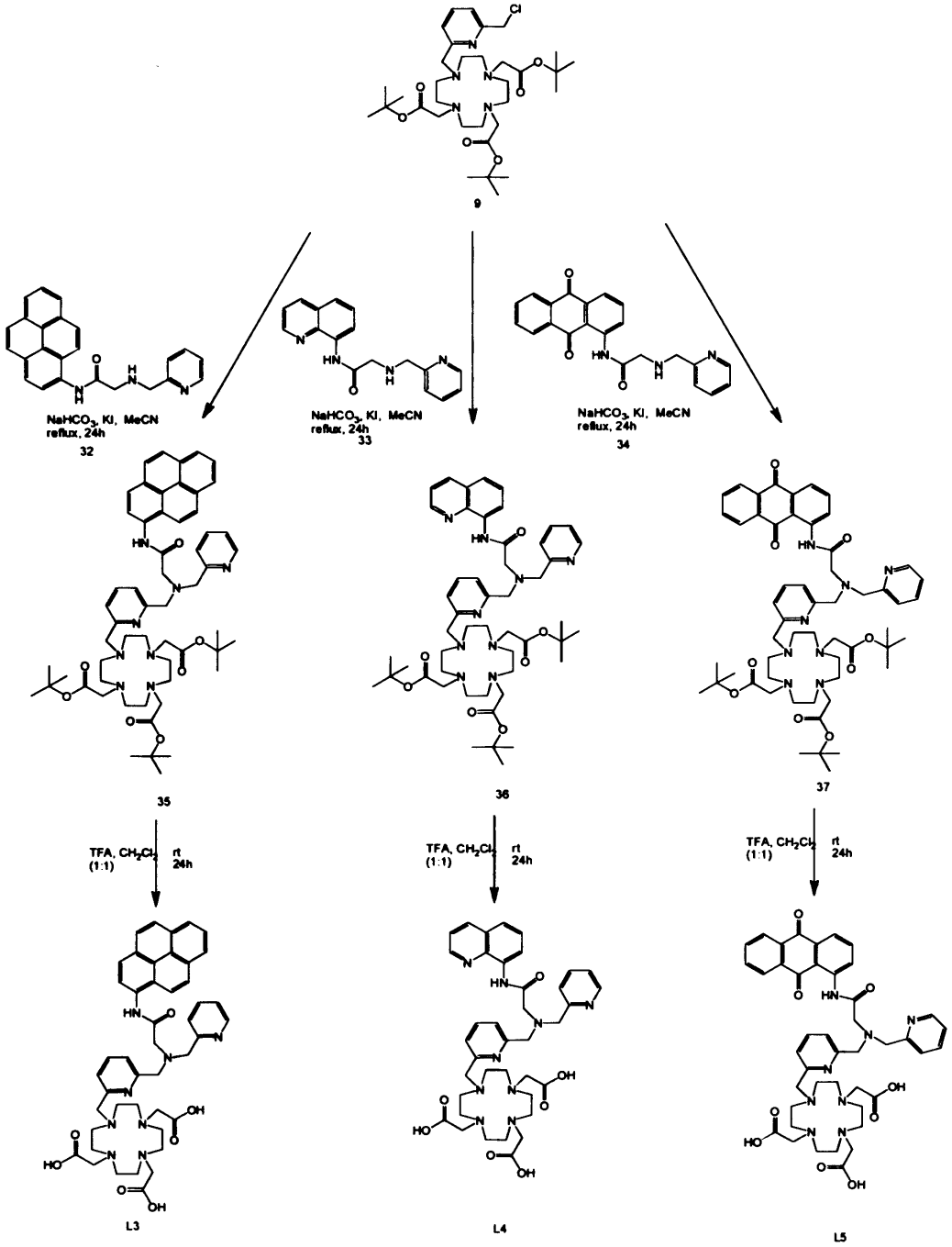

Figure 5.16 – Synthesis of **L3**, **L4** and **L5**.

5.2.2 – Photophysical Studies

The UV-Vis absorption spectrum of each complex showed intense absorption bands below 300 nm due to the $\pi \rightarrow \pi^*$ transitions of the pyridine groups. By

comparison the absorption bands of the long wavelength chromophores are much weaker. **L1** showed a broad shoulder at approximately 310 nm extending up to 350 nm due to the absorption of the hydroxyquinoline group. **L4** showed stronger quinoline absorption with distinct peaks at 323 and 333 nm, the incorporation of the amide into the aromatic system causing a red shift in the absorption. This corresponds well with the UV-Vis absorption profile of the amidoquinoline-containing system reported by Nagano *and co-workers.*[30] The ligand containing an anthracene-based chromophore, **L2**, did not show a typical structured anthracene absorbance. Instead a broad, low energy absorption bands were observed, peaking at 407 nm and 354 nm respectively. This has been observed previously in aminoanthracene[65] and is presumably due to donation of the nitrogen lone pair into the aromatic system resulting in some $n \rightarrow \pi^*$ charge transfer character. In **L3** the pyrene group showed the strongest absorption of a long wavelength chromophore compared to the absorption of the pyridine groups with a peak at 342 nm of comparable intensity to the lowest energy pyridine absorption. The pyrene peak was weakly structured, with shoulders at approximately 330 nm and 315 nm. **L5** showed a broad structureless absorption band due to a charge transfer, n(amino)$\rightarrow\pi^*$(quinine) transition with a peak at 395 nm.

In order to elucidate the triplet state energy levels of the chromophores the gadolinium complexes of each ligand were synthesised. Since the lowest excited state of Gd(III), the $^6P_{7/2}$ level, lies at approximately 32000 cm^{-1} it cannot receive energy from chromophores which absorb above 300 nm.[1] In each case irradiation of the low energy absorption bands was followed by phosphorescence (time gate of 0.5 ms) in the visible region.

GdL1 showed a broad, structureless emission with an onset at 490 nm, indicating that the lowest triplet state is approximately 20400 cm^{-1}. **GdL4** showed a strong, structured emission typical of quinoline triplet states with a low-energy onset at approximately 460 nm (corresponding to a triplet energy level of *ca.* 21700 cm^{-1}) which is ideally suited to sensitise Eu(III) emission. Following excitation at 400 nm **GdL5** showed a broad structureless emission with an onset at around 480 nm, corresponding to a triplet energy level at

approximately 20800 cm^{-1}. The similarity between the triplet energy levels, compared to the significant differences between the UV-Vis absorption profiles, is a result of the small singlet-triplet gap in **L5**, typical of aromatic ketones such as anthraquinone.[49]

After excitation of the pyrene group, **GdL3** showed a strong, structured phosphorescence at 580 nm. This corresponds to a triplet energy level of approximately 17200 cm^{-1}, which matches well with literature reports. This is too low to allow efficient sensitisation of Eu(III), but should allow sensitisation of the NIR emissive lanthanides, Nd(III), Yb(III) and Er(III).

Following excitation of the pyridine group(s) at 280 nm, the Eu(III) compex of each ligand showed characteristic Eu(III) emission in the visible region. The emission was well resolved, even in the cases of **EuL2**, **EuL3** and **EuL5** where there was some slight overlap with ligand emission. This allowed the $J = 0$ (580 nm), 1 (592 nm), 2 (614), 3 (652 nm) and the $J = 4$ manifold (680 – 705 nm) to be distinguished. The series of complexes show variation in the ratio of the intensity of the $J = 1$ and $J = 2$ peaks, indicating that the coordination environment of the Eu(III) may vary subtly for the different ligands (Figure 5.17).

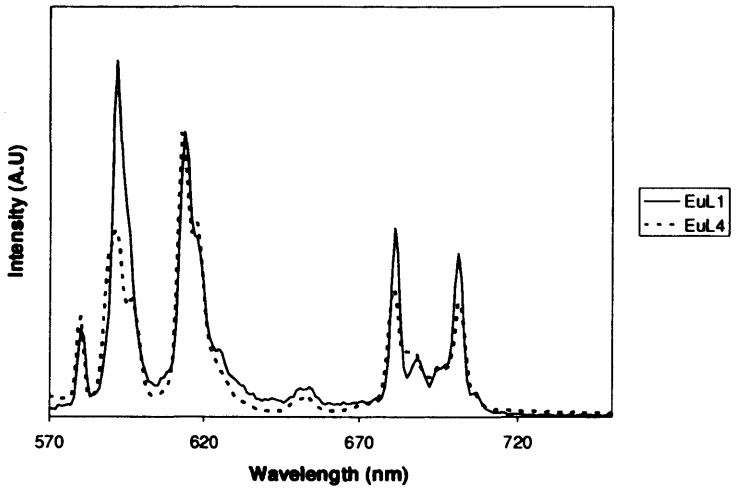

Figure 5.17 – Eu(III) emission of **EuL1** and **EuL4** (normalised for $J = 2$).

As expected only **L1**, **L4** and **L5**, the ligands containing relatively high energy

triplet states, could effectively sensitise Eu(III) emission following excitation at wavelengths of over 300 nm. Excitation of each complex at their peak absorbance lead to emission in the NIR by the Nd(III) and Yb(III) complexes. The Nd(III) complexes showed emission due to the $^4F_{3/2} \rightarrow {}^4I_{9/2}$, $^4F_{3/2} \rightarrow {}^4I_{11/2}$, and $^4F_{3/2} \rightarrow {}^4I_{13/2}$ transitions at approximately 880 nm, 1060 nm and 1350 nm respectively whereas the Yb(III) complexes showed emission due to the $^2F_{5/2} \rightarrow {}^4F_{7/2}$ transition at approximately 975 nm.

Interestingly, the pyrene emission of complexes of **L3** showed typical, structure peaks at approximately 400 nm as well as a broad, structureless emission at λ_{max} = 440 nm. At the same dilution in MeOH, this peak was not observed, therefore it was attributed to excimer or exciplex emission caused by the aggregation of hydrophobic pyrene groups.

The luminescence lifetime of each complex was measured in H_2O and D_2O (Table 5.1) and generally correlated well with reported values for similar complexes, i.e. in the order of milliseconds for Eu(III) and Tb(III) and on the order of microseconds for Yb(III) and Nd(III). In most cases they could be modelled as monoexponential decays, indicating the presence of a single emissive species in solution. In the cases where the lifetimes were double-exponential the lifetimes of the two components were very similar, most likely indicating reversible binding by one of the donors in the guest-metal receptor site. Using the modified versions of Horrocks' equation reported by Parker[66] and Faulkner[67] the difference in lifetimes in deuterated and non-deuterated solvent was used to calculate the degree of inner sphere hydration, q. In the cases which could not be modelled as single exponential decays, the q value was calculated for each componant (Table 5.1) In most cases q was between 0 and 1, which would correspond to nine- or eight-coordinate ligands. This indicates that pyridine and other donors present in the guest metal receptor sites are participating in the coordination sphere of the lanthanides, which is in accordance with literature reports.[59] The q values for **EuL2** and **TbL2** were 1.1 and 1.2 respectively, probably due to the steric bulk of the aminoanthracene unit preventing the binding of a ninth donor.

Complex	τ_H (μs)	τ_D (μs)	q
EuL1[a] *	640	1160	0.5
	900		0
TbL1[a]	1770	2560	0.6
NdL1[b]	0.09	0.312	0.6
YbL1[b]	1.40	5.69	0.33
EuL2[a]	590	1790	1.1
TbL2[a]	1230	1980	1.2
NdL2[b]	0.114	0.334	0.4
EuL3[a] *	490	910	0.8
	660	1240	0.6
NdL3[b]	0.144	0.383	0.2
YbL3[b]	2.71	6.60	0
EuL4[a]	840	1450	0.3
TbL4[a]	1890	2490	0.3
NdL4[b]	0.144	0.430	0.6
YbL4[b]	2.60	7.75	0
EuL5[a] *	680	1510	0.7
	980	1910	0.3
NdL5[b]	0.129	0.370	0.3
YbL5[b]	1.76	6.31	0.21

Table 5.1 – Lifetimes and q values for lanthanide complexes.

H_2O/D_2O, 298 K

[a] λ_{ex} = 280 nm

[b] λ_{ex} = 355 nm

* Could not be modelled as single exponential decay.

5.2.3 – Metal Binding Studies

The photophysical properties of the complexes were monitored in the presence of *d*-block and group 12 metals in order to assess their potential to act as responsive luminescent probes.

5.2.3.1 – Metal binding studies on complexes of L1

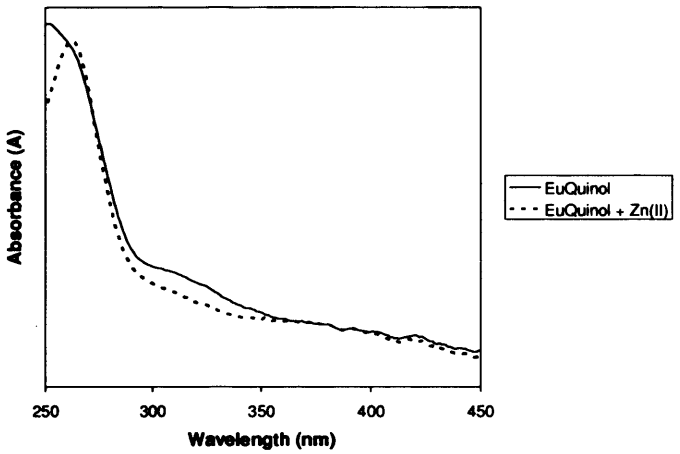

Figure 5.18 – UV-Vis spectrum of **EuL1** with and without Zn(II).

The addition of ten equivalents of $Zn(ClO_4)_2$ to a solution of **EuL1** caused a slight decrease in the absorbance between 290 and 350 nm (Figure 5.18), indicating that Zn(II) was binding to the ligand. However, as EuL1 was titrated against $Zn(ClO_4)_2$ the intensity and structure of the europium emission remained constant whereas the ligand luminescence showed a distinct increase in intensity (Figure 5.19). The excitation spectrum demonstrated that when irradiated at approximately 360 nm the ligand fluorescence showed a threefold increase in intensity after the addition of ten equivalents of Zn(II). This indicated that the Zn(II) was occupying the binding site without significantly influencing the coordination environment of the Eu(III) or the energy transfer from the chromophore.

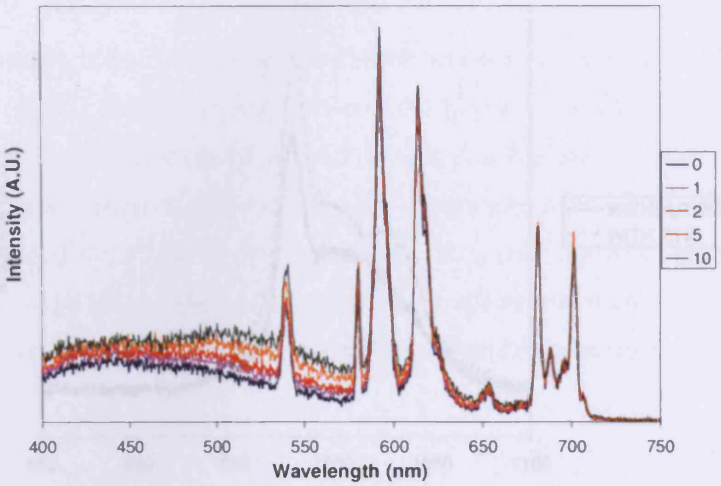

Figure 5.19 – Ligand and Eu(III) emission of **EuL1** following excitation at 280 nm, in the presence of Zn(II).

However, the addition of Zn(II) to a solution of **YbL1** causes a significant increase in the emission intensity, as well as subtle changes to the vibronic structure of the Yb(III) emission centred around 980 nm ($^2F_{5/2} \rightarrow {}^2F_{7/2}$ transition) (Figure 5.20). Time resolved data was obtained for the Yb(III) NIR emission in deuterated and non-deuterated solvents in the prescence of Zn(II), with the lifetimes being determined as 6.76 μs and 1.04 μs. The *q* value was calculated as 0.6, a slight increase compared to values obtained in the absence of Zn(II). This indicates that the presence of Zn(II) slightly increases the accessibility of the Yb(III) by surrounding solvent.

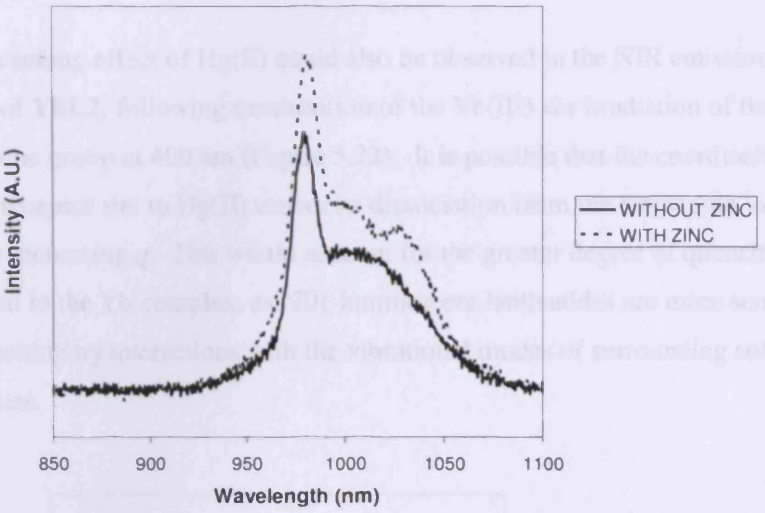

Figure 5.20 – Enhancement of **YbL1** emission on addition of Zn(II).

5.2.3.2 – Metal binding studies on complexes of L2

The addition of $Zn(ClO_4)_2$ to **LnL2** had very little effect on the absorption profile, ligand fluorescence or Eu(III) luminescence. However, the addition of ten equivalents of $Hg(ClO_4)_2$ caused a strong increase in the absorbance at $\lambda >$ 325 nm and a decrease in the intensity of the anthracene and Eu(III) emission. The quenching of the lanthanide-based emission was not accompanied by a change in the relative ratios of the $J = 1$ and $J = 2$ peaks, indicating that the coordination environment of the Eu(III) had not been affected (Figure 5.21).

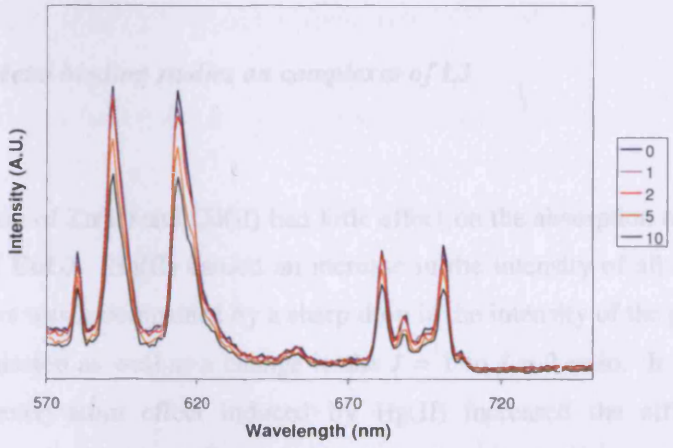

Figure 5.21 – Quenching of Eu(III) emission in **EuL2** on addition of Hg(II).

The quenching effect of Hg(II) could also be observed in the NIR emission profile of **YbL2**, following sensitisation of the Yb(III) *via* irradiation of the anthracene group at 400 nm (Figure 5.22). It is possible that the coordination of the **L2** receptor site to Hg(II) causes its dissociation from the lanthanide ion and slightly increasing q. This would account for the greater degree of quenching observed in the Yb complex, as NIR-luminescent lanthanides are more sensitive to quenching by interactions with the vibrational modes of surrounding solvent molecules.

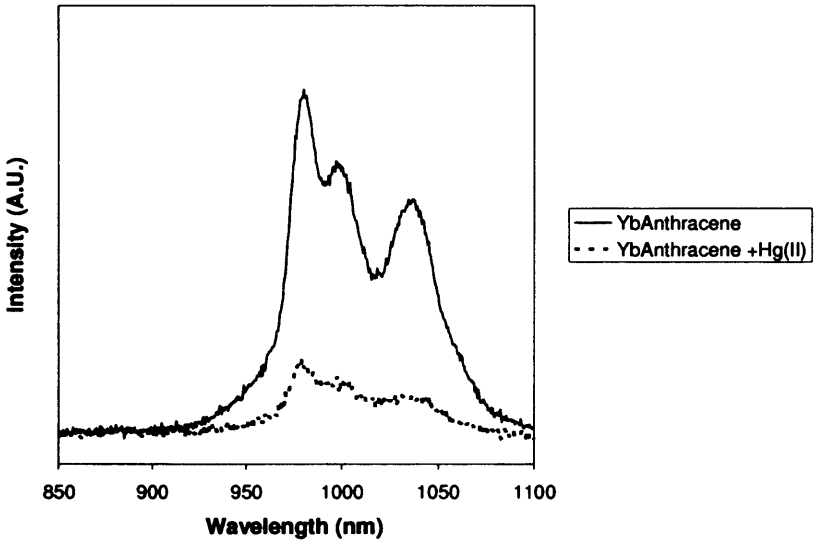

Figure 5.22 – NIR emission of **YbL2** with and without Hg(II).

5.2.3.3 – Metal binding studies on complexes of L3

The addition of Zn(II) and Cd(II) had little effect on the absorption or emission profiles of **EuL3**. Hg(II) caused an increase in the intensity of all absorption bands. This was accompanied by a sharp drop in the intensity of the pyrene and Eu(III) emission as well as a change in the $J = 1$ to $J = 2$ ratio. It is possible that the heavy-atom effect induced by Hg(II) increased the efficiency of intersystem-crossing, quenching the ligand singlet state and increasing the rate of BET from the lanthanide excited state.

The addition of $Cu(ClO_4)_2$ had little effect on the absorption profile but caused a significant change in the emission of **EuL3**. Along with a general quenching of both the ligand and lanthanide luminescence there was a change in structure of the pyrene luminescence. As the intensity dropped the structured fluorescence typical of pyrene (λ_{max} = 395 nm) was replaced by a broad, structureless emission at λ_{max} = 440 nm. This was attributed to the Cu(II) preferentially quenching the pyrene singlet emission, rather than the exciplex or excimer emission.[47]

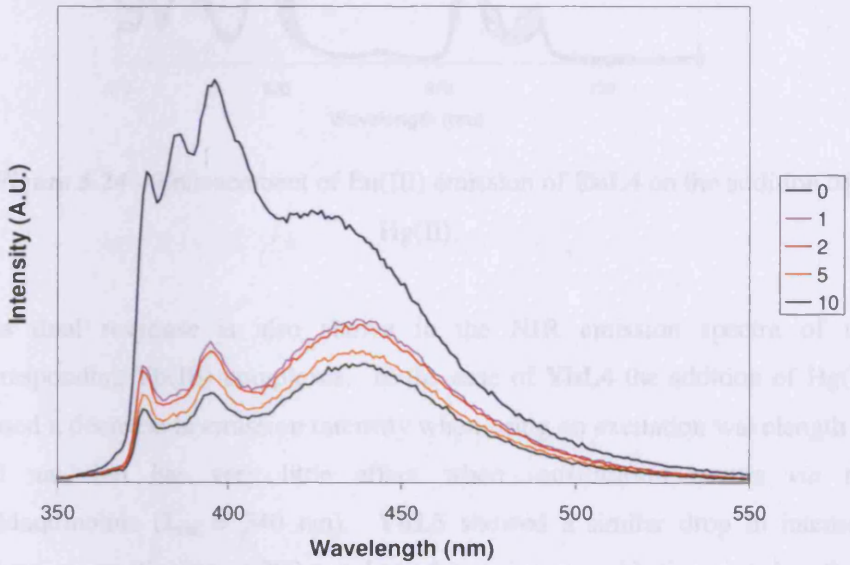

Figure 5.23 – Changes in ligand luminescence of **EuL3** on addition of Cu(II).

5.2.3.4 – Metal binding studies on complexes of L4 and L5

The complexes of **L4** and **L5** both show a slight decrease in absorption on addition of $Zn(ClO_4)_2$ and $Cd(ClO_4)_2$, however this change was not reflected in the Eu(III) emission spectra. On addition of $Hg(ClO_4)_2$ the absorption of the long-wavelength chromophores was increased. Following excitation at 280 nm the Eu(III) emission of both species was decreased and this was accompanied by a change in structure of the hypersensitive transitions. However, following excitation of the long-wavelength chromophores the addition of Hg(II) caused

an increase in intensity of the Eu(III) emission, also accompanied by a change in ratio of the $J = 1$ and $J = 2$ peaks (Figure 5.24).

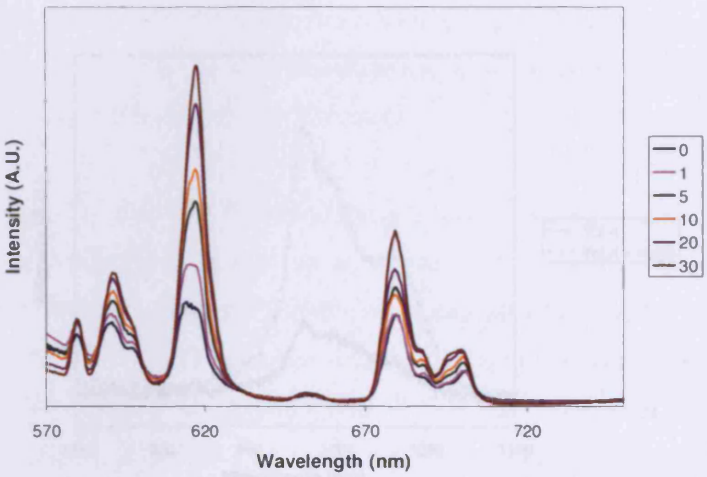

Figure 5.24 – Enhancement of Eu(III) emission of **EuL4** on the addition of Hg(II).

This dual response is also shown in the NIR emission spectra of the corresponding Yb(III) complexes. In the case of **YbL4** the addition of Hg(II) caused a decrease in emission intensity when using an excitation wavelength of 280 nm, but has very little effect when sensitisation occurs *via* the amidoquinoline (λ_{exc} = 340 nm). **YbL5** showed a similar drop in intensity following sensitisation at 280 nm, but when using an excitation wavelength of 400 nm the intensity of Yb(III) NIR emission increases significantly and showed a change in the vibronic structure (Figure 5.25). The lifetime of both complexes was measured in the presence of Hg(II) in H_2O and D_2O and in all cases were longer than the values obtained in the absence of Hg(II) (Table 2). In the case of **YbL5** the q value was also decreased, indicating that the presence of Hg(II) in the binding site limits access of surrounding solvent molecules to the lanthanide, partially accounting for the increased intensity.

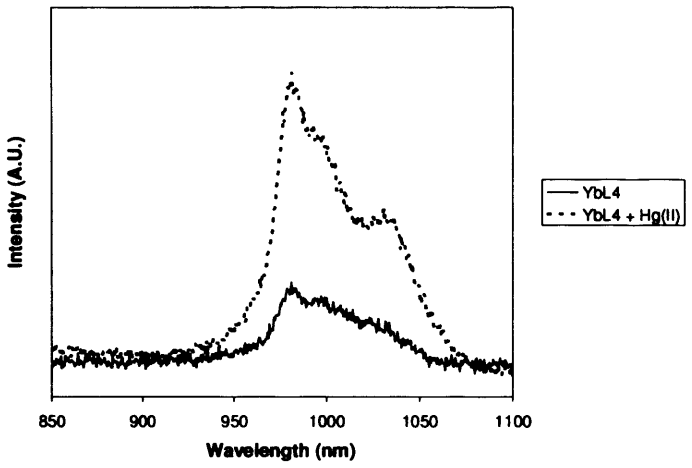

Figure 5.25 – **YbL4** emission profile with and without Hg(II).

Complex	τ_H (μs)	τ_D (μs)	*q*
YbL4	2.60	7.75	0
YbL4 + Hg(II)	3.80	10.98	0
YbL5	1.76	6.31	0.2
YbL5 + Hg(II)	3.85	10.60	0

Table 5.2 – Comparison of lifetimes of YbL4 and YbL5 with and without Hg(II).

5.3 - Conclusions

In conclusion, it has been shown that the synthetic strategy presented in Chapter 4 can be utilised to incorporate a range of long-wavelength chromophores into the receptor site of metal-ion responsive lanthanide complexes. Initially, the secondary amine precursors were synthesised by reductive amination. This approach was shown to be suitable for 8-hydroxyquinoline and aminoanthracene, however attempts to incorporate methylpyrene and

methylquinoline were unsuccessful due to cleavage of the chromophores during the TFA deprotection of the *tert* butyl ester groups. In response to this, aminopyrene, aminoquinoline and aminoanthraquinone were converted to chloroacetamides which then reacted with aminomethyl pyridine to form a secondary amine. The amido chromophores incorporated by this methodology were retained during the deprotection stage.

It was shown that the long-wavelength chromophores were capable of sensitising lanthanide emission. In accordance with literature precedent pyrene and anthracene were shown to capable of sensitising NIR emission from Nd(III) and Yb(III)[37, 38, 43, 44] and quinoline was also shown to be capable of sensitising visible emission from Eu(III) and Tb(III)[30, 68] As predicted from its triplet state anthraquinone (~ 20800 cm^{-1}) was shown to be capable of sensitising emission from Eu(III), Nd(III) and Yb(III).

Comparison between the lifetimes in H_2O and D_2O by application of the modified versions of Horrocks' equation demonstrated that the complexes had q values of between 0 and 1, indicating that there was at most one coordinated, inner sphere solvent molecule. This suggests that the ligands were eight or nine coordinate, implying that the long wavelength amido-chromophores may be involved in coordination to the Ln(III) ions.

Monitoring the UV-Vis absorption profile and ligand luminescence of **EuL1** during the addition of Zn(II) indicated that the ligand was binding to the metal ions, although this did not appear to influence the energy transfer processes to Eu(III) or the Eu(III) coordination environment. However, the addition of Zn(II) to a solution of **YbL1** resulted in an enhancement of emission intensity of the NIR emission coupled with subtle changes in the vibronic structure. Analysis of the luminescence lifetime indicated that the degree of inner sphere hydration was slightly higher after the addition of Zn(II). Due to the lanthanide contraction, Yb(III) is significantly smaller than Eu(III) and tends to form complexes with a coordination number of 8. It is possible that the greater coordination requirements of Eu(III) limited the degree of binding to Zn(II), prevented it from altering the Eu(III) coordination sphere, whereas the Yb(III)

complex allowed a greater degree of binding to Zn(II), which caused structural changes in the ligand and improved access of solvent molecules to the Yb(III).

Typically the complexes showed the greatest response in the presence of Hg(II), which caused increases the absorbance of all ligands. In complexes of **L2** and **L3** this was reflected in the lanthanide emission spectra as a decrease in emission from both the ligand singlet state and the excited lanthanide states. In the case of complexes of **L4** and **L5** the presence of Hg(II) caused a decrease in the intensity of the Eu(III) emission following excitation of *via* the pyridine groups, but an increase following excitation *via* the long wavelength chromophores. This dual-response was also observed in the NIR emission spectrum of **YbL5**. Luminescence lifetime studies indicated that the presence of Hg(II) decreased the access of solvent molecules to the Ln(III) ions, resulting in an enhancement of intensity and an extension of the lifetimes.

5.4 – Experimental

***N*(8-Hydroxyquinaldinyl-2-methyl)-aminoethyl acetate (5)** Glycine ethyl ester (0.40 g, 2.89 mmol, 1 eq.) was added to a stirred solution of 8-hydroxyquinaldine aldehyde (0.50 g, 0.289 mmol, 1 eq.) in MeOH (50 mL) and the mixture was stirred for 3 hours. The solution was then chilled to 0 °C and $NaBH(OAc)_3$ (1.24 g, 5.84 mmol, 2 eq.), was added in small portions over 30 min. The mixture was stirred for 3h then carefully quenched with a few drops of water. The MeOH was removed *in vacuo* and the residue was dissolved in CH_2Cl_2 (50 mL) then extracted with three portions of 0.1 M HCl (3 × 20 mL). The aqueous phases were combined and neutralised with $NaHCO_3$ then extracted with CH_2Cl_2 (100 mL). The organic phases were combined and dried over $MgSO_4$ then removed *in vacuo* to give pure **5** as a dark brown oil (0.59 g, 2.28 mmol, 78.9 %) . ^{1}H NMR (400 MHz, $CDCl_3$): δ_H = 1.18 (3H, t J_{HH} = 7.1, CH_2CH_3), 3.45 (2H, s, $NHCH_2$), 4.05 (2H, s, CH_2NH), 4.12 (2H, q J_{HH} = 7.1, OCH_2CH_3), 7.03 (1H, d J_{HH} = 7.2, aromatic), 7.15 (1H, d J_{HH} = 9, aromatic), 7.28 (2H, m, aromatic) and 7.91 ppm (1H, d J_{HH} = 8.3, aromatic). $^{13}C\{^1H\}$ NMR (62.5 MHz, $CDCl_3$) δ_C = 13.1, 49.2, 53.4, 59.9, 109.4, 116.6, 120.0, 126.2, 126.5, 135.5, 136.5, 151.1, 156.0 and 171.3 ppm. *m/z* (ES); 261. UV-Vis λ_{max} (ε/mol^{-1}dm^{3}cm^{-1}); 230 (600) and 339 (1200) nm. IR υ_{max}($CHCl_3$); 1194, 1474, 1509, 1736, 2253 and 3412 cm^{-1}.

1-(*N*(8-Hydroxyquinaldinyl-2-methyl)-*N*(ethylacetate)-6-aminomethylpyridine-2-methyl)-4,7,10-tris(butoxymethyl)-1,4,7,10-tetrazacyclododecane (10) A solution of **5** (0.063 g, 0.24 mmol, 2 eq.) in MeCN (10 mL) was added to a stirred solution of 9 (0.08 g, 0.12 mmol, 1 eq.), $NaHCO_3$ (0.02 g, 0.24 mmol, 2 eq.) and KI (cat) in MeCN (30 mL) and the mixture was heated to reflux for 2d. After which time it was allowed to cool, filtered over gravity and the solvent was removed *in vacuo*. The residue was dissolved in CH_2Cl_2, filtered over gravity and the solvent was removed *in vacuo*. The residue was dissolved in the minimum amount of hot toluene (~ 15 mL) and left to cool at –20 °C for two days, after which time to solution was decanted to leave the pure product as a dark brown oil (0.060 g, 0.068 mmol, 56.7 %). ^{1}H

NMR (400 MHz, $CDCl_3$): δ_H = 1.13 (3H, t J_{HH} = 7, CH_2CH_2), 1.26 (18H, s, $C(CH_3)_3$), 1.48 (9H, s, $C(CH_3)_3$), 1.60 – 2.55 (10H, br-m, ring CH_2) 2.69 – 3.03 (8H, br-m, ring-CH_2COO, ring-CH_2-pyr), 3.26 (2H, s, pyr-CH_2N), 3.83 (2H, s, quin-CH_2N), 3.91 (2H, s, NCH_2COO), 4.03 (2H, q J_{HH} = 7, CH_2CH_3), 7.07 (1H, d J_{HH} = 7.5, pyr), 7.24 (1H, d J_{HH} = 8, quin), 7.30 (1H, d J_{HH} = 7.5, pyr), 7.33 (1H, d J_{HH} = 7.5, pyr), 7.59 (1H, s, quin), 7.65 (1H, d J_{HH} = 8.5, quin), 7.97 (1H, d J_{HH} = 8.5, quin) and 8.05 ppm (1H, d J_{HH} = 8.5, quin). $^{13}C\{^1H\}$ NMR (62.5 MHz, $CDCl_3$) δ_C = 14.1, 27.8. 27.9, 28.1, 50.2, 53.7, 56.5, 59.7, 60.5, 60.6, 81.9, 82.2, 109.8. 117.7, 121.8, 122.8, 127.2, 127.4, 136.6, 137.0, 137.5, 151.7, 156.9, 157.4, 160.0, 170.8, 172.1 and 172.8 ppm. ES MS: *m/z* 900 $\{M+Na\}^+$.

General Procedure for the deprotection of ligands

The protected ligand precursor was added to a 1:1 mixture of trifluoroacetic acid:CH_2Cl_2 and the mixture was stirred at room temperature overnight. The solvent was removed *in vacuo* and the residue was re-dissolved three times in MeOH to eliminate excess acid. The residue was then dissolved in the minimum volume of MeOH and added dropwise to a stirred Et_2O at 0 °C. The precipitate was filtered and dried to give the deprotected ligand.

1-(*N*(8-Hydroxyquinaldinyl-2-methyl)-*N*(ethylacetate)-6-aminomethylpyridine-2-methyl)-4,7,10-tris(carboxymethyl)-1,4,7,10-tetrazacyclododecane (L1) was isolated as a dark brown powder (61 %). ^1H NMR (400 MHz, D_2O): δ_H 1.28 (3H, t J_{HH} = 7, CH_2CH_3), 3.07 - 3.72 (28H, br-m, ring CH_2), 3.97 (2H, br-s, NCH_2COO), 4.12 (4H, s, pyridine-CH_2N), 4.21 (2H, q J_{HH} = 7, CH_2CH_3), 4.31 (2H, br-s, quinoline-CH_2N), 7.33 (1H, d J_{HH} = 7.8, pyridine), 7.48 (1H, br-m, quinoline), 7.56 (1H, br-m, pyridine), 7.63 (2H, m, quinoline), 7.85 (2H, m, pyridine and quinoline) and 8.64 ppm (1H, d J_{HH} = 8, quinoline). ES^+ MS: *m/z* 836 $\{M + 2Cu\}^+$. HRMS (ESI^+) found *m/z* 710.3508 $\{M + H\}^+$; $C_{35}H_{48}N_7O_9$ requires 710.3493. UV-Vis λ_{max} (ε/$mol^{-1}dm^3cm^{-1}$); 211 (2100), 247 (2100) and 305 (200) nm. IR υ_{max}(ATR, solid); 3372, 1719, 1668, 1635, 1180 and 1126 cm^{-1}.

General Procedure for the formation of lanthanide complexes

A mixture of the ligand (approx. 0.020 g) and $Ln(OTf)_3$ was stirred in MeOH (10 mL) at 50 °C for 24h. The solution was reduced *in vacuo* then added dropwise to stirring diethyl ether at 0 °C. The precipitate was filtered, washed with diethyl ether and dried to give the lanthanide complex.

NdL1 was isolated as a pale brown powder. (0.022, 92 %) ES MS: *m/z* 873 {M + Na}$^+$. HRMS (ESI$^+$) found *m/z* 839.2351 {M + H}$^+$; $C_{35}H_{44}N_7O_9Nd_1$ requires 839.2350. IR υ_{max}(ATR, solid); 3429, 1594,1158 and 1082 cm^{-1}.

EuL1 was isolated as a yellow powder. (0.023, 95 %) ES MS: *m/z* 860 {M + H}$^+$, 882 {M + Na$^+$}, 898 {M + K$^+$} and 922 {M + Cu$^+$}. HRMS (ESI$^+$) found *m/z* 860.2489 {M + H}$^+$; $C_{35}H_{44}N_7O_9Eu_1$ requires 860.2472. IR υ_{max}(ATR, solid); 3490, 1583, 1164 and 1084 cm^{-1}.

GdL1 was isolated as a yellow powder. (0.021, 86 %) ES MS: *m/z* 865 {M + H}$^+$. IR υ_{max}(ATR, solid); 3527, 1595, 1160 and 1083 cm^{-1}.

TbL1 was isolated as a yellow powder. (0.022, 90 %) HRMS (ESI$^+$) found *m/z* 866.2527 {M + H}$^+$; $C_{35}H_{44}N_7O_9{}^{159}Tb$ requires 866.2524. IR υ_{max}(ATR, solid); 3568, 1594, 1162 and 1082 cm^{-1}.

YbL1 was isolated as a yellow powder. (0.023, 93 %) ES MS: *m/z* 943 {M + Cu}$^+$. HRMS (ESI$^+$) found *m/z* 881.2668 {M + H}$^+$; $C_{35}H_{44}N_7O_9Yb_1$ requires 881.2654. IR υ_{max}(ATR, solid); 3566, 1596, 1158 and 1081 cm^{-1}.

***N*(2-methylpyridine)-2-aminoanthracene (14)** pyridine-2-carboxaldehyde (0.100 g, 0.93 mmol, 1 eq.) was added to a solution of 2-aminoanthracene (0.180 g, 0.93 mmol, 1 eq) in MeOH (20 mL) and the mixture was stirred overnight after which time $NaBH_4$ (0.050 g, 1.40 mmol, 1.5 eq.) was added and the mixture was stirred for a further 1d. The mixture was carefully quenched with water and the solvent was removed *in vacuo*. The resultant oil solid was dissolved in CH_2Cl_2 (30 mL) and was washed three times with water (3 × 10

mL), the organic phase was dried over $MgSO_4$, filtered and removed *in vacuo* to give the desired product as a yellow/green solid (0.117 g, 0.62 mmol, 66.7 %). ^{1}H NMR (400 MHz, $CDCl_3$): δ_H 5.00 (2H, s, CH_2), 6.75 (1H, d J_{HH} = 1.9, aro), 7.06 (1H, dd J_{HH} = 2.2 and 9.0, aro), 7.12 (1H, t J_{HH} = 6.6, aro), 7.42 (2H, m, aro), 7.56 (1H, dt J_{HH} = 1.7 and 7.6, aro), 7.83 (1H, m, aro), 7.94 (2H, m, aro), 8.28 (1H, s, aro), 8.37 (1H, s, aro), 8.49 (1H, s, aro) and 8.63 ppm (1H, d J_{HH} = 4.0, aro). $^{13}C\{^1H\}$ (100 MHz, $CDCl_3$) δ_C 49.4, 102.3, 120.8, 122.2, 122.7, 123.1, 124.0, 125.7, 126.6, 127.8, 127.9, 128.7, 129.8, 129.9, 132, 9, 134.0, 137.2, 145.1, 149.6 and 158.2 ppm. ES^+ MS: *m/z* 284 $\{M + H\}^+$. HRMS (ESI^+) found *m/z* 285.1395 $\{M + H\}^+$; $C_{20}H_{17}N_2$ requires 285.1392. UV-Vis λ_{max} (ε/mol^{-1}dm^{3}cm^{-1}); 203 (1218), 249 (3684), 267 (5209), 320 (401), 336 (457), 350 (222) and 407 (287) nm. IR υ_{max}($CHCl_3$); 1201, 1423, 1476, 1520, 2400 and 3032 cm^{-1}.

***N*(2-methylpyridine)aminomethylpyrene (15)** pyridine-2-carboxaldehyde (0.079 g, 0.74 mmol, 1eq.) was added to a solution of aminomethylpyrene (0.200 g, 0.74 mmol, 1 eq.) in MeOH (50 mL) and the mixture was stirred for 3h. $NaBH(OAc)_3$ (0.237 g, 1.11 mmol, 1.5 eq.) was added at 0 °C over 30 min and the solution was allowed to warm to ambient temperature and stirred overnight. A few drops of water was added to quench the reaction and the solvent was removed *in vacuo* and the residue was dissolved in CH_2Cl_2 (30 mL) and washed three times with water (3 × 10 mL). The organic phase was dried over $MgSO_4$ and filtered under gravity before being removed *in vacuo* to yield the pure product as a dark brown oil (0.182 g, 0.59 mmol, 79.7 %). ^{1}H NMR (400 MHz, $CDCl_3$): δ_H 3.28 (1H, br-s, NH), 3.99 (2H, s, CH_2), 4.43 (1H, s, CH_2), 7.06 (1H, dt, J_{HH} = 4 and 8, pyridine), 7.24 (1H, d, J_{HH} = 8, pyridine), 7.53 (1H, dt J_{HH} = 4 and 8, pyridine), 7.86 – 7.94 (4H, m, pyrene), 7.99 – 8.08 (4H, m, pyrene) 8.27 (1H, d J_{HH} = 12, pyrene) and 8.49 pmm (1H, d J_{HH} = 4, pyridine). $^{13}C\{^1H\}$ (62.5 MHz, $CDCl_3$) ($_C$ 49.8, 53.3, 121.2, 121.5, 122.0, 123.7, 123.9, 124.0, 124.1 (br), 124.8, 126.1, 126.4, 126.7, 128.2, 129.7, 129.8, 130.2, 131.2, 135.5, 148.2 and 157.5 ppm. HRMS (ESI^+) found *m/z* 323.1538 $\{M + H\}^+$; $C_{23}H_{18}N_2$ requires 323.1548. UV-Vis λ_{max} (ε / mol^{-1} dm^3 cm^{-1}); 206.5 (4217), 237.5 (7399), 270.5 (4381) and 338.5 (3826) nm. IR υ_{max}($CHCl_3$);

1200.5, 1213.0, 1225.5, 1236.15 (C-N), 1433.8, 1476.2, 1509.0, 1597.7 and 3036 cm^{-1}.

Quinolin-2-ylmethanamine (18) 2-(bromomethyl)quinoline (1.40 g, 6.3 mmol, 1 eq.) was added to a solution of potassium phthalimide (1.16 g, 6.3 mmol, 1 eq.) in DMF and the mixture was heated to 90 °C for 1 h. The solution was then allowed to cool and CH_2Cl_2 was added. The organic phase was washed with H_2O and KOH (0.1 M) before the solvent was removed *in vacuo* to give 1-(quinolin-2-ylmethyl)pyrrolidine-2-5-dione as a brown oil (1.36 g, 5.7 mmol, 90 %). ^{1}H NMR (400 MHz, $CDCl_3$): δ_H 5.13 (2H, s, CH_2), 7.30 (1H, d J_{HH} = 8.4, quin), 7.43 (1H, t J_{HH} = 7.6, quin), 7.59 (1H, t J_{HH} = 7.6, quin), 7.70 (3H, m, quin + pyr), 7.85 (2H, m, pyr), 7.91 (1H, d J_{HH} = 8.0, quin) and 8.04 (1H, d J_{HH} = 8.4, quin). 1-(quinolin-2-ylmethyl)pyrrolidine-2-5-dione (1.36 g, 5.7 mmol, 1 eq.) was then mixed with hydrazine (0.18, 5.6 mmol, 1 eq.) in ethanol (50 mL) and heated to reflux for 2 h, after which time to solvent was removed *in vacuo* and residue dissolved in ethyl acetate (50 mL). The organic phase was then washed with KOH (3 x 20 mL, 1 M) before being dried *in vacuo* to yield the title compound as a brown oil (0.72 g, 4.6 mmol, 81 %). ^{1}H NMR (400 MHz, $CDCl_3$): δ_H 2.99 (2H, br-s, NH_2), 4.16 (2H, s, CH_2), 7.29 (1H, d J_{HH} = 8.4, quin), 7.45 (1H, t J_{HH} = 7.2, quin), 7.627 (1H, t J_{HH} = 7.6. quin), 7.70 (1H, d J_{HH} = 5.6, quin), 7.97 (1H, d J_{HH} = 4.8, quin) and 8.03 ppm (1H, d J_{HH} = 8.4, quin).

Bis(quinolin-2-ylmethyl)amine (20) quinolin-2-ylmethanamine (0.72 g, 4.6 mmol, 1 eq.) was mixed with quinoline-2-carbaldehyde (0.72, 4.6 mmol, 1 eq.) in methanol (30 mL) and stirred at room temperature for 3h, after which time the solution was chilled to 0 °C and $NaBH(OAc)_3$ (3.90 g, 18.4 mmol, 4 eq.) was added. The solution was allowed to warm to room temperature and stirred overnight, after which time the solvent was removed *in vacuo*. The residue was dissolved in $CHCl_3$ (50 mL) and washed with water, then HCl (5 x 10 mL, 0.1 M). The acid solution was then neutralised and extracted with $CHCl_3$ (3 x 20 mL) which was then removed *in vacuo* to give the desired product as a brown oil (0.59 g, 2.0 mmol, 43 %). ^{1}H NMR (400 MHz, $CDCl_3$): δ_H 2.66 (1H, s, NH_2), 4.85 (4H, s, $(CH_2)_2NH$), 7.21 (2H, s J_{HH} = 8.4. quin), 7.65 (2H, s J_{HH} = 7.6, quin), 7.65 (2H, t J_{HH} = 6.8, quin), 8.01 (2H, d, quin) and 8.09 ppm (2H, d,

quin).

1-(*N*(2-methylpyridine)-*N*(2-anthracene)-6-aminomethylpyridine-2-methyl)-4,7,10-tris(*tert*-butoxycarbonyl)-1,4,7,10-tetrazacyclododecane (21) *N*(2-methylpyridine)-2-aminomethylanthracene (0.03 g, 0.11 mmol, 1 eq), $NaHCO_3$ (0.02, 0.23 mmol, 2 eq.)) and KI (cat) were added to a stirred solution of 1-(6-chloromethylpyridine-2-methyl)-4,7,10-tris(*tert*-butoxycarbonyl)-1,4,7,10-tetraazacyclododecane (0.07, 0.11, 1 eq.) in MeCN (15 mL) and the mixture was heated to reflux for 2d. After which time it was allowed to cool, filtered over gravity and the solvent was removed *in vacuo*. The crude mixture was separated by column chromatography (CH_2Cl_2) to give the pure product as a yellow-green oil (0.03, 0.03 mmol, 27.2 %). NMR (400 MHz, $CDCl_3$): δ_H 1.28 (18H,s, $C(CH_3)_3$), 1.39 (9H, s, $C(CH_3)_3$), 1.95 – 2.52 (10H, br-m, ring CH_2) 2.52 – 3.07 (14H, br-m, ring CH_2), 4.83 (2H, s, NCH_2), 4.89 (2H, s, NCH_2), 6.61 (1H, d J_{HH} = 1.8, aro), 6.82 (1H, s, aro), 7.06 (1H, dd J_{HH} = 2.2 and 8.6, aro), 7.17 (2H, m, aro), 7.20 (1H, dd J_{HH} = 3.1 and 8.3, aro), 7.28 (1H, m, aro), 7.31 (1H, m, aro), 7.54 (2H, m, aro), 7.75 (2H, m, aro), 7.83 (1H, m, aro), 7.92 (1H, s, aro), 8,17 (1H, s, aro) and 8.56 ppm (1H, d J_{HH} = 4.9, aro). ES^+ MS: *m/z* 903 $\{M+H^+\}^+$, 924 $\{M+Na^+\}^+$. λ_{max} (ε/$mol^{-1}dm^3cm^{-1}$); 205 (21524), 230 (22490), 268 (36929), 338 (4367), 356 (2457) and 407 (2642) nm. $\upsilon_{max}(CHCl_3)$; 1227, 1425, 1521, 1726, 3015 cm^{-1}.

1-(*N*(2-methylpyridine)-*N*(methylpyrene)-6-aminomethylpyridine-2-methyl)-4,7,10-tris(*tert*-butoxycarbonyl)-1,4,7,10-tetrazacyclododecane (22) *N*(2-methylpyridine)aminomethylpyrene (0.066 g, 0.20 mmol, 1 eq.), $NaHCO_3$ (0.018 g, 0.21 mmol, 1 eq.) and KI (cat) were added to a stirred solution of 1-(6-chloromethylpyridine-2-methyl)-4,7,10-tris(*tert*-butoxycarbonyl)-1,4,7,10-tetraazacyclododecane (0.14 g, 0.21 mmol, 1 eq.) in MeCN (20 mL) and the mixture was heated to reflux for 2d. After which time it was allowed to cool, filtered over gravity and the solvent was removed *in vacuo*. The organic phase was then dissolved in the minimum amount of hot toluene (~ 30 mL). The solution was allowed to cool in a freezer for two weeks, after which time the solution was decanted to leave the product as a yellow brown oil (0.13 g, 0.14

mmol, 65.9 %). ^{1}H NMR (400 MHz, $CDCl_3$): δ_H 1.34 (18H, s, $C(CH_3)_3$), 1.40 (9H, s, $C(CH_3)$, 1.94 (8H, br-s, ring CH_2) 2.89 (6H, br-s, ring CH_2), 2.97 (4H, br-s, ring CH_2), 3.24 (4H, br-s, ring CH_2), 3.60 (2H, br-s), 3.95 (2H, br-s), 4.64 (2H, br-s), 7.00 (1H, t J_{HH} = 4, pyridine), 7.15 (1H, d J_{HH} = 8, pyridine), 7.27 (1H, d J_{HH} = 8, linker pyridine), 7.40 (1H, d J_{HH} = 8, linker pyridine), 7.47 (1H, dt J_{HH} = 4 and 8, pyridine), 7.63 (1H, t J_{HH} = 8, linker pyridine), 7.89 – 7.96 (5H, m, pyrene), 7.99 (1H, d J_{HH} = 8, pyrene) 8.04 (1H, d J_{HH} = 8, pyrene), 8.10 (1H, s, pyrene), 8.12 (1H, s, pyrene) and 8.37 ppm(1H, d J_{HH} = 8, pyridine). $^{13}C\{^1H\}$ (62.5 MHz, $CDCl_3$) ($_C$ 27.9, 28.3, 50.2, 56.8, 61.1, 77.3, 82.0, 82.3, 122.9, 123.0, 124.4, 124.6, 125.1, 126.0, 127.4, 128.2, 129.0, 129.8, 130.8, 131.2, 132.2, 136.4, 137.4, 157.0, 159.7, 160.7, 172.2 and 173.0 ppm. ES^+ MS: *m/z* 940 $\{M + H\}^+$. HRMS (ESI^+) found *m/z* 940.5694 $\{M + H\}^+$; $C_{56}H_{73}N_7O_6$ requires 940.5701. UV-Vis λ_{max} (ε / mol^{-1} dm^3 cm^{-1}); 208 (3597), 238 (4402), 272 (2544) and 340 (2074) nm. IR $\upsilon_{max}(CHCl_3)$; 1016, 1156 (C-O) and 1727 (C=O) cm^{-1}.

1-(*N*(bisquinolin-2-yl)-6-aminomethylpyridine-2-methyl)-4,7,10-tris(carboxymethyl)-1,4,7,10-tetrazacyclododecane (23) Bis(quinolin-2-ylmethyl)amine (0.215 g, 0.72 mmol, 1 eq.) was added to a stirred solution of 1-(6-chloromethylpyridine-2-methyl)-4,7,10-tris(*tert*-butoxycarbonyl)-1,4,7,10-tetraazacyclododecane (0.47 g, 0.72 mmol, 1 eq.), $NaHCO_3$ (0.12 g, 1.4 mmol, 2 eq.) and KI (cat.) in MeCN (20 mL) and the mixture was stirred at reflux for 2 days, after which time it was allowed to cool, filtered over gravity and the solvent was removed *in vacuo*. The residue was dissolved in the minimum volume of hot toluene (~ 50 mL) and left at – 20 °C for 2 days. The solution was decanted to leave the product as a brown oil (0.166 g, 0.18 mmol, 25 %). ^{1}H NMR (400 MHz, $CDCl_3$): 1.32 (18H, s, $C(CH_3)_3$), 1.44 (9H, s, $C(CH_3)$, 2.11 – 2.49 (8H, br-m, ring CH_2) 2.63 – 3.13 (16H, br-m, ring CH_2), 4.40 (2H, s, ring-CH_2-pyr), 4.57 (2H, s, pyr-CH_2-N), 4.85 (4H, s, NCH_2-pyr), 7.11 (1H, d J_{HH} = 7, pyr), 7.23 (2H, d J_{HH} = 9, quin), 7.26 (1H, d J_{HH} = 7, pyr), 7.47 (2H, t J_{HH} = 9, quin), 7.58 (2H, d J_{HH} = 8, quin), 7.65 (1H, d J_{HH} = 7, pyr), 7.76 (2H, d J_{HH} = 8, quin), 8.00 (2H, d J_{HH} = 9, quin) and 8.07 ppm (2H, d J_{HH} = 8, quin).

1-(*N*(2-methylpyridine)-*N*(2-anthracene)-6-aminomethylpyridine-2-methyl)-4,7,10-tris(carboxymethyl)-1,4,7,10-tetrazacyclododecane (L2) was isolated as a brown solid (0.0132 g, 54 %). ^{1}H NMR (400 MHz, D_2O): δ_H 2.80 – 3.65 (22H, br-m, ring-CH_2), 4.71 (2H, s, NCH_2), 5.08 (2H, s, NCH_2), 5.13 (1H, s, NCH_2), 6.98 (1H, s, aro), 7.08 (1H, d J_{HH} = 9.1, aro), 7.21 (1H, t J_{HH} = 7.4, aro), 7.27 (1H, dt J_{HH} = 1.8 and 8.3, aro), 7.33 (1H, m, aro), 7.45 (1H, t J_{HH} = 8.1, aro), 7.54 (1H, d J_{HH} = 7.4, aro), 7.61 (1H, d J_{HH} = 5.9, aro), 7.72 – 7.87 (4H, m, aro), 7.92 (1H, s, aro), 8.00 (1H, s, aro), 8.16 (1H, s, aro) and 8.24 ppm (1H, s, aro).). ES$^+$ MS: *m/z* 732 {M + H}$^+$. UV-Vis λ_{max} (ε); 270 (15800) and 420 (1500) nm. IR υ_{max}(ATR, solid); 3454, 3094, 1670, 1626, and 1179 cm^{-1}.

NdL2 was isolated as a brown powder. (0.023, 96 %) ES$^+$ MS: *m/z* 875 {M + H}$^+$. IR υ_{max}(ATR, solid); 3650, 1559, 1521, 1159 and 1084.

EuL2 was isolated as a brown powder. (0.021, 87 %) ES$^+$ MS: *m/z* 884 {M + H}$^+$. IR υ_{max}(ATR, solid); 3642, 1575, 1158 and 1078 cm^{-1}.

GdL2 was isolated as a brown powder. (0.021, 86 %) ES$^+$ MS: *m/z* 889 {M + H}$^+$. 889 IR υ_{max}(ATR, solid); 3630, 1624, 1577 and 1082 cm^{-1}.

TbL2 was isolated as a brown powder. (0.022, 90 %) ES$^+$ MS: *m/z* 890 {M + H}$^+$. HRMS (ESI$^+$) found *m/z* 890.2679 {M + H}$^+$; $C_{41}H_{44}N_7O_6{}^{159}Tb$ requires 890.2678. IR υ_{max}(ATR, solid); 3562, 1576, 1560, 1154 and 1079 cm^{-1}.

YbL2 was isolated as a brown powder. (0.023, 93 %) ES$^+$ MS: *m/z* 904 {M + H}$^+$. HRMS (ESI$^+$) found *m/z* 905.2815 {M + H}$^+$; $C_{41}H_{44}N_7O_6Yb_1$ requires 905.2820. IR υ_{max}(ATR, solid); 3650, 1653, 1559, 1521, 1159 and 1084 cm^{-1}.

General Procedure for the synthesis of secondary amines from chloracetamides

The chloroacetamide (1 eq.) was dissolved in MeCN and the solution was added dropwise to a stirred mixture of aminomethyl pyridine (2 eq.), $NaHCO_3$ (2 eq.)

and KI (cat.) at room temperature. The mixture was then heated to reflux and stirred overnight after which time it was left to cool, filtered over gravity and the solvent was removed *in vacuo*. The residue was purified by column chromatography $CH_2Cl_2 \rightarrow CH_2Cl_2$:MeOH (9:1).

N-(pyren-2-yl)-2-(pyridin-2-ylmethylamino)acetamide (32) was isolated as a yellow oil (88 %) NMR (400 MHz, $CDCl_3$): δ_H = 3.52 (2H, s, NHCH_2-pyr), 3.87 (2H, s, COCH_2NH), 7.21 (2H, d J_{HH} = 5.6, pyrene-H), 7.78 (1H, d J_{HH} = 9.2, pyridine-H), 7.88 (4H, m, pyrene-H, pyridine-H), 8.03 (3H, m, pyrene-H, pyridine-H), 8.53 (3H, m, pyrene-H) and 9.93 ppm(1H, br-s, CONH). $^{13}C\{^1H\}$ (62.5 MHz, $CDCl_3$) δ_C = 52.1, 54.1, 119.1, 119.2, 121.0, 121.4, 121.5, 123.7, 124.1, 124.2, 124.4, 125.0, 125.4, 126.4. 126.6, 127.4, 129.7, 129.8, 130.4, 135.7, 148.7, 157.3 and 169.2 ppm. HRMS (ESI^+) found *m/z* 365.1526 $\{M + H\}^+$; $C_{24}H_{19}N_3O_1$ requires 365.1528. λ_{max} (ε/mol^{-1}dm^{3}cm^{-1}); 207 (28000), 242 (50200), 277 (30100) and 341 (28900) nm. υ_{max}($CHCl_3$); 1200, 1417, 1524, 1556, 1602, 1686, 2253 and 3023 cm^{-1}.

2-(pyridin-2-ylmethylamino)-N-(quinolin-8-yl)acetamide (33) was isolated as a red oil (72.5 %); NMR (400 MHz, $CDCl_3$): δ_H = 3.42 (2H, s, NHCH_2-pyr), 3.92 (2H, s, COCH_2NH), 7.22 (1H, m, quin-H), 7.53 (1H, d J_{HH} = 7.6, pyr-H), 7.59 (1H, t J_{HH} = 7.2, pyr-H), 7.73 (1H, m, pyr-H, quin-H), 7.82 (1H, d J_{HH} = 0.8, pyr-H), 8.05 (2H, d J_{HH} = 6.8, quin-H), 8.45 (1H, d J_{HH} = 5.1, quin-H), 8.66 (1H, d J_{HH} = 2.4, quin-H) and 11.01 pmm(1H, s, CONH). $^{13}C\{^1H\}$ (62.5 MHz, $CDCl_3$) δ_C = 51.6, 53.5, 121.5, 121.7, 122.3, 126.1, 126.7, 127.1, 127.2, 127.9, 130.5, 135.9, 143.1, 144.0, 148.5, 156.6 and 169.4 ppm. ES+ MS: *m/z* 293 $\{M+H\}^+$. λ_{max} (ε/mol^{-1}dm^{3}cm^{-1}); 211 (28800), 250 (34500), 322 (3600) and 332 (3200) nm. υ_{max}($CHCl_3$); 1208, 1424, 1529, 1687, 2433 and 3013 cm^{-1}.

N-(anthraquinocen-2-yl)-2-(pyridin-2-ylmethylamino)acetamide (34) was isolated as a yellow powder (52.7 %). NMR (400 MHz, $CDCl_3$): δ_H = 3.54 (2H, s, NHCH_2-pyr), 4.04 (2H, s, COCH_2NH), 7.14 (1H, m, anth-H), 7.43 (1H, d J_{HH} = 7.6, pyr-H), 7.65 (1H, dt J_{HH} = 2 and 7.6, pyr-H), 7.72 (3H, m, pyr-H, anth-H), 8.03 (1H, dd J_{HH} = 1.2 and 7.6, pyr-H), 8.21 (2H, m, anth-H), 8.53 (1H, d J_{HH} =

4, anth-H), 9.18 (1H, dd J_{HH} = 1.2 and 8.8, anth-H) and 16.16 ppm(1H, s, CONH). $^{13}C\{^1H\}$ (62.5 MHz, $CDCl_3$) δ_C = 53.59, 55.13, 118.40, 122.28, 122.62, 122.68, 126.37, 126.97, 127.35, 132.78, 134.18, 134.24, 135.52, 136.56, 141.29, 149.45, 158.90, 172.36 and 186.49 ppm. ES+ MS: *m/z* 371 $\{M+H\}^+$. λ_{max} (ε/mol^{-1}dm^{3}cm^{-1}); 205 (7600), 223 (7100), 261 (9000), 329 (800) and 396 (1300) nm. $\upsilon_{max}(CHCl_3)$; 1017, 1211, 1423, 1520, 1579, 2434 and 3014 cm^{-1}.

General procedure for the reaction of amino-acetamides and 1

The amino-acetamide (1 eq.) was added to a mixture of 1 (1 eq.), $NaHCO_3$ (2 eq.) and KI (cat.) in MeCN, which was then heated to reflux and stirred overnight. The mixture was then allowed to cool, filtered over gravity and the solvent was removed *in vacuo*. The residue was then dissolved in the minimum amount of hot toluene and left to cool at -5 °C overnight. The solvent was then decanted to leave the pure product.

{N-(pyren-2-yl)-2-(pyridin-2-ylmethyl)acetamide}amino-6-methylpyridinyl-2-methyl-4,7,10-tris(*tert*-butoxycarbonyl)-1,4,7,10-tetrazacyclododecane (35) was isolated as a brown oil. (0.135 g, 81.0 %); NMR (400 MHz, $CDCl_3$): δ_H = 1.33 (18H, s, $C(CH_3)_3$), 1.48 (9H, s, $C(CH_3)_3$), 2.24 (6H, br-m, NCH_2), 2.68 (16H, br-m, ring-CH_2), 2.95 (2H, br-s, ring-CH_2-pyr), 3.42 (2H, s, $COCH_2N$), 3.54 (2H, s, CH_2N), 3.97 (2H, s, NCH_2), 7.12 (3H, m, pyrene-H, pyridine-H), 7.55 (2H, d J_{HH} = 4.7, pyrene-H), 7.58 (1H, m, pyridine-H), 7.95 (2H, m, pyrene-H, pyridine-H), 8.06 (2H, m, pyrene-H), 8.13 (3H, m, pyrene-H, pyridine-H), 8.48 (2H, d J_{HH} = 9.1, pyrene-H), 8.56 (1H, d J_{HH} = 8.4, pyridine) and 11.28 ppm(1H, s, CONH). $^{13}C\{^1H\}$ (62.5 MHz, $CDCl_3$) δ_C = 28.05, 28.13, 40.5, 50.0 (br), 55.8, 56.6, 61.4, 82.2, 82.3, 120.6, 121.1, 122.4, 122.9, 123.1, 123.2, 124.8, 125.3, 126.3, 126.5, 127.4, 127.8, 130.9, 131.4, 136.9, 137.6, 149.9, 157.4, 157.7, 159.0, 170.0, 172.4 and 172.9 ppm. HRMS (ESI^+) found *m/z* 1005.5549 $\{M + Na\}^+$; $C_{57}H_{74}N_8O_7Na$ requires 1005.5578. λ_{max} (ε/mol^{-1}dm^{3}cm^{-1}); 208 (15600), 242 (28900), 277 (17600) and 342 (15600) nm. $\upsilon_{max}(CHCl_3)$; 1225, 1424, 1476, 1520, 1567 and 1725 cm^{-1}.

{2-(pyridin-2-ylmethyl)-N-(quinolin-8-yl)acetamide}amino-6-

methylpyridinyl-2-methyl-4,7,10-tris(*tert*-butoxycarbonyl)-1,4,7,10-tetrazacyclododecane (36) was isolated as a brown/red oil (0.220 g, 63.3 %); NMR (400 MHz, $CDCl_3$): δ_H = 1.36 (18H, s, $C(CH_3)_3$), 1.49 (9H, s, $C(CH_3)_3$), 2.07 – 2.41 (6H, br-m, NCH_2), 2.41 – 3.10 (16H, br-m, ring-CH_2), 2.97 (2H, br-s, ring-CH_2-pyr), 3.42 (2H, s, $COCH_2N$), 3.84 (2H, s, CH_2N), 3.88 (2H, s, NCH_2), 7.08 (2H, m, pyr-H, quin-H), 7.33 (1H, d J_{HH} = 7.7, link pyr-H), 7.48 (2H, m, pyr-H, link pyr-H), 7.56 (3H, dq J_{HH} = 1.8 and 7.6, pyr-H, quin-H), 7.73 (1H, d J_{HH} = 7.4, link pyr-H), 7.97 (1H, d J_{HH} = 8.4, quin-H), 8.75 (1H, d J_{HH} = 4.6, pyr-H), 8.82 (1H, d J_{HH} = 2.4, quin-H), 9.01 (1H, d J_{HH} = 2.5, quin-H) and 11.33 ppm(1H, s, CONH). $^{13}C\{^1H\}$ (250 MHz, $CDCl_3$) δ_C = 28.05, 28.14, 40.49, 50.15, 55.93, 56.65, 58.13, 60.95, 82.16, 82.29, 122.52, 123.09, 123.24, 127.11, 127.72, 128.33, 128.80, 132.19, 137.62, 144.32, 144.88, 149.62, 157.25, 157.74, 158.99, 170.52, 172.33 and 172.94 ppm. ES+ MS: *m/z* 932 $\{M+Na\}^+$. λ_{max} (ε/mol^{-1}dm^{3}cm^{-1}); 221 (21400), 250 (25600), 323 (3500) and 333 (3300) nm. υ_{max}($CHCl_3$); 1211, 1424, 1522, 1674, 1725 and 3015 cm^{-1}.

{N-(anthraquinocen-2-yl)-2-(pyridin-2-ylmethyl)acetamide}amino-6-methylpyridinyl-2-methyl-4,7,10-tris(*tert*-butoxycarbonyl)-1,4,7,10-tetrazacyclododecane (37) was isolated as a yellow oil (0.125 g, 41.2 %); NMR (400 MHz, $CDCl_3$): δ_H = 1.30 (18H, s, $C(CH_3)_3$), 1.49 (9H, s, $C(CH_3)_3$), 2.17 (6H, br-m, NCH_2), 2.20 – 2.90 (16H, br-m, ring-CH_2), 2.98 (2H, br-s, ring-CH_2-pyr), 3.47 (2H, s, $COCH_2N$), 3.82 (2H, s, CH_2N), 3.89 (2H, s, NCH_2), 7.06 (1H, t J_{HH} = 4.0, pyr-H), 7.17 (1H, d J_{HH} = 7.8, link pyr-H), 7.60 (1H, dt J_{HH} = 1.7 and 7.6, pyr-H), 7.67 (2H, q J_{HH} = 7.6, link pyr-H, anth-H), 7.80 (1H, dt J_{HH} = 1.4 and 7.6, link pyr-H), 7.88 (1H, dt J_{HH} = 1.3 and 7.5, anth-H), 7.94 (1H, d J_{HH} = 7.9, pyr-H), 8.00 (1H, dd J_{HH} = 1.1 and 7.6, anth-H), 8.15 (1H, d J_{HH} = 7.8, anth-H), 8.24 (1H, dd J_{HH} = 7.3 and 11.6, anth-H), 8.33 (1H, dd J_{HH} = 0.9 and 7.8, anth-H), 8.40 (1H, d J_{HH} = 4.0, pyr-H), 9.03 (1H, dd J_{HH} = 1.1 and 8.6, anth-H) and 13.00 ppm(1H, s, CONH). $^{13}C\{^1H\}$ (250 MHz, $CDCl_3$) δ_C = 28.03, 28.21, 50.26, 56.75, 58.21, 62.02, 82.16, 82.43, 118.22, 122.70, 123.25, 126.11, 127.10, 134.04, 134.58, 134.73, 135.47, 136.74, 141.15, 149.01, 157.26, 157.88, 159.16, 171.12, 172.27, 172.86, 182.8 and 186.7 ppm. ES+ MS: *m/z* 989 $\{M+H\}^+$. λ_{max} (ε/mol^{-1}dm^{3}cm^{-1}); 224 (22700), 258 (24600), 334 (3000) and 401

(4100) nm. $\upsilon_{max}(CHCl_3)$; 1228, 1311, 1417, 1509, 1593, 1650, 1725, 2253 and 2836 cm^{-1}.

{N-(pyren-2-yl)-2-(pyridin-2-ylmethyl)acetamide}amino-6-methylpyridinyl-2-methyl-4,7,10-tris(carboxycarbonyl)-1,4,7,10-tetrazacyclododecane (L3) was isolated as a brown solid (0.103 g, 91 %) . NMR (400 MHz, D_2O): δ_H = 3.03 (6H, br-m, ring-H), 3.07 – 3.76 (16H, br-m, ring-H), 3.88 (2H, br-s, ring-NCH_2), 4.19 (2H, br-s, NCH_2), 4.33 (2H, br-s, NCH_2), 4.47 (2H, br-s, NCH_2), 7.44 (1H, m, pyridine-H), 7.54 (1H, t J_{HH} = 6.1, pyridine-H), 7.61 (1H, d J_{HH} = 7.2, pyridine-H), 7.77 (1H, d J_{HH} = 8.0, pyridine-H), 7.88 (1H, m, pyridine), 7.97 – 8.19 (10H, m, 1 pyridine-H, 9 pyrene-H) and 8.63 ppm (1H, d J_{HH} = 4.1, pyridine-H). ES+ MS: *m/z* 939 $\{M+2Cu\}^+$. HRMS (ESI^+) found *m/z* 815.3875 $\{M + H\}^+$; $C_{45}H_{51}N_8O_7$ requires 815.3861. λ_{max} (ε/$mol^{-1}dm^3cm^{-1}$); 205 (28000), 243 (30500), 267 (16300), 277 (19200), 329 (11400) and 341 (15800) nm.

{2-(pyridin-2-ylmethyl)-N-(quinolin-8-yl)acetamide}amino-6-methylpyridinyl-2-methyl-4,7,10-tris(carboxycarbonyl)-1,4,7,10-tetrazacyclododecane (L4) was isolated as a brown solid. (0.120 g, 72 %) NMR (400 MHz, D_2O): δ_H =2.95 (6H, br-m, ring-H), 3.03 – 3.56 (16H, br-m, ring-H), 4.03 4.51 (2H, s, NCH_2), 4.55 (4H, br-s, $N(CH_2)_2$), 7.84 (3H, m, 2 pyr-H, 1 quin-H), 7.90 (1H, d J_{HH} = 8.1, pyr-H), 8.00 (2H, m, pyr-H, quin-H), 8.11 (2H, m, pyr-H, quin-H), 8.66 (1H, d J_{HH} = 5.8, pyr-H), 8.93 (1H, s, quin-H) and 9.35 ppm(1H, d J_{HH} = 2.2, quin-H). ES+ MS: *m/z* 804 $\{M+Cu\}^+$. HRMS (ESI^+) found *m/z* 742.3671 $\{M + H\}^+$; $C_{38}H_{48}N_9O_7$ requires 742.3659. λ_{max} (ε/$mol^{-1}dm^3cm^{-1}$); 208 (20900), 250 (19700), 322 (2900) and 333 (2800) nm.

{N-(anthraquinocen-2-yl)-2-(pyridin-2-ylmethyl)acetamide}amino-6-methylpyridinyl-2-methyl-4,7,10-tris(carboxycarbonyl)-1,4,7,10-tetrazacyclododecane (L5) was isolated as a brown solid (0.086 g, 83 %). NMR (400 MHz, D_2O): δ_H = 2.88 (6H, br-m, ring-H), 2.97 – 3.83 (16H, br-m, ring-H), 3.68 (2H, br-s, ring-NCH_2), 4.32 (2H, br-s, NCH_2), 4.41 (2H, br-s, NCH_2), 4.44 (2H, br-s, NCH_2), 7.44 (1H, t J_{HH} = 8.8, anth-H), 7.62 (1H, d J_{HH} =

7.2, pyr-H), 7.71 (1H, t J_{HH} = 8.8, pyr-H), 7.76 (1H, t J_{HH} = 8.3, anth), 7.80 (2H, t J_{HH} = 6.5, anth-H), 7.89 (2H, t J_{HH} = 7.5, 2 pyr-H, anth-H), 8.03 (1H, d J_{HH} = 7.8, pyr-H), 8.17 (1H, d J_{HH} = 8.1, anth-H), 8.26 (1H, d J_{HH} = 7.9, anth-H), 8.39 (1H, t J_{HH} = 8.1, anth-H), 8.57 (1H, d J_{HH} = 6.5, anth-H) and 8.70 ppm (1H, d J_{HH} = 6.0, pyr-H). ES+ MS: *m/z* 883 $\{M+Cu\}^+$. HRMS (ESI^+) found *m/z* 821.3617 $\{M + H\}^+$; $C_{43}H_{49}N_8O_9$ requires 821.3611. λ_{max} (ε/$mol^{-1}dm^3cm^{-1}$); 206 (13400), 263 (11500), 316 (1000) and 396 (1400 nm).

NdL3 was isolated as a pale brown powder. (0.022, 94%) ES+ MS: *m/z* 956 $(M+H)^+$. HRMS (ESI^+) found *m/z* 956.2751 $\{M + H\}^+$; $C_{45}H_{48}N_8O_7Nd_1$ requires 956.2750. IR υ_{max}(ATR, solid); 3590, 1653, 1583, 1446 and 1417 cm^{-1}.

EuL3 was isolated as a pale brown powder. (0.021, 89 %) ES+ MS: *m/z* 965 $(M+H)^+$. HRMS (ESI^+) found *m/z* 965.2858 $\{M + H\}^+$; $C_{45}H_{48}N_8O_7Eu_1$ requires 965.2855. IR υ_{max}(ATR, solid); 3669, 1601, 1572 and 1457 cm^{-1}.

GdL3 was isolated as a pale brown powder. (0.021, 89 %) ES+ MS: *m/z* 970 $(M+H)^+$. HRMS (ESI^+) found *m/z* 970.2892 $\{M + H\}^+$; $C_{45}H_{48}N_8O_7Gd_1$ requires 970.2889. IR υ_{max}(ATR, solid); 3568, 1580, 1445 and 1413 cm^{-1}.

YbL3 was isolated as a pale brown powder. (0.022, 91 %) ES+ MS: *m/z* 986 $(M+H)^+$. HRMS (ESI^+) found *m/z* 986.3038 $\{M + H\}^+$; $C_{45}H_{48}N_8O_7Yb_1$ requires 986.3037. IR υ_{max}(ATR, solid); 3537, 1593, 1446, and 1412 cm^{-1}.

NdL4 was isolated as a dark brown powder. (0.022, 92 %) ES+ MS: *m/z* 881 $(M+H)^+$. HRMS (ESI^+) found *m/z* 881.2523 $\{M + H\}^+$; $C_{38}H_{45}N_9O_7Nd_1$ requires 881.2514. IR υ_{max}(ATR, solid); 3500 and 1576 cm^{-1}.

EuL4 was isolated as a dark brown powder. (0.022, 91 %) ES+ MS: *m/z* 892 $(M+H)^+$. HRMS (ESI^+) found *m/z* 892.2653 $\{M + H\}^+$; $C_{38}H_{45}N_9O_7Eu_1$ requires 892.2653. IR υ_{max}(ATR, solid); 3494, 1577, 1444 and 1406 cm^{-1}.

GdL4 was isolated as a dark brown powder. (0.022, 95 %) ES+ MS: *m/z* 897 $(M+H)^+$. HRMS (ESI^+) found *m/z* 897.2686 $\{M + H\}^+$; $C_{38}H_{45}N_9O_7Gd_1$ requires 897.2669. IR υ_{max}(ATR, solid); 3490, 1576, 1445 and 1405 cm^{-1}.

TbL4 was isolated as a dark brown powder. (0.023, 95 %) ES+ MS: *m/z* 898 $(M+H)^+$. HRMS (ESI^+) found *m/z* 898.2691 $\{M + H\}^+$; $C_{38}H_{45}N_9O_7Tb_1$ requires 898.2690. IR υ_{max}(ATR, solid); 3490, 1576 and 1459 cm^{-1}.

YbL4 was isolated as a dark brown powder. (0.024, 97 %) ES+ MS: *m/z* 913 $(M+H)^+$. HRMS (ESI^+) found *m/z* 913.2831 $\{M + H\}^+$; $C_{38}H_{45}N_9O_7Yb_1$ requires 913.2821. IR υ_{max}(ATR, solid); 3471, 1576, 1456 and 1400 cm^{-1}.

NdL5 was isolated as a brown powder. (0.023, 98 %) ES+ MS: *m/z* 960 $(M+H)^+$. HRMS (ESI^+) found *m/z* 960.2464 $\{M + H\}^+$; $C_{43}H_{46}NdN_8O_9$ requires 960.2459. IR υ_{max}(ATR, solid); 3451, 1734, 1578, 1508, 1456 and 1408 cm^{-1}.

EuL5 was isolated as a brown powder. (0.022, 93 %) ES+ MS: *m/z* 969 $(M+H)^+$. HRMS (ESI^+) found *m/z* 969.2585 $\{M + H\}^+$; $C_{43}H_{46}EuN_8O_9$ requires 969.2581. IR υ_{max}(ATR, solid); 3500, 1617, 1590 and 1477 cm^{-1}.

GdL5 was isolated as a brown powder. (0.023, 97 %) ES+ MS: *m/z* 973 $(M+H)^+$. HRMS (ESI^+) found *m/z* 973.2614 $\{M + H\}^+$; $C_{43}H_{46}GdN_8O_9$ requires 973.2608. IR υ_{max}(ATR, solid); 3473, 1734, 1576, 1507, 1456, 1442 and 1406 cm^{-1}.

YbL5 was isolated as a brown powder. (0.022, 91 %) ES+ MS: *m/z* 992 $(M+H)^+$. IR υ_{max}(ATR, solid); 3491, 1734, 1590, 1516 and 1457 cm^{-1}.

5.5 - References

1. G. A. Crosby, R. M. Alire and R. E. Whan, *J. Chem. Phys.*, 1961, **34**, 743-&.
2. F. J. Steemers, W. Verboom, D. N. Reinhoudt, E. B. Vandertol and J. W. Verhoeven, *J. Am. Chem. Soc.*, 1995, **117**, 9408-9414.
3. M. Latva, H. Takalo, V. M. Mukkala, C. Matachescu, J. C. RodriguezUbis and J. Kankare, *J. Lum.*, 1997, **75**, 149-169.
4. M. H. V. Werts, M. A. Duin, J. W. Hofstraat and J. W. Verhoeven, *Chem. Commun.*, 1999, 799-800.
5. A. Beeby, L. M. Bushby, D. Maffeo and J. A. G. Williams, *J. Chem. Soc. Perkin Trans. 2*, 2000, 1281-1283.
6. A. Dadabhoy, S. Faulkner and P. G. Sammes, *J. Chem. Soc. Perkin Trans. 2*, 2002, 348-357.
7. R. Van Deun, P. Nockemann, P. Fias, K. Van Hecke, L. Van Meervelt and K. Binnemans, *Chem. Commun.*, 2005, 590-592.
8. P. Coppo, M. Duati, V. N. Kozhevnikov, J. W. Hofstraat and L. De Cola, *Angew. Chem. Int. Ed. Engl.*, 2005, **44**, 1806-1810.
9. F. F. Chen, Z. Q. Bian, Z. W. Liu, D. B. Nie, Z. Q. Chen and C. H. Huang, *Inorg. Chem.*, 2008, **47**, 2507-2513.
10. J. Ni, L. Y. Zhang and Z. N. Chen, *Journal of Organometallic Chemistry*, 2009, **694**, 339-345.
11. T. Lazarides, G. M. Davies, H. Adams, C. Sabatini, F. Barigelletti, A. Barbieri, S. J. A. Pope, S. Faulkner and M. D. Ward, *Photochem. Photobiol. Sci.*, 2007, **6**, 1152-1157.
12. R. M. Supkowski, J. P. Bolender, W. D. Smith, L. E. L. Reynolds and W. D. Horrocks, *Coord. Chem. Rev.*, 1999, **185-6**, 307-319.
13. M. I. Gaiduk, V. V. Grigoryants, A. F. Mironov, V. D. Rumyantseva, V. I. Chissov and G. M. Sukhin, *J. Photochem. Photobiol. B*, 1990, **7**, 15-20.
14. M. H. V. Werts, J. W. Hofstraat, F. A. J. Geurts and J. W. Verhoeven, *Chem. Phys. Lett.*, 1997, **276**, 196-201.
15. G. A. Hebbink, L. Grave, L. A. Woldering, D. N. Reinhoudt and F. van Veggel, *J. Phys. Chem. A*, 2003, **107**, 2483-2491.
16. K. Aita, T. Temma, Y. Kuge and H. Saji, *Luminescence*, 2007, **22**, 455-461.
17. S. I. Klink, P. O. Alink, L. Grave, F. G. A. Peters, J. W. Hofstraat, F. Geurts and F. van Veggel, *J. Chem. Soc. Perkin Trans. 2*, 2001, 363-372.
18. N. M. Shavaleev, S. J. A. Pope, Z. R. Bell, S. Faulkner and M. D. Ward, *Dalton. Trans.*, 2003, 808-814.
19. R. F. Ziessel, G. Ulrich, L. Charbonniere, D. Imbert, R. Scopelliti and J. C. G. Bunzli, *Chem. Eur. J*, 2006, **12**, 5060-5067.
20. S. I. Klink, H. Keizer, H. W. Hofstraat and F. van Veggel, *Synth. Met.*, 2002, **127**, 213-216.
21. N. M. Shavaleev, L. P. Moorcraft, S. J. A. Pope, Z. R. Bell, S. Faulkner and M. D. Ward, *Chem. Eur. J*, 2003, **9**, 5283-5291.
22. T. K. Ronson, T. Lazarides, H. Adams, S. J. A. Pope, D. Sykes, S. Faulkner, S. J. Coles, M. B. Hursthouse, W. Clegg, R. W. Harrington and M. D. Ward, *Chem. Eur. J*, 2006, **12**, 9299-9313.
23. F. Kennedy, N. M. Shavaleev, T. Koullourou, Z. R. Bell, J. C. Jeffery, S.

Faulkner and M. D. Ward, *Dalton. Trans.*, 2007, 1492-1499.
24. J. M. Herrera, S. J. A. Pope, A. Meijer, T. L. Easun, H. Adams, W. Z. Alsindi, X. Z. Sun, M. W. George, S. Faulkner and M. D. Ward, *J. Am. Chem. Soc.*, 2007, **129**, 11491-11504.
25. K. Senechal-David, S. J. A. Pope, S. Quinn, S. Faulkner and T. Gunnlaugsson, *Inorg. Chem.*, 2006, **45**, 10040-10042.
26. S. J. A. Pope, B. J. Coe and S. Faulkner, *Chem. Commun.*, 2004, 1550-1551.
27. A. P. deSilva, H. Q. N. Gunaratne, T. E. Rice and S. Stewart, *Chem. Commun.*, 1997, 1891-1892.
28. M. A. Kessler, *Anal. Chim. Acta.*, 1998, **364**, 125-129.
29. C. Li, G. L. Law and W. T. Wong, *Org. Lett.*, 2004, **6**, 4841-4844.
30. K. Hanaoka, K. Kikuchi, H. Kojima, Y. Urano and T. Nagano, *J. Am. Chem. Soc.*, 2004, **126**, 12470-12476.
31. J. B. Coldwell, C. E. Felton, L. P. Harding, R. Moon, S. J. A. Pope and C. R. Rice, *Chem. Commun.*, 2006, 5048-5050.
32. K. J. Latas and A. M. Nishimura, *J. Phys. Chem.*, 1978, **82**, 491-495.
33. Y. Shiraishi, C. Ichimura and T. Hirai, *Tett. Lett.*, 2007, **48**, 7769-7773.
34. Y. Mikata, M. Wakamatsu and S. Yano, *Dalton. Trans.*, 2005, 545-550.
35. Y. Weng, Z. L. Chen, F. Wang, L. Xue and H. Jiang, *Anal. Chim. Acta.*, 2009, **647**, 215-218.
36. M. R. Padhye, S. P. McGlynn and M. Kasha, *J. Chem. Phys.*, 1956, **24**, 588-594.
37. N. S. Baek, Y. H. Kim, S. G. Roh, B. K. Kwak and H. K. Kim, *Ad. Funct. Mater.*, 2006, **16**, 1873-1882.
38. T. Lazarides, M. A. H. Alamiry, H. Adams, S. J. A. Pope, S. Faulkner, J. A. Weinstein and M. D. Ward, *Dalton. Trans.*, 2007, 1484-1491.
39. L. Fabbrizzi, M. Licchelli, P. Pallavicini, A. Perotti, A. Taglietti and D. Sacchi, *Chem. Eur. J*, 1996, **2**, 75-82.
40. F. Unob, Z. Asfari and J. Vicens, *Tett. Lett.*, 1998, **39**, 2951-2954.
41. Y. J. Lee, D. Seo, J. Y. Kwon, G. Son, M. S. Park, Y. H. Choi, J. H. Soh, H. N. Lee, K. D. Lee and J. Yoon, *Tetrahedron*, 2006, **62**, 12340-12344.
42. J. Langelaar, J. W. V. Beek, H. Ten Brink and J. D. W. Van Voorst, *Chem. Phys. Lett.*, 1970, **7**, 368-370.
43. S. Faulkner, M. C. Carrie, S. J. A. Pope, J. Squire, A. Beeby and P. G. Sammes, *Dalton. Trans.*, 2004, 1405-1409.
44. S. J. A. Pope, *Polyhedron*, 2007, **26**, 4818-4824.
45. J. E. S. Sohna and F. Fages, *Tett. Lett.*, 1997, **38**, 1381-1384.
46. H. F. Ji, R. Dabestani, G. M. Brown and R. L. Hettich, *Photochem. Photobiol.*, 1999, **69**, 513-516.
47. B. C. Roy, B. Chandra, D. Hromas and S. Mallik, *Org. Lett.*, 2003, **5**, 11-14.
48. Z. Wang, D. Q. Zhang and D. B. Zhu, *Anal. Chim. Acta.*, 2005, **549**, 10-13.
49. G. N. Lewis and M. Kasha, *J. Am. Chem. Soc.*, 1944, **66**, 2100-2116.
50. S. A. Carlson and D. M. Hercules, *J. Am. Chem. Soc.*, 1971, **93**, 5611-&.
51. H. Yang, Z. G. Zhou, J. Xu, F. Y. Li, T. Yi and C. H. Huang, *Tetrahedron*, 2007, **63**, 6732-6736.
52. M. Kadarkaraisamy and A. G. Sykes, *Inorg. Chem.*, 2006, **45**, 779-786.
53. W. Fang-ying, H. Mei-hua, W. Yu-mei, T. Xiao-fang, Z. Yong-qiang and

J. Zhao-jun, *Spectrochim. Acta, Part A*, 2006, **65**, 633-637.
54. K. L. McGilvray, M. N. Chretien, M. Lukeman and J. C. Scaiano, *Chem. Commun.*, 2006, 4401-4403.
55. V. G. H. Lafitte, W. X. Wang, A. S. Yashina and N. S. Lawrence, *Electrochem. Commun.s*, 2008, **10**, 1831-1834.
56. B. L. Vallee and K. H. Falchuk, *Physiol. Rev.*, 1993, **73**, 79-118.
57. T. Budde, A. Minta, J. A. White and A. R. Kay, *Neuroscience*, 1997, **79**, 347-358.
58. J. Kaiser, *Science*, 1994, **265**, 1365-1365.
59. S. J. A. Pope and R. H. Laye, *Dalton. Trans.*, 2006, 3108-3113.
60. C. He and S. J. Lippard, *Tetrahedron*, 2000, **56**, 8245-8252.
61. L. S. Hegedus, M. M. Greenberg, J. J. Wendling and J. P. Bullock, *J. Org. Chem.*, 2003, **68**, 4179-4188.
62. Y. Zhang, X. F. Guo, W. X. Si, L. H. Jia and X. H. Qian, *Org. Lett.*, 2008, **10**, 473-476.
63. J. H. Kim, A. R. Hwang and S. K. Chang, *Tett. Lett.*, 2004, **45**, 7557-7561.
64. S. Kumar, V. Luxami and A. Kumar, *Org. Lett.*, 2008, **10**, 5549-5552.
65. C. A. Butts, J. Xi, G. Brannigan, A. A. Saad, S. P. Venkatachalan, R. A. Pearce, M. L. Klein, R. G. Eckenhoff and I. J. Dmochowski, *Proc. Nat. Acad. Sci. USA*, 2009, **106**, 6501-6506.
66. A. Beeby, I. M. Clarkson, R. S. Dickins, S. Faulkner, D. Parker, L. Royle, A. S. de Sousa, J. A. G. Williams and M. Woods, *J. Chem. Soc. Perkin Trans. 2*, 1999, 493-503.
67. S. Faulkner, A. Beeby, M. C. Carrie, A. Dadabhoy, A. M. Kenwright and P. G. Sammes, *Inorg. Chem. Commun.* 2001, **4**, 187-190.
68. C. S. Bonnet and T. Gunnlaugsson, *New J. Chem.*, 2009, **33**, 1025-1030.

Chapter Six
The development of responsive luminescent dimeric lanthanide complexes

6.1 – Introduction

While the luminescent properties of lanthanide ions show great promise their application in diagnostic medicine is dominated by the paramagnetic character of gadolinium complexes, which makes them ideal candidates for magnetic resonance imaging (MRI) contrast agents. The relaxation accelerating effect, known as the relaxivity, of Gd(III) complexes is the sum of short-range dipole interactions between the unpaired electrons and the proton nuclei of water molecules in the inner hydration sphere and long-range dipole-dipole coupling between the paramagnetic metal ion and outer sphere water molecules. Inner sphere relaxivity is dependant on the number of coordinated solvent molecules (q) and the correlation time (τ_c), which in turn depends on the rotational correlation time (τ_R) of the complex, the residence time of inner sphere water molecules (τ_m) and the longitudinal and transverse electronic relaxation rates (T_1 and T_{2e}).[1, 2] There are currently several gadolinium contrast agents currently approved for use in the EU and the USA[1] and they are used in about 40 - 50 % of MRI exams[3] and their success has led to the development of second generation contrast agents, in which the relaxivity is modulated by the presence of various biomolecules or biorelevant ions. Responsive contrast agents have been designed to signal the expression of β-galactosidase,[4] esterase activity[5] and pH.[6] This chapter focused on the development of a metal-responsive gadolinium contrast agent.

Among the earliest metal-responsive MRI contrast agents to be developed was a dimeric gadolinium complexes reported by Meade *et al*, in which two DO3A units were linked by BAPTA, to form a Ca(II) receptor (Figure 6.1).[7, 8] In the presence of Ca(II) the BAPTA carboxylate arms dissociate from the Gd(III) centres, allowing direct binding of water and causing an 80 % increase in the relaxivity.

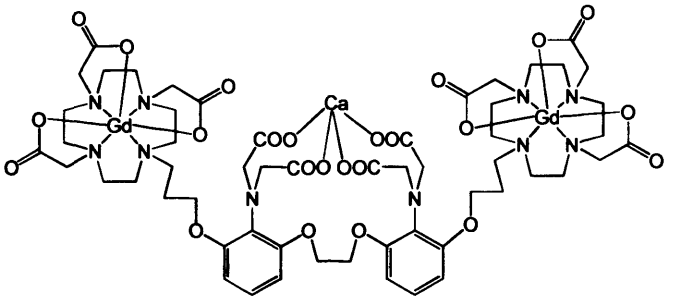

Figure 6.1 - Ca(II) responsive MRI contrast agent.

Due to the biological importance of Zn(II) and its association with neurological disorders[9-11] several gadolinium complexes have been reported as potential probes for Zn(II) concentration (Figure 6.2). In several responsive systems developed by Nagano *et al* the binding of Zn(II) causes the ligands to fold, limiting the access of water molecules to the Gd(III) centres and decreasing the relaxivity.[12-14] A similar system was designed by Sherry *et al* to be a paramagnetic chemical exchange saturation transfer (CEST) agent to signal the presence in Zn(II).[15] In this case the occupation of the binding site by Zn(II) did not cause a change in the coordination geometry of the Eu(III) ion but instead catalyses the rate of prototopic exchange between the lanthanide and the bulk solvent.

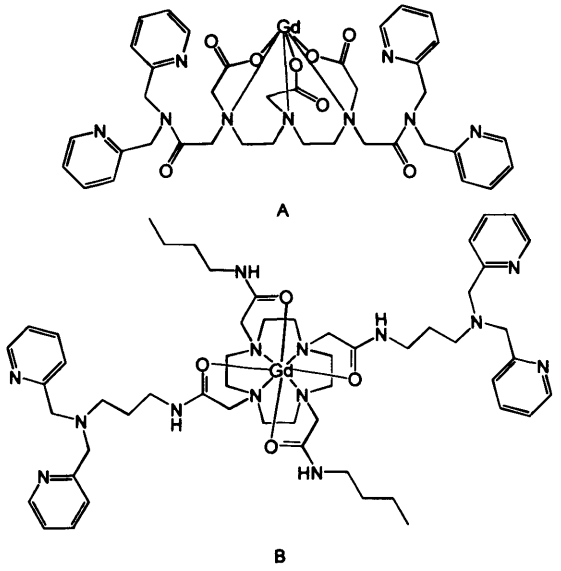

Figure 6.2 – Zn(II) gadolinium complexes developed by Nagano *et al* (A) and Sherry *et al* (B).

A 'hydration switch'-style Zn(II) responsive luminescence probe has been developed by Pope *et al* (Figure 6.3).[16] The presence of Zn(II) caused the pyridine chromophores to dissociate from the Eu(III), altering the hyperfine transitions and allowing direct access of surrounding solvent which resulted in a decrease of the luminescence lifetime.

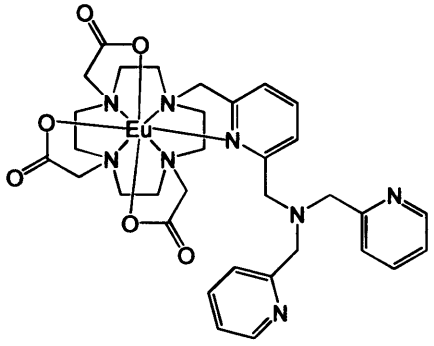

Figure 6.3 – Zn(II) responsive luminescent lanthanide probe.

In vivo concentration of Cu(II) has been linked to Alzheimer's, prion and Parkinson's diseases and amyotrophic lateral sclerosis.[17] Chang has developed a hydration switch probe in which the presence of Cu(II) causes an increase in the relaxivity (Figure 6.4)[18, 19] and by adopting the synthetic strategy developed by Pope has incorporated several soft thioether donors into the binding site to induce a high degree of selectivity for Cu(I) over Cu(II).[19]

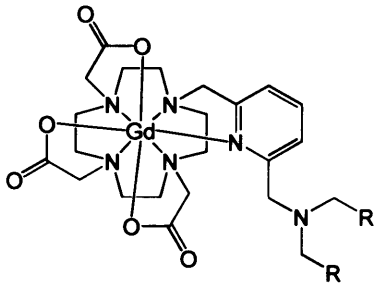

Figure 6.4 – General architecture of Chang's Cu(II) responsive MRI contrast agent.

In order to produce target-specific contrast agents for *in vivo* applications the

relaxivity of probes may need to be increased to enable monitoring of the target at low concentration. Increasing the degree of hydration of the Gd(III) often results in instability of the complex.[20] A particularly effective method of increasing the relaxivity of is by slowing the tumbling rate of the gadolinium to allow faster exchange with water. This can be achieved by increasing the molecular weight of the contrast agent while also increasing to number of gadolinium centres. This can be accomplished by a variety of approaches such as incorporating gadolinium complexes into polymers,[21] binding them to proteins[22] and incorporating them into dendrimers.[23]

Some of the earliest attempts to increase the molecular weight of contrast agents while maintaining a high Gd(III) payload were based around dimeric complexes in which two DO3A macrocycles were bound by coordinating linker groups (Figure 6.5 A)[24, 25] It was found that the greatest gain in relaxivity was obtained in dimeric systems in which the linker group was rigid, preventing the independent rotation of individual chelating units. However it was observed that the eight-coordinate ligands used in these studies limited the water-exchange rates and prevented further enhancements in relaxivity.[25]

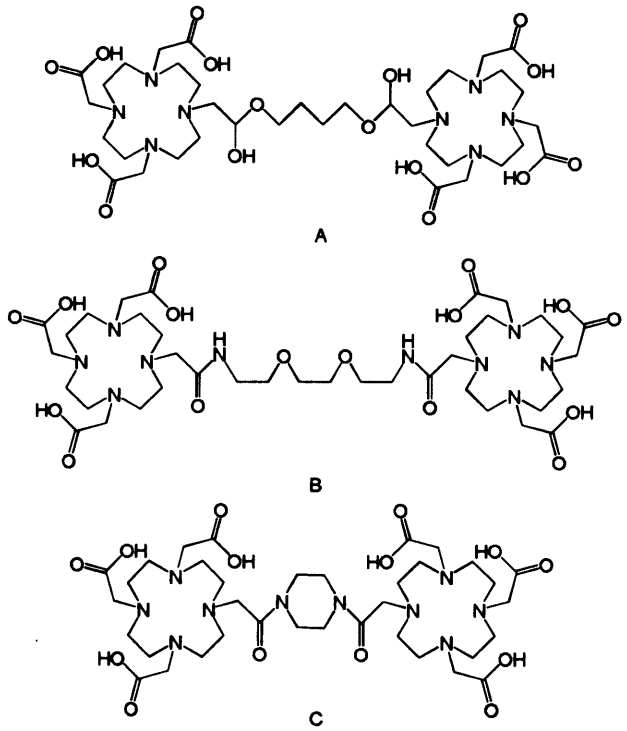

Figure 6.5 – Dimeric ligands developed by Merbach.

Later attempts to synthesise dimeric contrast agents focused on enhancing the relaxivity by increasing the water exchange rate. Two dimeric complexes reported by Merbach *et al* in which a pair of seven-coordinate DTTA binding sites were linked by rigid xylene cores (Figure 6.6) showed relaxivities of approximately 8 $mM^{-1} s^{-1}$ per Gd(III) ion.[26]

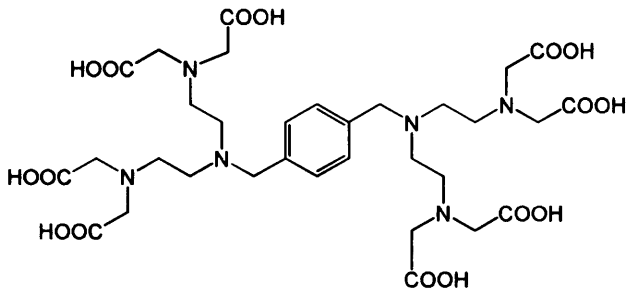

Figure 6.6 – Ligand of dimeric contrast agent with high relaxivity.

Similar systems in which two DO3A binding sites were linked by a xylyl unit (Figure 6.7) showed highly field-dependent relaxivities and a lower degree of hydration than expected (q = 1).[27] This was due to the formation of slowly rotating aggregates of approximately ten complexes, in which the coordination sites of complexes in the interior of the aggregates may have been blocked. This behaviour was attributed to π-stacking and hydrogen bonding between chelates.

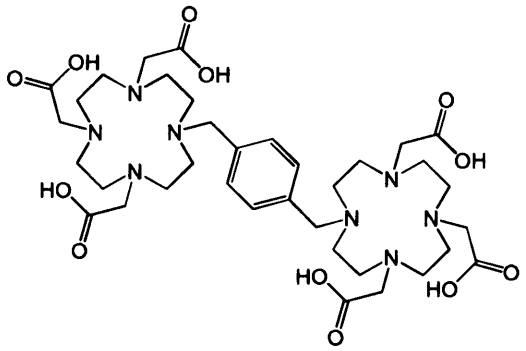

Figure 6.7 – Bis-macrocyclic ligand of a dimeric contrast agent which undergoes aggregation in solution.

The aim of this chapter was to synthesise a ligand capable of forming responsive

dimeric lanthanide complexes. The linker, a pyridine functionalised piperazine unit, would provide the molecule with a degree of rigidity as well as the potential binding site for target metal ions. This work utilised a combined approach to study the effect of binding to guest metal ions, monitoring changes in the emission profile and lifetime of Eu(III) luminescence as well as increases of relaxivity of the Gd(III) complex. The focus of the chapter was the group 12 metals and Cu(II).

6.2 – Results and Discussion

6.2.1 – Synthesis and characterisation of ligand and complexes

The synthetic strategy was based on that of the metal probes discussed previously in Chapters 4 and 5. 2,6-bis(chloromethyl)pyridine (**1**) was reacted with 4,7,10-tris(carboxymethyl)-1,4,7,10-tetraazacyclododecane (**2**) to form the chloromethyl pyridine- functionalised macrocyle **3**. Two equivalents of this were mixed with piperazine (**4**), $NaHCO_3$ and a catalytic amount of KI in MeCN, which was heated to reflux for 1 day. After this time the residue was purified by precipitation from hot toluene. The product (**5**) was characterised primarily by NMR (^1H, ^{13}C) which showed slight shifts in the aromatic pyridine resonances as well as the absence of peaks associated with the chloromethyl group. Electrospray Mass Spectrometry (ES MS) showed a parent ion peak with an *m/z* corresponding to $\{M+H\}^+$ as well as a peak associated with the doubly-charged $\{M+2H\}^{2+}$ species at *m/z* 661.5. Deprotection of the *tert*-butyl ester groups was carried out according to standard procedure by stirring 5 in trifluoroacetic acid (TFA) and CH_2Cl_2 (1:1) for 24 hours, after which time the ligand **L1** was purified by precipitation in diethyl ether. ^1H NMR confirmed that the reaction had reached completion and ES MS showed a parent ion peak corresponding to $\{M+H\}^+$ at *m/z* 984.

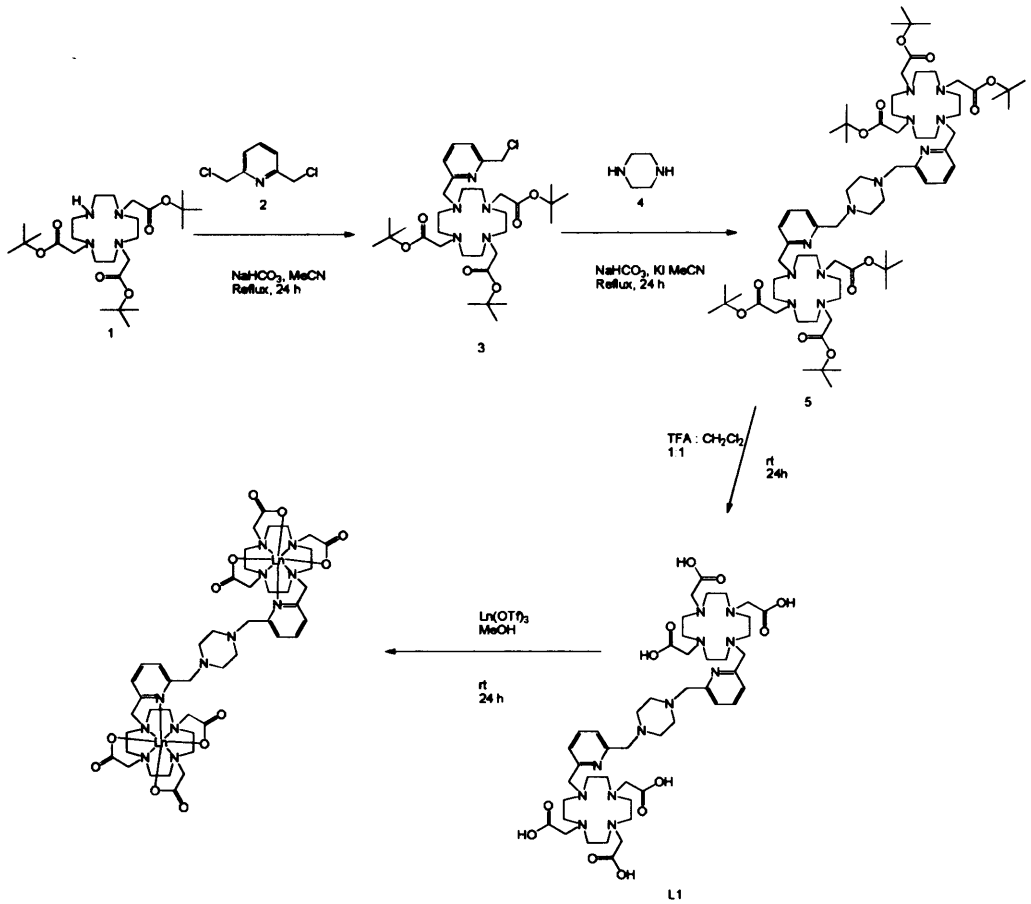

Figure 6.8 – Synthetic strategy towards $\mathbf{Ln_2L1}$.

Complexation was carried out by mixing **L1** with two equivalents of lanthanide triflate salt in methanol at 50 °C for 24 h. Complexes were characterised primarily by MS, which in all cases showed a parent ion peak corresponding to $\mathbf{Ln_2L1}$ with the isotope patterns correlating well with theoretical results (Figure 6.8).

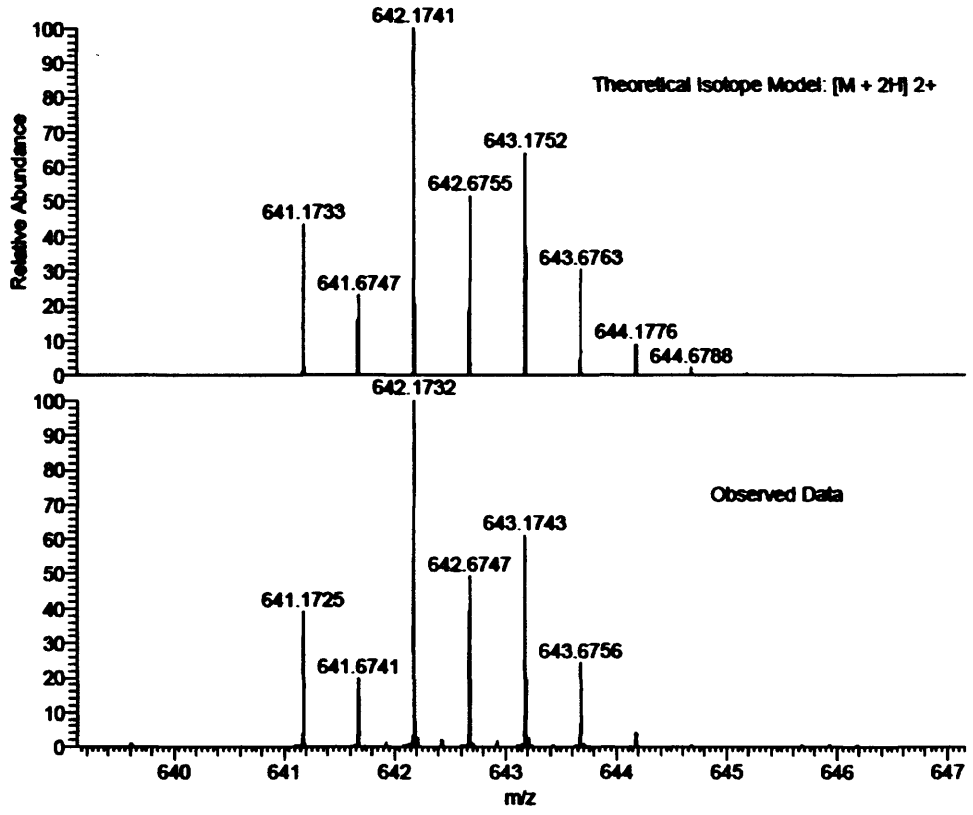

Figure 6.9 – Isotope pattern observed for **Eu_2L1** (bottom), with theoretical isotope pattern (top).

6.2.2 – Photophysical studies

The UV-Vis spectra of all complexes showed absorption bands corresponding to the pyridine $^1\pi\pi^*$ transitions at $\lambda < 300$ nm. Irradiation of the gadolinium complex at these wavelengths at room temperature showed a broad, structureless ligand emission, typical of pyridine $^1\pi\pi^*$ fluorescence, with λ_{max} at approximately 400 nm. In an optical glass (ethanol, 77 K) **Gd_2L1** showed phosphorescence which was assigned to the pyridine $^3\pi\pi^*$ state and from the onset (~ 350 nm) it was calculated to have an energy of 28500 cm^{-1}. This is too low to sensitise emission from Gd(III), in which the lowest emissive state has an energy of approx. 32000 cm^{-1} ($^6P_{7/2}$)[28], but allows sensitisation of visibly emissive ions Sm(III), Eu(III) and Tb(III). Following excitation at 277 nm **Sm_2L1** showed characteristic emission arising from the $^4G_{5/2} \rightarrow {}^6H_{5/2}$ (565 nm), $^4G_{5/2} \rightarrow {}^6H_{7/2}$ (603 nm) and $^4G_{5/2} \rightarrow {}^6H_{9/2}$ (653 nm) transitions.[29] **Eu_2L1** showed

strong, well-resolved emission from the $^5D_0 \rightarrow {}^7F_J$ (J = 0,1 2, 3 and 4) transitions. Tb(III) showed emission originating from the $^5D_4 \rightarrow {}^7F_J$ (J = 6, 5, 4 and 3).

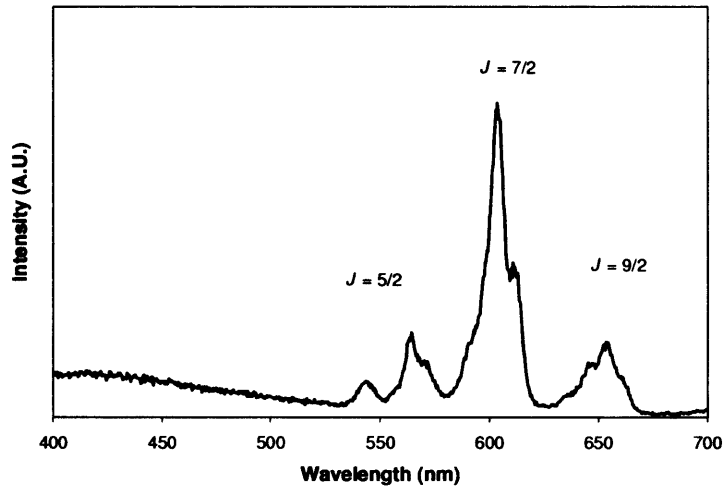

Figure 6.10 – **Sm_2L1** emission spectrum (540 nm – 675 nm) and residual ligand luminescence (400 nm – 540 nm) in H_2O.

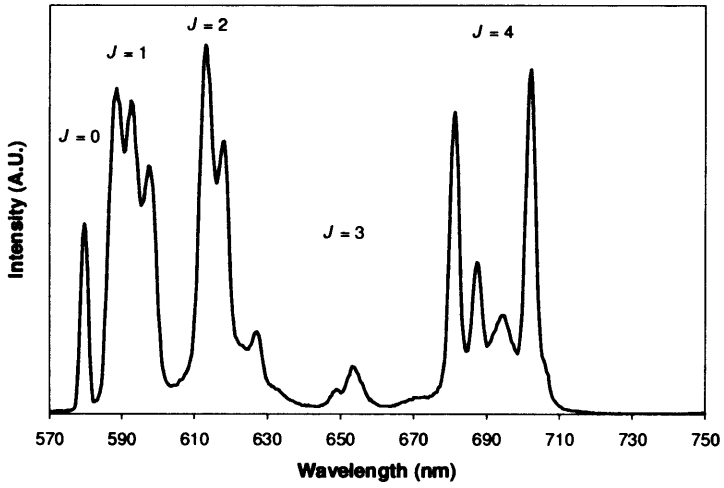

Figure 6.11 –**Eu_2L1** emission spectrum in H_2O.

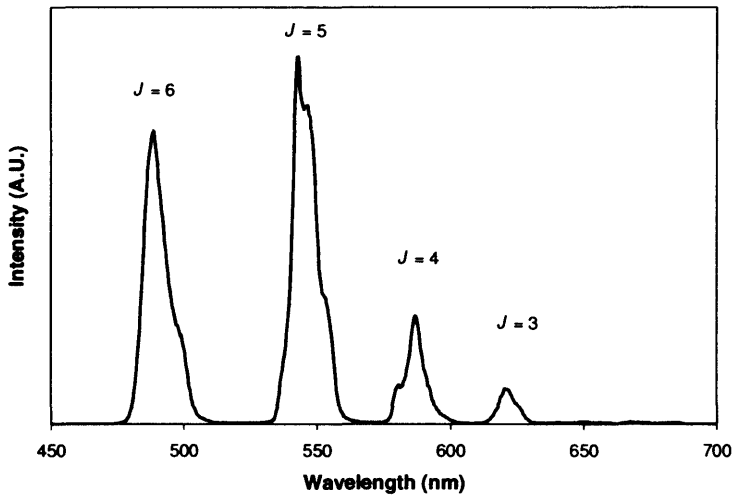

Figure 6.12 **–Tb_2L1** emission spectrum in H_2O.

In each case the ligand luminescence was comparatively very weak, indicating efficient energy transfer from the chromophore to the lanthanide ion.

The luminescent lifetimes of **Eu_2L1** and **Tb_2L1** were measured and could be modelled as single exponential decays. By measuring the lifetime of **Eu_2L1** in H_2O and D_2O and using Parker's modification of Horrocks' equation,[30] which takes into account quenching contributions by outer-sphere solvent molecules, the degree of inner-sphere hydration, q, was calculated to be 0.4 which suggests that one Eu(III) ion has a coordination number (CN) of nine while the other has a CN of eight, allowing access of one water molecule. This is consistent with previous work in which pyridine participates in the coordination sphere of Eu(III). It is likely that steric hindrance prevents the ligand from completely satisfying the coordination requirements of both Eu(III) centres simultaneously but the two binding modes are interchangeable on the timescale of the lifetime measurements, resulting in a single exponential decay with an averaged lifetime. The presence of two emissive environments is supported by the steady-state luminescence spectrum, in which the hyperfine structure shows unusual complexity.

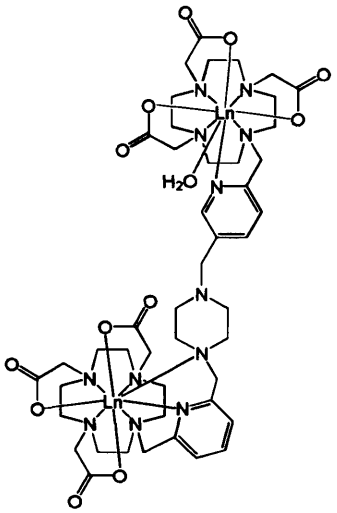

Figure 6.13 – Proposed binding mode of L1.

Steady-state luminescence spectra of $\mathbf{Eu_2L1}$ measured at 1.0 mM, 0.1 mM and 0.01 mM showed no change in the $J = 1/J = 2$ or the hyperfine structure, indicating that the complex was not undergoing aggregation as observed in a related complex by Merbach *et al.*[27]

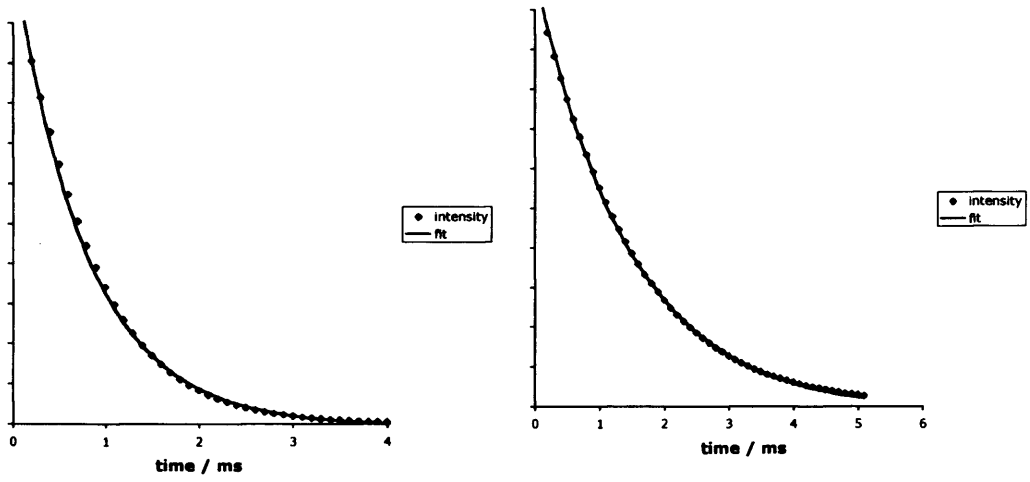

Figure 6.14 – Luminescence lifetimes of $\mathbf{Eu_2L1}$ in H_2O (left) and D_2O (right).

6.2.3 – Metal binding studies

In order to study the potential for $\mathbf{Ln_2L1}$ to act as a metal responsive probe a

buffered (HEPES) solution of **Eu_2L1** was titrated against various metals ions. Zn(II), Cd(II) and Fe(II) had little effect but Hg(II) and Cu(II) both quenched the steady-state luminescence intensity to some degree.

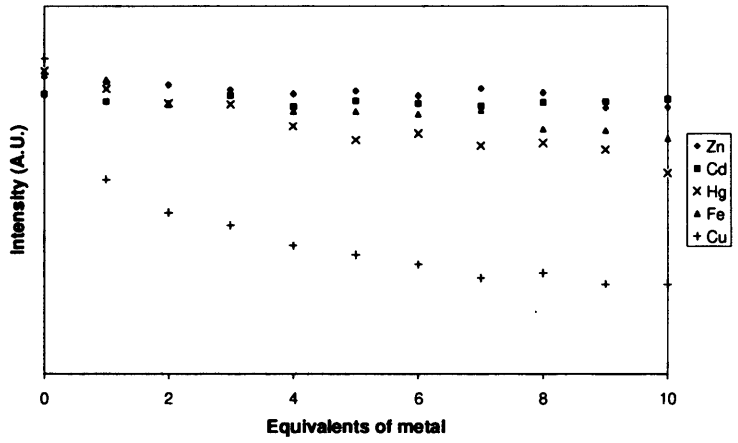

Figure 6.15 –Effect of metal ion on the intensity of the $J = 1$ (590 nm) transition of **Eu_2L1**.

The quenching effect of Hg(II) was accompanied by a slight decrease in the $J = 2$ / $J = 1$ ratio and other slight changes in the hyperfine structure, indicating a change in the coordination environment of the Eu(III) centres. In contrast to this Cu(II) had a general quenching effect, with very little change in the $J = 1$ / $J = 2$ ratio or hyperfine structure.

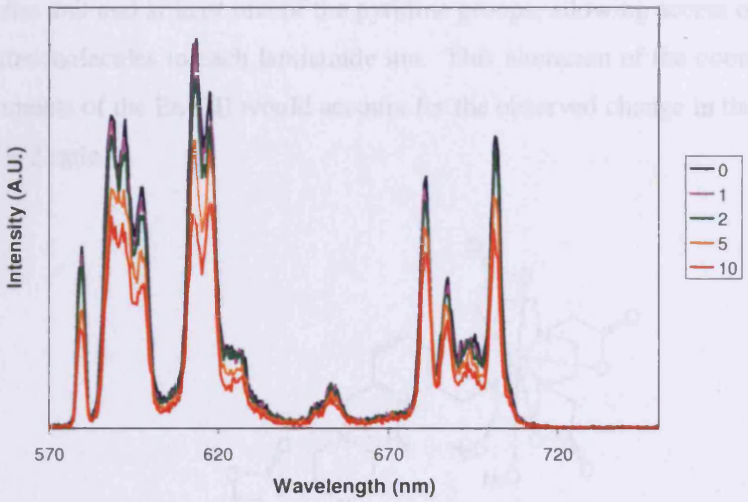

Figure 6.16 – Effect of adding ten equivalents of Hg(II) to a solution of **Eu_2L1**.

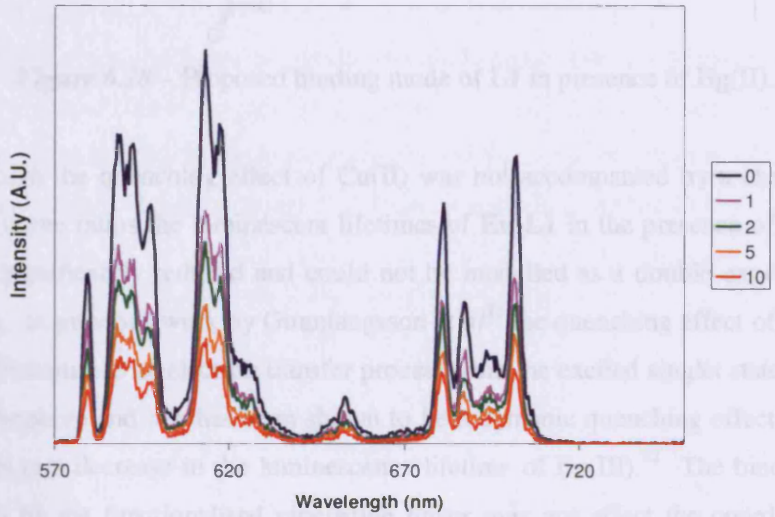

Figure 6.17 – Effect of adding ten equivalents of Cu(II) to a solution of **Eu_2L1**.

Luminescence lifetime measurements on **Eu_2L1** in the presence of Hg(II) were fitted as a bi-exponential decay with the relative contribution roughly the same in D_2O and H_2O, indicating the presence of two emissive species. Applying the modified version of Horrocks' equation demonstrated that the minor componant (20 %) had a q of 0.4, corresponding to that of the free complex, whereas the major componant had a q of 1.6, which corresponds to 1-2 bound water molecules per Eu(III) centre. This indicates that Hg(II) binds to the central

piperazine unit and at least one of the pyridine groups, allowing access of one or two water molecules to each lanthanide ion. This alteration of the coordination environments of the Eu(III) would account for the observed change in the $J = 1/J = 2$ ratio.

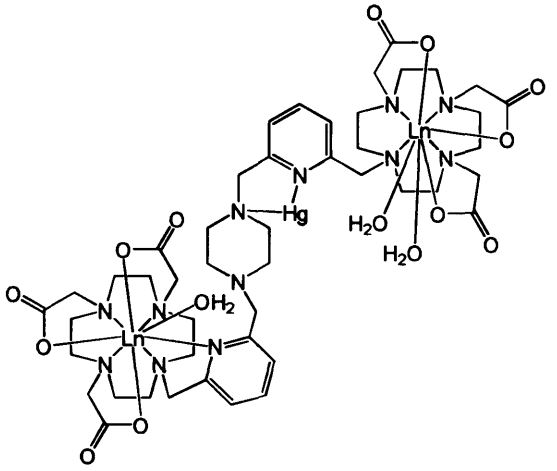

Figure 6.18 – Proposed binding mode of **L1** in presence of Hg(II).

Although the quenching effect of Cu(II) was not accompanied by a change in the relative ratios the luminescent lifetimes of $\mathbf{Eu_2L1}$ in the presence of Cu(II) were significantly reduced and could not be modelled as a double exponential decay. In previous work by Gunnlaugsson *et al*[31] the quenching effect of Cu(II) was attributed to an electron transfer process from the excited singlet state of the chromophore and this has been shown to be a dynamic quenching effect which results in a decrease in the luminescence lifetime of Eu(III).[32] The binding of Cu(II) by the functionalised piperazine linker may not effect the coordination environment of the Eu(III) but would still quench luminescence by an electron transfer process from the pyridine units, which would account for the retention of the coordination environment of the Eu(III) during the general quenching of luminescence intensity and lifetime

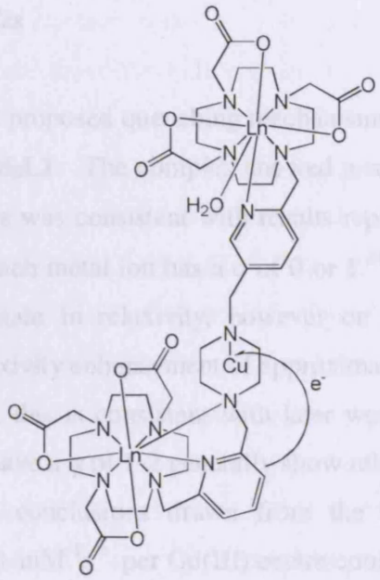

Figure 6.19 – Proposed binding mode and quenching mechanism of Cu(II).

The electron transfer from the pyridine excited singlet state would also result in a quenching of ligand luminescence. In order to study this a solution of **Gd_2L1**, in which the ligand luminescence is clearly visible due to the absence of energy transfer process to lanthanide excited states, was titrated against Cu(II).

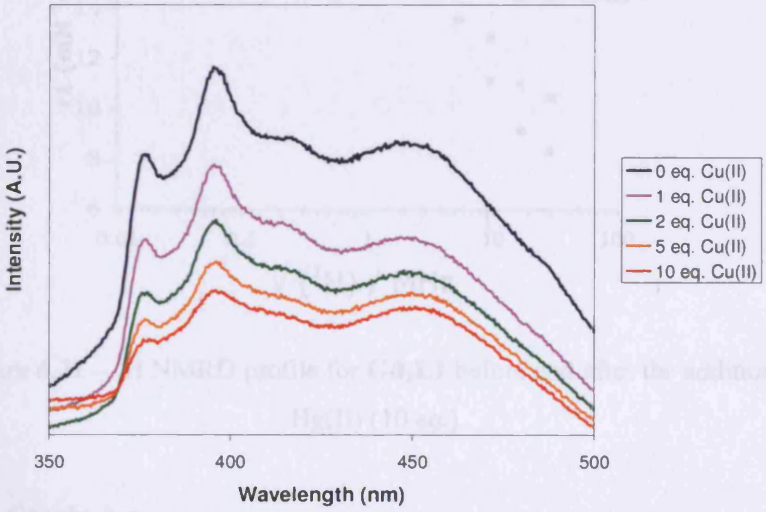

Figure 6.20 – Effect of Cu(II) on **Gd_2L1** ligand luminescence.

6.2.4 – Relaxivity studies

In order to confirm the proposed quenching mechanisms NMRD measurements were carried out on **Gd_2L1**. The complex showed a relaxivity of 8.3 $mM^{-1}s^{-1}$ (30 MHz, 25 °C). This was consistent with results reported by Merbach *et al*, for systems in which each metal ion has a *q* of 0 or 1.[24, 25] In the prescence of Cu(II) there was no gain in relaxivity, however on addition of Hg(II) the complex showed a relaxivity enhancement of approximately 25 %, resulting in a value of 10.3 $mM^{-1}s^{-1}$, this is consistent with later work by Merbach *et al* in which systems which have a *q* of 1-2 generally show relaxivities of > 10 $mM^{-1}s^{-1}$ which supports the conclusions drawn from the luminescence results.[26] However, a change of 1 $mM^{-1}s^{-1}$ per Gd(III) centre could also be accounted for by the water molecules in the Hg(II) hydration sphere being held in relatively close proximity to the gadolinium ions when Hg(II) occupies the binding site of **Gd_2L1**.

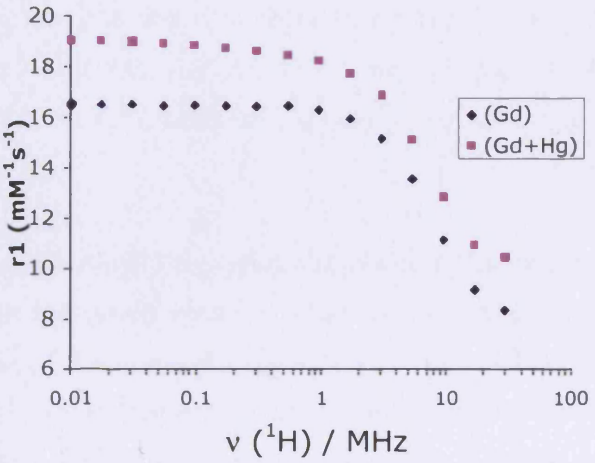

Figure 6.21 – ^{1}H NMRD profile for **Gd_2L1** before and after the addition of Hg(II) (10 eq.).

6.2.5 – Conclusions

In conclusion a new ligand capable of forming dimeric complexes with trivalent lanthanide ions has been developed by exploiting the novel chloromethyl

pyridine functionalised cyclen synthon. A combined luminescent and relaxometric study has shown that in solution the free complex has a q value of 0-1 per lanthanide ion. On the binding of Hg(II) the number of coordinated solvent molecules increases to 1-2 per Gd(III) centre, increasing the relaxivity of **Gd_2L1** and decreasing the luminescence lifetime and thus quenching the overall emission intensity of **Eu_2L1** and resulting in a change in the $J = 1/J = 2$ ratio and hyperfine structure of the emission profile. The binding of Cu(II) does not influence the binding mode of the ligand, and thus has no effect on the relaxivity of **Gd_2L1** or $J = 1/J = 2$ ratio in the Eu(III) emission profile, but an electron transfer process from the ligand excited singlet state would account for the general quenching of the Eu(III) emission profile. The complexes show good selectivity for Hg(II) and Cu(II) over other metal ions such as Zn(II), Fe(II) and Cd(II).

6.3 – Experimental

bis(6-methylpyridinyl-2-methyl-4,7,10-tris(tert-butoxycarbonyl)-1,4,7,10-tetrazacyclododecane)piperazine (17) Piperazine (0.013 g, 0.15 mmol, 1 eq.) was added to a stirred solution of 1 (0.204 g, 0.30 mmol. 2 eq.), $NaHCO_3$ (0.039 g, 0.45 mmol, 3 eq.) and KI (cat.) in MeCN (10 mL) and the mixture was heated to refluxed and stirred overnight under N_2. The mixture was then allowed to cool, filtered over gravity and the solvent was removed in vacuo. The residue was dissolved in the minimum amount of hot toluene and left to cool at -5 °C for 3d, the solvent was then decanted to leave the pure product as a brown oil (0.180 g, 0.13 mmol, 90 %); ^{1}H NMR (400 MHz, $CDCl_3$): δ_H = 1.34 (32H, s, $C(CH_3)_3$), 1.46 (18H, s, $C(CH_3)_3$), 2.20 (12H, br-m, NCH_2), 2.29 – 2.94 (36H, br-m, piperazine-CH_2, ring-CH_2), 2.98 (4H, br-s, ring-CH_2-pyr), 3.56 (4H, s, $COCH_2N$), 7.17 (2H, d J_{HH} = 7.6, pyr-H), 7.34 (2H, d J_{HH} = 7.7, pyr-H) and 7.60 ppm(2H, t J_{HH} = 7.8, pyr-H). ^{13}C{1H} (62.5 MHz, CDCl3) δ_C = 27.08, 27.20,49.31, 55.60, 80.97, 81.21, 121.63, 136.46,156.09,159.09, 171.11 and 171.85 ppm. ES+ MS: m/z 1321 {M+H}+ and 661.5 {M+2H}2+. λ_{max} (ε / mol^{-1} dm^3 cm^{-1}); 206 (29991) and 265 (7383) nm. IR υ_{max} (CHCl3): 1016, 1211, 1424, 1520, 1578, 1727, 2400 and 3015 cm^{-1}.

bis(6-methylpyridinyl-2-methyl-4,7,10-tris(tert-butoxycarbonyl)-1,4,7,10-tetrazacyclododecane)piperazine (L1) 17 (0.200, 1 eq., 1.5 mmol) was dissolved in a 1:1 solution of CH_2Cl_2:TFA (10 mL) and the reaction was left to stir overnight. After this time the solvent was removed *in vacuo* and the residue was dissolved in CH_3OH (10 mL). This was then removed *in vacuo* and the process was repeated two more times to eliminate excess acid. The residue was then dissolved in the minimum amount of CH_3OH, which was slowly added to stirred Et_2O at 0 °C. The suspension was then filtered and dried to give L1 as a yellow powder (0.108 g, 72 %); NMR (400 MHz, D_2O):δ_H = 2.92 – 3.60 (48 H, br-m, CH_2COOH, piperazine-CH_2, ring-CH_2), 3.47 (4H, br-s, NCH_2pyr),3.88 (4H, br-s, CH_2piperazine), 7.48 (4H, m, pyr-H) and 7.86 ppm (2H, t J_{HH} = 7.6, pyr-H). ES+ MS: m/z 984 {M+H}+. λ_{max} (ε / mol^{-1} dm^3 cm^{-1}); 209 (11657) and

263 (4975) nm. IR υ_{max} (ATR, solid): 1125, 1183, 1462, 1673, 1726, 1980, 2051 and 2165 cm^{-1}.

General Procedure for the formation of lanthanide complexes

A mixture of the ligand (0.02 g, 1 eq., 0.2 mmol) and $Ln(OTf)_3$ (2 eq.)was stirred in MeOH at 50 °C for 24h. The solution was reduced in vacuo then added dropwise to stirring diethyl ether at 0 °C. The precipitate was filtered, washed with diethyl ether and dried to give the lanthanide complex.

EuL10 was isolated as a pale yellow powder (0.024, 92 %); ES+ MS: m/z 1283 {M+H}+. HRMS: 1281.3400 {M+H}+; $\{C_{46}H_{66}N_{12}O_{112}{}^{151}Eu_2\}$+ requires 1281.3406 and 641.1725 {M+2H}2+; $\{C_{46}H_{66}N_{12}O_{112}{}^{151}Eu_2\}$2+ requires 641.1733. λmax (ε / mol-1 dm3 cm-1); 207 (8849) and 266 (3507) nm. IR υMAX (ATR, solid): 1028, 1166, 1410, 1444, 1593, 2048 and 2162 cm^{-1}.

GdL10 was isolated as a pale yellow powder (0.025, 95 %); ES+ MS: m/z 648 $\{M+2H\}^+$. UV-Vis λ_{max} (ε / mol^{-1} dm^3 cm^{-1}); 210 (7595) and 267 (5918) nm. IR υ_{max} (ATR, solid): 1029, 1170, 1412, 1444, 1597, 2048 and 2162 cm^{-1}.

TbL10 was isolated as a pale yellow powder (0.025, 95 %); ES+ MS: m/z 1297 {M+H}+. UV-Vis λ_{max} (ε / mol^{-1} dm^3 cm^{-1}); 208 (9193) and 267 (4166) nm. IR υ_{max} (ATR, solid): 1028, 1170, 1411, 1444, 1598, 2046 and 2161 cm^{-1}.

SmL10 was isolated as a pale yellow powder (0.023, 88 %); ES+ MS: m/z 1282 {M+H}+. UV-Vis λ_{max} (ε / mol^{-1} dm^3 cm^{-1}); 209 (9182) and 266 (3481) nm. IR υ_{max} (ATR, solid): 1028, 1167, 1411, 1444, 1544, 2039 and 2162 cm^{-1}.

6.4 – References

1. P. Caravan, J. J. Ellison, T. J. McMurry and R. B. Lauffer, *Chem. Rev.*, 1999, **99**, 2293-2352.
2. R. B. Lauffer, *Chem. Rev.*, 1987, **87**, 901-927.
3. K. N. Raymond and V. C. Pierre, *Bioconj. Chem.*, 2005, **16**, 3-8.
4. A. Y. Louie, M. M. Huber, E. T. Ahrens, U. Rothbacher, R. Moats, R. E. Jacobs, S. E. Fraser and T. J. Meade, *Nature Biotechnol.*, 2000, **18**, 321-325.
5. M. Giardiello, M. P. Lowe and M. Botta, *Chem. Comm.*, 2007, 4044-4046.
6. M. P. Lowe, D. Parker, O. Reany, S. Aime, M. Botta, G. Castellano, E. Gianolio and R. Pagliarin, *J. Am. Chem. Soc.*, 2001, **123**, 7601-7609.
7. W. H. Li, G. Parigi, M. Fragai, C. Luchinat and T. J. Meade, *Inorg. Chem.*, 2002, **41**, 4018-4024.
8. W. H. Li, S. E. Fraser and T. J. Meade, *J. Am. Chem. Soc.*, 1999, **121**, 1413-1414.
9. T. Budde, A. Minta, J. A. White and A. R. Kay, *Neuroscience*, 1997, **79**, 347-358.
10. B. L. Vallee and K. H. Falchuk, *Physiol.Rev.*, 1993, **73**, 79-118.
11. J. Kaiser, *Science*, 1994, **265**, 1365-1365.
12. K. Hanaoka, K. Kikuchi and T. Nagano, *J. Inorg. Biochem.*, 2003, **96**, 141-141.
13. K. Hanaoka, K. Kikuchi, Y. Urano, M. Narazaki, T. Yokawa, S. Sakamoto, K. Yamaguchi and T. Nagano, *Chem. Biol.*, 2002, **9**, 1027-1032.
14. K. Hanaoka, K. Kikuchi, Y. Urano and T. Nagano, *J. Chem. Soc.-Perkin Trans. 2*, 2001, 1840-1843.
15. R. Trokowski, J. M. Ren, F. K. Kalman and A. D. Sherry, *Angew. Chem.-Int. Ed. Engl.*, 2005, **44**, 6920-6923.
16. S. J. A. Pope and R. H. Laye, *Dalton Trans.*, 2006, 3108-3113.
17. E. Gaggelli, H. Kozlowski, D. Valensin and G. Valensin, *Chem. Rev.*, 2006, **106**, 1995-2044.
18. E. L. Que and C. J. Chang, *J. Am. Chem. Soc.*, 2006, **128**, 15942-15943.
19. E. L. Que, E. Gianolio, S. L. Baker, A. P. Wong, S. Aime and C. J. Chang, *J. Am. Chem. Soc.*, 2009, **131**, 8527-8536.
20. T. H. Cheng, Y. M. Wang, K. T. Lin and G. C. Liu, *J. Chem. Soc.-Dalton Trans.*, 2001, 3357-3366.
21. C. Casali, M. Janier, E. Canet, J. F. Obadia, S. Benderbous, C. Corot and D. Revel, Symposium on Contrast Media Research, Kyoto, Japan, 1997.
22. Z. D. Zhang, M. T. Greenfield, M. Spiller, T. J. McMurry, R. B. Lauffer and P. Caravan, *Angew. Chem.-Int. Ed. Engl.*, 2005, **44**, 6766-6769.
23. M. Rohrer, H. Bauer, J. Mintorovitch, M. Requardt and H. J. Weinmann, *Invest. Radiol.*, 2005, **40**, 715-724.
24. E. Toth, S. Vanthey, D. Pubanz and A. E. Merbach, *Inorg. Chem.*, 1996, **35**, 3375-3379.
25. D. H. Powell, O. M. NiDhubhghaill, D. Pubanz, L. Helm, Y. S. Lebedev, W. Schlaepfer and A. E. Merbach, *J. Am. Chem. Soc.*, 1996, **118**, 9333-9346.
26. J. Costa, E. Toth, L. Helm and A. E. Merbach, *Inorg. Chem.*, 2005, **44**, 4747-4755.
27. J. Costa, E. Balogh, V. Turcry, R. Tripier, M. Le Baccon, F. Chuburu, H. Handel, L. Helm, E. Toth and A. E. Merbach, *Chem. Eur. J.*, 2006, **12**, 6841-

6851.
28. G. A. Crosby, R. M. Alire and R. E. Whan, *J.Chem. Phy.*, 1961, **34**, 743-&.
29. K. Annapurna, R. N. Dwivedi, P. Kundu and S. Buddhudu, *Mater. Res. Bull.*, 2003, **38**, 429-436.
30. A. Beeby, I. M. Clarkson, R. S. Dickins, S. Faulkner, D. Parker, L. Royle, A. S. de Sousa, J. A. G. Williams and M. Woods, *J. Chem. Soc.-Perkin Trans. 2*, 1999, 493-503.
31. T. Gunnlaugsson, J. P. Leonard, K. Senechal and A. J. Harte, *Chem. Comm.*, 2004, 782-783.
32. M. A. Kessler, *Anal. Chim. Acta*, 1998, **364**, 125-129.